PART I

STRUCTURAL STUDIES ON THE Bi_2O_3-Nb_2O_5 SYSTEM

PART II

STUDIES ON SOME NOVEL FLUORITE-TYPE SUPERSTRUCTURES

PART III

THE CRYSTAL STRUCTURE OF DICALCIUM NITRIDE

A thesis submitted for the degree of Doctor of Philosophy of the University of London

by

EDWARD THOMAS KEVE B.Sc., D.I.C., Grad.Inst.P., A.M.C.S.T.

Department of Chemistry

Imperial College

July 1968

ABSTRACT

Part I

An investigation of some of the crystal structures occurring in the Bi_2O_3-Nb_2O_5 binary system was undertaken by X-ray methods.

The structure of triclinic $BiNbO_4$ was solved from visually estimated single-crystal diffraction data. The unit cell has a = 7.611, b = 5.536, c = 7.919 Å, $\alpha = 89^\circ 54'$, $\beta = 77^\circ 28'$, $\gamma = 87^\circ 9'$, the space group is $P\bar{1}$. The structure, which consists of sheets of niobium-oxygen octahedra linked through bismuth atoms, is of an entirely new type. The mode of joining of the octahedra in the sheets found in this compound is novel. Least-squares refinement with isotropic temperature factors converged to R = 0.122.

The correct structural formula of the compound "$Bi_2O_3.6Nb_2O_5$" was shown to be $3Bi_2O_3.17Nb_2O_5$, on the basis of single-crystal structural analysis. This compound is orthorhombic, with a = 12.516, b = 37.14, c = 3.922 Å, and has the space group Pba2. The structure, which was solved from visually estimated single-crystal intensity data, is related to the tetragonal bronze structure, but has a three-fold increase in the a cell parameter. The bismuth atoms are distributed among a number of possible sites in the cavities of a rigid $Nb_{34}O_{94}$ niobium-oxygen framework. Least-squares refinement, with anisotropic thermal parameters

for the metal atoms gave a final R-value of 0.092.

The hexagonal unit cell of the compound "$4Bi_2O_3 \cdot 9Nb_2O_5$" was corrected to $a = 7.445$, $c = 19.778$ Å, on the basis of single-crystal photographs. Intensity data for this compound were collected on an automatic diffractometer.

The published X-ray powder pattern of the compound "$Bi_2O_3 \cdot 5Nb_2O_5$" was indexed using an orthorhombic unit cell of $a = 17.632$, $b = 3.949$, $c = 17.167$ Å. A structure related to the tetragonal bronzes is postulated. The space group $Pmn2_1$ is thought likely.

Part II

Some preliminary studies are described on a family of compounds containig lead, niobium, oxygen, fluorine and in all but one case, a rare earth metal. All the compounds, which are themselves rhombohedral, have a rhombohedral subcell, with $a_{hex} = 3.75$, $c_{hex} = 9.45$ Å. The true cells all have $a = 2a_{sub}$, and have c parameters 5, 7 or 10 times that of the subcell. Single crystal intensity data collection on the automatic diffractometer is described for two of the compounds, and structural postulates are made.

Part III

The solution of the crystal structure of a new compound, dicalcium nitride, is described. Ca_2N is rhombohedral, with the space group $R\bar{3}m$,

and has $a = 6.603$ Å, $\alpha = 31^{\circ}59'$ ($a_{hex} = 3.638$, $c_{hex} = 18.78$ Å). The layer structure of Ca_2N is of the anti-$CdCl_2$ type. These layers are widely separated, their closest approach being a Ca-Ca distance of 4.35 Å. The structure refined to $R = 0.132$ on the basis of visually estimated intensity data. An essentially ionic structure is proposed for Ca_2N, and novel electrical properties are predicted for a single crystal.

ACKNOWLEDGEMENTS

I wish to thank sincerely Dr. A. C. Skapski and Professor D. Rogers for their guidance and helpful advice during the course of this work. Their friendly supervision in the last three years has been much appreciated.

I am also grateful to Dr. A. E. D. White for the preparation of the materials discussed in Part II, and for the way in which the facilities of the Crystal Growing Laboratory were made available to me. Professor J. W. Tomlinson and Mr. C. Lammas were kind enough to provide crystals of Ca_2N.

The facilities of the IBM 7090 computer at Imperial College, and of the London University Atlas computer are gratefully acknowledged. My thanks are due to all the authors of the X-ray '63 system of crystallographic computer programs, especially to Professor J. M. Stewart. The authors of the ATSYS system of programs, including Drs. M. G. B. Drew and D. J. Hunt, and Drs-to-be P. G. H. Troughton and F. H. Allen, are similarly thanked.

I am indebted to G. I. K. (working wife) and S. R. C. (Research Studentship) for their financial help.

The encouragement I received from my wife, parents, relatives and friends was a great help to me throughout.

"It is a pleasure to stand upon the shore,
and to see ships tost upon the sea,
a pleasure to stand in the window of a castle,
and to see a battle and the adventures thereof below:
but no pleasure is comparable to the standing
upon the vantage ground of truth
and to see the errors, and wanderings, and mists, and tempests,
in the vale below."

Francis Bacon

To my wife

CONTENTS

A SUMMARY OF X-RAY DIFFRACTION TECHNIQUES AND THEORY

1. Theoretical Background and Computational Methods 11
2. Experimental Method 24

PART I - STRUCTURAL STUDIES ON THE Bi_2O_3-Nb_2O_5 SYSTEM

Introduction 31
3. The Bi_2O_3-Nb_2O_5 System 32
4. The Crystal Structure of Triclinic $BiNbO_4$ 40
5. Discussion of the Crystal Structure of Triclinic $BiNbO_4$ 60
6. The Crystal Structure of $3Bi_2O_3.17Nb_2O_5$ ($Bi_2O_3.6Nb_2O_5$) 86
7. Discussion of the Crystal Structure of $3Bi_2O_3.17Nb_2O_5$ 115
8. Investigations on "$Bi_2O_3.5Nb_2O_5$" and Discussion of Some Related Compounds 150
9. "$4Bi_2O_3.9Nb_2O_5$" 172
10. Summary to Part I 177

References I 184

PART II - STUDIES ON SOME NOVEL FLUORITE-TYPE SUPERSTRUCTURES

Introduction 189

11. Some Superstructures of the Fluorite-Type 189

References II 219

PART III - THE CRYSTAL STRUCTURE OF DICALCIUM NITRIDE

Introduction 221

12. The Crystal Structure of Ca_2N 224

13. Discussion of the Crystal Structure of Ca_2N 261

References III 278

Appendix 280

A SUMMARY OF

X-RAY DIFFRACTION TECHNIQUES AND THEORY

1. Theoretical Background and Computational Methods

Crystal Symmetry

Any crystal may be thought of as being built up by the periodic repetition in three dimensions of a certain atomic arrangement. This fundamental set of atoms is contained in the unit cell. The three-dimensional array of points having identical and parallel environment in a crystal defines its lattice, and the unit cell can in principle be chosen from this in an infinity of ways. In practice the choice is guided by the symmetry of the pattern of atoms inside the unit cell. The cell chosen may be primitive, i.e. have one lattice point at each of its corners only, or it can be non-primitive, having more than one lattice point per cell. Thus each of the six crystal systems has a unit cell of a distinctive shape, embodying the symmetry of the structure, and may in some systems also contain lattice points at face or body centres, resulting in the 14 Bravais lattices.

When a motif is repeated in three dimensions using the symmetry operations of 1,2,3,4 or 6-fold rotation, inversion and the mirror image, together with combinations of these and linear translations, 230 distinct three-dimensional symmetry patterns or space-groups may be built up. Any crystal therefore belongs to one of these 230 space-groups.

For a complete determination of the structure of a crystal,

the space-group, the size and shape of the unit cell, and the positions of all atoms in the asymmetric unit must be known. X-ray crystallography is concerned with finding these by the interpretation of the X-ray diffraction pattern of the crystal.

Scattering of Radiation

When a beam of monochromatic X-rays of wavelength λ falls on a body with non-uniform electron density, the scattered wave at B can be written with respect to the wave at A as

$$\rho(\underline{r})dV(\exp(\frac{2\pi i}{\lambda}(\cos\psi - \cos\phi))) ,$$

where the vector $\overrightarrow{AB}$ is denoted by $\underline{r}$, and B is contained in the volume element dV with local electron density $\rho(\underline{r})$. The angles ψ and ϕ are shown in Figure 1.1.

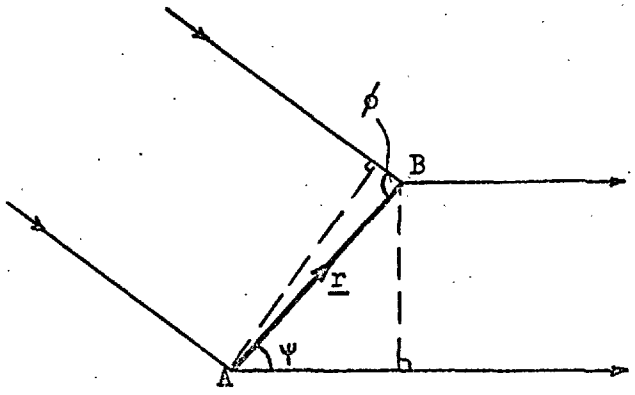


Figure 1.1

The total scattered wave is given by the integral over the whole volume of the body

$$\int \rho(\underline{r}) \exp\left(\frac{2\pi i |\underline{r}|}{\lambda}(\cos\psi - \cos\phi)\right) dV$$

Defining vectors $\underline{S}$, $\underline{s}_1$ and $\underline{s}_2$ such that

$$\underline{r}.\underline{s}_1 = |\underline{r}|\cos\phi / \lambda, \qquad \underline{r}.\underline{s}_2 = |\underline{r}|\cos\psi / \lambda, \qquad \underline{S} = \underline{s}_1 - \underline{s}_2$$

then the total scattered wave, denoted by $G(\underline{S})$, becomes

$$\int \rho(\underline{r}) \exp 2\pi i \underline{r}.(\underline{s}_1 - \underline{s}_2) dV \text{ , or}$$

$$G(\underline{S}) = \int \rho(\underline{r}) \exp 2\pi i \underline{r}.\underline{S} dV$$

The vector $\underline{S}$ is reciprocally related to $\underline{r}$, thus it is considered to be a vector in "reciprocal space" as opposed to the real space occupied by the scattering material. The result for $G(\underline{S})$ is a "Fourier Transform". The intensity I, of the scattered wave is given by $I = G(\underline{S}).G^*(\underline{S})$, where $G^*(\underline{S})$ is the complex conjugate of $G(\underline{S})$. Thus to determine $\rho(\underline{r})$, it is not sufficient to know I, and thence $|G(\underline{S})|$, but it is also necessary to be able to derive its phase.

In practice I is found by direct measurement, whereas the phase must be arrived at indirectly, hence the so called "phase problem" of crystallography.

Diffraction by a Single Crystal

If there are N atoms in the unit cell, each with co-ordinates

$\underline{X}_n$, $\underline{Y}_n$, $\underline{Z}_n$ with respect to the origin of the cell, the nth atom will be $\underline{r}_n = \underline{X}_n + \underline{Y}_n + \underline{Z}_n$ from the cell origin. The wave scattered by one of the N atoms in the unit cell can be written as

$$\int \rho(\underline{r}) \exp 2\pi i(\underline{r} + \underline{r}_n) \cdot \underline{S} dV \qquad \text{or}$$

$$\left\{ \int \rho(\underline{r}) \exp 2\pi i \underline{r} \cdot \underline{S} dV \right\} \exp 2\pi i \underline{r}_n \cdot \underline{S}$$

The portion in brackets is the same for all chemically equivalent atoms and can be replaced by f_n, the scattering factor for a spherically symmetric atom. The total wave scattered by the N atoms in the unit cell is given by a summation since the electron densities of adjacent atoms do not appreciably overlap. Thus

$$G_u(\underline{S}) = \sum_{n=1}^{N} f_n \exp 2\pi i \underline{r}_n \cdot \underline{S}$$

If the unit cell of a crystal has edges defined by vectors $\underline{a}$, $\underline{b}$, $\underline{c}$, all atoms in the crystal may be designated by the ends of vectors of the form $u\underline{a} + v\underline{b} + w\underline{c} + \underline{r}_n$, where u, v, and w are integers. The total transform of the crystal is therefore

$$G_t(\underline{S}) = \sum_{u=0}^{U-1} \sum_{v=0}^{V-1} \sum_{w=0}^{W-1} G_u(\underline{S})$$

Each of these summations is of the form

$$\sum_{t=0}^{T-1} = (1 + \exp 2\pi i \underline{a} \cdot \underline{S} + \ldots + \exp 2\pi i t \underline{a} \cdot \underline{S} + \ldots + \exp 2\pi i (T-1) \underline{a} \cdot \underline{S})$$

$$= \frac{1 - \exp 2\pi i T \underline{a} \cdot \underline{S}}{1 - \exp 2\pi i \underline{a} \cdot \underline{S}}, \text{ which reduces to } \frac{\sin T\pi \underline{a} \cdot \underline{S}}{\sin \pi \underline{a} \cdot \underline{S}}.$$

Its value is T when $\underline{a}.\underline{S}$ is an integer, but is negligible otherwise.

Therefore $G_t(\underline{S})$ can be written

$$G_t(\underline{S}) = G_u(\underline{S})\left(\frac{\sin(U\pi\underline{a}.\underline{S})}{\sin(\pi\underline{a}.\underline{S})}\right)\left(\frac{\sin(V\pi\underline{b}.\underline{S})}{\sin(\pi\underline{b}.\underline{S})}\right)\left(\frac{\sin(W\pi\underline{c}.\underline{S})}{\sin(\pi\underline{c}.\underline{S})}\right).$$

$G_t(\underline{S})$ therefore is zero, unless $\underline{a}.\underline{S}$, $\underline{b}.\underline{S}$ and $\underline{c}.\underline{S}$ all have integer values, h, k, l say.

i.e. $G_t(\underline{S}) = 0$ in general,

$G_t(\underline{S}) = UVWG_u(\underline{S})$ when $\underline{a}.\underline{S} = h$, $\underline{b}.\underline{S} = k$, $\underline{c}.\underline{S} = l$ simultaneously.

The conditions for non-zero $G_t(\underline{S})$ are the Laue equations. Thus the total diffraction pattern of the crystal is directly proportional to that of the unit cell contents, $G_u(\underline{S})$, at points in reciprocal space defined by the trio of integer co-ordinates (h,k,l), but is zero elsewhere. These points define a three-dimensional reciprocal lattice.

The Structure Factor

The value of $G_u(\underline{S})$ at a reciprocal lattice point is called the structure factor, F_{hkl}, at that point. Using the fractional co-ordinates x_n, y_n, z_n, (the atomic parameters) for the n^{th} atom, such that

$$\underline{r}_n = x_n\underline{a} + y_n\underline{b} + z_n\underline{c},$$

$$F_{hkl} = \sum_{n=1}^{N} f_n \exp 2\pi i(x_n\underline{a}.\underline{S} + y_n\underline{b}.\underline{S} + z_n\underline{c}.\underline{S})$$

$$F_{hkl} = \sum_{n=1}^{N} f_n \exp 2\pi i(hx_n + ky_n + lz_n)$$

$$= \sum_{n=1}^{N} f_n \cos 2\pi(hx_n + ky_n + lz_n) + i\sum_{n=1}^{N} f_n \sin 2\pi(hx_n + ky_n + lz_n)$$

which may be written

$$F_{hkl} = A_{hkl} + iB_{hkl} = |F_{hkl}| \exp(i\phi_{hkl}),$$

where ϕ_{hkl} is the phase angle, and $|F_{hkl}|$ is the structure amplitude.

For a centrosymmetric arrangement within the unit cell, taking atoms in pairs $\underline{r}_n$, $\underline{r}'_n$ such that $\underline{r}'_n = -x_n\underline{a} - y_n\underline{b} - z_n\underline{c}$, we have that $B = 0$, since $\sin\theta + \sin(-\theta) = 0$ for any angle θ. Therefore $|F_{hkl}| = A_{hkl}$ with phase 0 or π for the centrosymmetric case. In general, the previous statement that $I = G(\underline{S}).G^*(\underline{S})$ can be rewritten as $I = A^2 + B^2$.

The symmetry with which the motifs are repeated within the unit cell by the space-group may cause certain combinations of h, k and l to give structure factors of zero. The recognition of such "systematic absences" will help to limit the possible space-groups of a given crystal.

The Temperature Factor

All the above equations are derived for stationary atoms, but thermal motion can be accomodated by substituting $f_o \exp\left(\frac{-B\sin^2\theta}{\lambda^2}\right)$ for f, where B is the isotropic temperature factor, and θ is the

Bragg angle, equal to half the angle of scattering.

Often a more sophisticated allowance for thermal movement is required, and a set of anisotropic vibrational parameters, β_{ij}, is then used, with f being replaced by

$$f_o \exp(-(\beta_{11}h^2 + \beta_{22}k^2 + \beta_{33}l^2 + 2\beta_{12}hk + 2\beta_{13}hl + 2\beta_{23}kl)) .$$

Corrections to Intensity

Several corrections must be applied to an experimental intensity value before it can be considered to be representative of the square of the structure factor.

The polarisation correction allows for the fact that the process of "reflection" introduces partial polarisation. If the incident beam is unpolarised the correction is expressed in terms of the Bragg angle, θ, as

$$p^{-1} = \frac{1}{1 + \cos^2 2\theta} .$$

The Lorentz factor is a geometrical correction dependent on the method of collection of data, and represents the rate at which the crystal is swept through the reflecting position. In this work, when photographic methods were adopted, the equiinclination Weissenberg technique was used. The combined Lorentz and polarisation factors for this method are given by

$(Lp)^{-1} = \frac{2\xi\cos\theta}{1 + \cos^2 2\theta}$, where ξ is the radial cylindrical co-ordinate of the reciprocal-lattice point concerned.

When a four-circle diffractometer was used for data collection, the correction made was

$$(Lp)^{-1} = \frac{2\sin 2\theta}{(1 + \cos^2 2\theta)} .$$

Absorption of monochromatic radiation is in general of the form $I = I_o \exp(-\mu t)$, where t is the path length of material traversed, and μ is the linear absorption coefficient of the material for the wavelength used. The mass absorption coefficient, μ_m, of an element may be defined by $\mu = \rho \sum_{i=1}^{n} p_i \mu_{m_i}$, where p_i is the fraction by weight of the i^{th} element present, and ρ is the density of the material.

For a crystal of general shape, individual diffracted rays have to pass through different thicknesses of material. When the absorption errors are not negligible, a correction may be computed by working out the path lenths of the incident and diffracted rays for a number of sample points within the crystal. A summation is then carried out, which approximates to the integral

$$A_{hkl} = \frac{1}{V} \int_V \exp(-\mu t)\, dV$$

over the volume of the crystal, where A_{hkl} is the transmission factor for a given hkl.

The phenomenon of extinction arises because part of the energy of a diffracted beam can be doubly reflected back into the incident beam. As there is a phase change of $\pi/2$ at each scattering, the doubly scattered beam will be π out of phase with the primary beam, thus progressively cutting down its effective intensity as it penetrates

deeper into the crystal. This phenomenon of primary extinction arises only in perfect regions of the crystal, usually a single mosaic block. Secondary extinction has a similar basis, but arises from the mosaic structure of a single crystal. The deeper blocks are partially screened by any parallel blocks which may be situated closer to the irradiated surface.

No correction for extinction was made, but "reflections" thought to be suffering severely from it were removed in the final stages of least-squares refinement.

The diffracted beams fulfil the geometry of reflection of the incident beam off a stack of parallel planes within the crystal, with an angle of deviation between the incident and the reflected beam of 2θ, where θ is the Bragg angle. They are commonly termed "reflections" but they only occur in the immediate neighbourhood of θ_B, defined by Bragg's law, which connects the distance d, between the reflecting planes with θ_B by

$$2d\sin\theta_B = n\lambda \quad \text{for the } n^{th} \text{ order diffraction.}$$

These planes are said to have Miller indices hkl. Thus such an interpretation identifies each F_{hkl} with a set of planes (hkl), from which the beam is reflected.

After these corrections have been applied, or have been shown to be negligible, the observed intensities of the diffracted beams will be proportional to the squares of the moduli of the corresponding structure factors.

Fourier Synthesis

The three-dimensional electron-density function, ρ_{xyz}, is the Fourier transform of the sum of all the structure factors, F_{hkl}, with their appropriate phases. Thus at any point x,y,z

$$\rho_{xyz} = \frac{1}{V} \sum_{h=-\infty}^{\infty} \sum_{k=-\infty}^{\infty} \sum_{l=-\infty}^{\infty} F_{hkl} \exp(-2\pi i(hx + ky + lz)),$$

where V is the volume of the unit cell.

Since the vector $\underline{S}$, being defined as $(\underline{s}_1 - \underline{s}_2)$, has a maximum length equal to $2\underline{s}_1$, i.e. is confined to a sphere of this radius in reciprocal space, only reflections corresponding to those reciprocal lattice points which lie within this limiting sphere are observable. This can lead to series termination errors in the calculated electron density, which take the form of ripples around atomic peaks, (Bessel function cross section). They are only serious if the intensity data are severely truncated at the limiting sphere.

Patterson Function

The Fourier transform of the intensities is often very helpful, as this function was shown by Patterson to give a vectorial representation of the crystal structure:

$$P_{uvw} = \frac{1}{V} \sum_{h=-\infty}^{\infty} \sum_{k=-\infty}^{\infty} \sum_{l=-\infty}^{\infty} |F_{hkl}|^2 \exp(-2\pi i(hu + kv + lw)).$$

Since $|F_{hkl}|^2 = F_{hkl} F^*_{hkl}$, the Patterson function, P_{uvw}, can also be

described as the "convolution" of the structure with its inverse.

Difference-Fourier Synthesis

Sometimes structure factors are calculated for a partial structure, and are subtracted from the observed structure amplitudes. The Fourier transform of the resultant, $F_{obs}-F_{part}$ is referred to as the difference Fourier, and it often shows those details of the structure which were omitted from the structure factor calculation.

Least-Squares Refinement

The crystal structures comprising this work were solved using Patterson, Fourier and difference-Fourier syntheses, followed by the refinement of the atomic co-ordinates, temperature factors and sometimes inter-layer scale-factors. This is achieved by minimising $\Sigma\omega\Delta^2$, where Δ is the difference between the observed structure amplitudes, $|F_o|$, and the calculated structure factors, $|F_c|$, and ω is a weight.

Agreement is usually expressed in terms of R, where

$$R = \frac{\sum_l \| |F_o| - |F_c| \|}{\sum_l |F_o|} .$$

Computation

The bulk of the calculations were carried out on the Imperial College

IBM 7094 computer using the "X-ray 63" system of crystallographic programs. This system treats programs as links, enabling the user to feed the output of one program into the next, thus performing several different calculations successively in one run. All essential crystallographic data are saved on magnetic tapes so that the input of only those items which have changed from the previous run are required to initiate a new one. The versatility of this system was found ideal for the type and size of problems met by the author.

The links used were as follows:-

DATRDN - for reduction of data, application of Lorentz and polarisation corrections, scaling, square rooting of intensities and the generation of the primary data magnetic tapes;

FC - structure factor calculation and reflection statistics;

FOURR - Patterson, Fourier and difference-Fourier syntheses;

ORFLS - Busing-Levy full-matrix least-squares refinement, patched by the author as necessary to incorporate the various symmetry requirements;

BLOKLS - least-squares refinement, similar to the above, but using a block diagonal approximation of the matrix;

BONDLA - bond-lengths, angles and their standard deviations;

DELSIG - weighting scheme analysis;

LISTFC - final structure factor listing in a format suitable for publication.

Other computer programs used on the Imperial College machine were:-

ICABS - an absorption/extinction correction program originally written by Coppens, Leiserowitz and Rabinovich for a CDC 1604 computer and adapted for the IBM machine by P.G.H.Troughton;

TRNS - a program for the transformation of indices written by the author.

The major use made of the programs available within the ICSYS system on the Atlas computer was connected with the preparation and processing of the punched paper tape input to and output from the Siemens diffractometer. The numerous other crystallographic programs were little used, because of the convenience of the IBM 7094 and the fact that the size of problems dealt with did not necessitate the superior speed of Atlas. The following computer programs were used:-

SEKO - written by P.G.H.Troughton, generates the punched paper tape required for steering the Siemens diffractometer;

SODI - written by P.G.H.Troughton processes the paper tape output of the diffractometer, applies the $(Lp)^{-1}$ correction and punches the data onto cards for input to the X-ray 63 system;

LSCD - least-squares refinement of cell dimensions, written by R.Diamand;

SOSO - indexing powder lines from approximate cell dimensions written by M.G.B.Drew and modified by F.H.Allen;

BOSS - structure factor calculation and Fourier synthesis written by M.M.Harding, adapted by M.G.B.Drew;

SFLS - a structure factor least-squares refinement program, using a block diagonal approximation written by R.Diamand;

CEDI - least-squares refinement of cell dimensions written by P.G.H.Troughton.

2. Experimental Method

Preliminary Examination

Crystals were first subjected to optical examination under a microscope. Morphology, colour, the occurrence and directions of uniform extinction between crossed polars, perfection of crystals etc., were all noted.

Suitable crystals were mounted on glass fibres with vacuum grease. Use of the diffractometer, however, neccesitated mounting the crystals on the much stiffer quartz fibres with araldite. Oscillation and Weissenberg photographs were taken to determine the unit-cell dimensions and the space group. More accurate cell parameters were obtained either by indexing the powder pattern of the appropriate compound, and least-squares refinement, or from some very accurate θ-values obtained from a single crystal on the four-circle diffractometer.

The crystals selected for intensity work were measured using a calibrated graticule on the microscope. In the cases where the diffractometer was used, and where an absorption correction was essential, the crystals were drawn and measured from five orthogonal directions while still on the Eulerian cradle, using the attached calibrated microscope.

Photographic Data Collection

Where intensity data were recorded photographically, the equiinclination Weissenberg technique was adopted. In every case, a pack of four Ilford Industrial G films was used with CuKα radiation for each layer. As this gave an attenuation of about 2.6-2.8 per film, a useful intensity range could be covered with one pack. The exposure was taken as the longest necessary (or practicable in the case of $3Bi_2O_3.17Nb_2O_5$). A short exposure pack was not required in any of the cases.

The four films were developed and fixed together in darkness for five minutes each. Intensities were estimated using wedges made by exposing a given reflection for accurately known lengths of time. In one case, ($BiNbO_4$), part of the data was measured on a Joyce-Loeble integrating microdensitometer. The structure was solved in projection on the basis of these measurements, but the same films, when estimated visually, gave better agreement. Visual measurement was therefore adopted throughout. It is thought that the extremely small, sharp reflections of this crystal were paricularly unfavourable for correct integration by the densitometer.

Measurements of intensities on each film were scaled up to the top film of each pack and a mean value was calculated for each reflection. Where appropriate, a correlating layer was taken, rotating about a different axis; otherwise the inter-layer scales were used as parameters

in the least-squares refinement of the structure.

In general, it was not possible to make use of the integrating mechanism of the camera, as the exposure times were already near the maximum practicable.

Diffractometer Data Collection

A Siemens Automatic Single-Crystal Diffractometer was used to collect intensity data for three crystals. This is a four-circle off-line instrument using punched paper tape input and output.

A set of digitizer drums ensures that each of the four circles (Figure 2.1) can be positioned to an accuracy of 1/100th of a degree, or one "bit". The crystal under study is set up with one axis parallel to the axis of the ϕ circle, and the ϕ=0.00° datum line is set to coincide with a reciprocal axis. This is accomplished with the aid of a set of horizontal and vertical half-shutters and automatic scanning of θ for successive values of ϕ, (θ-ϕ scan) to an accuracy of 1/100th of a degree.

Accurate unit-cell constants are determined from values of θ for a number of reflections, measured using a slit collector aperture for maximum resolution.

For the collection of intensity data, a "steering" paper tape is generated, which gives the incremental angle change for each successive reflecting position, followed by a command to check the digitizers

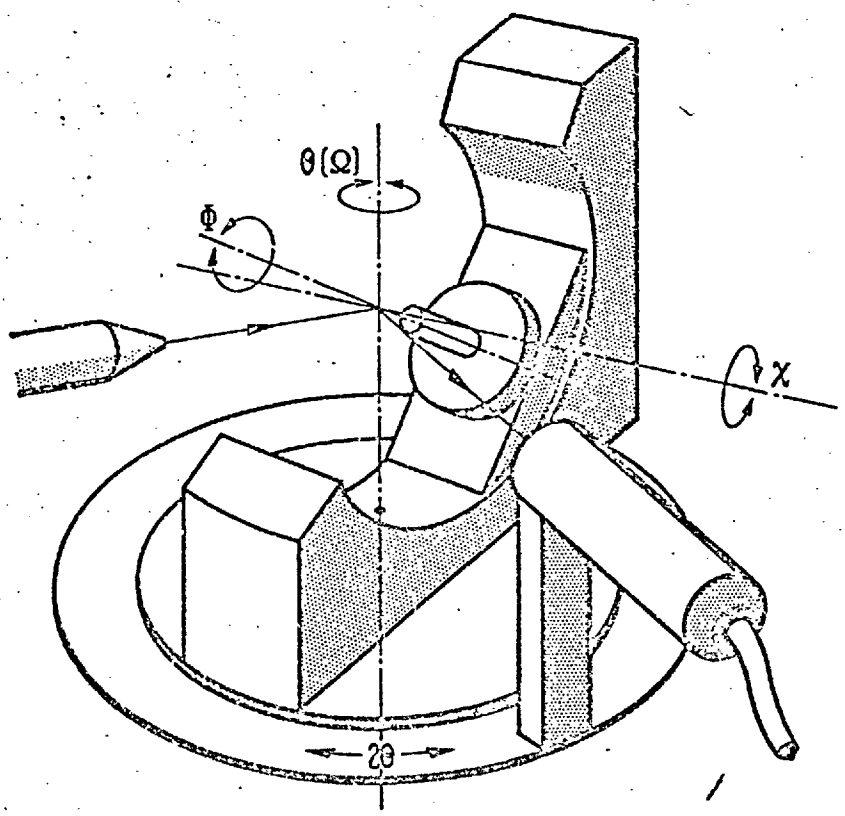


Figure 2.1

Basic design of the Automatic Single Crystal Diffractometer

against the fractional parts of the correct values of the angles. If this check is successful, a five-point measurement is initiated, (Figure 2.2), in which the two halves of an intensity peak are measured as two integrated totals, as well as the complete peak, and

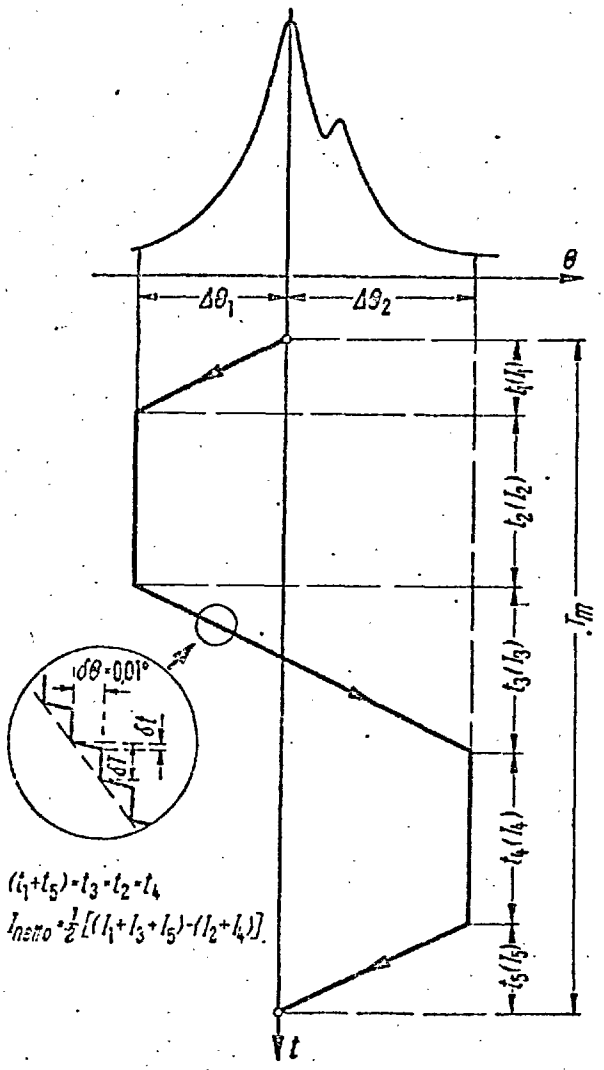


Figure 2.2

Intensity determination according to the five values method.

two background counts are taken. All these values are output together with relevant information for the given reflection. A maximum measuring time per reflection is preset, but the logic of the instrument is capable of reducing this substantially, to give a narrower range of actual counts throughout, thereby ensuring that the minimum time is taken for a given accuracy of the results.

If a digitizer check fails, this is indicated on the output, and the instrument automatically searches for the correct fractional part over a range of $\bar{+}20$ bits. If it is found, the machine locks on this value and proceeds with data collection; otherwise it halts. Periodically a zero check is introduced, thereby checking the correct absolute values of the previous angle settings. Checks on the intensity of a reference reflection and positions of control reflections are also made periodically, and included in the output.

The output tapes are examined for digitizer checks and the balance of the control reflections. The intensity values of the reference reflection are used to scale groups of data, to allow for slight variations with time of various operating factors, then the data are treated in the normal way.

In all cases CuK_α radiation and a scintillation (Na(Tl)I) counter plus photomultiplier were used.

"... the schoolmen are like astronomers, which feign eccentrics and epicycles, and such engines of orbs, to save phenomena, though they know there are no such things."

A 16th century Councillor of Trent

PART I

STRUCTURAL STUDIES ON THE Bi_2O_3-Nb_2O_5 SYSTEM

PART I - Introduction

The first compound in the Bi_2O_3-Nb_2O_5 system to be studied by the author was triclinic $BiNbO_4$. This is a member of the family of some $A^{III}B^{V}O_4$ oxides of group V metals shown in Table 3.1. These compounds exhibit three structure types, two of which had been determined recently by Rogers and Skapski[I.1,I.5], and were found to be unique to this family. The crystal structure of triclinic $BiNbO_4$ was therefore attempted and solved to complete the trilogy of novel structural types exhibited in this group.

The work on $BiNbO_4$ had drawn attention to other compounds in the Bi_2O_3-Nb_2O_5 system recorded by Roth and Waring[I.2]. It was hoped that the analysis of some of these structures would prove fruitful not only in themselves but also in predicting the other structures in the group, and possibly showing a common, unifying building principle throughout.

An account of this work forms Part I of this thesis.

3. The Bi_2O_3-Nb_2O_5 System

Compounds of the Formula $xBi_2O_3.yNb_2O_5$

The phase relationships in the binary system Bi_2O_3-Nb_2O_5 were extensively studied by Roth and Waring[I.2,I.3]*. They constructed the phase equilibrium diagram reproduced in Figure 3,1, from observations of fusion characteristics and X-ray powder data. In the system they found five binary compounds with Bi_2O_3:Nb_2O_5 ratios of 5:3, 1:1, 4:9, 1:5 and 1:6, details of which are given below. The 1:1 compound had previously been synthsised by Aurivillius[I.4], but Roth was able to show that a low temperature form also exists.

$5Bi_2O_3.3Nb_2O_5$

This compound was found to give poor quality powder patterns, which could be partially indexed on the basis of a pseudo-tetragonal cell of a = 10.912, c = 10.496 Å.

---

* For the sake of brevity, the work of "Roth" is usually quoted when reference is made to paper I.2

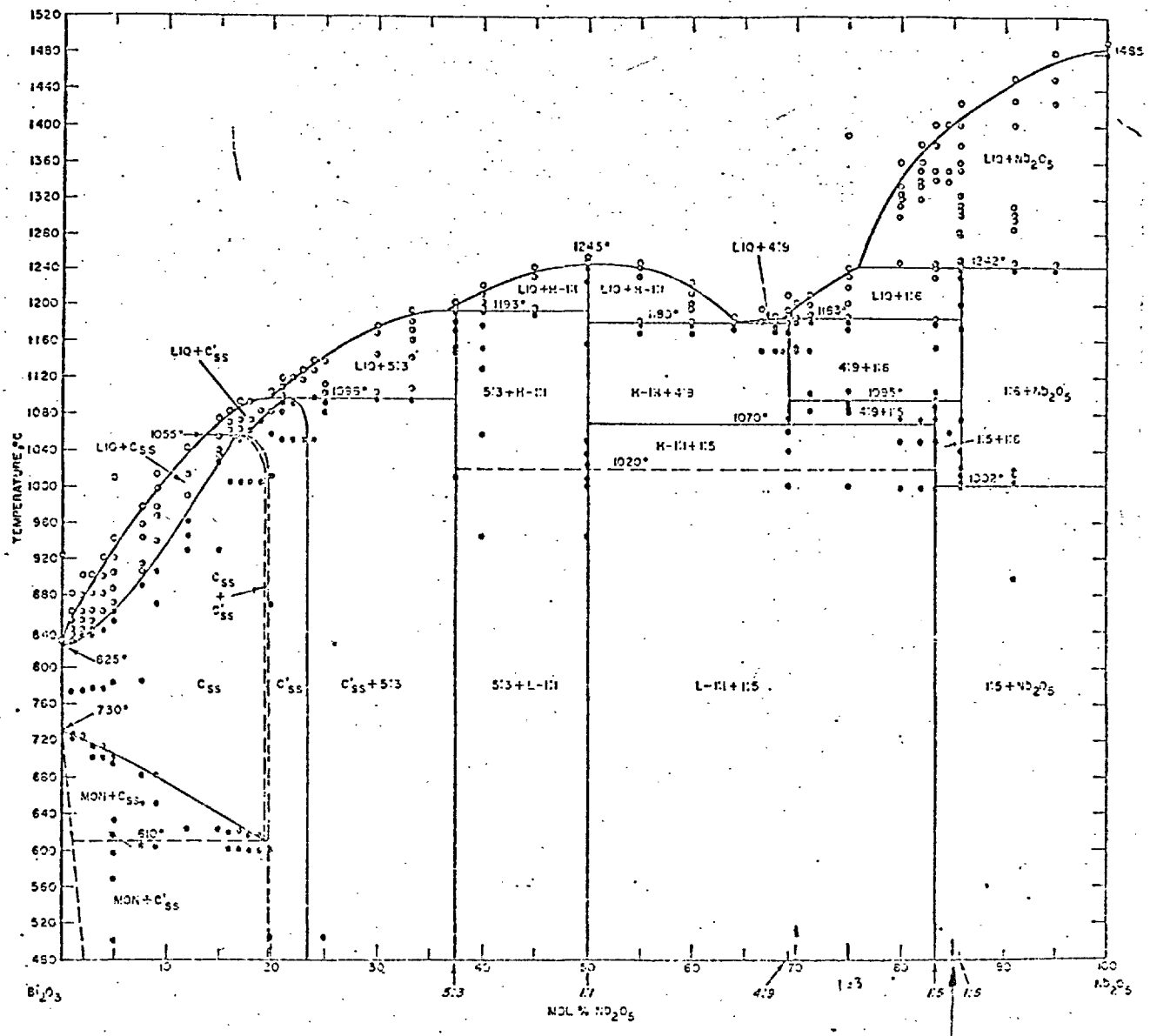


FIGURE 3. *Phase equilibrium diagram for the system* Bi_2O_3-Nb_2O_5

O—no melting
Ø—partially melted
O—completely melted
L—low temperature modification
H—high temperature modification
C—cubic
C'—pseudocubic
Mon—monoclinic
LIQ—liquid

$Bi_2O_3 \cdot Nb_2O_5$ ($BiNbO_4$) - low temperature form

All preparations below 1200°C of the 1:1 compound yielded an orthorhombic modification. Once the high temperature form appeared, however, the transformation could not be reversed. The X-ray powder pattern was indexed on the basis of an orthorhombic unit cell with $a = 4.980$, $b = 11.70$, and $c = 5.675$ Å.

$Bi_2O_3 \cdot Nb_2O_5$ ($BiNbO_4$) - high temperature form

Aurivillius first prepared the triclinic modification of $BiNbO_4$ and deduced its unit-cell dimensions from single crystal Weissenberg photographs as $a = 7.71$, $b = 5.55$, $c = 7.97$ Å, $\alpha = 89°$, $\beta = 77°$, $\gamma = 87°$. Roth also found this phase from 1020°C to the melting point of 1245°C. He was able to index the X-ray powder pattern on the basis of the triclinic cell, and obtained the following dimensions:- $a = 7.611$, $b = 5.536$, $c = 7.919$ Å, $\alpha = 89.88°$, $\beta = 77.43°$, $\gamma = 87.15°$.

$4Bi_2O_3 \cdot 9Nb_2O_5$

A phase stable from 1070°C to the melting point of 1183°C was assigned this formula. The X-ray powder pattern was indexed on the basis of a hexagonal unit cell with $a = 6.447$ and $c = 19.778$ Å.

$Bi_2O_3 \cdot 5Nb_2O_5$

This compound was found to be stable from room temperature to a

dissociation temperature of 1095°C. The powder pattern was not indexed.

$Bi_2O_3 \cdot 6Nb_2O_5$

The 1:6 compound was found to be stable from 1002°C to the melting point of 1242°C. The X-ray powder pattern was thought to bear resemblance to the 1:5 compound, but was not indexed.

ABO_4 Compounds

$BiNbO_4$ may further be discussed in the context of $A^{III}B^{V}O_4$ compounds of some group V metals. Table 3.1 shows six such compounds, some of which appear twice, as the low temperature form and as the stable high temperature modification. The three structural types found in this group are also indicated.

The monoclinic structure, as exemplified by β-Sb_2O_4 was determined by Rogers and Skapski[I.1]. The cell has a = 12.060, b = 4.834, c = 5.383Å, β = 104°35'. The structure consists of Sb^{V}-O octahedra linked by corner sharing to form corrugated sheets. Adjacent sheets are linked by the Sb^{III} ions.

The structure of $SbNbO_4$, representative of the orthorhombic members of the group was determined by Skapski and Rogers[I.5]. The cell has a = 5.561, b = 4.939, c = 11.810 Å. The structure has many features in common with β-Sb_2O_4. It can in fact be derived from the latter by an

	Nb^V	Sb^V	Ta^V
Sb^{III}	$SbNbO_4$ (o-rh) a = 5.561 b = 4.939 c = 11.810 Ref. (I.5)	α-Sb_2O_4 (o-rh) a = 5.443 b = 11.787 c = 4.807 Ref. (I.6)	$SbTaO_4$ (o-rh) a = 4.927 b = 5.554 c = 11.81 Ref. (I.3)
	–	β-Sb_2O_4 (mon) a = 12.060 b = 4.834 c = 5.383 β = 104°35' Ref. (I.1)	–
Bi^{III}	$BiNbO_4$ (o-rh) a = 4.980 b = 11.709 c = 5.675 Ref. (I2)	–	$BiTaO_4$ (o-rh) a = 4.957 b = 11.763 c = 5.633 Ref. (I.3)
	$BiNbO_4$ (tric) a = 7.611 b = 5.536 c = 7.919 α = 89.88° β = 77.43° γ = 87.15° Ref. (I.2)	$BiSbO_4$ (mon) a = 5.464 b = 4.887 c = 11.81 β = 101.0° Ref. (I.4)	$BiTaO_4$ (tric) a = 7.652 b = 5.584 c = 7.772 α = 89.92° β = 77.12° γ = 86.45° Ref. (I.3)

Table 3.1 $A^{III}B^VO_4$ compounds - cell dimensions in Å

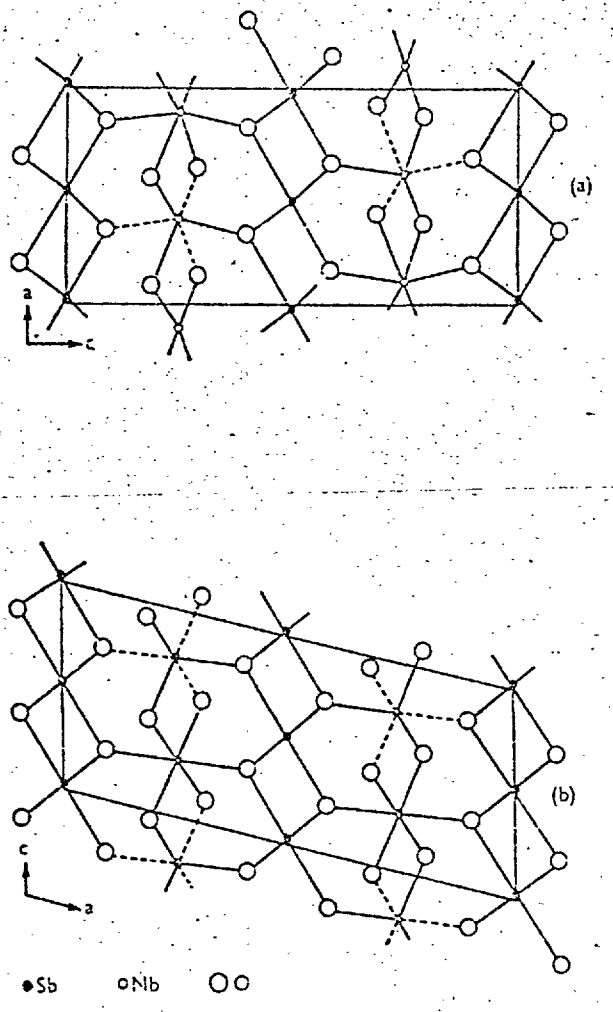


FIGURE 3.2 (a) [010] *Projection of* $SbNbO_4$.
(b) [010] *Projection of* β-Sb_2O_4 *(origin moved to facilitate comparison).*

(Dashed lines indicate bonds between niobium and oxygens in the cell below. The octahedra are joined at corners, not edges.)

alternative way of stacking the sheets of distorted octahedra. The similarity between the two structures is illustrated in Figure 3.2.

Aurivillius[I.4] showed from the Patterson projections, that triclinic $BiNbO_4$ and $BiTaO_4$ were isostructural, although he did not attempt to solve these structures.

Preparation of Compounds During the Study of the Bi_2O_3-Nb_2O_5 System

High purity Nb_2O_5 (Koch-Light Laboratories) and > 99°/o pure Bi_2O_3 (British Drug Houses) were used for all preparations in this group. The moisture contents of the two starting products were determined (negligible for Nb_2O_5, 0.25°/o for Bi_2O_3) and allowed for in the preparations.

About 0.1 mg of a mixture of the appropriate proportions were ground thoroughly in a small agate mortar. Short lengths of platinum tubing were boiled in concentrated nitric acid to remove the lubricant used in the extrusion of the tube, from the inside. The mixtures were sealed in the platinum tubes and fired at the temperatures listed below. The weights of the capsules were checked before and after heating to ensure that no loss occurred.

a) A 1:1 ratio of oxides was heated at 1150°C for 46 hours. The temperature chosen was mid-way between the transformation from the orthorhombic to the stable monoclinic form of $BiNbO_4$ at 1020°C and the melting point at 1245°C. The capsule was quenched in air. The product was crystalline, and was shown to consist of triclinic $BiNbO_4$. A suitable crystal was picked for structural studies.

b) 1;5 and 1:6 ratio mixtures were prepared and sealed in separate capsules. They were both fired for twenty hours at 1060°C. The temperature was a compromise, since $Bi_2O_3.5Nb_2O_5$ is stable from room temperature to 1095°C, and $Bi_2O_3.6Nb_2O_5$ from 1002°C to 1245°C. After quenching in air, only micro-crystalline products were found in each case.

c) A 1:6 ratio mixture was fired at 1200°C for 72 hours and was quenched. The product was partially crystalline. A Guinier photograph showed all the powder lines recorded by Roth for $Bi_2O_3.6Nb_2O_5$, plus some more, which could be explained by the presence of small quantities of various other phases, mainly triclinic $BiNbO_4$.

d) A 1:5 mixture was heated at 1080°C for 4 days and cooled over a period of one day to 700°C. The product was micro-crystalline, but its powder pattern agreed with that given by Roth for $Bi_2O_3.5Nb_2O_5$.

e) A 1:6 mixture was heated at 1230°C for 3 days and quenched. The product was crystalline, and contained single crystals of $Bi_2O_3.6Nb_2O_5$ as well as $4Bi_2O_3.9Nb_2O_5$.

f) A 4:9 mixture was heated at 1160°C for 3 days and quenched. The product was micro-crystalline. Its Guinier powder pattern showed it to consist of triclinic $BiNbO_4$, and to a less extent, the 4.9 compound.

g) A 7:33 ratio mixture was heated to 1060°C for 16 hours and cooled slowly. Guinier photographs and an XRD-6 diffractometer trace were taken of the powder produced. It was shown to consist mainly of the "1.5" compound plus some triclinic $BiNbO_4$.

4. The Crystal Structure of Triclinic $BiNbO_4$

Crystal Data

$BiNbO_4$, M = 365.9, Triclinic, a = 7.611, b = 5.536, c = 7.919 Å, $\alpha = 89.88^\circ$, $\beta = 77.43^\circ$, $\gamma = 87.15^\circ$,* U = 324.0 $Å^3$, D_m = 7.5 g.cm.$^{-3}$ (I.4), D_c = 7.3 g.cm.$^{-3}$ for Z = 4; F(000) = 752

Space Group $P\bar{1}$, (C_i^1, No.2)

For CuKα radiation μ = 1299 cm.$^{-1}$

* Note:- the triclinic cell chosen by both Aurivillius(I.4) and Roth is preserved.

Preliminary Examination

The crystals were pale yellow elongated prisms. The extinction direction between crossed polarisers showed no obvious relationship to the morphology.

All the crystals which were examined by oscillation and Weissenberg photographs were twinned in two ways. One of these appeared to be of the polysynthetic type. On the Weissenberg photographs the h0l and the hk0 reflections were doubled; the h00 line showed no doubling however. A similar description of the twinning was given by Aurivillius(I.4), who found that all crystals examined were twinned in these two ways.

After numerous attempts, a crystal plate was found which, although it twinned in the two aforementioned ways, gave otherwise clear and sharp reflections. An attempt was made to break this crystal up, with a view to decreasing the absorption errors of the plate. On exerting pressure under benzene with a sharp point, the original crystal cleaved easily along two parallel planes to give a rectangular prism.

An h0l Weissenberg photograph of this crystal showed no doubling of spots, but splitting occurred on a first layer photograph. On plotting out the first layer of the reciprocal lattice, (hl1), the angle between the twins was seen to be $\sim 6^{\circ}$, corresponding to the fact that $\gamma^{*} = 90 \pm 3^{\circ}$.

The twinning in $BiNbO_4$ is discussed more fully later.

It was clear that no single crystal of $BiNbO_4$ could be found, and due to the polysynthetic nature of the twinning, no absorption correction could be applied. It was therefore imperative to reduce absorption effects by choosing a crystal as small as possible, and with a favourable shape. Small crystal size was also dictated by the imperfections and macro-twinning of the larger ones. Due to the small crystal size $CuK\alpha$ radiation was chosen as opposed to $MoK\alpha$, otherwise exposures would have been unreasonably long. If a large enough "single" crystal free of macro-twinning could have been found, Mo radiation would have provided an effective means of reducing absorption errors.

The only crystal found, which was usable for intensity work was already too small for consideration of Mo radiation before it was split. After splitting, the crystal was a prism with a rectangular base, and approximately 0.006cm x 0.0025cm x 0.0010cm in size. This small crystal required exposures of up to two weeks, which proved quite practicable.

Unit Cell

The unit-cell dimensions obtained from Weissenberg and oscillation photographs were in agreement with those quoted by previous workers. Roth's values for the unit cell were adopted throughout, since these were more accurate than any obtainable from photographs, having been calculated from a high-resolution diffractometer powder diagram.

Data Collection

Single-crystal intensity data were collected photographically, using the equiinclination Weissenberg technique to register layers h0l to h5l with CuKα radiation. A total of 662 reflections were estimated visually. An attempt was made to use a Joyce-Loebl integrating microdensitometer, but the reflections were found to be too small and sharp for correct measurement, and visual estimation proved superior.

The Structure in Projection

The structure was solved from the h0l data with the aid of a model, while the full three-dimensional data were being collected, since this took rather a long time. The Patterson map of the ac projection shown in Figure 4.1 was calculated initially using the Boss program on Atlas.

The subsequent Fourier calculations were also completed using Boss. The scattering factors used were for Bi^{+}, Nb^{3+} and O^{-}, as a compromise between a purely ionic and a purely covalent compound. Scattering factors for Bi^{+} were obtained by interpolating between those for Bi and Bi^{3+} given by Cromer et al(I.7). Those for Nb^{3+} were calculated by applying the differences between Nb^{3+} and Nb given by Thomas and Umeda(I.8) to values for Nb tabulated by Cromer et al(I.7). Scattering factors for O^{-} were taken from International Tables(I.9). The real parts of the anomalous dispersion correction were included for bismuth and niobium.

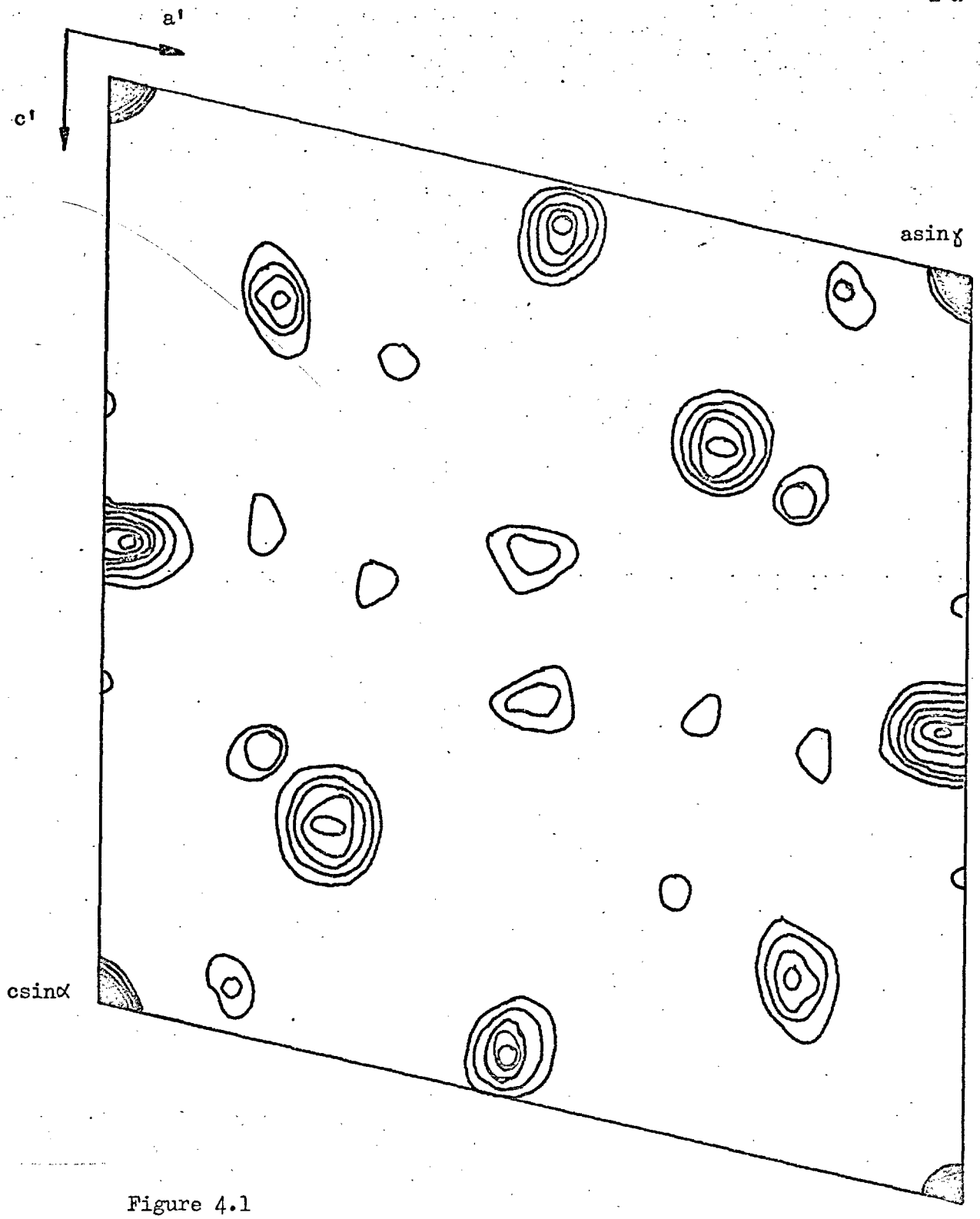


Figure 4.1

Triclinic $BiNbO_4$ - [010] Patterson projection

Due to the heavy nature of bismuth and the relatively small number of reflections, no statistical test was attempted to find out whether the structure was centrosymmetric or not. Piezo and pyro-electric tests were judged to be dubious in view of the known twinning. Thus it was decided to treat the space group as P1 until it could be shown otherwise.

Primarily the determination of the bismuth positions was attempted, as phasing on these was likely to show the niobium atoms on a Fourier map, and the combination of all the heavy atoms, it was hoped, would determine the oxygen positions.

It was clear from looking at the photographs that festoons of even l index were very strong compared with those of odd l. This indicated a halving of the unit cell, which would approximately repeat the contents of volume A in Figure 4.2 in B.

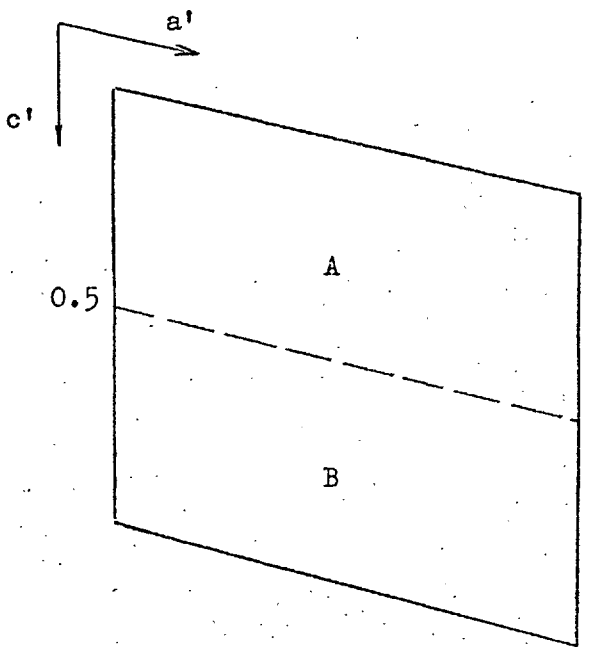


Figure 4.2

This was also borne out by the large peak in the Patterson (Figure 4.1) at u,w = ±0.05,0.5 and the recurrence of these vectors elsewhere on the map.

The initial Fourier calculation was completed with a bismuth at the origin and one at 0.05 in a and 0.5 in c. An R factor of 0.33 was obtained, but the two heavy-atom positions specified effectively halved the cell along c, introduced a false centre of symmetry and represented too small a proportion of the scattering material to dominate the phases. Hence no new peaks could be clearly seen. The approach then adopted was to place a bismuth or a niobium atom at points corresponding to each of the other major peaks in the Patterson. Many permutations were tried, but progress only began when the initial "symmetry" of halving along c was deliberately broken, by inputting three (A, B and C in Figure 4.3) of what later turned out to be the four bismuth positions. The heavy atoms were then identified as bismuth or niobium, and the arrangement corresponding to Figure 4.3 was obtained. The positions corresponded to a centrosymmetric projection, and the heavy atoms were refined in space group $P\bar{1}$. For the purposes of least-squares refinement, the computation was transferred to X-ray 63, where the full-matrix refinement program in the ORFLS link was used. The heavy atoms refined to an R value of 0.15.

The eight oxygen atoms in the asymmetric unit could be seen in a partial difference synthesis, $F_{obs}-F_{Bi+Nb}$. Figure 4.4 shows this

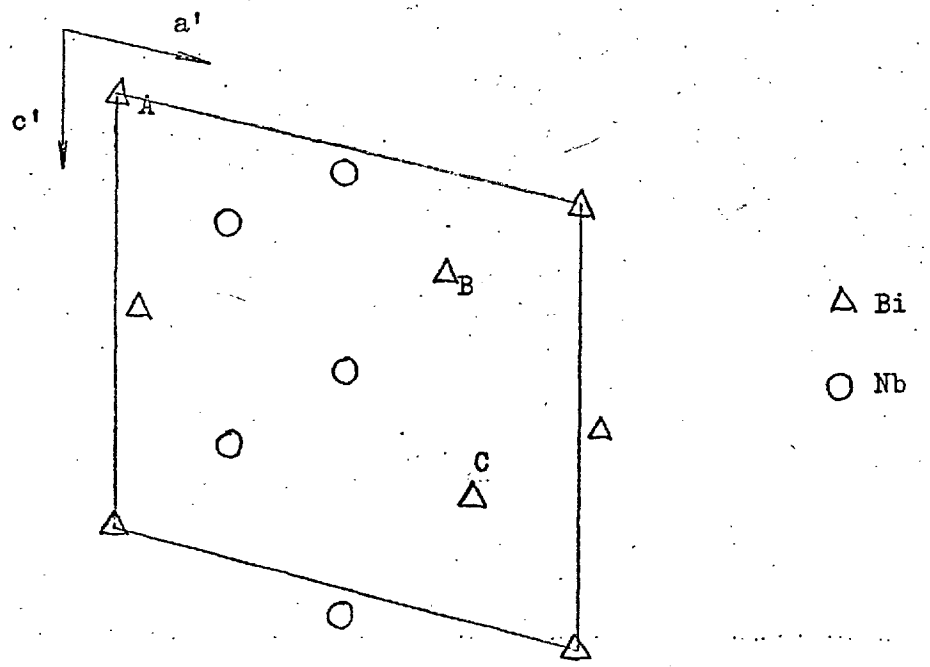


Figure 4.3

synthesis, together with the final, refined positions of the oxygen atoms.

Further refinement was continued until shifts in positional and thermal parameters were less than one fifth of a standard deviation. A weighting scheme of the type recommended by Hughes[I.10] was used in refinement, with $F^{*} = 60$. The agreement factor, R, fell to 0.091. The two-dimensional positions and temperature factors with standard deviations are shown in Table 4.1. The negative temperature factors are caused by absorption errors, which could not be corrected for.

A final Fourier synthesis and error synthesis were calculated. The latter showed no peaks higher than the equivalent of 1/3 of an oxygen.

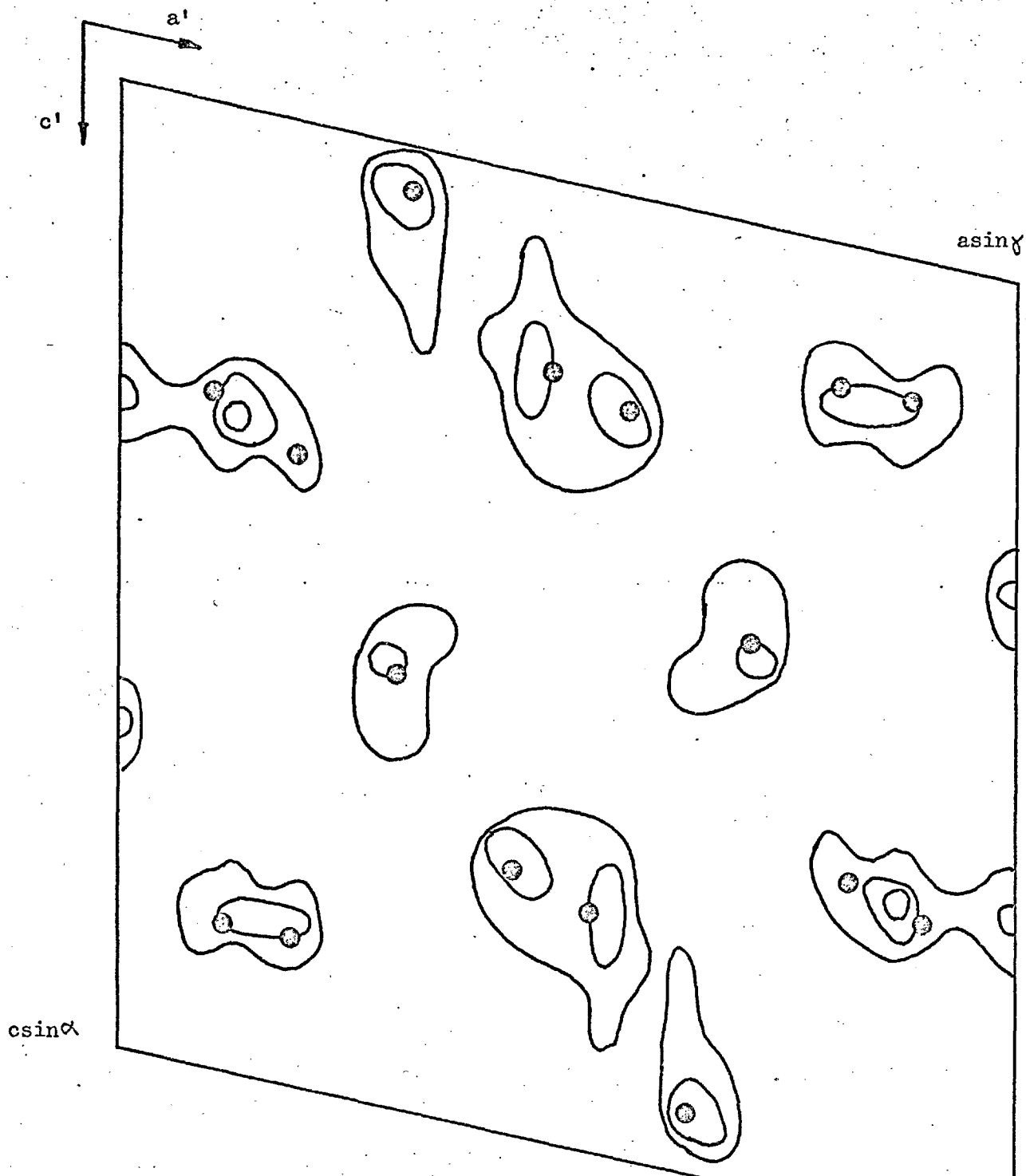


Figure 4.4

[010] Difference Fourier, $F_{obs} - F_{Bi+Nb}$, Synthesis

⊙ Final oxygen positions

Table 4.1

Triclinic $BiNbO_4$ - Final Positional Parameters and Temperature Factors - 2D Refinement

Atom	x	σ(x)	z	σ(z)	B	σ(B)
Bi(1)	0.1227	0.0008	0.6274	0.0009	-0.53	0.18
Bi(2)	0.8333	0.0009	0.8736	0.0011	-0.14	0.19
Nb(1)	0.655	0.002	0.678	0.002	-0.06	0.35
Nb(2)	0.322	0.002	0.821	0.002	-0.42	0.33
O(1)	0.310	0.007	0.050	0.008	-3.5	1.1
O(2)	0.100	0.010	0.307	0.015	-1.3	2.2
O(3)	0.185	0.015	0.361	0.020	0.4	3.3
O(4)	0.307	0.008	0.556	0.010	-2.9	1.4
O(5)	0.104	0.008	0.828	0.009	-3.5	1.2
O(6)	0.188	0.009	0.836	0.010	-3.3	1.3
O(7)	0.547	0.008	0.273	0.010	-2.8	1.5
O(8)	0.460	0.010	0.259	0.011	-3.0	1.3

Determination of the Three-Dimensional Structure

At this stage a model was made using the two-dimensional co-ordinates. Assuming an octahedral arrangement of oxygens about each niobium, and Nb-O distances of about 2 Å, there was only one satisfactory way of arranging the atoms due to the relatively short (5.5Å) repeat in the b direction. This involved placing the heavy atoms at heights of about $\frac{1}{4}$ and $\frac{3}{4}$, and joining octahedra by corners. A centre of symmetry was assumed.

The full data contained 662 independent reflections, which were used to calculate a three-dimensional Patterson map using X-ray 63. All large peaks were at $v \simeq 0$ or $\frac{1}{2}$, thus confirming the approximate heavy-atom co-ordinates deduced from the model. Least-squares refinement in three dimensions was then carried out on the heavy-atom positions, followed by a difference Fourier map on which the oxygens could be seen. The full contents of the unit cell were then put into a full-matrix least-squares program. Inter-layer scaling had only been approximate previously, deduced from exposure times. In order to correct this and to allow for spot-shape distortion separate scale-factors were used as parameters in refinement for the upper and lower halves of films. With isotropic temperature factors the total number of parameters was 57. Some 20 reflections were removed from refinement, as they were thought to suffer from extinction, leaving a total of 642.

Refinement was continued until shifts in positional and thermal parameters were less than 0.1 of a standard deviation, the agreement factor, R, falling to 0.122. As with the two-dimensional refinement, a weighting scheme of the type recommended by Hughes was used, initially with $F^* = 60$. A weighting scheme analysis showed, however, that F^* should be increased. A refinement using weights w, where

$\sqrt{w} = F^*/F$ for $F>F^*$ and $w = 1$ for $F<F^*$, with $F^* = 90$

gave no reduction in R, but did improve the standard deviations significantly.

Table 4.2 shows the final atomic positional parameters and temperature factors with their standard deviations. The negative temperature factors are caused by absorption. Their internal consistency is a better measure of their validity than their absolute values if one takes into account the appropriate standard deviations. Orthogonalised co-ordinates in Å are given in Table 4.4.

Table 4.3 lists the observed structure amplitudes and calculated structure factors. Those marked with an e were thought to be suffering from extinction and were removed from refinement. Unobserved reflections are labelled with an asterisk. They were not included in the least-squares refinement. It was intended to include these in the structure factor list at a value of F corresponding to $I_t/2$, where I_t is the observable threshold. Due to an error in the estimation of I_t, the entry under F_{obs} for these reflections should be taken as $F_t/2$ (i.e. $I_t/4$).

Structure factors are on a ten times absolute scale in Table 4.3.

Table 4.2

Triclinic $BiNbO_4$ - Final Positional Parameters, Temperature Factors and their Standard Deviations

Atom	x	σ(x)	y	σ(y)	z	σ(z)	B Å^2	σ(B)
Bi(1)	0.1215	0.0004	0.7644	0.0006	0.6272	0.0004	-0.01	0.08
Bi(2)	0.8335	0.0004	0.2820	0.0007	0.8745	0.0004	0.04	0.08
Nb(1)	0.6556	0.0009	0.7752	0.0015	0.6784	0.0008	0.34	0.12
Nb(2)	0.3243	0.0009	0.7752	0.0015	0.8228	0.0008	0.06	0.12
O(1)	0.325	0.004	0.292	0.007	0.471	0.004	-2.2	0.5
O(2)	0.106	0.007	0.988	0.011	0.320	0.006	-0.2	0.8
O(3)	0.167	0.008	0.464	0.013	0.360	0.008	0.8	1.1
O(4)	0.312	0.006	0.167	0.009	0.551	0.005	-0.9	0.7
O(5)	0.108	0.009	0.439	0.014	0.822	0.008	1.0	1.1
O(6)	0.169	0.007	0.973	0.011	0.863	0.006	-0.2	0.8
O(7)	0.448	0.007	0.918	0.011	0.226	0.006	-0.3	0.8
O(8)	0.540	0.009	0.449	0.014	0.278	0.008	1.4	1.3

Table 4.3

Triclinic $BiNbO_4$- Observed Structure Amplitudes and Calculated Structure Factors

Tabulated as:

h $|F_o|$ F_c

e indicates a reflection affected by extinction and omitted from least-squares refinement

* indicates a reflection too weak to be observed

H,0,6

1	666	1173
2	1036	-1376
3	1130	-1289
4	2062	-2672
5	1026	-1006
6	1844	1925
7	930	791
8	146*	-23
9	584	608

H,0,-1

0	51*	21
1	73*	-57
2	693	-853
3	684	-785
4	443	-494
5	622	626
6	1602	1925
7	1000	1006
8	728	-596
9	810	-1030

H,0,-2

0	1329	-1152
1	1493	1544
2	1890c	2969
3	437	544
4	1102	-1079
5	716	-678
6	1428	-1408
7	51*	-170
8	1304	1070
9	51*	77

H,0,3

0	89*	40

H,0,-3

1	351	329
2	637	563
3	475	-401
4	1160	-1337
5	855	-955
6	164*	-167
7	908	987
8	1657	1854

H,0,-4

0	2262	-2845
1	563	-517
2	137*	-54
3	1385	1755
4	1821c	2737
5	609	-489
6	1235	-1027
7	127*	-275

H,0,-5

0	137*	-50
1	146*	119
2	347	470
3	753	826
4	553	594
5	845	-813
6	1411	-1511
7	563	-614

H,0,-6

0	1152	1018
1	1770	-1944
2	1498c	-2165
3	164*	-191
4	155*	-78
5	1273	1146
6	1230	1319

H,0,-7

0	164*	-33
1	366	-360
2	401	-386
3	359	410
4	811	869
5	682	831

H,0,-8

0	765	1104
1	936	1245
2	237	265
3	1885	-2211
4	779	-1007

H,0,1

1	463	-367
2	446	-385
3	103*	173
4	1197	1517
5	984	1262
6	200	-146
7	930	-960
8	1496	-1675
9	1166	-1037

H,0,2

1	878	-909
2	2110c	-2975
3	1062	-1181
4	1540	1954
5	1165	1231
6	760	745
7	722	565
8	1057	-951
9	1270	-849

H,0,3

1	89*	8
2	815	756
3	1034	1007
4	127*	78
5	656	-613
6	1396	-1565
7	1211	-1441
8	735	683
9	1472	1530

H,0,4

1	2500	-2947
2	1657	1753
3	1772	1961
4	1029	934
5	1328	1273
6	1064	-1150
7	1443	-1649
8	207	183
9	179	247

H,0,5

1	137*	233
2	137*	206
3	146*	-236
4	960	-1041
5	1182	-1292
6	164*	163
7	1150	1252
8	1108	1251
9	898	985

H,0,6

1	1616	1670
2	1300	1405
3	1574	1499
4	1011	-1101
5	1723	-2177
6	164*	-194
7	207	-280
8	115*	246

H,0,7

1	164*	-15
2	366	-449
3	930	-857
4	164*	-139
5	783	849
6	887	1085
7	950	1073
8	89*	-170

H,0,8

1	1491	1756
2	311	-396
3	1632c	-2368
4	709	-871
5	146*	84
6	127*	223
7	1334	1523

H,0,9

1	137*	-182
2	164*	-52
3	220	289
4	688	687
5	790	947
6	89*	23

H,1,0

-3	680	-765
-2	1412c	-3804
0	81*	-0
1	525	784
2	2196c	3979
3	1329	1424
4	1748	-2178
5	1109	-958
6	1353	-1234
7	1017	-749
8	1577	1359
9	994	863

H,1,-1

9	740	843
8	1487	1606
7	729	637
6	257*	-123
5	564	-544
4	1150	-1130
3	163*	-69
2	115*	199
1	115*	16
0	468	-373
-1	81*	52
-2	1151	1265
-3	598	670

H,1,-2

8	949	-658
7	762	-721
6	1406	-1407
5	230*	363
4	1909c	2831
3	1251	1335
2	627	419
1	968	-995
0	2435c	-3896
-1	1580	-1504
-2	1593	1567
-3	1378	1293
-4	1528	1676

H,1,-3

7	949	-1015
6	1600	-1560
5	515	-599
4	461	495
3	431	512
2	364	467
1	163*	-71
0	364	277
-1	1406	1072
-2	461	410
-3	182*	-124
-4	1740	-1909
-5	1357	-1634
-6	257*	157

H,1,-4

7	182*	-90
6	1609	1873
5	1092	950
4	244*	463
3	230*	5
2	2152c	-3110
1	1754	-2121
0	1592	1511
-1	1230	1127
-2	1692	1990
-3	1725	1726
-4	1646	-1653
-5	1556	-1792
-6	244*	24

H,1,-5

7	732	-807
6	199*	434
5	721	783
4	623	669
3	257*	351
2	244*	-205
1	230*	-244
0	215*	80
-1	215*	-217
-2	906	-811
-3	1276	-1133
-4	423	354
-5	692	655

H,1,-6

6	546	599
5	199*	125
4	1651	-2082
3	1350	-1804
2	686	430
1	691	927
0	1564	1937
-1	1768	2002
-2	1236	-1357
-3	1520	-1823
-4	576	-614
-5	631	-723

H,1,-7

5	528	565
4	469	-484
3	461	-499
2	244*	-170
1	257*	79
0	257*	-146
-1	515	-513
-2	446	-486
-3	364	380
-4	729	948
-5	1439	1420
-6	230*	-16

H,1,-8

4	115*	250
3	182*	510
2	1205	1323
1	1550	2059
0	244*	-540
-1	1636	-2102
-2	244*	-835
-3	909	-840
-4	230*	388
-5	1213	1959
-6	182*	465

H,1,-9

2	141*	28
1	141*	15
0	182*	147
-1	199*	124
-2	199*	656
-3	864	916
-4	182*	54
-5	713	-1174

H,1,1

9	1480	-1279
8	253*	-327
7	1594	1337
6	1563	1673
5	237*	371
4	200*	-283
3	1114	-1200
2	126*	-276
1	89*	-14
0	89*	-335
-1	126*	-652
-2	696	-767
-3	690	613
-4	1318e	1940

H,1,2

-4	1357e	-2313
-3	1173	-1312
-2	563	-511
-1	541	584
0	2236e	3777
1	1930	1999
2	1332	-1437
3	1494	-1554
4	1293	-1918
5	1275	-1332
6	1471	1752
7	1124	1352

H,1,3

-4	269*	-620
-3	929	-996
-2	931	-932
-1	179*	-275
0	179*	201
1	566	466
2	179*	-26
3	200*	340
4	797	834
5	1041	1042
6	269*	-470
7	954	-948
8	1061	-1183
9	1196	-1096

H,1,4

-4	283*	-300
-3	253*	-311
-2	2169	2718
-1	1864	2387
0	1278	-1266
1	1214	-1232
2	1589	-1964
3	1644	-2107
4	1460	1481
5	2031	2354
6	283*	311
7	283*	454
8	253*	-496
9	1478	-1381

H,1,5

-4	1336	-1322
-3	283*	-655
-2	900	771
-1	611	573
0	237*	147
1	237*	-236
2	237*	254
3	688	581
4	253*	506
5	269*	-470
6	1088	-1118
7	1364	-1247
8	219*	180
9	1283	1440

H,1,6

-4	1358	1532
-3	1587	1737
-2	283*	-276
-1	674	-738
0	1455	-1794
1	1860	-2253
2	1204	1098
3	1843	2136
4	960	954
5	957	826
6	269*	-720
7	1784	-1990
8	200*	-161
9	89*	365

H,1,7

-2	269*	588
-1	283*	321
0	283*	-188
1	283*	19
2	283*	-203
3	283*	-284
4	283*	-688
5	938	-930
6	253*	56
7	1309	1317
8	1068	1118

H,1,8

-2	822	-1008
-1	1604	-2138
0	253*	212
1	2021	2131
2	857	1006
3	910	985
4	253*	-285
5	1726	-2211
6	912	-871
7	687	529

H,1,9

0	179*	-95
1	219*	132
2	219*	-15
3	200*	-412
4	200*	-158
5	179*	442
6	639	769

H,2,0

1	746	-1192
2	1140	1420
3	786	749
4	1847	2338
5	1298	1199
6	1794	-1931
7	1128	-1140
8	223*	-353

H,2,-1

8	206*	349
7	997	-888
6	1333	-1390
5	239*	-263
4	206*	357
3	169*	279
1	482	416
0	504	522
-1	1091	951
-2	752	630
-3	582	-518

H,2,-2

8	1750	-1421
7	329	426
6	1601	1877
5	1034	1186
4	1172	1236
3	704	-895
2	2303e	-3951
1	1301	-1456
0	841	646
-1	1411	1492
-2	2478	2826
-3	1246	1081
-4	1802	-1784

H,2,-3

8	756	-1401
7	630	-570
6	253*	138
5	253*	633
4	676	756
3	223*	-160
2	188*	121
1	169*	218
0	590	423
-1	169*	-125
-2	1225	-1212
-3	1509	-1443
-4	206*	1

H,2,-4

7	169*	500
6	1110	1009
5	253*	-62
4	1689e	-2632
3	1106	-1276
2	760	663
1	206*	437
0	2053	2553
-1	1572	1545
-2	1742	-1811
-3	1582	-1315
-4	573	-510
-5	970	-876

H,2,-5

6	960	962
5	239*	596
4	253*	-423
3	253*	-234
2	253*	7
1	239*	104
0	833	-814
-1	956	-793
-2	223*	-232
-3	239*	363
-4	1476	1631
-5	1480	1591

H,2,-6

5	1617	-1382
4	239*	-256
3	239*	320
2	1699	2295
1	1764	2118
0	1133	-1079
-1	1355	-1355
-2	1200	-1270
-3	1412	-1261
-4	1157	1142
-5	1374	1475
-6	239*	-135

H,2,-7

4	188*	-459
3	223*	-228

H,2,-7

2	239*	207
1	253*	-260
0	253*	-189
-1	253*	203
-2	846	844
-3	1104	1196
-4	253*	-11
-5	794	-1080
-6	970	-1358

H,2,-8

3	1604	1875
2	606	-620
1	1134	-1410
0	753	-1029
-1	1407	-1457
-2	699	677
-3	1645	2017
-4	223*	380
-5	188*	102

H,2,-9

2	84*	61
1	146*	-123
0	164*	369
-1	758	848
-2	188*	155
-3	492	-657
-4	653	-860

H,2,1

9	1184	986
8	1207	1247
7	876	847
6	248*	-60
5	888	-829
4	467	-505
3	165*	-139
2	116*	-73
1	352	-388
-1	116*	-9
-2	1439	1709
-3	1023	1077

H,2,2

9	1493	1256
8	1404	1183
7	1026	-827
6	906	-909
5	1418	-1739
4	1390	-1701
3	1549	2167
2	1969e	3099
1	982	1001
0	116*	81
-1	1928	-1994
-2	2493	-3134
-3	202*	217
-4	1149	1007

H,2,3

9	1242	-1308
8	218*	-307
7	1121	1177
6	1036	1062
5	233*	113
4	202*	-50
3	184*	-255
2	184*	-145
1	165*	85
0	573	-508
-1	827	-910
-2	992	-902
-3	1029	954
-4	1393	1646
-5	938	946
-6	233*	165

H,2,4

9	143*	-87
8	218*	182
7	1798	2214
6	970	985
5	1079	-1279
4	1026	-1132
3	1637	-2034
2	1528	-1513
1	1983	2363
0	2165	2259
-1	202*	271
-2	930	640
-3	1385	-1391
-4	1536	-1814

H,2,5

8	1177	-1242
7	736	-796
6	248*	-10
5	731	752
4	589	490
3	233*	200
2	218*	-46
1	645	423
0	549	649
-1	746	-550
-2	907	-892
-3	1110	-1111

H,2,6

7	218*	-34
6	233*	659
5	1730	2391
4	734	885
3	1555	-1799
2	1216	-1354
1	1443	-1443
0	348	-463
-1	2034	2270
-2	1393	1477
-3	233*	-138
-4	248*	-272

H,2,7

8	116*	-7
7	963	-902
6	218*	-538
5	233*	-520
4	248*	110
3	248*	245
2	248*	-104
1	248*	-76
0	248*	412
-1	928	1011
-2	523	459
-3	640	-611
-4	1046	-1138

H,2,8

6	165*	-210
5	202*	241
4	759	1041
3	1766	2442
2	233*	95
1	1407	-1665
0	775	-993
-1	986	-1285
-2	233*	-169
-3	1522	1797

H,3,0

-3	184*	82
-2	2343	2803
-1	1067	1120
1	299	-413
0	82*	98
2	1763e	-3396
3	1374	-1541
4	1316	1471
5	1312	1336
6	1245	1296
7	999	1015
8	1598	-1492

H,3,1

8	184*	191
7	617	-677
6	576	-655
5	385	-372
4	202*	-68
3	164*	-71
2	348	-470
1	82*	151
0	1267	1167
-1	1018	907
-2	816	778
-3	687	-580
-4	2049	-2108

H,3,2

9	116*	-234
8	184*	-306
-1	164*	-166
7	1768	-1926
6	1423	-1455
5	1341	1421
4	1298	1907
3	1034	1268
2	1196	1395
1	1839	-2110
0	2357	-2680
-2	184*	236
-3	1053	886
-4	1765	1534

H,3,3

7	218*	420
6	233*	-48
5	646	-716
4	202*	-322
3	164*	344
2	164*	-64
1	799	-767
0	893	-762
-1	686	565
-2	1274	1211
-3	1251	1239
-4	749	614
-5	1547	-1398

H,3,4

8	184*	654
7	218*	-487
6	233*	-698
5	1551	-2239
4	1123	-1217
3	1653	2245
2	1268	1515
1	1223	1086
0	804	577
-1	2031	-2026
-2	1857	-1855
-3	620	515
-4	233*	206
-5	233*	336

H,3,5

7	485	672
6	699	766
5	466	387
4	233*	-19
3	233*	221
2	202*	224
1	690	-447
0	636	-526
-1	1023	-1119
-2	848	-808
-3	1040	1012
-4	1292	1559

H,3,6

7	1680	2166
6	494	535
5	720	-919
4	660	-997
3	1752	-2253
2	665	-503
1	1886	2045
0	1289	1434
-1	618	531
-2	233*	250
-3	1422	-1475
-4	999	-1009

H,3,7

6	184*	245
5	451	486
4	218*	-83
3	218*	-170
2	233*	215
1	641	730
0	233*	525
-1	218*	-162
-2	772	-971

H,3,8

5	1760	2305
4	184*	65
3	826	-963
2	822	-1065
1	1457	-1715
0	184*	-37
-1	1477	1869
-2	116*	523

H,3,-1

8	1430	-1447
7	213*	-358

H,3,-1

6	228*	248
5	388	473
4	733	458
3	120*	112
2	197*	-29
1	571	618
0	857	906
-1	620	-499
-2	1801	-1914
-3	1143	-1264
-4	213*	-225

H,3,-2

6	1554	1676
5	872	-837
4	1839	-2590
3	801	-1073
2	161*	-211
1	760	862
0	2115e	3017
-1	987	813
-2	1858	-1500
-3	573	-534
-4	1238	-1157

H,3,-3

6	796	744
5	228*	58
4	228*	13
3	213*	3
2	508	156
1	180*	85
0	973	-904
-1	1103	-1046
-2	180*	-215
-3	703	593
-4	1454	1691
-5	1275	1377

H,3,-4

6	2070	-2176
5	720	-969
4	228*	-534
3	228*	495
2	2111e	2952
1	1315	1472
0	1315	-1213
-1	1047	-980
-2	1601	-1429
-3	1497	-1270
-4	1533	1448
-5	856	838

H,3,-5

5	197*	-440
4	213*	-161
3	228*	-88
2	228*	-314
1	448	-394
0	536	-541
-1	213*	-29
-2	1428	1634
-3	1464	1563
-4	228*	-125
-5	801	-977

H,3,-6

5	139*	-44
4	2005	2251
3	1402	1524
2	559	-702
1	559	-788
0	1439	-1747
-1	1273	-1363
-2	1257	1263
-3	1208	1450
-4	228*	142

H,3,-7

4	139*	263
3	180*	-68
2	197*	-36
1	213*	152
0	213*	600
-1	769	931
-2	228*	85
-3	484	-793
-4	1183	-1356
-5	1071	-1152
-6	161*	414

H,3,-8

2	1044	-1424
1	1284	-1814
0	726	844
-1	1176	1551

H,4,0

-3	634	-499
-2	953	-942
-1	88*	19
1	854e	1650
2	601	-642
3	759	-870
4	1697	-2341
5	1420	-1445
6	1632	1588
7	1441	1435

H,4,1

7	139*	-346
6	152*	146
5	500	340
4	139*	-182
3	124*	77
2	384	483
1	440	568
0	688	1031
-1	757	-646
-2	1614	-1765
-3	1017	-1138
-4	164*	-113

H,4,2

-5	152*	102
7	1090	903
6	884	900
5	1491	1791
4	1151	1392
3	1240	-1899
2	1355	-2005
1	481	-568
0	329	-568
-1	1256	1238
-2	1529	1879
-3	575	-271
-4	466	-351

H,4,3

7	787	-836
6	440	-396
5	152*	-65
4	152*	-139
3	455	-486
2	465	-382
1	259	263
0	871	770
-1	1304	1487
-2	771	743
-3	1230	-1108
-4	1645	-1826
-5	820	-812

H,4,4

7	2152	-2290
6	811	-870
5	1158	1391
4	989	1170
3	1339	1664
2	718	689
1	1856	-2255
0	1589	-1593
-1	152*	109
-2	164*	-47
-3	1354	1073
-4	1168	1065
-5	827	-658

H,4,5

6	335	-190
5	152*	45
4	164*	-34
3	164*	51
2	164*	-153
1	1082	-1061
0	854	-803
-1	874	696
-2	1076	1182
-3	862	1026
-4	648	702

H,4,6

6	808	-974
5	2044	-2310
4	373	-381
3	1491	1530
2	1050	1084
1	1444	1358
0	461	368
-1	1726	-1789
-2	886	-924
-3	107*	46

H,4,7

5	107*	134
4	124*	163
3	124*	176
2	438	389
1	139*	-36
0	769	-779
-1	1042	-1253
-2	264	-424

H,4,8

3	1294	-2087
2	303	125
1	1089	1547
0	337	604

H,4,-1

7	600	393
6	632	697
5	165*	40
4	153*	-103
3	529	505
2	476	570
1	88*	-188
0	1052	-1202
-1	967	-927
-2	963	-952
-3	789	825

H,4,-2

7	960	-770
6	1504	-1669
5	832	-859
4	1105	-1025
3	590	841
2	1852e	2790
1	481	497
0	711	-603
-1	547	-473
-2	1600	-1711
-3	504	-417
-4	1013	1151

H,4,-3

6	125*	-65
5	153*	-328
4	165*	-28
3	153*	26
2	418	-526
1	816	-874
0	435	-347
-1	139*	212
-2	1777	1870
-3	1215	1429
-4	432	-197
-5	744	-1119

H,4,-4

5	380	466
4	2411	2649
3	970	1247
2	419	-392
1	695	-750
0	1815	-2306
-1	1060	-1089
-2	1430	1450
-3	717	740
-4	392	360
-5	527	582

H,4,-5

5	108*	-219
4	139*	29
3	153*	2
2	646	-583
1	165*	44
0	895	1085
-1	958	1052
-2	165*	68
-3	391	-420

H,4,-5		
-4	1263	-1736
-5	1144	-1487

H,4,-6		
2	1471	-1964
1	1324	-1334
0	1358	1228
-1	920	954
-2	498	632
-3	855	873
-4	926	-845
-5	831	-839

H,4,-7		
1	610	735
0	139*	426
-1	139*	-439
-2	953	-1245
-3	1045	-1388
-4	125*	67

Table 4.4 - Triclinic $BiNbO_4$, Orthogonal Co-ordinates in Å

(Right-Handed System of Orthogonal Axes, X,Y,Z; X is parallel to a, Y is perpendicular to a in the plane of a and c, Z is perpendicular to X and Y.)

Atom	X	Y	Z
Bi(1)	2.302	4.221	4.787
Bi(2)	7.965	1.557	6.735
Nb(1)	6.460	4.281	5.182
Nb(2)	3.988	1.364	6.339
O(1)	2.664	1.612	0.341
O(2)	1.740	5.457	2.391
O(3)	2.074	2.562	2.743
O(4)	3.392	0.922	4.241
O(5)	2.415	2.424	6.321
O(6)	3.150	5.373	6.591
O(7)	4.147	5.070	1.673
O(8)	4.761	2.479	2.113

Choice of Space-Group

It can be stated with reasonable certainty that the heavy-atom arrangement is centrosymmetric, since this was not assumed initially, but was shown to be the case on refinement. It is likely that the oxygen atoms are also in centrosymmetric positions. Points in favour of this view are the ease of refinement of oxygen atoms, the appearence of the difference Fourier syntheses and the final Fourier maps. It must be noted however, that when heavy atoms are centrosymmetrically related there is a tendency for non-existent light atoms to appear in positions related by this symmetry to actual light atoms. This phenomenon, called "inverse overlap" is discussed in detail by Geller(I.11) and Rae and Maslen(I.12). It is thus impossible to tell with certainty whether the complete structure is centrosymmetric or only nearly so. As statistical tests for the recognition of centrosymmetric structures(I.13) are unreliable in the presence of a few heavy atoms, or for a relatively small number of reflections or near-centrosymmetric structures, they were not tried.

An attempt was made to refine the structure in the space group P1. There was no improvement in agreement or standard deviations. Atoms refined to positions very close to the centrosymmetric ones. The imaginary part of the structure factor had negligible effect on the calculated F-s.

This was thought to indicate that the correct space group is $P\bar{1}$, but it cannot be regarded as rigorously proved.

5. Discussion of the Structure of Triclinic $BiNbO_4$

Description of the Structure

Figures 5.1 and 5.2 show that the structure contains puckered sheets in the bc plane consisting of Nb-O octahedra, each being joined by corners to four others. Each sheet has the composition $(NbO_4)_n$, and can be derived by taking a diagonal slice of an ReO_3-type structure (parallel to (110) of the ReO_3 unit cell), Figure 5.3(a) and (a'), separating these sheets of octahedra, Figure 5.3(b) and (b'), and sidestepping them to permit more economical packing - Figure 5.3(c) and (c'). The voids in this framework are then filled with bismuth atoms - Figure 5.3(d) and (d').

This type of octahedral sheet had not previously been reported, nor has the mode of co-ordination in which two free vertices on each octahedron are adjacent (or cis). The only other way of joining octahedra at four vertices to form a sheet of composition $(AX_4)_n$ makes the two free vertices trans, and is found in many compounds, e.g. $SbNbO_4$ (I.5). Comparison may also be made with sheets two octahedra thick found in $Sr_3Ti_2O_7$ (I.14) and Bi_3NbTiO_9 (I.15), (as perovskite units).

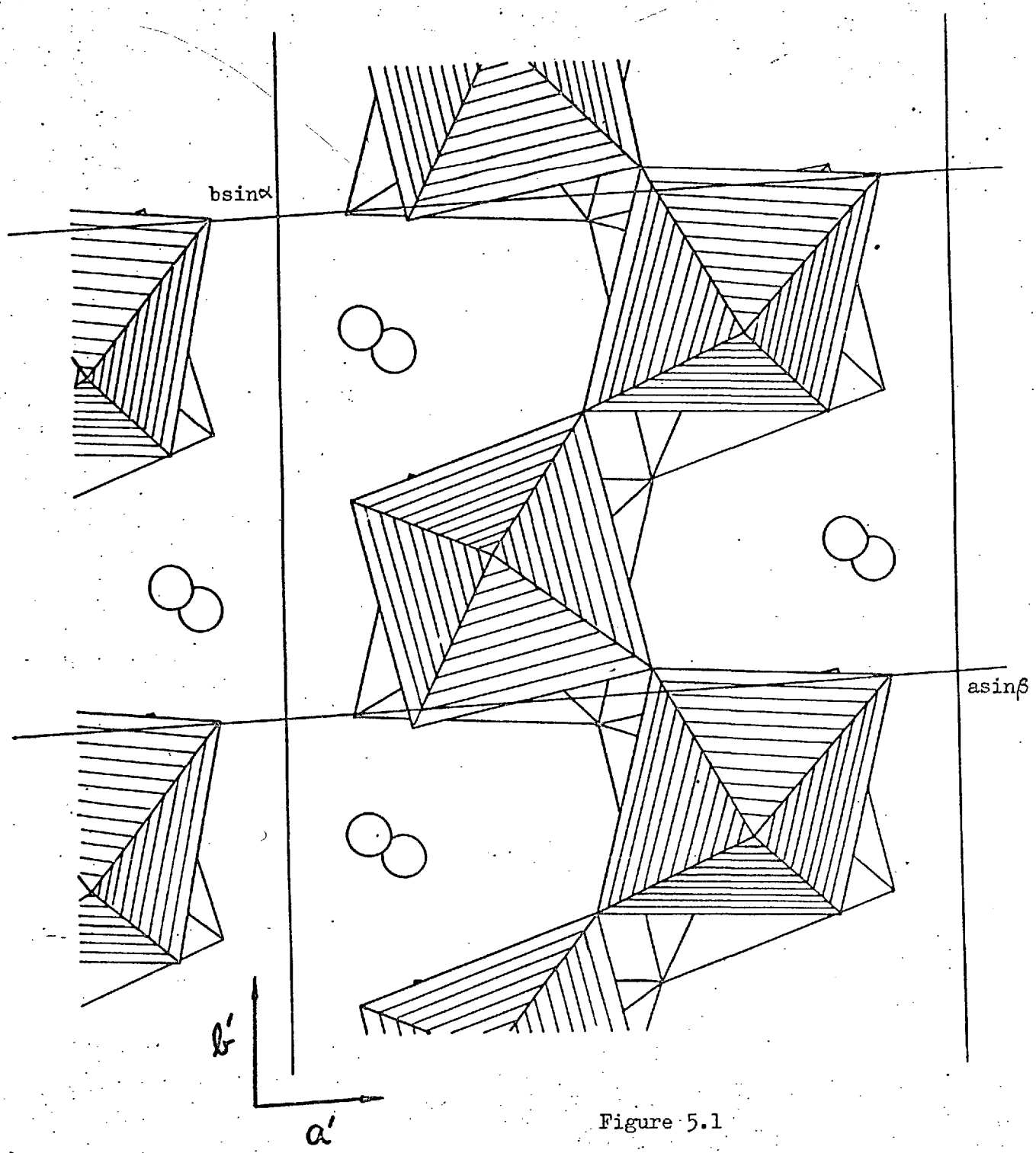


Figure 5.1

[001] projection of the triclinic $BiNbO_4$ structure

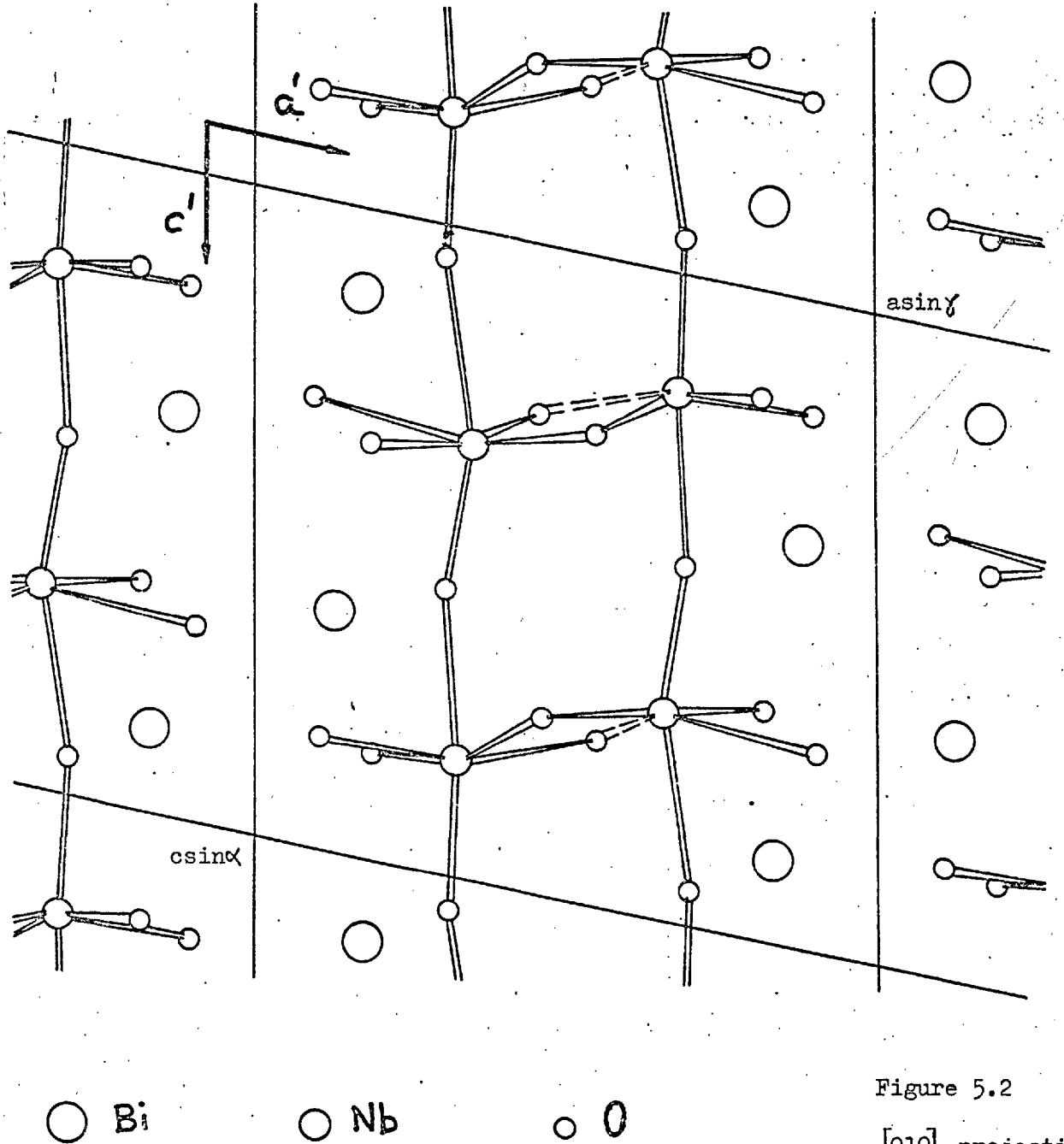


Figure 5.2

[010] projection of the triclinic $BiNbO_4$ structure

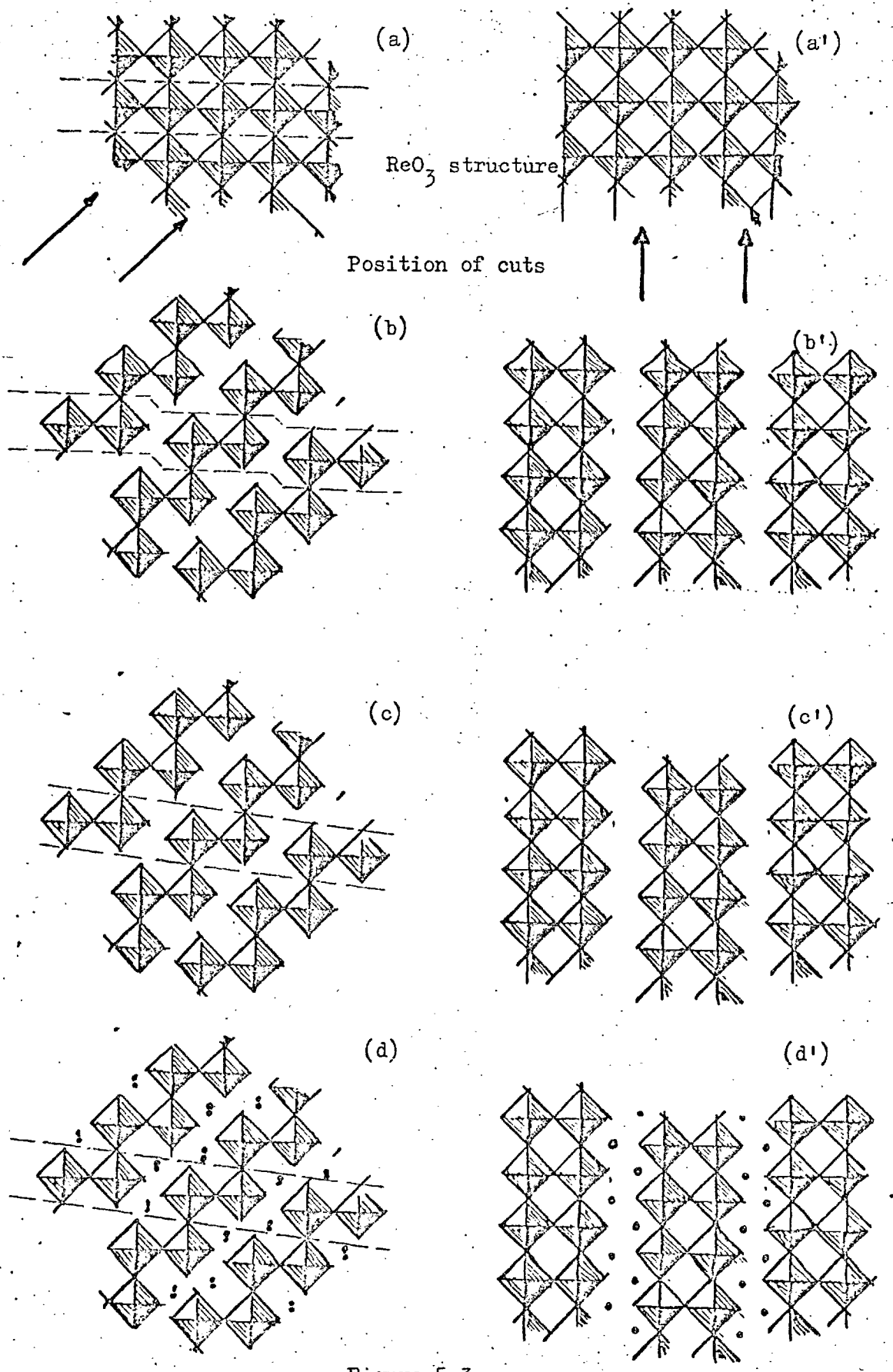


Figure 5.3
a' is the projection of the part of the structure shown between broken lines in a. Similarly for b and b', etc.

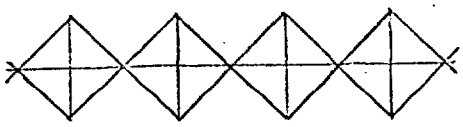
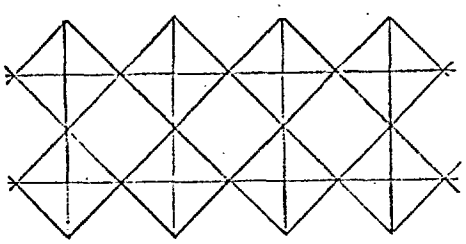
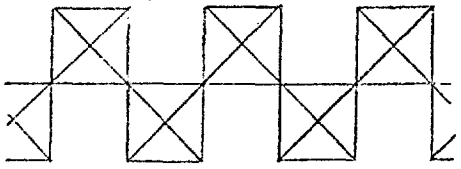
Idealised Sheet	Thickness	Formula	Found In	No of Free Vertices
	d	$(AX_4)_n$	e.g. $SbNbO_4$	2n at opposite ends -trans-
	2d	$(AX_{7/2})_n$	Bi_3NbTiO_9 $Sr_3Ti_2O_7$	n
	$\sqrt{2}$d	$(AX_4)_n$	tric. $BiNbO_4$	2n at adjacent ends -cis-

Table 5.1

All these sheets differ from that found in triclinic $BiNbO_4$ in that they correspond to slices parallel to (100) of the ReO_3 structure. The various types of octahedral sheets discussed are listed in Table 5.1.

This in fact is the essential difference between the structures of the triclinic members of the ABO_4 group and the monoclinic and orthorhombic ones. In $BiNbO_4$ the octahedral sheet is of this novel

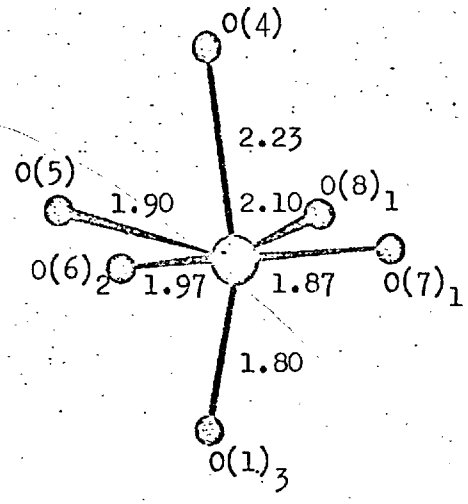
type, "$\sqrt{2}$" octahedra thick, whereas the crystals of higher symmetry have more orthodox octahedral sheets, only one unit thick.

The Niobium and Bismuth Co-ordinations

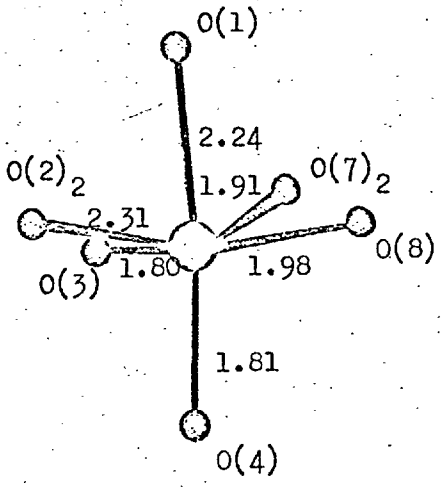
The final atomic parameters were used to work out a set of interatomic distances and angles which are given in Tables 5.4 and 5.5. (The symmetry operations used are listed in Table 5.3.) Figure 5.4 shows the oxygen co-ordination about the two independent niobium and bismuth atoms.

The oxygen atoms are arranged about the niobiums in the form of a distorted octahedron, with Nb-O distances of 1.80 - 2.23 Å in one case, (a), and 1.80 - 2.31 Å in the other, (b). The mean values are 1.98 and 2.00 Å respectively. Four of these bonds are distinctly shorter than the other two, in each case, thus the niobium atom can be pictured as being displaced toward one edge of the distorted octahedron. This is analogous to the niobium co-ordination found in $SbNbO_4$ (I.5).

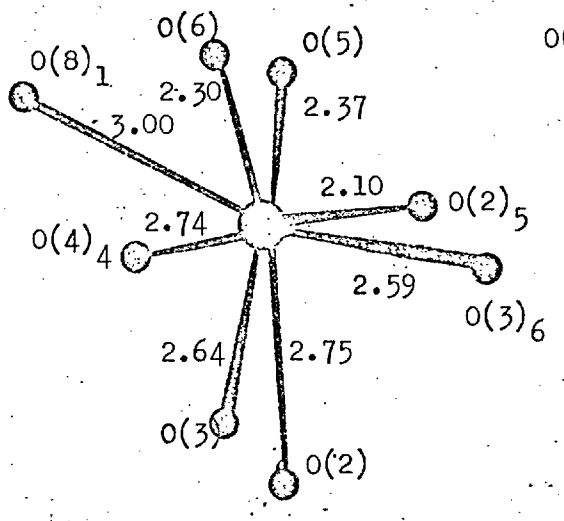
The bismuth co-ordination is difficult to describe. Figure 5.4(c) and (d) show Bi-O contacts of less than 3.48 Å. There are further oxygens at 3.52 Å for (c) and 3.48 Å for (d). In each case the eight nearest neighbours around the bismuth form a very distorted square anti-prism. This may be compared with the nine-co-ordination found for bismuth in $BiOHSeO_4.H_2O$ (I.16) and the two forms of $BiOHCrO_4$ (I.17), in which the



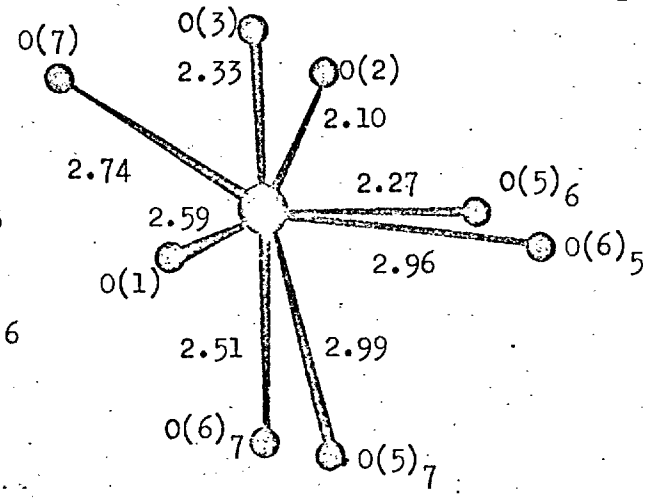
(a) Nb2



(b) Nbl
(actually Nbl_1)



(c) Bi(1)



(d) Bi(2)
(actually $Bi(2)_1$)

Figure 5.4

(a),(b) Nb co-ordination

(c),(d) Bi co-ordination (< 3.48Å)

Table 5.3 - Triclinic $BiNbO_4$, Symmetry Operations Used in the Calculation of Interatomic Distances and Angles.

Suffix	Symmetry Operation
1	1-x, 1-y, 1-z;
2	x, y-1, z;
3	x, y, z+1;
4	x, y+1, z;
5	-x, 2-y, 1-z;
6	-x, 1-y, 1-z;
7	x, y, z-1.

eight nearest neighbours form a square antiprism, far less distorted than that in triclinic $BiNbO_4$, the ninth oxygen being bonded through one of the basal planes of the antiprism.

Figures 5.4(c) and (d) show a distinct similarity in the distortions of the co-ordination polyhedra of the bismuth atoms. In both cases there is a very short Bi-O distance of 2.10Å, two in the range 2.27 - 2.37Å, and five more Bi-O distances between 2.50 and 3.00Å. The means of the nearest eight oxygen distances are 2.562 and 2.560Å respectively for (c) and (d).

All the oxygen atoms are associated with octahedra. The nearest approach of oxygens to each other is 2.50Å, which is unremarkable.

Table 5.4 - Triclinic $BiNbO_4$, Final Interatomic Distances and Standard Deviations in Å.

See Figure 5.4

Nb(2)	- O(4)	2.225	0.043	
Nb(2)	- O(5)	1.897	0.068	
Nb(2)	- $O(6)_2$	1.971	0.059	(a)
Nb(2)	- $O(7)_1$	1.868	0.049	
Nb(2)	- $O(8)_1$	2.101	0.075	
Nb(2)	- $O(1)_3$	1.795	0.032	
$Nb(1)_1$	- O(1)	2.240	0.031	
$Nb(1)_1$	- $O(2)_2$	2.310	0.057	
$Nb(1)_1$	- O(3)	1.799	0.065	(b)
$Nb(1)_1$	- O(4)	1.807	0.041	
$Nb(1)_1$	- $O(7)_2$	1.906	0.054	
$Nb(1)_1$	- O(8)	1.975	0.075	
Bi(1)	- O(2)	2.752	0.051	
Bi(1)	- O(3)	2.642	0.065	
Bi(1)	- O(5)	2.365	0.070	(c)
Bi(1)	- O(6)	2.302	0.055	

Table 5.4 - continued

$Bi(1) - O(8)_1$	3.005	0.072	
$Bi(1) - O(2)_5$	2.101	0.051	
$Bi(1) - O(4)_4$	2.737	0.049	(c)
$Bi(1) - O(3)_6$	2.593	0.069	
.....			
$Bi(1) - O(4)$	3.517	0.048	
$Bi(2)_1 - O(1)$	2.586	0.037	
$Bi(2)_1 - O(2)$	2.102	0.053	
$Bi(2)_1 - O(3)$	2.327	0.082	
$Bi(2)_1 - O(7)$	2.739	0.055	
$Bi(2)_1 - O(5)_7$	2.986	0.070	(d)
$Bi(2)_1 - O(6)_7$	2.510	0.053	
$Bi(2)_1 - O(5)_6$	2.273	0.068	
$Bi(2)_1 - O(6)_5$	2.957	0.054	
.....			
$Bi(2)_1 - O(1)_4$	3.479	0.037	

Table 5.5 - Triclinic $BiNbO_4$, Final Interatomic Angles and Standard Deviations in °.

See Figure 5.4

O(4)	- Nb(2) -	O(5)	83.1	2.2
O(4)	- Nb(2) -	$O(6)_2$	80.8	1.9
O(4)	- Nb(2) -	$O(8)_1$	85.6	2.2
O(4)	- Nb(2) -	$O(7)_1$	87.0	1.9
$O(1)_3$	- Nb(2) -	O(5)	96.9	2.2
$O(1)_3$	- Nb(2) -	$O(6)_2$	94.9	1.9
$O(1)_3$	- Nb(2) -	$O(8)_1$	98.7	2.2
$O(1)_3$	- Nb(2) -	$O(7)_1$	93.5	1.9
O(5)	- Nb(2) -	$O(6)_2$	85.3	2.8
$O(7)_1$	- Nb(2) -	$O(8)_1$	85.5	2.6
$O(8)_1$	- Nb(2) -	O(5)	86.3	2.9
$O(6)_2$	- Nb(2) -	$O(7)_1$	100.6	2.4

(a)

O(1)	- $Nb(1)_1$ -	$O(2)_2$	82.8	1.6
O(1)	- $Nb(1)_1$ -	O(3)	81.2	2.2
O(1)	- $Nb(1)_1$ -	$O(7)_2$	82.0	1.8
O(1)	- $Nb(1)_1$ -	O(8)	85.9	2.2
O(4)	- $Nb(1)_1$ -	$O(2)_2$	87.5	2.0
O(4)	- $Nb(1)_1$ -	O(3)	91.5	2.4
O(4)	- $Nb(1)_1$ -	$O(7)_2$	101.2	2.2
O(4)	- $Nb(1)_1$ -	O(8)	103.5	2.5
O(8)	- $Nb(1)_1$ -	$O(7)_2$	106.8	2.5

(b)

Table 5.5 - continued

$O(7)_2$ - $Nb(1)_1$ - $O(2)_2$	73.5	2.0	
$O(2)_2$ - $Nb(1)_1$ - $O(3)$	82.5	2.6	(b)
$O(3)$ - $Nb(1)_1$ - $O(8)$	94.0	3.1	
$O(2)_5$ - $Bi(1)$ - $O(6)$	78.5	2.0	
$O(6)$ - $Bi(1)$ - $O(4)_4$	64.8	1.6	
$O(4)_4$ - $Bi(1)$ - $O(2)$	63.1	1.5	
$O(2)$ - $Bi(1)$ - $O(2)_5$	73.7	1.7	
$O(5)$ - $Bi(1)$ - $O(8)_1$	59.9	2.1	
$O(8)_1$ - $Bi(1)$ - $O(3)$	91.3	2.0	
$O(3)$ - $Bi(1)$ - $O(3)_6$	69.8	1.9	(c)
$O(3)_6$ - $Bi(1)$ - $O(5)$	69.0	2.3	
$O(3)_6$ - $Bi(1)$ - $O(2)_5$	70.4	2.2	
$O(5)$ - $Bi(1)$ - $O(6)$	81.6	2.2	
$O(3)$ - $Bi(1)$ - $O(2)$	65.9	1.9	
$O(8)_1$ - $Bi(1)$ - $O(6)$	71.0	1.9	
$O(8)_1$ - $Bi(1)$ - $O(4)_4$	84.2	1.7	
$O(6)_5$ - $Bi(2)_1$ - $O(2)$	64.3	1.8	
$O(2)$ - $Bi(2)_1$ - $O(7)$	61.7	1.7	
$O(7)$ - $Bi(2)_1$ - $O(6)_7$	96.8	1.7	(d)
$O(6)_7$ - $Bi(2)_1$ - $O(6)_5$	65.4	1.5	

Table 5.5 - continued

$O(5)_6$ - $Bi(2)_1$ - $O(3)$	75.5	2.4
$O(3)$ - $Bi(2)_1$ - $O(1)$	65.0	1.7
$O(1)$ - $Bi(2)_1$ - $O(5)_7$	59.0	1.5
$O(5)_7$ - $Bi(2)_1$ - $O(5)_6$	67.6	2.0
$O(5)_6$ - $Bi(2)_1$ - $O(6)_5$	58.4	2.2
$O(2)$ - $Bi(2)_1$ - $O(3)$	82.9	2.2
$O(6)_7$ - $Bi(2)_1$ - $O(5)_7$	66.8	1.9
$O(1)$ - $Bi(2)_1$ - $O(7)$	97.1	1.4
$O(7)$ - $Bi(2)_1$ - $O(3)$	84.7	2.1

Twinning in Triclinic $BiNbO_4$

The unit cells of the two components of a twinned triclinic crystal meet in the composition plane, which has the shape of a parallelogram.

Two types of twin may be distinguished. In one, (a), the discontinuity between the twin portions may arise from a rotation of this parallelogram through 180° about a normal to the composition plane. The parallelograms of the two twin components are then congruent and may be superimposed to give a complete plane in common, (Figure 5.5(a)).

In the second case, (b), the parallelogram is rotated through 180°

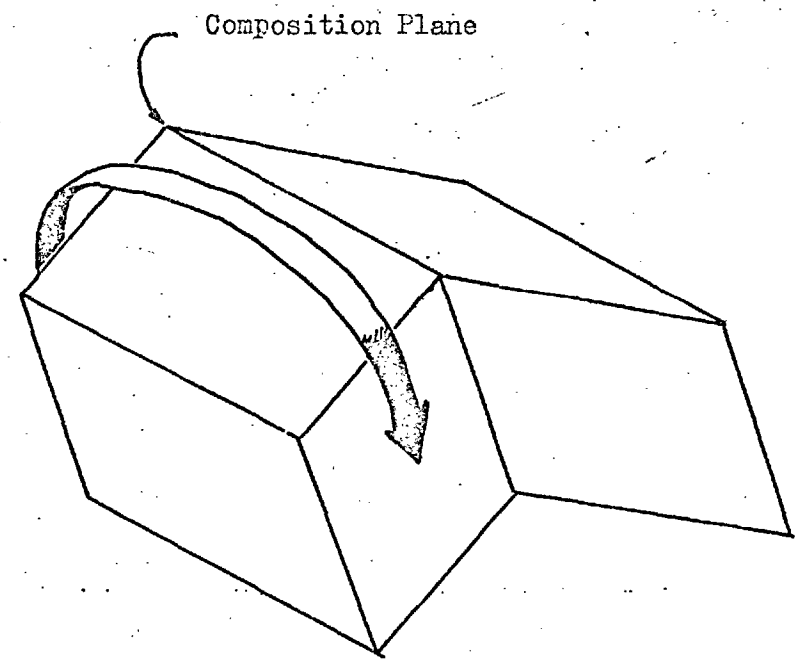


Figure 5.5 (a)

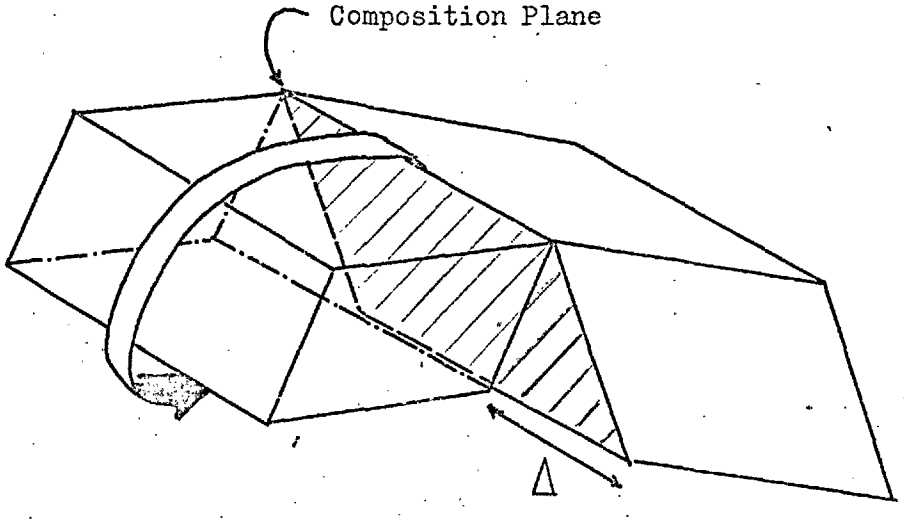


Figure 5.5 (b)

about an axis within its plane. The resultant parallelogram is the reverse of the original, and therefore the two are no longer congruent. In this case, at most one cell edge may be in common between the twins (Figure 5.5(b)).

If (100) is taken arbitrarily as the composition plane, then the first case corresponds to a 180° rotation of the real lattice about a^* (Figure 5.6 (a)), with the result in reciprocal space that only the a^* reciprocal axis is common (Figure 5.7(a)). In a Weissenberg photograph therefore, all but the h00 reflections would be split.

In the second instance, (b), if the twinning occurs on the bc plane, the rotation may be about an axis parallel to b or c. (Non-axial rotations are possible, but not considered.) Rotation about b is illustrated in Figure 5.6(b). In reciprocal space, (Figure 5.7(b)), a_1^* and a_2^* are then colinear; as are c_1^* and c_2^*. Hence in this case, all the h0l reflections are common, whereas others are split.

Photographic evidence in triclinic $BiNbO_4$, illustrated in Figure 5.8, is as follows:-

Polysynthetically twinned crystals have h0l in common, all other reflections occur in pairs parallel to the h0l zone. Therefore these twins are of the second type, (b), and are related by rotation about an axis parallel to b. The composition plane must then be a plane parallel to b. Structural considerations, however show that the composition plane is in fact bc, the plane parallel to the octahedral sheets.

Case (a) - Real

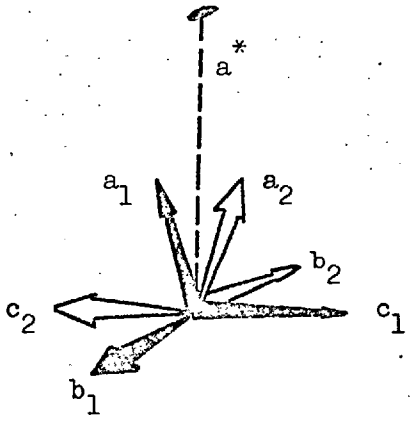


Figure 5.6 (a)

bc plane common
rotate about normal (a^*)

Case (b) - Real

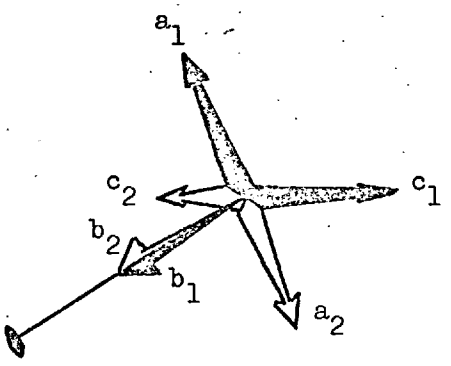


Figure 5.6 (b)

Rotate bc plane about b
(b in common)

Case (a) - Reciprocal

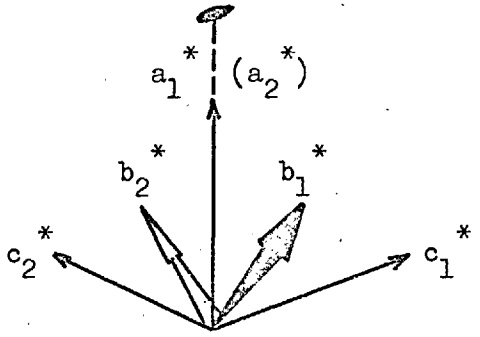


Figure 5.7 (a)

a^* common (h00)

Case (b) - Reciprocal

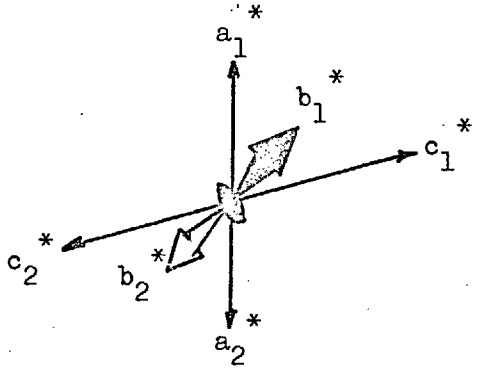


Figure 5.7 (b)

a_1^* b_1c_1 } colinear
a_2^* b_2c_2 }

c_1^* a_1b_1 } colinear
c_2^* a_2b_2 }

a^*c^* plane in common (h01)

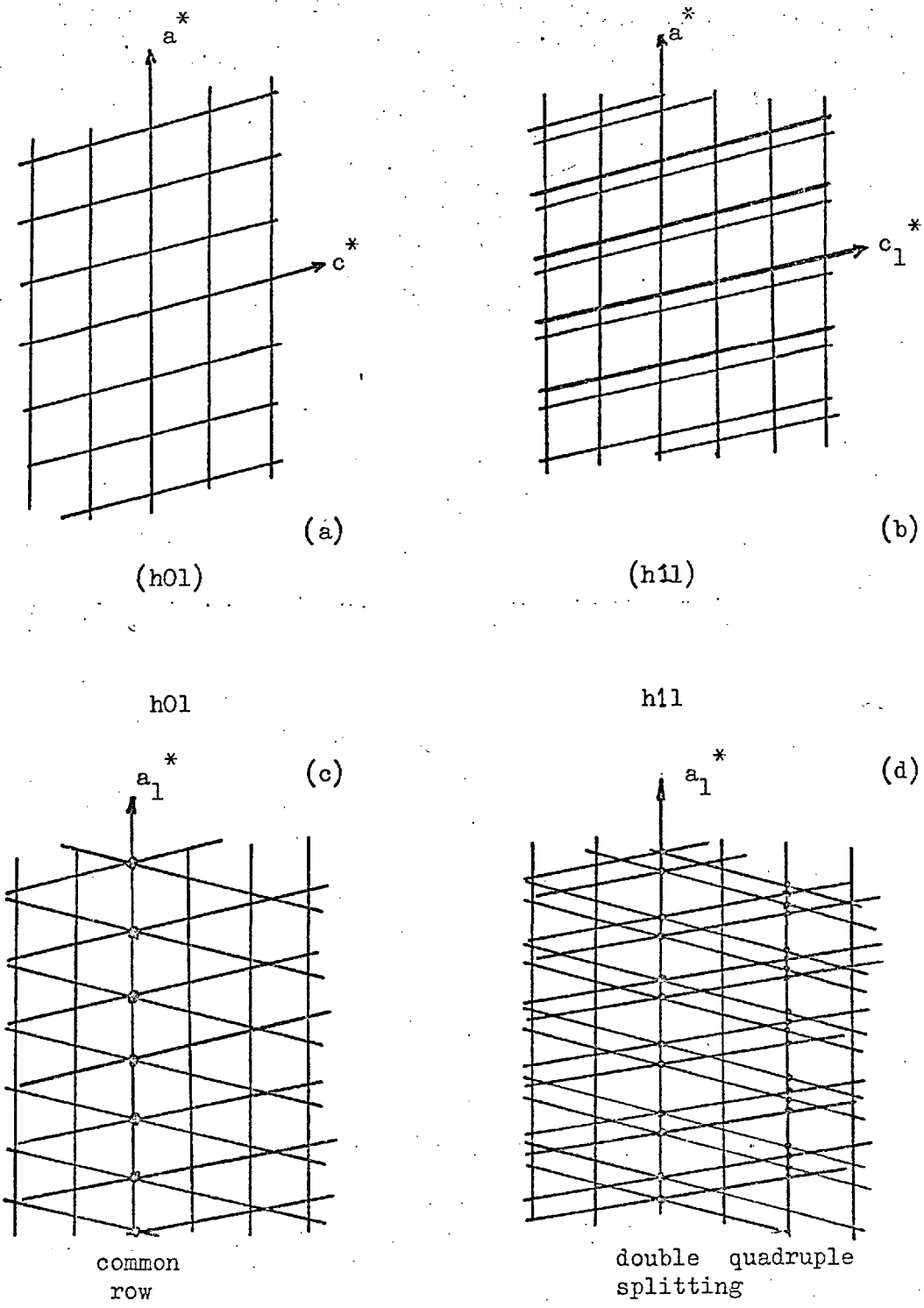


Figure 5.8 - Triclinic $BiNbO_4$, Reciprocal Lattice

(a), (b) Polysynthetic Twin

(c), (d) Double twin

Doubly twinned crystals give Weissenberg photographs for which

h00 are single

hk0 are doubled

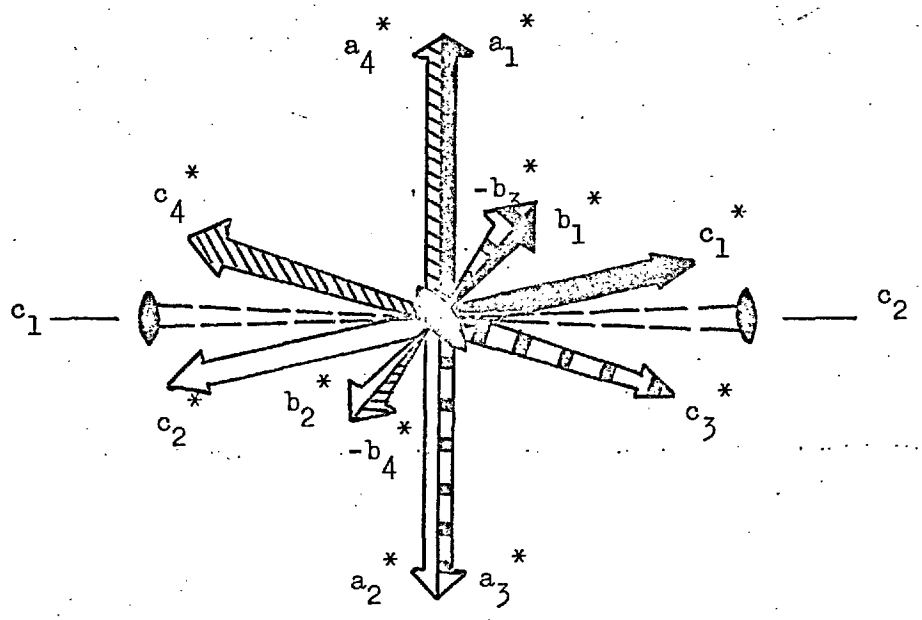
h0l are doubled

hkl are quadrupled.

In every case, the multiple spots occurred at symmetrical positions on festoons parallel to a^*. This is a special case of the reciprocal lattice to be expected if different parts of the crystal represent twins (all compounded on bc), some being rotated about b, (polysynthetic), and some about c. The fact that the four-fold spots occur in a row parallel to a^* arises only because α and α^* are so close to 90°.

If one considers a crystal, which has polysynthetic twinning of type (b) with rotation about b, plus twinning with rotation about c in each polysynthetic case, the reciprocal axes will look like Figure5.9. The $(hl\ell)_1$ sheet is not coplanar with the $(hl\ell)_3$ sheet, hence an $(hl\ell)_1$ photograph would contain only reflection-pairs $(hl\ell)_1$ and $(hl\ell)_2$.

If, however, the special case is considered, where α^* is approximately equal to 90°, (as in $BiNbO_4$, where $\alpha^* = 90^\circ 40'$), the various b axes of Figure 5.9 will fall on top of the a axes in the diagram, and c_1 and c_2 will now be in the plane of the paper. The special case is illustrated in Figure 5.10. All the planes $(hl\ell)_i$ now coincide, and an $hl\ell$ photograph will contain reflections $(hl\ell)_1$, $(hl\ell)_2$, $(h\bar{l}\ell)_3$, $(h\bar{l}\ell)_4$; Figure 5.11(a).



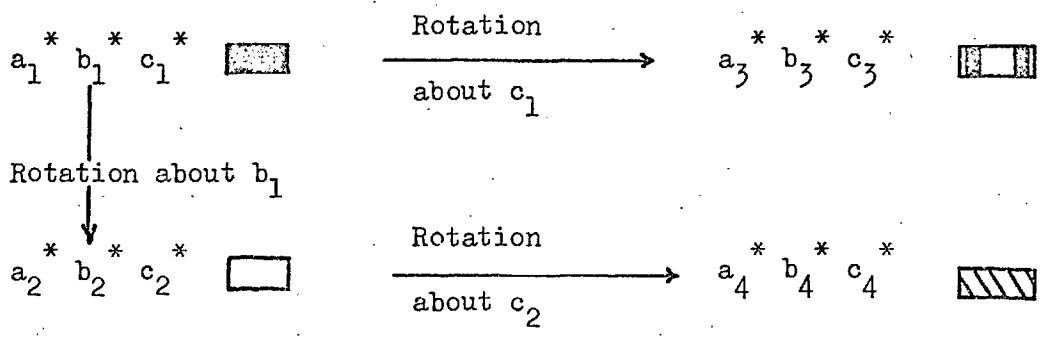


Figure 5.9

General triclinic "double" twin of the type discussed in the text

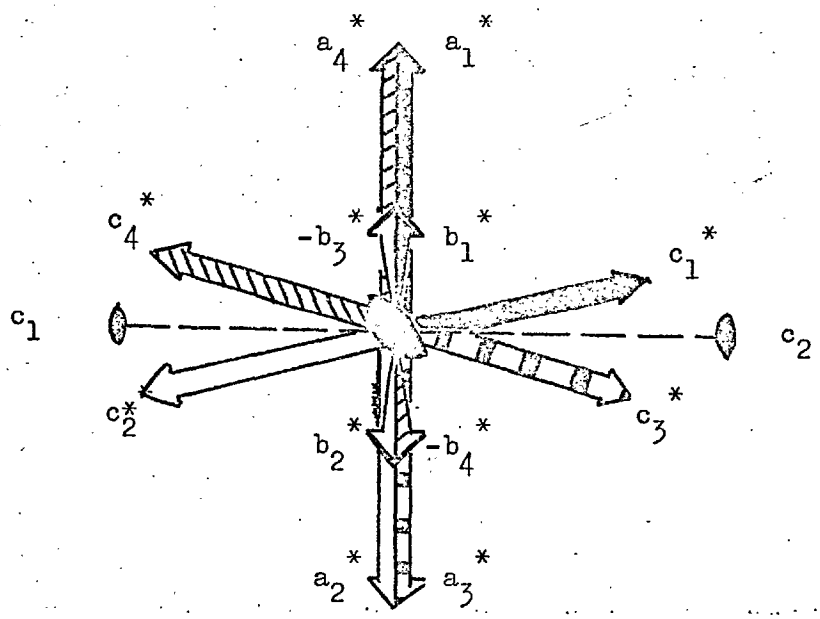
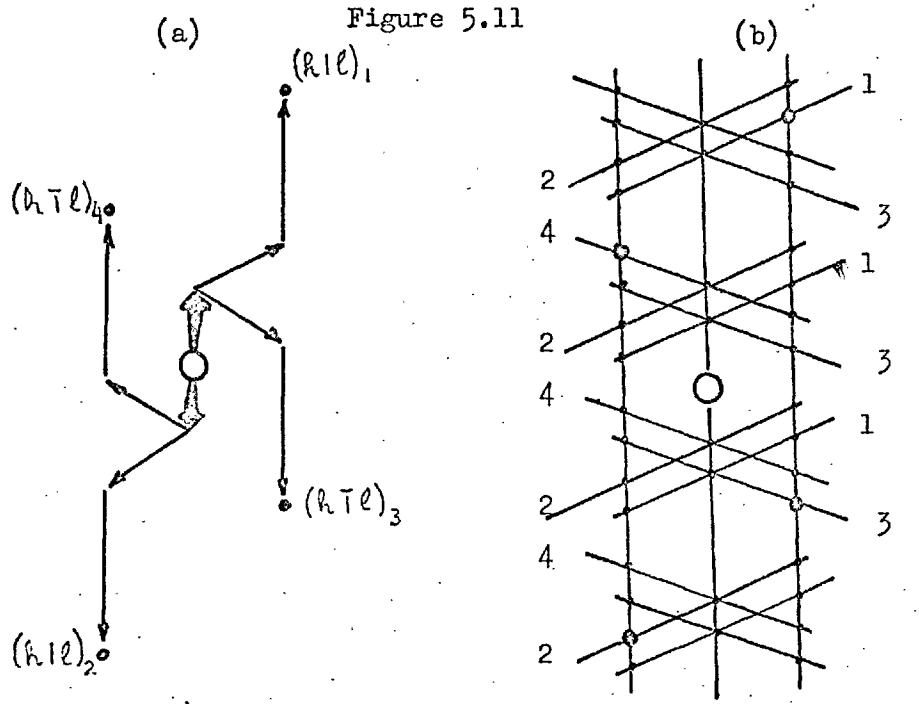


Figure 5.10

Special case of "double" twin when $\alpha^* = 90^\circ$

Figure 5.11



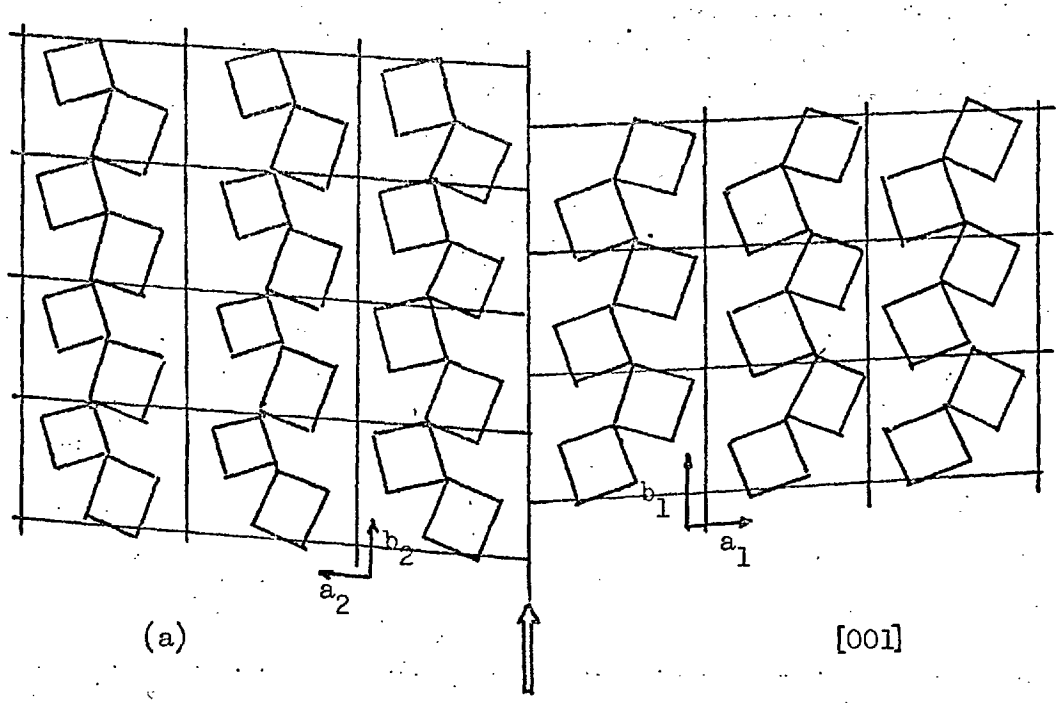
The four reciprocal lattice sheets, $(h\,l\,\ell)_i$, superimpose (Figure 5.11(b)), to give quadrupling along rows of constant h. In fact the four reflections in a row will be $(h\,l\,\ell)_1$, $(h\,l\,\bar{\ell})_2$, $(h\,\bar{l}\,\ell)_3$ and $(h\,\bar{l}\,\bar{\ell})_4$.

Figure 5.11(b) illustrates exactly what was found for doubly twinned triclinic $BiNbO_4$ crystals (Figure 5.8(d))

Thus both the twins found in triclinic $BiNbO_4$ are of type (b), obtained by rotation about b in the polysynthetic case, and c in the other case. Structural considerations make it clear that the composition plane is bc in both cases. Since the angle α is very nearly 90°, the bc face is almost a rectangle, i.e. the "incongruence" of the parallelograms, Δ in Figure 5.5(b), is small. Therefore twinning of type (b) is particularly easy on this face.

The twins may be pictured structurally as alternative ways of stacking the octahedral sheets. Figure 5.12 shows [001] and [010] projections of the polysynthetically twinned structure. By suitable slip on the composition plane, an almost perfect continuity can be envisaged. The twin is derived by rotating the octahedral sheet about an axis parallel to b and stacking on the previous sheet.

The second mode of twinning, which was not polysynthetic, is derived by rotating the octahedral sheet about an axis parallel to c. A small slip on the composition plane will again give reasonably good continuity through the twin structure. (See Figure 5.13).



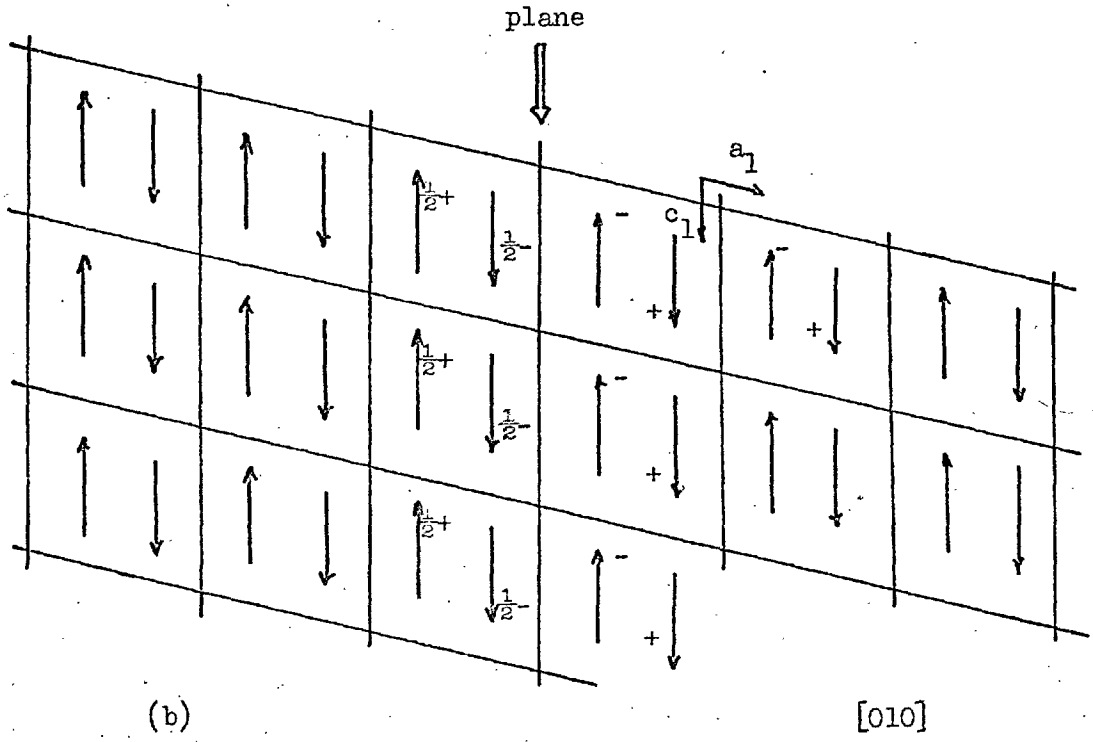


Figure 5.12 - Triclinic $BiNbO_4$, Polysynthetic Twin

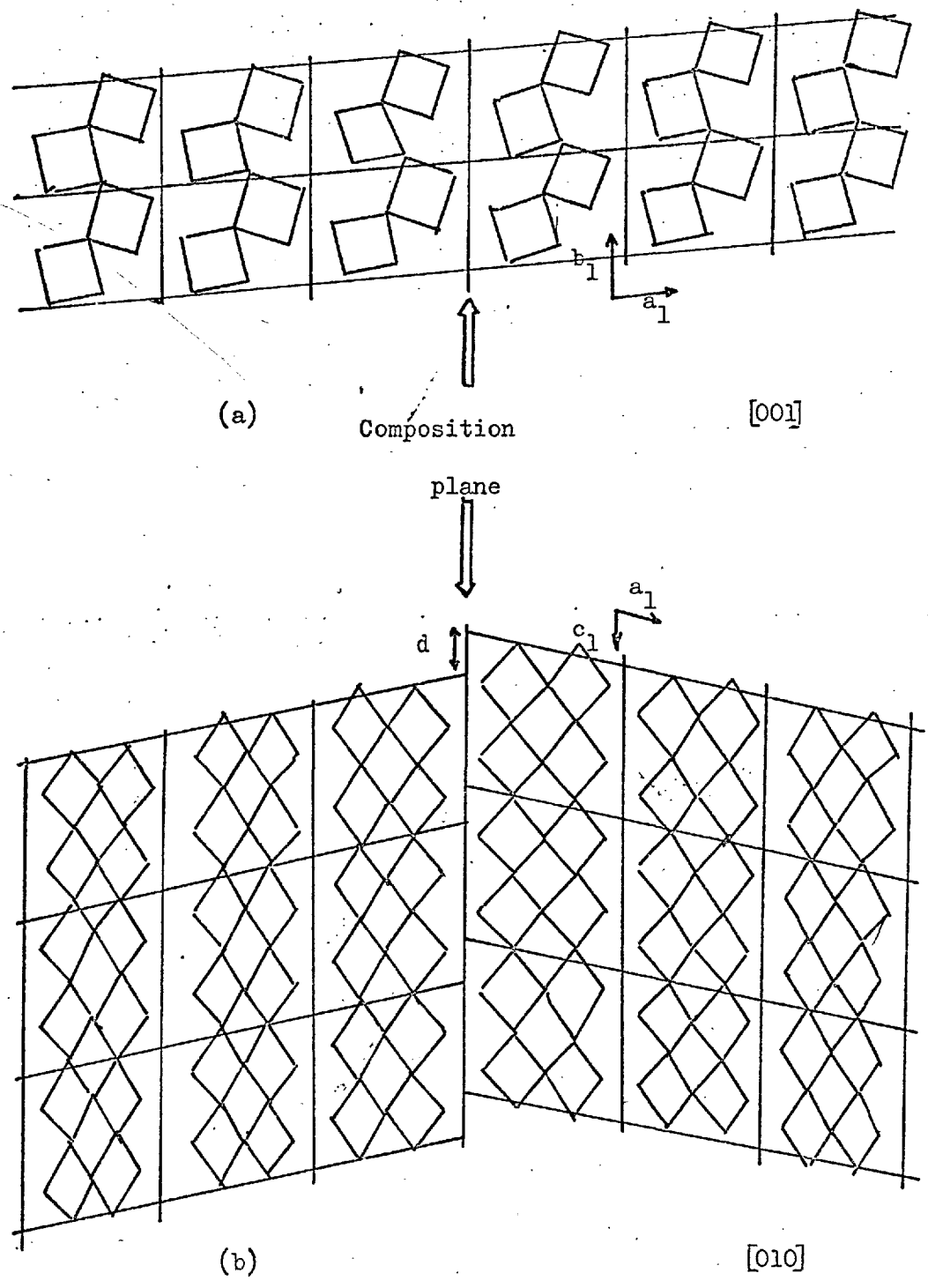
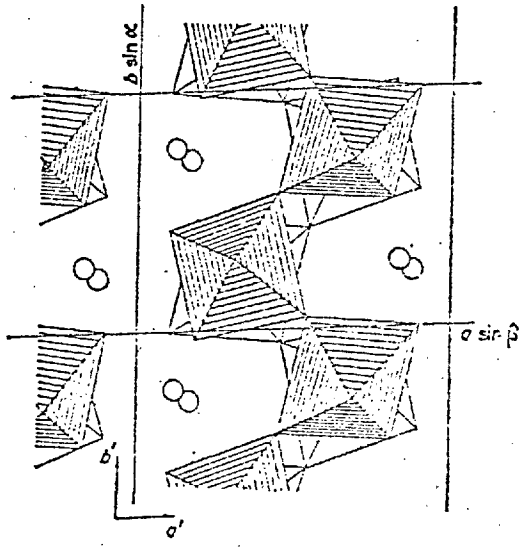


Figure 5.13 - Triclinic $BiNbO_4$, Second Mode of Twinning

Triclinic $BiNbO_4$ in relationship to other ABO_4 compounds

Table 5.6 shows the structural relationships found in the ABO_4 group of compounds under discussion. It is important to note that whereas the orthorhombic and monoclinic structures are simply related to one another, (see Chapter 3 and Figure 3.2), the triclinic structure type is not derivable from either of the other two in simple terms. They are related only in a general way, in that they are all built up of corrugated sheets of B^V-O octahedra. Whereas the orthorhombic and monoclinic structures differ only in the manner of stacking these sheets, in the triclinic structure an entirely new type of double sheet is formed. The manner of corrugation is however quite similar, as shown in Figure 5.14.



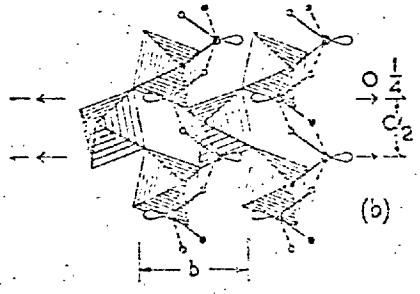


Figure 5.14

Cut across the "double" sheet of the triclinic structure

View of the single sheet in the monoclinic structure

Form		Symmetry	Sb^{III}			Bi^{III}		
			Nb^{V}	Sb^{V}	Ta^{V}	Nb^{V}	Sb^{V}	Ta^{V}
Low Temp.	non-centrosymmetric	Orthorhombic U in $Å^3$	$SbNbO_4$ * 324.4	α-Sb_2O_4 308.4	$SbTaO_4$ * ~~330.9~~ 323	$BiNbO_4$ 330.9	?	$BiTaO_4$ 328.5
High Temp.	centrosymmetric	Monoclinic U in $Å^3$	—	β-Sb_2O_4 * 303.7	—		$BiSbO_4$ * 308.5	
		Triclinic U in $Å^3$				$BiNbO_4$ * 325.2		$BiTaO_4$ * 325

Table 5.6

* stable form

The irreversible transformation from the low temperature form to the high temperature form in each case involves a reduction in the cell volume of about 1%, and in the monoclinic case a centre of symmetry is gained. The triclinic structure probably also contains a centre of symmetry, hence a gain of a centre of symmetry accompanied by a $1\frac{1}{2}\%$ increase in density on the transformation to the stable high temperature modifications may be taken as a characteristic of the group as a whole.

6. The Crystal Structure of $3Bi_2O_3.17Nb_2O_5$ ($Bi_2O_3.6Nb_2O_5$)

Crystal Data

$Bi_6Nb_{34}O_{94}$, M = 5916.8, Orthorhombic, a = 12.516 ± 0.005,
b = 37.14 ± 0.02, c = 3.922 ± 0.002 Å, U = 1828.3 Å^3, D_c = 5.37 g.cm.$^{-3}$
for Z=1, F(000) = 2644.
Space Group Pba2, (C_{2v}^8, No.32)
For CuKα radiation, μ = 727.6 cm^{-1}.

Preliminary Examination

The crystals were yellow irregular plates, often relatively thick. All aspects of the crystals showed sharp extinction directions. Oscillation and Weissenberg photographs indicated orthorhombic symmetry with $a \sim 12.46$, $b \sim 37.4$, $c \sim 3.93$ Å; though often the crystals were twinned so as to give a pseudo-tetragonal unit cell with $a \sim 37.4$ Å. Many crystals were examined from preparations (c) and (d), Section 3, to find one completely free of this twinning. One such crystal was found, but this showed the presence of a fragment at a random orientation to the main crystal. As this did not in general interfere with intensity measurement, this crystal, the best of many examined, was used for data collection.

Unit Cell and Space Group

The Laue symmetry of mmm was quite clear from oscillation and Weissenberg photographs. Examination of the latter for systematic absences showed that of the type

h0l only $h = 2n$, whereas of the

0kl only $k = 2n$ were present. No other systematic absences occurred. This indicated Pba2 (No.32) or Pbam (No.55) as possible space groups. The former has four-fold, whereas the latter

has eight-fold general positions. Due to the short c axis, the eight-fold general position in Pbam could not be considered. Of the four-fold positions in this space group the most general are of the type x, y, 0 or x, y, $\frac{1}{2}$. Therefore the space groups differ essentially only in whether atoms occur in two strict planes at z = 0 and $\frac{1}{2}$, or not. The strict planarity was thought unlikely and in fact Pba2 emerged as the correct space group.

The initial unit cell constants were used to index the first few lines of Roth's powder pattern for "$Bi_2O_3.6Nb_2O_5$". These were refined by least-squares to produce more accurate values. The complete powder pattern was then indexed with the aid of the list of single-crystal intensity measurements. All reflections with intensities greater than a particular threshold appeared as lines in the powder pattern. Least-squares refinement on the basis of all the uniquely indexed lines gave the final cell parameters of a = 12.516 ± 0.005, b = 37.14 ± 0.02, c = 3.922 ± 0.002 Å. The complete indexed powder pattern is listed in Table 6.1.

Data Collection

Intensity data were collected using a Nonius Weissenberg camera from a crystal approximately 0.05 x 0.04 x 0.01 mm in size, mounted about the c axis. Layers hk0 to hk3 were photographed, but due to the small crystal size exposures of over three weeks duration had to be taken with

Table 6.1 - $3Bi_2O_3 \cdot 17Nb_2O_5$, X-ray Powder Pattern

Cu Kα radiation

$\lambda = 1.54178$ Å

Roth and Waring(I.2)						
I	d(Å)	$\sin^2\theta_{obs}$	h	k	l	$\sin^2\theta_{calc}$
5	7.49	0.01059	1	4	0	0.01072
5	6.15	0.01571	2	1	0	0.01565
			0	6	0	0.01556
			2	0	0	0.01522
10	5.92	0.01696	2	2	0	0.01694
100	3.929	0.03850	0	0	1	0.03848
			3	3	0	0.03809
			1	9	0	0.03876
25	3.673	0.04405	1	2	1	0.04400
15	3.619	0.04537	0	4	1	0.04538
30	3.455	0.04978	3	6	0	0.04973
35	3.442	0.05016	2	9	0	0.05015
10	3.310	0.05424	2	1	1	0.05410
20	3.274	0.05544	2	2	1	0.05539
40	3.206	0.05782	1	6	1	0.05780
25	3.129	0.06070	4	0	0	0.06078
			2	4	1	0.06057

Table 6.1 continued -

I	d(Å)	$\sin^2\theta_{obs}$	h	k	l	$\sin^2\theta_{calc}$
20	3.089	0.06228	3	8	0	0.06180
			4	2	0	0.06250
40	3.032	0.06464	4	3	0	0.06466
			2	5	1	0.06445
60	3.000	0.06603	1	12	0	0.06592
15	2.964	0.06764	2	11	0	0.06739
			4	4	0	0.06767
40	2.930	0.06922	2	6	1	0.06919
			3	9	0	0.06913
10	2.854	0.07296	3	1	1	0.07308
30	2.788	0.07645	4	6	0	0.07630
			3	3	1	0.07653
55	2.773	0.07728	1	9	1	0.07720
			2	12	0	0.07731
10	2.736	0.07939	3	4	1	0.07954
40	2.596	0.08818	3	6	1	0.08816
35	2.592	0.08845	2	9	1	0.08859
5	2.439	0.09990	4	1	1	0.09964
10	2.402	0.10300	4	3	1	0.10309

Table 6.1 continued -

I	d(Å)	$\sin^2\theta_{obs}$	h	k	l	$\sin^2\theta_{calc}$
10	2.386	0.10439	1	12	1	0.10435
10	2.352	0.10743	3	9	1	0.10756
5	2.294	0.11293	4	11	0	0.11293
10	2.275	0.11482	4	6	1	0.11473

Cu-Kα radiation. In spite of this, much of the data were recorded only on the top two films of the packs.

The crystal was remounted about the a axis, and the 2kl layer was recorded for correlation. A total of 1299 reflections were measured visually. Data were punched on cards and processed using X-ray 63. Scattering factors used were for Bi^+, Nb^{3+} and O^-. (See Section 4). The real part of the anomalous dispersion correction was applied for bismuth and niobium[I.9].

The Structure in Projection

The size of the unit cell suggested immediately a connection between this structure and that of $Nb_{16}W_{18}O_{94}$, determined in projection by Sleight[I.18]. This is orthorhombic with a = 12.251, b = 36.62, c = 3.94 Å and space group $P2_12_12$. The structure illustrated in Figure 6.1 is related to that of tetragonal potassium tungsten bronze[I.19] shown in Figure 6.2, but has one cell edge tripled.

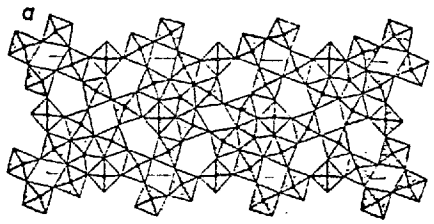


Figure 6.1
The crystal structure of $Nb_{16}W_{18}O_{94}$

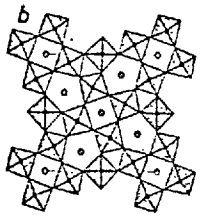


Figure 6.2
The crystal structure of tetragonal potassium tungsten bronze

The bronze structure consists of a complex network of WO_3 octahedra, sharing corners. The resulting pentagonal tunnels and perovskite-like

cages are partially filled with potassium atoms. $Nb_{16}W_{18}O_{94}$ has the same basic MO_3 octahedral network with extra metal and oxygen atoms in four out of every twelve pentagonal tunnels, producing pentagonal bipyramids. The niobium and tungsten atoms are statistically distributed at the various sites.

A check on the intensities of an hk0 Weissenberg photograph of "$Bi_2O_3.6Nb_2O_5$" showed surprisingly good agreement with those published for $Nb_{16}W_{18}O_{94}$. Sleight[I.18] found that the most frequent type of twinning occurring in $Nb_{16}W_{18}O_{94}$ was one which gave an apparently tetragonal cell with $a \sim 37$ Å. This corresponds to the mode of twinning often found in crystals of "$Bi_2O_3.6Nb_2O_5$".

The formula given by Roth, $Bi_2O_3.6Nb_2O_5$, cannot easily be reconciled with this strucure, However it would be expected that niobium atoms occupied the metal sites of $Nb_{16}W_{18}O_{94}$, giving a unit cell content of 34Nb + 94 O. The nearest approximation to this is three 1:6 formula units giving $3x(Bi_2O_3.6Nb_2O_5)$ or 6 Bi + 36 Nb + 99 O. A reduction in the niobium content of the cell to 34 results in 6 Bi + 34 Nb + 94 O or $3Bi_2O_3.17Nb_2O_5$. It was thought that the structure was based on a $M_{34}O_{94}$ matrix, and therefore the ideal formula is in fact "3:17" and not "1:6". The difference between the two compositions is very slight (15.0% Bi_2O_3, 85.0% Nb_2O_5, D_{calc} = 5.37g.cm.$^{-3}$ for 3:17 ; and 14.3% Bi_2O_3, 85.7% Nb_2O_5, D_{calc} = 5.30g.cm.$^{-3}$ for 1:6). The density of this compound was not measured since the product of the preparation was always a

mixture of phases. In any case, a density measurement would not have been accurate enough to distinguish between these two alternatives.

When data for the hk0 projection became available, a structure analogous to $Nb_{16}W_{18}O_{94}$ was tried. Refinement on just the Nb-O framework with oxygens fixed gave an R of 0.27. A difference Fourier synthesis showed electron density in all three of the still unfilled pentagonal tunnels, as well as the diamond shaped hole at the origin. When bismuth atoms were placed at some of these peaks and refined, they were found to have very high temperature factors. Difference Fourier syntheses showed appreciable electron density left both in the "unfilled" tunnels and in the ones where a bismuth atom had already been placed.

In projection, a bismuth atom with a high temperature factor could not be distinguished from a niobium. In three dimensions however it was expected that a niobium in a pentagonal tunnel would be at the same level as the other niobium atoms with octahedral environment, whereas the bismuth atoms were thought to be approximately half way between the niobium layers.

Three-Dimensional Refinement of the Structure

In the initial stages of three-dimensional refinement only data from layers hk0-hk2 were used. The third layer was included when it became available.

The first refinement was based on just the niobium atoms of the $M_{34}O_{94}$

network. x and y co-ordinates were those obtained from the two-dimensional refinement, whereas the z co-ordinates were taken to be approximately 0.5 with a small variation from atom to atom. This arrangement gave R = 0.29, and a difference Fourier synthesis showed all the oxygen atoms of the skeleton structure, though some of those at $z \sim 0$ were rather indefinite.

A large peak was visible at $z \sim 0$ in pentagonal tunnel A, (Figure 6.3), its height was however less than that expected for a bismuth atom. There was more electron density elsewhere in tunnel A and also some in B and C.

Refinement on the niobium atoms, a bismuth at the highest electron density peak in tunnel A, all the oxygen atoms at $z \sim \frac{1}{2}$ and four of those at $z \sim 0$ reduced R to 0.23. On the basis of a difference Fourier synthesis

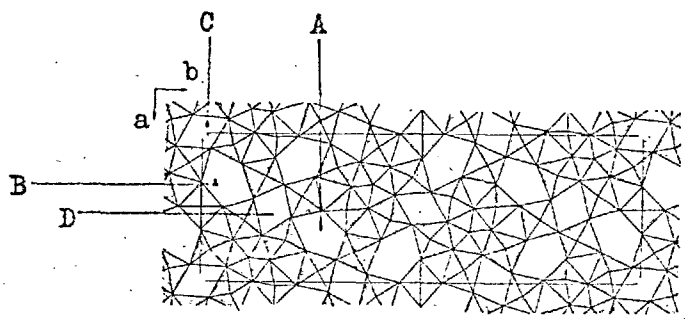


Figure 6.3

further bismuth atoms were added; one more into tunnel A and one into B and C. Although it was realised that neither tunnel was large enough for two separate bismuth atoms, it was decided to try to refine this configuration. The refinement which was otherwise normal, gave individual temperature factors of 6.0 - 9.0 for the bismuth atoms, compared with a very uniform value of approximately 1.0 for the niobiums.

In the next round of refinement the occupancies of the various bismuth sites were used as parameters. This gave occupancies ranging from 0.5 to 0.2, with temperature factors of about 2.0, and R fell to 0.18.

The correlation coefficient between occupancies and temperature factors was between 0.8 and 0.9, but refining them together did not appear to have any adverse effects. Some experimental runs with the two-dimensional data, with one or other of these fixed and with different initial values produced very similar final results. A bismuth atom in tunnel D was added to one run, but its occupancy refined to a very low level in a few cycles.

A difference Fourier synthesis indicated the need to add two further fractional occupancy bismuth atoms into tunnel B, and to allow the atom in C to move off the special position 0, 0, z thereby reducing R to 0.15.

With the complete set of intensity data (1299 reflections) and the full complement of oxygen atoms, the structure refined to R = 0.138. A weighting scheme of the type recommended by Hughes[I.10] was used throughout with F^{*} = 110. The occupancies obtained are listed in Table 6.1.

In all previous refinements inter-layer scale factors were allowed to refine. At this stage the 2kl layer photographs were used for correlation of the data. There were approximately 30 common reflections per layer. The data were brought to a common scale before the start of anisotropic refinement, although absorption errors must have reduced the accuracy of the correlation process.

Tunnel	Atom	Site Occupancy	σ		Occupancy per cell
A	Bi(1)	0.51	0.02		2.04
	Bi(10)	0.24	0.02		0.96
B	Bi(2)	0.23	0.02		0.92
	Bi(21)	0.16	0.02		0.64
	Bi(22)	0.09	0.01		0.36
C	Bi(3)	0.16	0.02		0.64
Total		1.39	0.05	(r.m.s.)	5.56

Table 6.1

A few cycles of anisotropic refinement of the metal atoms (with the bismuth occupancies fixed from the isotropic refinement) reduced R to

0.122. On removal of nine of the strongest reflections which were thought to be suffering from extinction, and the release of the oxygen atoms in block-diagonal refinement, R dropped to 0.101. A further 12 reflections were removed for extinction and R of 0.098 was reached.

A difference Fourier synthesis showed evidence of small peaks (2 - 3 e) at a site in tunnel D and one further position in tunnel A. These were far too small however for inclusion in refinement as very low occupancy bismuth sites.

At this stage it was thought that the values of the occupancies of the bismuth sites obtained from isotropic refinement in which inter-layer scales were refined, were no longer valid, since different inter-layer scales, derived from correlating data, were now used, and also the dispersion correction had not been applied previously. At this stage therefore, the real part of the dispersion correction was included for bismuth and niobium. (After the final convergence of least-squares refinement, further cycles were completed to test in which sense the imaginary part should be applied. Neither sense gave an improvement in R, or changed the positional parameters significantly. The imaginary part of the correction was therefore neglected.)

Isotropic refinement with the dispersion correction applied, and scales fixed at the "correlated" values gave a total bismuth content of 5.5 per unit cell, with the individual occupancies virtually unchanged. Table 6.2 shows these occupancies, which were fixed parameters in subseqent anisotropic refinement. It was felt that the occupancies of

the bismuth atoms could not be determined with very good precision due to the high correlation between temperature factors or scale parameters and the occupancies. The agreement between these values and those quoted in Table 6.1 (different inter-layer scales and no dispersion correction) appears to indicate however that these occupancies are real effects and not simply artefacts of neglected corrections. As a further check, some

Table 6.2 - $3Bi_2O_3.17Nb_2O_5$, Final occupancies of bismuth sites

Tunnel	Atom	Site occupancy	σ	Occupancy per cell
A	Bi(1)	0.51	0.02	2.04
	Bi(10)	0.24	0.02	0.96
B	Bi(2)	0.23	0.02	0.92
	Bi(21)	0.15	0.02	0.60
	Bi(22)	0.09	0.01	0.36
C	Bi(3)	0.16	0.02	0.64
	Total	1.38	0.05 (r.m.s.)	5.52

cycles of refinement in projection were completed, using hk0 data. Two runs, of which one had occupancies and temperature factors refining, and the other had bismuth temperature factors fixed at B=2.0 $Å^2$ but occupancies

varied, gave results which were not significantly different from one another or from those in Table 6.2.

For the final cycles of anisotropic block-diagonal least-squares refinement, the occupancies listed in Table 6.2 were retained. (The meaning and relevance of these fractions is discussed in Section 7.) Only 0.4 of the calculated shifts were applied at first, but this restriction was raised to 0.7 later on. After 12 cycles of refinement 5 parameters still had shifts greater than 0.2 (but less than 0.3) standard deviations. The five atoms concerned were then refined by full-matrix least-squares for two more cycles, when the maximum parameter change was less than 1/5 of the corresponding standard deviation.

The average shift/error for the 224 parameters refined on the last cycle was 0.05. The final value of R was 0.092 for 1279 independent reflections, 20 having been previously removed for suspected extinction.

Calculation of structure factors on the basis of the final parameters for all 1279 observed data gave R = 0.097. Structure factors were also calculated for the 608 "unobserved" reflections which were too weak to appear on the photographs. A few reflections calculated greater than the minimum observable F, but none exceeded twice F_{min}.

The final atomic positional parameters and their standard deviations are listed in Table 6.3. The final thermal parameters are given in Table 6.4, either as B for the isotropically refined oxygen atoms, or as β_{ij} for the metal atoms.

Table 6.3 - $3Bi_2O_3.17Nb_2O_5$, Final Positional Parameters and Standard Deviations.

Atom	x	σ_x	y	σ_y	z	σ_z
Bi(1)	0.7509	0.0003	0.2929	0.0001	0.060	0.002
Bi(10)	0.7367	0.0008	0.2619	0.0003	0.070	0.005
Bi(2)	0.4080	0.0007	0.0588	0.0003	0.065	0.006
Bi(21)	0.3370	0.0015	0.0362	0.0005	0.049	0.007
Bi(22)	0.2822	0.0010	0.0687	0.0004	0.081	0.008
Bi(3)	0.0228	0.0010	0.0062	0.0003	0.068	0.007
Nb(1)	0.3361	0.0003	0.39084	0.00008	0.553	0.
Nb(2)	0.0771	0.0003	0.07056	0.00009	0.565	0.003
Nb(3)	0.0779	0.0003	0.40151	0.00010	0.593	0.003
Nb(4)	0.4505	0.0003	0.23193	0.00008	0.558	0.003
Nb(5)	0.2943	0.0003	0.47821	0.00008	0.565	0.003
Nb(6)	0.2268	0.0003	0.30777	0.00009	0.575	0.003
Nb(7)	0.3002	0.0003	0.13816	0.00009	0.566	0.003
Nb(8)	0.0200	0.0003	0.17166	0.00009	0.520	0.003
Nb(9)	0.5	0.	0.0	0.	0.578	0.004
O(1)	0.337	0.002	0.0033	0.0008	0.527	0.015
O(2)	0.109	0.002	0.0196	0.0007	0.604	0.014

Table 6.3 continued

Atom	x	σ_x	y	σ_y	z	σ_z
O(3)	0.501	0.002	0.0513	0.0008	0.608	0.016
O(4)	0.442	0.002	0.1228	0.0008	0.612	0.012
O(5)	0.212	0.002	0.0917	0.0008	0.521	0.015
O(6)	-0.004	0.001	0.1176	0.0005	0.544	0.014
O(7)	0.172	0.002	0.1652	0.0008	0.636	0.010
O(8)	0.346	0.002	0.1913	0.0008	0.561	0.022
O(9)	0.293	0.003	0.2628	0.0009	0.577	0.022
O(10)	0.073	0.002	0.2940	0.0007	0.614	0.011
O(11)	0.019	0.002	0.2251	0.0008	0.516	0.013
O(12)	0.363	0.002	0.3359	0.0007	0.507	0.011
O(13)	0.190	0.002	0.3625	0.0006	0.514	0.011
O(14)	0.218	0.002	0.4300	0.0006	0.523	0.011
O(15)	0.415	0.002	0.4419	0.0006	0.520	0.011
O(16)	0.335	0.002	0.3898	0.0005	0.135	0.007
O(17)	0.078	0.002	0.0703	0.0008	-0.029	0.009
O(18)	0.077	0.004	0.4004	0.0014	0.171	0.015
O(19)	0.422	0.003	0.2320	0.0010	0.106	0.018
O(20)	0.295	0.003	0.4795	0.0009	0.162	0.011
O(21)	0.223	0.003	0.3059	0.0009	0.172	0.010

Table 6.3 continued

Atom	x	σ_x	y	σ_y	z	σ_z
O(22)	0.302	0.005	0.1428	0.0015	0.131	0.022
O(23)	0.022	0.002	0.1712	0.0008	0.087	0.018
O(24)	0.5	0.	0.0	0.	-0.048	0.014

.....

Table 6.4 - $3Bi_2O_3.17Nb_2O_5$, Final Thermal Parameters

	β_{11}*	β_{22}	β_{33}	β_{12}	β_{13}	β_{23}
Bi(1)	0.0031	0.00075	0.036	-0.00039	-0.002	0.0036
Bi(10)	0.0042	0.00076	0.036	0.00130	0.016	0.0051
Bi(2)	0.0040	0.00060	0.041	0.00057	-0.009	-0.0009
Bi(21)	0.0091	0.00062	0.033	0.00200	-0.001	-0.0007
Bi(22)	-0.0002	0.00009	0.008	0.00014	0.000	-0.0048
Bi(3)	0.0046	0.00037	0.043	-0.00011	0.010	0.0038

*coefficients in the expression $f_o \exp(-(\beta_{11}h^2 + \beta_{22}k^2 + \beta_{33}l^2 + 2\beta_{12}hk + 2\beta_{13}hl + 2\beta_{23}kl))$

Table 6.4 - continued

	β_{11}	β_{22}	β_{33}	β_{12}	β_{13}	β_{23}
Nb(1)	0.0013	0.00002	0.073	0.00009	0.004	0.0004
Nb(2)	0.0020	0.00006	0.072	0.00026	-0.003	0.0024
Nb(3)	0.0011	0.00012	0.066	-0.00004	-0.001	0.0005
Nb(4)	0.0017	0.00007	0.028	0.00000	0.003	-0.0007
Nb(5)	0.0025	0.00006	0.084	-0.00008	-0.004	0.0037
Nb(6)	0.0017	0.00017	0.071	-0.00012	0.020	-0.0001
Nb(7)	0.0013	0.00024	0.042	0.00018	0.042	0.0004
Nb(8)	0.0014	0.00003	0.098	-0.00006	0.024	0.0012
Nb(9)	0.0069	0.00032	0.013	-0.00122	0.	0.

	$B(\text{Å})^2$		$B(\text{Å}^2)$		$B(\text{Å}^2)$
O(1)	1.2	O(9)	2.0	O(17)	0.8
O(2)	1.1	O(10)	0.3	O(18)	3.8
O(3)	1.6	O(11)	1.0	O(19)	2.7
O(4)	1.2	O(12)	0.4	O(20)	1.5
O(5)	1.5	O(13)	0.2	O(21)	1.5
O(6)	0.1	O(14)	-0.1	O(22)	5.2
O(7)	0.8	O(15)	-0.1	O(23)	2.3
O(8)	1.9	O(16)	-0.8	O(24)	1.4

It is felt that the positions of the oxygen atoms at the bismuth level are less certain than the standard deviations would indicate, since the presence or absence of a bismuth atom at a neighbouring site must effect the precise position of any particular oxygen atom. This is reflected in the rather high temperature factors of two of these oxygens.

Some of the anisotropic thermal parameters are non-positive definate, and a few isotropic ones are negative. These are probably due to various errors, the most significant of which is uncorrected absorption. No attempt is made to discuss the anisotropy of the bismuth and niobium atoms.

The observed structure amplitudes and the calculated structure factors are listed in Table 6.5. (The decimal parts of F should not be regarded as significant.) Reflections marked with an asterisk are those removed from refinement for suspected extinction. Three reflections were inadvertently omitted from least-squares refinement and from Table 6.5. These are

h	k	l	F_o	F_c
1	20	0	108	99
7	41	0	102	90
0	28	2	90	115.

A final Fourier synthesis and an error synthesis were calculated. The latter showed no remarkable features. In the Fourier synthesis multiple peaks appeared for some of the oxygens in the bismuth layer, as well as two small extra peaks in tunnels A and D, possibly corresponding to very

low occupancy bismuth sites. Both these indications were noted, but refinement was not continued further.

Table 6.5

$3Bi_2O_3.17Nb_2O_5$ - Final Structure Factor List

Tabulated as:

h k l $|F_o|$ $|F_c|$ A B

* indicates a reflection affected by extinction,

and omitted from least-squares refinement

H	K	L		FO	FC	A	B
0	10	0		263.04	303.38	303.38	-0.0
0	12	0		117.03	108.04	108.04	-0.0
0	16	0		154.04	165.06	165.06	0.0
0	18	0		125.59	114.63	114.63	-0.0
0	22	0		89.30	94.87	-94.87	-0.0
0	24	0		305.99	324.22	-324.22	-0.0
0	28	0		81.66	71.86	71.86	-0.0
0	30	0	*	344.06	419.24	419.24	0.0
0	32	0		215.11	250.25	-250.25	0.0
0	36	0		48.85	63.84	63.84	-0.0
0	40	0		39.71	31.88	31.88	-0.0
0	42	0		259.10	241.00	241.00	-0.0
0	44	0		115.23	100.88	100.88	-0.0
1	0	0		334.10	361.92	-361.92	-0.0
1	11	0		185.49	218.08	218.08	-0.0
1	12	0	*	492.33	640.49	640.49	0.0
1	16	0		130.68	132.28	-132.28	0.0
1	17	0		108.39	100.73	100.73	0.0
1	19	0		58.38	47.14	-47.14	-0.0
1	21	0	*	465.53	541.19	-541.19	-0.0
1	22	0		237.20	203.09	203.09	-0.0
1	24	0		99.20	106.41	-106.41	-0.0
1	26	0		139.27	121.51	-121.51	-0.0
1	27	0		52.94	51.95	51.95	-0.0
1	28	0		126.30	122.04	122.04	-0.0
1	29	0		93.58	79.07	79.07	-0.0
1	30	0		221.45	214.45	-214.45	0.0
1	31	0		201.73	203.18	-203.18	0.0
1	33	0		112.28	107.56	-107.56	-0.0
1	34	0		139.57	142.64	-142.64	-0.0
1	36	0		197.55	197.08	-197.08	-0.0
1	39	0		135.83	139.90	-139.90	-0.0
1	40	0		68.49	61.20	-61.20	-0.0
1	41	0		103.75	96.58	96.58	-0.0
1	42	0		62.32	51.94	51.94	0.0
1	43	0		92.64	85.48	-85.48	0.0
1	44	0		100.52	117.79	-117.79	0.0
1	45	0		155.47	161.48	161.48	0.0
1	46	0		93.05	68.44	-68.44	-0.0
2	6	0		148.82	153.31	-153.31	-0.0
2	7	0		46.41	41.84	-41.84	0.0
2	8	0		27.41	13.20	-13.20	0.0
2	9	0		435.94	441.61	441.61	0.0
2	10	0		115.44	111.51	-111.51	-0.0
2	11	0		181.47	168.28	168.28	-0.0
2	12	0		435.33	440.68	440.68	-0.0
2	13	0		88.82	92.73	-92.73	-0.0
2	15	0		125.43	108.47	-108.47	-0.0
2	16	0		49.80	39.97	39.97	0.0
2	17	0		89.20	69.36	-69.36	0.0
2	18	0	*	510.17	577.61	577.61	-0.0
2	19	0		89.02	91.28	91.28	-0.0
2	20	0		145.09	134.11	-134.11	-0.0
2	22	0		251.25	246.80	246.80	-0.0
2	23	0		102.85	93.66	93.66	-0.0
2	24	0		177.61	172.57	172.57	0.0
2	25	0		120.22	114.66	-114.66	-0.0
2	27	0		80.99	73.68	73.69	-0.0
2	30	0		154.73	171.12	171.12	-0.0
2	33	0		228.11	260.58	-260.58	-0.0
2	34	0		147.97	149.12	149.12	0.0
2	35	0		105.26	96.93	-96.93	-0.0
2	36	0		135.61	149.78	-149.78	0.0
2	37	0		95.51	81.08	81.08	0.0
2	38	0		108.44	103.13	-103.13	-0.0
2	39	0		198.44	237.81	237.81	0.0
2	40	0		187.16	205.71	205.71	-0.0
2	43	0		157.08	172.78	-172.78	-0.0
2	44	0		85.21	87.78	-87.78	-0.0
2	45	0		55.45	60.38	-60.38	-0.0
2	46	0		96.16	95.24	-95.24	-0.0
3	1	0		58.59	49.14	-49.14	-0.0
3	3	0		307.35	318.00	-318.00	-0.0
3	4	0		90.44	82.73	-82.73	0.0
3	5	0		114.10	118.68	118.68	0.0
3	6	0		400.50	387.96	-387.96	-0.0
3	8	0		216.00	217.22	-217.22	-0.0
3	9	0		411.83	408.66	-408.66	-0.0
3	10	0		125.57	119.85	119.85	-0.0
3	12	0		80.20	66.52	66.52	-0.0
3	15	0		316.63	303.25	303.25	-0.0
3	17	0		96.04	69.92	-69.92	0.0
3	18	0		531.41	564.92	-564.92	-0.0
3	19	0		159.26	148.54	-148.54	-0.0
3	21	0		66.03	49.24	49.24	0.0
3	23	0		297.25	279.60	279.60	-0.0
3	24	0		228.77	226.93	226.93	-0.0
3	25	0		55.70	51.05	-51.05	-0.0
3	26	0		87.91	77.71	77.71	-0.0
3	28	0		202.70	190.37	-190.37	0.0
3	29	0		135.19	124.02	124.02	0.0
3	30	0		169.25	138.50	138.50	0.0
3	31	0		92.88	75.24	75.24	-0.0
3	32	0		103.32	93.68	-93.68	-0.0
3	34	0		132.00	128.41	128.41	0.0
3	37	0		109.55	105.48	-105.48	0.0
3	39	0		203.44	198.61	-198.61	-0.0
3	40	0		114.34	116.97	116.97	-0.0
3	41	0		111.83	113.42	113.42	-0.0
3	43	0		96.96	87.03	-87.03	-0.0
3	45	0		100.34	99.99	-99.99	-0.0
4	0	0	*	334.02	466.77	466.77	-0.0
4	1	0		145.22	171.98	-171.98	0.0
4	2	0		272.14	315.37	-319.37	0.0

H	K	L		FO	FC	A	B
4	3	0	*	409.56	549.37	-549.37	-0.0
4	4	0		270.24	315.89	315.89	-0.0
4	5	0		91.60	90.49	90.49	-0.0
4	6	0		299.40	311.75	311.75	0.0
4	10	0		132.36	121.36	121.36	-0.0
4	11	0		192.33	230.98	-230.98	0.0
4	12	0		40.37	25.90	25.90	0.0
4	13	0		213.25	209.89	-209.89	-0.0
4	14	0		115.04	114.38	114.38	-0.0
4	15	0		189.47	189.72	-189.72	0.0
4	16	0		146.62	124.22	124.22	-0.0
4	18	0		86.35	84.14	-84.14	-0.0
4	19	0		62.79	64.64	-64.64	-0.0
4	21	0		148.25	122.45	-122.45	-0.0
4	22	0		116.34	97.97	97.97	-0.0
4	23	0		77.40	62.79	62.79	-0.0
4	24	0		134.40	111.66	111.66	-0.0
4	27	0	*	370.87	420.83	420.83	-0.0
4	28	0		102.64	88.43	-88.43	-0.0
4	29	0		137.13	118.91	-118.91	-0.0
4	30	0		97.91	83.05	83.05	-0.0
4	31	0		151.01	160.62	-160.62	-0.0
4	32	0		85.47	66.41	-66.41	-0.0
4	34	0		127.36	124.16	124.16	0.0
4	35	0		132.90	144.18	144.18	-0.0
4	36	0		59.84	55.46	55.46	-0.0
4	37	0		85.09	82.38	82.38	-0.0
4	39	0		149.03	136.34	136.34	-0.0
4	40	0		55.11	53.15	53.15	-0.0
4	42	0		117.34	129.92	129.92	-0.0
5	2	0		199.33	211.84	-211.84	0.0
5	3	0		32.56	14.91	14.91	-0.0
5	4	0		72.28	67.83	67.83	-0.0
5	8	0		226.80	216.85	216.85	-0.0
5	9	0		225.71	190.01	190.01	-0.0
5	10	0		162.60	136.75	-136.75	-0.0
5	11	0		174.30	164.21	164.21	0.0
5	12	0		287.00	279.93	279.93	-0.0
5	13	0		168.12	139.10	-139.10	0.0
5	14	0		181.91	142.67	-142.67	-0.0
5	15	0	*	504.25	587.40	-587.40	-0.0
5	16	0		224.69	198.77	198.79	-0.0
5	17	0		105.04	81.46	81.46	-0.0
5	18	0		243.36	224.98	-224.98	-0.0
5	19	0		157.03	140.12	140.12	0.0
5	20	0		237.32	219.00	-219.00	0.0
5	21	0		178.61	162.92	-162.92	-0.0
5	22	0		78.77	78.37	78.37	-0.0
5	23	0		53.22	40.73	-40.73	-0.0
5	24	0		124.79	118.15	118.15	0.0
5	25	0		150.65	121.08	-121.08	-0.0
5	27	0		319.33	271.28	-271.28	-0.0
5	28	0		81.46	63.24	63.24	0.0
5	29	0		82.12	73.86	-73.86	0.0
5	30	0		289.17	269.40	-269.40	0.0
5	31	0		144.68	142.29	-142.29	-0.0
5	34	0		105.37	109.88	109.88	0.0
5	35	0		73.11	69.16	69.19	-0.0
5	36	0		135.00	125.52	-125.52	0.0
5	37	0		74.67	76.67	-76.67	0.0
5	39	0		75.72	86.71	86.71	-0.0
5	40	0		147.68	142.21	-142.21	-0.0
5	41	0		51.62	39.51	39.51	0.0
5	42	0		117.02	126.13	126.13	0.0
5	43	0		98.84	116.68	-116.68	0.0
6	0	0		135.59	152.28	-152.28	0.0
6	1	0		46.83	54.09	-54.09	0.0
6	2	0		150.05	145.43	145.43	-0.0
6	4	0		144.31	132.35	-132.35	-0.0
6	5	0		136.66	118.04	118.04	-0.0
6	6	0	*	384.10	440.68	440.68	-0.0
6	7	0		150.73	139.10	-139.10	-0.0
6	8	0	*	311.39	354.38	354.38	-0.0
6	9	0	*	378.95	439.75	439.75	-0.0
6	10	0		58.71	52.85	-52.85	-0.0
6	11	0		112.40	113.24	113.24	-0.0
6	12	0		79.19	70.74	70.74	-0.0
6	13	0		89.43	71.96	-71.96	-0.0
6	14	0		250.13	220.83	-220.83	-0.0
6	15	0		285.51	251.51	251.51	-0.0
6	17	0		129.30	103.09	103.09	-0.0
6	18	0		274.04	232.41	232.41	-0.0
6	19	0		61.45	62.71	62.71	-0.0
6	20	0		59.45	54.09	-54.09	0.0
6	21	0		98.92	95.17	-95.17	-0.0
6	22	0		134.79	116.14	116.14	0.0
6	23	0		106.56	102.07	102.07	-0.0
6	24	0		131.25	161.61	161.61	0.0
6	25	0		100.81	87.75	-87.75	-0.0
6	26	0		65.18	56.00	56.00	-0.0
6	28	0		163.34	161.52	161.52	0.0
6	29	0		88.28	75.23	-75.23	-0.0
6	30	0		135.80	122.98	-122.98	0.0
6	32	0		133.61	133.29	-133.29	-0.0
6	33	0		182.38	184.58	-184.58	-0.0
6	34	0		79.25	87.68	87.68	-0.0
6	36	0		310.73	324.42	324.42	-0.0
6	37	0		135.57	142.61	-142.61	-0.0
6	40	0		68.31	67.16	-67.16	-0.0
6	42	0		107.96	122.97	-122.97	0.0
6	43	0		102.09	115.39	-115.39	-0.0
7	1	0		82.49	83.52	83.52	-0.0
7	3	0	*	423.57	536.19	-536.19	0.0
7	4	0		191.16	199.69	199.69	-0.0

H	K	L	FO	FC	A	B
7	5	0	136.67	115.76	-115.75	-0.0
7	6	0	50.91	28.04	28.04	-0.0
7	7	0	45.35	20.25	-20.25	-0.0
7	8	0	171.59	157.59	-157.59	0.0
7	9	0	143.65	123.08	123.08	-0.0
7	10	0	141.17	115.30	115.30	-0.0
7	12	0	57.91	52.57	52.57	-0.0
7	13	0	178.41	148.22	-148.22	-0.0
7	14	0	128.19	121.03	-121.03	-0.0
7	15	0	151.27	133.40	-133.40	-0.0
7	16	0	106.96	87.37	87.37	-0.0
7	17	0	71.57	63.13	63.13	0.0
7	18	0	117.61	97.76	-97.76	-0.0
7	19	0	104.46	85.56	85.56	-0.0
7	20	0	230.59	216.85	216.85	-0.0
7	21	0	196.63	186.43	186.43	0.0
7	24	0	184.84	157.37	-157.37	0.0
7	25	0	127.91	106.97	-106.97	-0.0
7	26	0	73.08	64.20	-64.20	-0.0
7	29	0	75.92	74.97	74.97	0.0
7	30	0	81.25	63.29	63.29	-0.0
7	31	0	82.97	76.10	76.10	-0.0
7	32	0	200.66	187.22	-187.22	-0.0
7	33	0	181.51	155.13	-155.13	0.0
7	35	0	102.11	94.30	94.30	-0.0
7	36	0	145.85	164.34	-164.34	0.0
7	39	0	83.93	80.10	-80.10	-0.0
7	42	0	75.97	102.08	-102.08	-0.0
7	43	0	69.02	71.73	-71.73	-0.0
8	0	0	168.53	178.19	-178.19	0.0
8	1	0	163.66	156.30	156.30	-0.0
8	2	0	170.92	158.64	-158.64	-0.0
8	3	0	75.37	53.96	53.96	-0.0
8	4	0	179.90	185.36	185.36	-0.0
8	5	0	99.44	88.00	88.00	0.0
8	6	0	236.62	233.18	233.18	0.0
8	7	0	247.86	273.42	-273.42	-0.0
8	8	0	187.12	175.50	-175.50	0.0
8	9	0	271.92	255.53	-255.53	0.0
8	10	0	129.37	123.93	123.93	-0.0
8	11	0	191.05	156.83	156.83	-0.0
8	13	0	74.69	66.47	66.47	-0.0
8	15	0	143.18	131.06	-131.06	-0.0
8	16	0	87.83	80.41	80.41	-0.0
8	18	0	154.19	109.93	109.93	-0.0
8	19	0	168.50	159.22	-159.22	0.0
8	20	0	138.30	110.34	110.34	-0.0
8	21	0	150.85	121.64	121.64	0.0
8	24	0	297.65	297.05	297.05	-0.0
8	25	0	267.45	293.35	-293.35	-0.0
8	27	0	160.61	153.39	153.39	-0.0
8	30	0	116.81	103.66	-103.65	0.0
8	31	0	119.65	121.18	121.18	-0.0
8	33	0	171.87	183.90	183.90	-0.0
8	34	0	69.64	83.60	83.60	-0.0
8	36	0	58.51	66.43	66.43	-0.0
8	37	0	65.47	58.16	-58.15	0.0
8	38	0	46.61	24.62	-24.62	-0.0
8	39	0	78.31	64.34	64.34	-0.0
8	40	0	52.97	26.15	26.15	-0.0
9	1	0	81.60	66.78	-66.78	-0.0
9	3	0	84.29	74.56	74.56	0.0
9	4	0	159.46	150.33	150.33	-0.0
9	5	0	138.67	127.37	127.37	-0.0
9	6	0	175.36	177.51	-177.51	-0.0
9	8	0	83.94	74.27	74.27	-0.0
9	9	0	96.16	81.08	81.08	0.0
9	10	0	143.08	134.50	-134.50	-0.0
9	11	0	134.88	110.40	-110.40	-0.0
9	12	0	301.08	258.60	-258.60	-0.0
9	13	0	161.04	148.41	148.41	-0.0
9	14	0	231.50	228.96	-228.95	-0.0
9	15	0	301.39	278.85	-278.85	-0.0
9	16	0	157.44	145.27	145.27	-0.0
9	18	0	81.88	84.84	84.84	-0.0
9	19	0	182.56	168.12	-168.12	-0.0
9	20	0	73.10	65.80	-65.80	0.0
9	23	0	92.27	84.48	84.48	0.0
9	24	0	138.30	125.36	-125.35	0.0
9	26	0	138.94	139.82	-139.82	-0.0
9	27	0	197.02	217.07	-217.07	0.0
9	28	0	111.66	132.55	132.55	-0.0
9	32	0	68.89	83.77	83.77	-0.0
9	33	0	84.55	64.69	64.68	-0.0
9	37	0	147.58	189.51	-189.51	0.0
9	38	0	122.80	129.97	129.97	-0.0
10	0	0	87.14	69.85	69.85	-0.0
10	1	0	130.32	126.01	-126.01	0.0
10	2	0	279.92	278.60	278.60	-0.0
10	3	0	162.78	155.81	155.81	0.0
10	4	0	104.03	81.67	-81.67	-0.0
10	5	0	131.24	121.71	121.71	-0.0
10	6	0	198.03	163.54	163.54	-0.0
10	7	0	109.25	113.96	-113.95	-0.0
10	10	0	118.72	122.68	-122.68	-0.0
10	11	0	75.38	67.97	-67.97	0.0
10	12	0	81.73	77.22	77.22	0.0
10	13	0	79.03	62.82	-62.82	-0.0
10	14	0	107.69	91.81	91.81	0.0
10	15	0	223.60	222.99	222.99	-0.0
10	18	0	134.10	138.26	-138.25	-0.0
10	20	0	75.84	64.02	-64.02	-0.0
10	22	0	52.83	41.37	41.37	-0.0
10	26	0	218.10	221.75	-221.75	0.0

H	K	L	FO	FC	A	B
10	27	0	104.59	101.70	-101.70	-0.01
10	32	0	56.38	56.28	56.28	-0.00
10	33	0	173.44	146.01	146.01	-0.00
10	34	0	55.25	45.28	-45.28	-0.00
10	35	0	84.50	89.58	89.58	-0.00
10	36	0	80.81	95.75	95.75	-0.00
11	2	0	185.10	160.06	-160.05	-0.00
11	3	0	120.38	106.11	-106.11	-0.00
11	5	0	76.24	75.91	75.91	-0.00
11	6	0	295.51	297.58	297.58	0.00
11	7	0	169.31	164.86	-164.85	0.00
11	10	0	62.42	53.57	53.57	0.00
11	12	0	120.72	116.19	-116.19	-0.01
11	16	0	179.39	186.08	186.08	-0.00
11	17	0	89.12	103.06	103.06	-0.00
11	18	0	111.40	110.84	110.84	-0.00
11	19	0	121.92	129.11	-129.11	-0.01
11	21	0	92.65	92.03	-92.03	-0.01
11	22	0	70.36	55.61	-55.61	-0.00
11	23	0	105.34	126.37	-126.37	0.00
11	24	0	196.44	208.75	-208.75	0.00
11	25	0	92.54	84.92	84.92	-0.00
11	27	0	139.58	119.22	119.22	-0.00
11	29	0	100.17	77.72	-77.72	-0.00
11	30	0	135.06	139.80	-139.80	0.00
11	32	0	102.47	77.52	-77.52	-0.00
11	33	0	106.37	113.46	-113.45	-0.00
11	34	0	74.07	92.43	92.89	0.00
12	0	0	159.64	150.74	150.74	-0.00
12	2	0	61.99	54.16	54.16	-0.00
12	3	0	81.95	67.43	67.43	-0.00
12	4	0	127.60	117.82	-117.82	-0.00
12	5	0	53.53	44.88	44.83	0.00
12	6	0	191.24	148.85	-168.85	0.00
12	8	0	118.92	102.83	-102.83	-0.00
12	10	0	192.74	202.04	202.04	0.00
12	13	0	91.94	90.89	-90.89	0.00
12	17	0	169.39	168.84	168.84	-0.01
12	18	0	201.29	210.08	210.08	-0.00
12	19	0	178.34	183.22	-183.22	-0.00
12	20	0	177.83	170.08	170.08	-0.01
12	21	0	99.12	97.00	97.00	-0.00
12	22	0	131.52	118.33	-118.33	0.00
12	23	0	55.96	56.16	56.16	0.00
12	24	0	59.22	61.99	61.99	-0.00
12	25	0	92.98	88.23	-88.23	-0.00
12	28	0	162.73	183.65	183.65	-0.00
12	30	0	66.43	63.69	63.69	-0.00
13	3	0	50.79	53.68	-53.68	-0.00
13	4	0	107.46	108.92	108.92	-0.00
13	5	0	123.67	142.60	-142.60	-0.01
13	6	0	213.28	217.08	-217.08	0.00
13	8	0	134.58	120.66	-120.65	0.00
13	10	0	95.76	88.09	88.09	-0.00
13	11	0	196.70	194.83	-194.83	-0.00
13	12	0	110.56	102.92	-102.92	0.00
13	13	0	126.49	117.24	117.24	-0.00
13	14	0	84.99	69.14	-69.14	-0.00
13	16	0	89.80	77.93	-77.93	-0.00
13	17	0	87.88	96.87	96.87	-0.00
13	19	0	81.67	79.25	-79.25	-0.00
13	20	0	87.33	86.46	-86.45	-0.00
13	21	0	79.64	78.22	-78.22	-0.00
13	22	0	85.14	85.35	85.35	-0.01
13	24	0	43.62	45.46	-45.46	0.00
13	26	0	88.53	86.78	-86.78	-0.00
13	27	0	83.32	81.24	81.24	-0.00
14	0	0	132.41	139.93	139.93	-0.01
14	1	0	205.51	201.55	-201.55	-0.00
14	2	0	140.86	137.85	137.85	0.00
14	3	0	86.48	78.93	78.93	0.00
14	4	0	84.12	57.35	-57.35	-0.00
14	7	0	88.02	85.91	-85.91	0.00
14	8	0	66.54	45.62	-45.62	-0.00
14	11	0	78.17	68.53	68.53	-0.00
14	12	0	85.42	71.89	71.89	0.00
14	13	0	80.40	77.84	-77.84	-0.01
14	15	0	69.81	72.02	-72.02	-0.00
14	16	0	64.24	58.54	58.54	-0.00
14	17	0	105.44	113.66	-113.66	0.00
14	18	0	80.66	78.93	-78.93	-0.00
14	21	0	142.68	135.95	135.95	-0.00
15	2	0	50.05	39.03	39.03	-0.01
15	3	0	115.31	105.38	105.38	-0.00
15	4	0	57.72	48.54	-48.54	-0.00
15	5	0	144.42	132.00	132.00	-0.00
15	6	0	61.87	35.44	35.44	-0.00
15	7	0	128.54	103.96	-103.76	0.00
15	8	0	155.96	132.67	-132.67	-0.00
15	9	0	115.69	100.20	-100.20	-0.00
15	10	0	182.50	172.69	172.69	-0.00
15	12	0	89.58	87.56	87.56	-0.00
15	15	0	80.81	65.32	65.32	-0.00
0	8	1	148.98	156.54	-142.16	-65.54
0	10	1	157.55	150.33	-127.18	-80.15
0	12	1	181.05	191.90	-176.35	-74.25
0	14	1	142.74	146.06	145.92	4.87
0	16	1	70.42	59.45	-51.52	-29.67
0	20	1	150.39	169.84	168.15	23.91
0	22	1	83.93	95.52	-73.48	-54.46
0	24	1	309.00	331.74	318.71	92.08
0	30	1	192.57	215.60	-211.32	-42.74
0	32	1	157.01	164.42	159.44	40.13
0	34	1	144.94	149.38	111.55	99.36

H	K	L		FO	FC	A	B
0	36	1		135.28	140.11	-140.10	-1.65
0	40	1		88.49	93.27	-75.20	-50.84
0	42	1		247.48	221.22	-197.91	-99.03
0	44	1		86.43	88.49	-81.62	-34.17
1	7	1		89.50	97.36	80.63	54.58
1	8	1		170.43	179.76	154.06	90.67
1	9	1	*	346.72	383.96	357.07	141.17
1	10	1		138.39	124.68	-117.29	-42.27
1	12	1		237.37	259.60	-243.78	-89.25
1	13	1		79.17	88.55	87.88	10.82
1	14	1		48.20	46.24	44.91	10.99
1	15	1		66.46	52.61	50.40	-15.11
1	16	1		48.00	27.02	26.33	6.10
1	17	1		64.03	44.64	-43.97	9.27
1	18	1		77.84	85.55	81.07	27.32
1	20	1		133.63	134.96	-131.36	-31.04
1	21	1	*	372.85	422.51	394.72	150.72
1	22	1		158.67	167.15	-133.65	-100.38
1	23	1		84.87	89.51	63.05	63.53
1	24	1		194.63	193.64	187.30	49.14
1	25	1		69.52	70.97	69.89	12.35
1	28	1		85.56	79.56	70.81	36.27
1	31	1		144.19	136.93	121.48	63.18
1	32	1		73.78	86.13	83.21	22.24
1	33	1		53.97	52.15	47.90	20.64
1	36	1		120.40	116.24	115.18	15.64
1	39	1		146.18	130.54	126.11	33.68
1	41	1		74.33	59.98	-59.72	-5.61
1	43	1		109.27	92.73	88.10	28.93
1	44	1		95.78	63.77	51.30	37.88
1	45	1		148.68	126.39	-116.05	-50.08
2	5	1		125.59	123.59	108.30	69.33
2	6	1		234.78	252.74	221.80	121.18
2	7	1		146.67	125.30	116.83	45.30
2	8	1		95.81	89.26	88.06	14.60
2	9	1		248.54	268.05	-248.16	-101.32
2	11	1		141.64	141.28	-130.85	-53.26
2	12	1		74.84	75.85	-75.82	2.23
2	13	1		44.97	44.72	-42.61	13.56
2	14	1		65.12	53.04	-19.66	-49.26
2	16	1		87.90	90.19	89.08	14.12
2	17	1		33.00	13.50	-1.91	-13.37
2	18	1		294.13	295.23	-285.39	-75.61
2	20	1		78.98	73.00	72.58	-7.78
2	23	1		69.19	66.12	-52.94	-39.62
2	24	1		194.70	203.53	-196.84	-51.73
2	25	1		51.57	51.58	51.42	-4.06
2	27	1		100.89	100.83	-87.33	-50.39
2	30	1		181.03	185.71	-160.57	-93.29
2	32	1		71.37	65.21	65.01	-5.17
2	33	1		188.77	205.44	193.27	69.66
2	34	1		181.32	196.81	-172.01	-91.44
2	35	1		95.66	103.22	98.81	29.86
2	36	1		234.85	245.02	228.71	87.90
2	38	1		55.38	62.33	59.74	-17.79
2	39	1		188.31	173.98	-165.77	-52.79
2	40	1		160.89	140.45	-115.62	-79.74
2	43	1		111.80	112.17	95.40	59.01
2	44	1		55.41	61.30	56.36	-24.11
3	1	1		169.54	185.01	154.84	101.26
3	2	1		89.02	87.59	79.79	36.13
3	3	1		308.62	306.00	292.90	88.59
3	4	1		207.99	233.01	-224.77	-61.42
3	6	1	*	342.89	417.33	391.42	144.74
3	8	1		110.45	108.81	-103.14	-34.67
3	9	1		233.38	229.62	220.66	63.53
3	10	1		87.85	85.00	83.19	17.45
3	12	1		56.00	41.61	-29.82	-29.02
3	14	1		72.21	63.27	62.92	6.61
3	15	1		210.32	211.19	-198.68	-71.62
3	16	1		134.61	129.85	110.43	68.31
3	17	1		77.55	70.29	35.00	60.95
3	18	1		330.75	314.67	278.50	146.48
3	19	1		148.77	144.87	130.63	62.63
3	22	1		58.76	51.72	-50.64	-10.51
3	23	1		160.03	160.19	-157.66	-28.33
3	24	1		299.77	319.46	-288.77	-136.62
3	25	1		63.26	69.56	66.85	19.15
3	27	1		57.72	58.08	55.57	-16.87
3	29	1		45.42	47.35	19.32	43.56
3	29	1		53.12	56.97	-55.90	-10.99
3	34	1		67.95	63.02	-49.16	-39.43
3	38	1		117.66	127.64	-114.18	-57.05
3	39	1		189.42	161.90	155.44	45.26
3	40	1		102.90	88.92	-82.45	-33.28
3	41	1		105.82	97.60	-95.59	-19.71
3	42	1		67.10	77.62	-66.47	-40.09
3	43	1		69.86	70.90	70.15	10.23
3	44	1		45.58	50.89	50.82	2.60
3	45	1		47.41	50.10	50.07	1.62
4	0	1		40.49	49.17	-47.67	11.84
4	1	1		133.69	129.06	120.93	46.08
4	2	1		51.19	56.67	-30.01	-43.08
4	3	1		269.59	289.73	267.45	111.42
4	5	1		44.94	46.48	-39.24	24.91
4	6	1		167.80	153.93	-146.55	-47.27
4	7	1		53.26	59.14	-42.78	-40.54
4	8	1		41.91	50.89	47.93	-17.11
4	10	1		153.90	148.66	141.03	47.03
4	11	1		67.17	57.70	56.83	9.93
4	12	1		36.51	32.02	-32.01	1.44
4	13	1		101.77	96.43	96.38	3.17
4	14	1		95.44	93.80	93.30	9.75
4	15	1		75.71	54.22	39.36	44.25

H	K	L		FO	FC	A	B
4	16	1		114.73	104.67	-85.82	-59.96
4	20	1		136.37	131.60	130.75	14.95
4	21	1		167.66	143.74	136.33	45.54
4	22	1		195.13	200.95	-184.77	-74.71
4	26	1		51.76	35.51	-19.47	-29.35
4	27	1		299.49	333.12	-313.96	-113.84
4	28	1		102.79	109.03	105.73	26.66
4	31	1		66.10	64.24	63.81	13.67
4	33	1		68.01	52.73	-52.39	-5.97
4	34	1		43.25	34.25	-32.32	-11.40
4	35	1		153.15	150.46	-142.48	-49.36
4	36	1		141.43	141.24	-128.36	-57.71
4	37	1		86.70	89.41	-54.67	-70.82
4	38	1		40.47	38.42	38.32	4.22
4	39	1		99.98	110.80	-91.99	-61.77
4	40	1		47.59	47.07	-47.37	-3.18
4	41	1		58.67	52.68	-42.92	-33.54
4	42	1		30.80	23.62	-20.99	-13.49
4	44	1		50.40	41.73	41.56	3.74
5	1	1		69.30	79.47	54.25	53.07
5	2	1		31.62	40.04	17.35	-35.03
5	3	1		67.34	43.45	35.01	25.73
5	4	1		141.19	141.72	110.25	89.05
5	5	1		57.68	51.33	38.33	37.29
5	6	1		187.31	181.95	-169.02	-67.36
5	8	1		79.19	80.89	78.35	20.09
5	9	1		130.14	126.68	-117.64	-46.98
5	10	1		42.43	37.21	36.08	9.13
5	11	1		168.70	145.41	-139.34	-41.55
5	12	1		135.85	137.04	-116.04	-72.90
5	13	1		179.61	156.01	146.12	54.66
5	14	1		152.45	146.17	143.67	26.91
5	15	1		441.41	456.14	435.18	136.69
5	16	1		275.61	268.66	-261.05	-63.48
5	17	1		96.68	95.03	80.51	51.48
5	18	1		168.91	163.07	147.95	68.57
5	19	1		73.67	51.62	-42.27	-29.63
5	21	1		248.03	227.03	219.95	59.66
5	22	1		132.46	125.78	-104.91	-69.38
5	24	1		66.30	45.85	-38.00	-25.65
5	25	1		78.29	82.50	69.91	43.80
5	26	1		92.31	99.42	-80.95	-57.71
5	27	1		106.61	125.19	106.03	66.56
5	28	1		83.29	78.80	61.06	49.80
5	30	1		89.45	99.13	93.39	33.42
5	31	1		32.11	32.72	31.28	15.37
5	32	1		67.32	74.71	74.22	8.52
5	34	1		101.20	128.86	-126.71	-23.43
5	36	1		92.74	89.56	88.38	14.22
5	37	1		98.70	111.39	93.78	60.11
5	39	1		97.40	82.13	-80.49	-16.34
5	40	1		87.20	77.22	64.75	41.78
5	41	1		75.54	67.57	-67.39	-4.89
5	42	1		77.08	72.93	-72.47	-6.10
5	43	1		59.97	58.64	55.45	19.09
6	0	1		165.95	178.48	-176.05	-27.34
6	2	1		137.47	153.55	143.58	54.43
6	3	1		65.30	61.92	57.55	22.55
6	5	1		138.54	136.09	-133.24	-27.71
6	6	1		156.86	136.63	-126.31	-52.79
6	7	1		110.08	120.01	118.13	21.15
6	8	1		170.08	109.83	-100.29	-44.76
6	9	1		374.06	395.46	-369.51	-140.91
6	11	1		81.52	74.09	-70.04	-24.03
6	12	1		80.15	74.60	65.12	36.39
6	15	1		143.40	117.16	-105.43	-51.09
6	17	1		82.03	83.42	-79.31	-28.74
6	18	1		208.51	197.33	-182.98	-73.86
6	21	1		56.71	45.85	42.26	17.77
6	22	1		54.43	51.37	49.61	-13.35
6	23	1		131.68	135.16	-121.08	-60.09
6	24	1		108.74	121.75	-114.51	-41.56
6	26	1		81.89	80.64	80.62	2.07
6	27	1		53.92	57.36	-44.92	-35.67
6	29	1		73.90	69.59	-69.50	-3.52
6	29	1		68.61	57.30	54.19	18.62
6	30	1		65.47	58.79	57.87	10.38
6	32	1		183.09	171.18	163.37	51.11
6	33	1		182.03	172.05	159.19	65.27
6	34	1		167.50	189.67	-149.72	-72.33
6	36	1		182.26	187.71	-175.85	-65.67
6	37	1		95.78	90.80	89.80	13.40
6	38	1		74.12	70.82	-64.04	-30.25
6	39	1		88.51	79.97	-77.63	-19.17
6	40	1		82.43	76.49	62.09	44.66
6	42	1		96.82	85.77	71.19	47.83
7	2	1		150.51	174.23	154.20	85.32
7	3	1	*	360.34	415.37	392.24	135.67
7	4	1		253.98	274.67	-259.69	-89.46
7	5	1		77.25	76.39	62.32	44.17
7	6	1		188.33	198.95	188.70	63.03
7	8	1		199.67	216.39	-192.11	-95.86
7	9	1		110.41	125.14	-106.28	-56.06
7	12	1		170.62	174.44	-162.71	-62.87
7	13	1		159.77	168.98	138.56	96.73
7	15	1		231.56	201.37	186.12	76.85
7	16	1		52.24	48.35	-44.08	-19.87
7	20	1		132.01	89.83	-74.37	-50.39
7	21	1		181.15	207.73	-185.97	-92.56
7	22	1		57.65	66.00	46.28	47.05
7	24	1		95.45	84.84	84.75	3.77
7	26	1		111.25	124.11	120.09	31.31
7	28	1		122.52	126.99	-118.72	-45.07
7	29	1		62.07	68.16	-65.96	-17.23

H	K	L		FO	FC	A	B
7	32	1		53.06	54.17	45.43	29.19
7	33	1		162.13	147.82	147.48	10.00
7	35	1		47.83	42.59	-39.57	-16.54
7	36	1		125.79	127.09	117.50	46.40
7	39	1		82.98	73.02	72.00	12.16
7	41	1		46.71	66.17	60.11	27.67
8	0	1	*	270.31	339.86	307.22	145.33
8	1	1		119.86	132.70	-111.70	-71.64
8	2	1		36.46	80.37	-58.54	-55.06
8	3	1		118.19	124.36	-115.55	-45.97
8	5	1		112.21	118.52	-104.96	-55.05
8	6	1		196.64	186.86	-169.61	-78.41
8	7	1		157.31	144.20	138.20	41.14
8	8	1		102.83	118.16	117.67	10.81
8	9	1		252.98	260.69	244.93	89.26
8	11	1		62.70	64.95	-64.60	-5.67
8	12	1		94.62	92.17	-91.48	-11.29
8	14	1		117.67	124.97	118.16	40.68
8	15	1		60.95	44.19	40.76	17.06
8	16	1		91.58	81.67	-72.55	-37.50
8	18	1		83.83	77.33	-72.49	-26.92
8	21	1		171.08	163.52	-157.33	-44.60
8	23	1		96.93	100.53	-98.81	-47.11
8	24	1		122.74	137.34	-133.24	-33.31
8	25	1		187.81	211.46	202.30	61.54
8	26	1		86.71	83.04	-70.24	-44.30
8	27	1		104.24	109.42	-105.62	-28.56
8	30	1		124.03	122.79	103.65	65.84
8	31	1		95.81	84.98	-74.01	-41.78
8	32	1		120.54	131.31	-112.04	-68.48
8	33	1		173.24	173.80	-161.05	-65.33
8	36	1		132.91	131.78	-110.97	-71.07
8	38	1		76.34	78.16	77.80	-7.47
8	39	1		50.88	54.99	-54.48	-7.46
9	4	1		73.11	81.00	70.85	39.25
9	8	1		62.57	54.68	53.76	-9.96
9	11	1		96.65	85.87	71.32	47.82
9	12	1		148.11	134.62	125.59	48.48
9	13	1		123.57	129.98	-126.72	-28.92
9	14	1		156.79	174.74	162.29	64.76
9	15	1		130.54	141.32	134.99	41.85
9	16	-1		179.60	200.62	-186.50	-73.93
9	19	1		60.34	70.80	68.50	17.92
9	21	1		83.40	73.88	72.16	15.86
9	22	1		46.42	46.21	41.98	33.36
9	23	1		67.87	59.44	-59.25	4.86
9	24	1		116.45	110.21	92.31	60.20
9	25	1		81.94	80.43	65.48	46.71
9	27	1		150.88	150.75	138.88	58.64
9	28	1		97.50	83.57	-79.97	-24.26
9	29	1		77.45	72.49	62.43	36.85
9	30	1		150.88	142.91	-126.54	-66.41
9	36	1		48.77	46.66	45.22	11.50
9	37	1		146.83	164.75	148.98	70.33
10	0	1		130.35	155.56	-147.56	-49.20
10	1	1		64.52	49.17	44.17	-21.60
10	2	1		69.74	45.37	-41.72	-17.83
10	3	1		79.17	81.93	-69.00	-44.16
10	5	1		130.81	137.85	-128.28	-50.47
10	6	1		118.85	133.63	-123.58	-50.84
10	7	1		100.44	102.54	94.16	40.60
10	8	1		59.65	41.99	-13.55	-39.74
10	9	1		83.51	77.39	-77.37	1.89
10	11	1		46.55	48.28	47.36	9.35
10	12	1		68.65	69.09	68.40	9.69
10	14	1		105.90	103.01	-93.71	-42.78
10	15	1		124.38	133.20	-116.90	-63.85
10	17	1		46.56	33.61	-31.67	11.26
10	18	1		157.28	161.46	149.88	60.05
10	24	1		86.61	76.74	-69.69	-32.14
10	26	1		206.75	182.33	175.39	49.82
10	27	1		61.36	49.72	-45.73	19.51
10	28	1		77.70	71.29	-68.82	-18.61
10	29	1		69.94	60.60	56.98	20.63
10	33	1		97.68	100.91	-97.49	-26.02
10	35	1		106.15	105.48	-101.47	-28.91
11	2	1		145.93	178.29	171.56	48.53
11	3	1		70.88	65.19	54.59	26.22
11	4	1		136.28	145.46	-134.50	-55.41
11	5	1		78.22	87.23	-75.65	-43.43
11	6	1		100.97	94.39	-90.00	-28.43
11	7	1		129.37	152.83	142.34	55.67
11	8	1		84.83	99.67	-83.77	-54.00
11	10	1		65.87	59.59	35.99	47.49
11	11	1		50.21	49.69	47.05	15.97
11	12	1		59.83	71.68	60.70	38.11
11	16	1		93.78	95.47	-93.20	-20.72
11	17	1		145.48	150.26	-143.96	-43.08
11	18	1		154.34	183.04	-162.99	-83.29
11	19	1		124.58	135.09	122.63	56.67
11	23	1		156.04	153.89	147.13	45.11
11	24	1		135.59	130.31	126.00	33.23
11	25	1		98.76	89.49	-74.28	-49.92
11	28	1		109.25	111.01	-96.95	-54.06
11	29	1		57.48	70.33	52.96	46.29
11	30	1		126.55	152.39	149.34	30.35
12	0	1		52.98	57.39	56.89	7.53
12	2	1		146.18	149.26	-129.79	-73.71
12	3	1		93.48	90.98	-87.02	-26.54
12	4	1		159.50	169.24	154.64	68.76
12	6	1		101.78	97.10	91.87	31.46
12	8	1		58.34	50.27	37.06	33.97
12	9	1		75.70	76.07	68.81	32.45
12	10	1		106.59	120.82	-109.53	-50.98

H	K	L		FO	FC	A	B
12	11	1		81.48	81.86	-81.72	-4.86
12	12	1		101.74	109.11	-99.13	-43.62
12	13	1		90.15	89.73	87.12	21.47
12	14	1		87.06	83.33	32.17	13.35
12	15	1		93.47	59.25	-53.34	-25.79
12	16	1		54.26	52.52	-52.21	-5.96
12	17	1		131.27	129.24	-120.60	-46.46
12	18	1		144.40	144.73	-140.14	-43.34
12	19	1		105.08	106.63	98.84	34.31
12	20	1		115.22	105.32	-92.65	-49.72
12	21	1		70.56	69.54	-69.04	-8.33
12	22	1		42.22	50.53	49.52	10.45
12	23	1		57.62	40.92	-35.56	-20.04
12	25	1		54.42	60.68	59.70	10.89
12	28	1		136.31	159.77	-145.07	-66.94
13	2	1		42.65	48.34	-42.67	-22.72
13	5	1		105.61	106.80	101.04	34.59
13	8	1		155.99	150.50	143.31	45.94
13	10	1		156.59	151.37	-148.07	-31.45
13	11	1		157.34	172.09	154.77	79.22
13	12	1		133.45	99.08	90.29	40.81
13	13	1		122.41	111.09	-94.72	-58.02
13	14	1		86.77	85.41	81.82	24.50
13	15	1		79.78	67.13	-62.02	-25.69
13	17	1		80.18	74.58	-70.66	-23.84
13	18	1		81.72	67.29	66.47	10.45
13	21	1		87.56	96.60	82.08	50.93
13	22	1		81.02	97.08	-95.65	-15.62
14	0	1		169.77	192.49	-168.54	-92.99
14	1	1		164.46	172.88	161.32	62.17
14	7	1		99.14	98.83	88.64	5.76
14	8	1		54.22	46.34	45.60	7.05
14	10	1		106.13	101.50	-83.68	-57.44
14	11	1		67.59	55.45	-54.90	-7.80
14	14	1		49.60	45.78	-44.67	-10.88
14	15	1		60.71	50.91	48.34	14.36
14	17	1		55.86	47.44	41.08	23.73
14	18	1		49.48	52.09	50.21	13.86
15	1	1		46.18	43.80	38.76	20.39
15	3	1		80.89	74.10	-71.45	-19.65
15	4	1		77.97	79.24	-76.52	-20.59
15	5	1		118.29	116.68	-109.35	-40.71
15	7	1		65.07	65.37	57.19	31.65
15	8	1		46.16	54.24	53.29	10.11
15	10	1		61.21	70.44	-64.55	-29.22
0	4	2		68.04	86.76	62.95	59.67
0	6	2		55.86	51.29	-40.22	-31.82
0	8	2		62.91	62.78	7.08	62.38
0	10	2		180.04	193.24	31.39	190.67
0	12	2		74.55	45.61	45.57	-1.97
0	14	2		66.52	67.61	60.02	31.12
0	16	2		143.93	120.52	95.36	73.69
0	18	2		85.37	90.56	90.36	-5.80
0	22	2		64.70	48.72	-31.97	-36.90
0	24	2		263.02	231.66	-97.53	-214.49
0	30	2		313.48	304.73	228.44	201.64
0	32	2		224.50	173.06	-102.99	-139.08
0	42	2		155.05	172.81	137.64	104.59
1	5	2		41.22	43.78	-42.91	-8.67
1	6	2		78.23	101.21	-90.91	-44.48
1	7	2		47.43	70.57	7.10	70.21
1	9	2		174.82	179.41	-136.04	-114.95
1	11	2		135.81	142.97	112.84	87.79
1	12	2	*	339.08	378.47	207.05	315.80
1	13	2		52.79	41.92	-31.78	-27.34
1	16	2		112.36	103.22	-79.25	-66.12
1	17	2		58.86	46.60	46.60	-0.15
1	20	2		82.73	73.41	48.00	55.54
1	21	2		320.07	328.35	-234.25	-230.09
1	22	2		126.74	113.67	59.13	102.94
1	23	2		55.67	37.08	-5.85	-36.61
1	24	2		93.20	64.50	-63.48	-11.40
1	26	2		113.20	85.89	-72.64	-45.84
1	27	2		77.51	52.76	2.63	52.70
1	28	2		119.82	105.65	54.03	90.79
1	29	2		64.31	57.65	57.33	-4.04
1	30	2		192.92	164.30	-127.00	-104.24
1	31	2		185.23	154.46	-59.47	-142.77
1	33	2		76.50	61.65	-22.41	-57.43
1	34	2		120.47	114.50	-103.65	-48.62
1	35	2		152.65	148.09	-75.25	-127.54
1	39	2		101.44	96.38	-71.93	-64.10
1	40	2		61.68	70.27	0.98	-70.27
1	41	2		69.35	88.17	86.13	15.66
1	42	2		42.75	47.67	42.49	21.60
1	43	2		55.81	61.65	-40.75	-45.26
2	0	2		100.61	110.49	-39.24	-103.29
2	1	2		82.75	86.10	71.07	48.59
2	2	2		111.98	137.61	53.28	126.87
2	5	2		40.51	42.10	41.80	5.02
2	6	2		102.36	113.82	12.97	-113.08
2	9	2		253.46	247.31	141.41	202.59
2	10	2		70.47	59.25	-51.50	-29.29
2	11	2		97.40	93.20	82.82	42.74
2	12	2		268.95	272.97	212.95	170.78
2	13	2		61.45	73.91	-7.15	-73.57
2	15	2		74.30	63.93	-42.28	-47.96
2	16	2		61.07	63.72	43.09	-8.83
2	17	2		72.82	73.89	-73.76	4.35
2	18	2		335.76	370.34	276.29	244.60
2	19	2		72.30	69.01	9.69	68.36
2	20	2		79.42	85.10	-79.13	-31.32
2	22	2		184.14	182.25	110.31	145.07
2	23	2		73.77	68.84	46.13	51.09

H	K	L		FO	FC	A	B
2	24	2		122.75	95.20	31.46	89.35
2	25	2		90.92	82.70	-42.85	-70.73
2	26	2		77.39	72.79	57.03	45.23
2	30	2		108.48	105.36	93.97	47.84
2	32	2		77.22	68.40	-1.13	68.39
2	33	2		172.60	174.42	-112.05	-133.67
2	34	2		100.54	103.30	82.51	62.16
2	35	2		72.17	61.61	-46.12	-33.47
2	36	2		96.50	99.66	-47.79	-87.45
2	37	2		66.84	68.70	24.53	64.18
2	38	2		68.66	92.78	-92.72	-3.27
2	39	2		185.30	167.01	123.26	112.69
2	40	2		136.29	144.99	84.85	117.57
2	43	2		98.76	127.05	-53.36	-115.30
3	3	2		175.78	154.92	-116.87	-101.69
3	4	2		72.34	83.31	-76.48	-33.03
3	5	2		57.14	55.62	54.02	13.24
3	6	2		201.27	200.70	-118.33	-162.10
3	8	2		131.30	131.94	-52.66	-120.97
3	9	2		201.18	240.74	-167.69	-172.73
3	10	2		83.67	85.47	80.26	29.40
3	12	2		58.73	51.94	49.72	15.05
3	15	2		187.32	203.06	122.22	162.16
3	17	2		80.22	87.16	-13.43	-86.12
3	18	2	*	277.39	350.88	-220.01	-273.34
3	19	2		101.58	98.57	-41.18	-89.55
3	23	2		180.06	187.19	167.56	83.46
3	24	2		137.51	133.10	101.30	86.34
3	26	2		95.58	73.18	71.45	15.84
3	28	2		142.05	166.65	-43.87	-160.77
3	29	2		78.72	86.60	68.77	52.62
3	30	2		108.40	116.25	79.66	84.65
3	31	2		74.23	58.95	25.01	53.38
3	32	2		76.39	81.32	-76.39	-27.91
3	34	2		94.20	88.37	51.25	71.99
3	36	2		65.12	57.08	-50.24	27.09
3	39	2		141.98	152.03	-115.54	-98.81
3	41	2		74.27	65.78	56.98	32.87
4	0	2		267.52	296.13	218.08	200.34
4	1	2		97.95	80.22	-41.79	-68.47
4	2	2		174.85	203.82	-154.03	-133.48
4	3	2		319.59	329.84	-192.66	-267.72
4	4	2		207.92	210.41	114.79	176.33
4	5	2		81.82	91.88	84.40	36.32
4	6	2		194.88	162.56	104.31	124.69
4	7	2		72.86	69.98	-54.53	43.86
4	9	2		56.32	26.37	-8.10	-25.10
4	10	2		95.70	91.03	67.52	61.05
4	11	2		110.68	127.78	-73.26	-104.69
4	13	2		119.13	110.08	-53.91	-95.98
4	14	2		97.44	103.58	52.38	89.36
4	15	2		120.84	125.62	-45.80	-116.98
4	16	2		94.70	100.99	18.61	99.26
4	18	2		75.70	66.65	-16.58	-64.55
4	20	2		55.76	42.44	-40.86	11.45
4	21	2		93.52	87.53	-19.23	-85.40
4	22	2		68.95	58.01	44.63	37.06
4	23	2		76.60	93.87	93.70	-5.60
4	24	2		92.23	90.30	88.04	20.10
4	27	2		259.37	297.27	189.47	229.07
4	28	2		78.70	81.27	6.98	-80.97
4	29	2		95.87	94.25	-64.69	-68.54
4	30	2		67.13	64.70	49.76	41.35
4	31	2		108.07	104.10	-70.91	-76.21
4	34	2		93.84	103.64	86.92	58.45
4	35	2		108.12	111.20	85.08	71.60
4	37	2		73.95	71.50	0.95	71.50
4	39	2		98.78	95.05	60.26	73.52
4	40	2		49.10	43.92	43.07	8.62
4	42	2		67.29	103.66	85.62	58.44
5	2	2		144.94	155.05	-144.18	-57.04
5	3	2		56.86	41.93	-6.30	41.51
5	4	2		59.71	73.36	71.74	15.34
5	6	2		63.48	63.95	-52.46	-36.56
5	8	2		165.08	173.61	120.49	124.99
5	9	2		136.77	113.82	63.25	94.63
5	10	2		116.70	111.14	-56.34	-95.80
5	11	2		97.80	87.96	58.83	65.40
5	12	2		197.65	188.84	116.15	148.89
5	13	2		105.27	95.20	-75.26	-58.31
5	14	2		110.88	104.94	-94.32	-46.00
5	15	2	*	283.33	354.73	-265.03	-235.78
5	16	2		117.00	120.83	87.19	83.66
5	17	2		65.59	63.01	57.28	26.24
5	18	2		135.14	154.11	-86.36	-127.64
5	19	2		91.00	100.22	48.42	87.75
5	20	2		137.68	140.57	-107.57	-90.49
5	21	2		96.14	91.33	-64.29	-64.86
5	24	2		75.13	89.30	41.17	79.24
5	25	2		81.97	77.61	-26.06	-73.11
5	27	2		179.99	181.45	-111.15	-143.42
5	29	2		70.46	79.33	-51.40	-60.43
5	30	2		202.34	190.29	-118.89	-143.58
5	31	2		115.36	104.18	-77.59	-69.53
5	34	2		76.00	70.37	51.21	43.26
5	36	2		94.45	91.76	-49.54	-77.24
5	38	2		53.97	55.46	21.79	51.00
5	39	2		69.42	67.31	56.67	35.32
5	40	2		103.94	118.45	-50.17	-107.31
6	0	2		135.31	140.95	-28.84	-137.97
6	2	2		140.59	128.72	69.41	108.40
6	4	2		107.00	92.45	-59.81	-60.60
6	5	2		73.99	63.54	52.12	36.35
6	6	2		267.34	272.93	205.40	179.72

H	K	L	FO	FC	A	B
6	7	2	86.49	90.86	-69.35	-58.71
6	8	2	217.77	242.23	176.02	166.43
6	9	2	232.97	272.71	153.51	225.40
6	11	2	62.90	70.03	68.38	12.63
6	13	2	57.93	54.58	-52.01	-16.97
6	14	2	129.79	151.93	-139.86	-59.35
6	15	2	146.07	167.71	102.67	132.62
6	17	2	68.49	67.80	41.04	51.96
6	18	2	135.14	135.16	89.64	102.03
6	19	2	62.68	69.11	-2.19	69.07
6	21	2	74.75	78.26	-55.56	-55.64
6	22	2	90.65	103.09	92.27	45.38
6	23	2	78.75	74.57	44.89	59.55
6	24	2	113.73	98.07	79.70	57.15
6	25	2	71.75	79.75	-78.66	-13.13
6	26	2	63.81	58.92	49.63	31.07
6	28	2	132.39	120.50	63.69	102.30
6	30	2	103.97	98.83	-34.75	-92.52
6	33	2	152.98	139.01	-86.82	-103.57
6	34	2	58.29	69.27	28.81	39.96
6	36	2	187.20	230.77	160.98	165.35
6	37	2	87.32	100.00	-76.72	-64.14
7	1	2	53.46	61.70	32.41	52.50
7	3	2	288.04	317.30	-212.59	-235.55
7	4	2	120.08	107.29	77.08	74.64
7	5	2	122.43	100.31	-20.95	-99.10
7	6	2	53.61	42.16	0.23	42.16
7	7	2	54.02	52.99	26.12	-46.11
7	8	2	116.48	104.79	-77.65	-70.36
7	9	2	88.15	87.41	35.05	80.08
7	13	2	114.37	97.14	-25.52	-93.73
7	14	2	75.60	92.28	-75.85	-52.55
7	15	2	79.42	61.58	-42.23	-44.82
7	16	2	76.96	78.89	78.87	1.71
7	18	2	78.04	80.68	-66.42	-45.79
7	20	2	143.68	165.68	117.01	117.30
7	21	2	142.07	130.71	41.51	123.94
7	24	2	110.29	107.63	-72.29	-79.73
7	25	2	89.22	87.83	-66.80	-74.39
7	30	2	69.70	54.23	34.05	42.21
7	31	2	72.72	70.75	-6.81	70.43
7	32	2	137.12	143.22	-98.61	-103.86
7	33	2	119.34	125.93	-117.39	-45.58
7	35	2	54.42	61.99	53.97	30.31
7	36	2	119.92	131.28	-110.09	-71.52
8	0	2	106.45	107.72	-55.68	-92.22
8	1	2	134.71	116.43	56.91	101.63
8	2	2	92.96	95.46	-74.75	-59.37
8	4	2	133.86	136.85	57.56	124.16
8	5	2	77.57	77.64	76.85	11.03
8	6	2	138.35	145.90	121.32	81.05
8	7	2	148.84	175.43	-123.94	-124.26
8	8	2	117.53	112.48	-65.79	-91.23
8	9	2	161.27	151.79	-71.77	-133.75
8	10	2	101.15	112.10	99.13	52.34
8	11	2	108.75	107.56	38.36	100.30
8	13	2	67.32	73.17	42.88	59.29
8	15	2	71.57	85.54	-51.34	-63.42
8	18	2	93.79	76.05	71.49	25.94
8	19	2	93.67	96.86	-41.01	-87.75
8	20	2	84.73	99.73	58.65	81.66
8	21	2	81.21	74.33	70.78	22.70
8	24	2	204.67	223.79	187.26	122.54
8	25	2	178.23	197.83	-137.25	-142.48
8	27	2	126.51	121.06	96.92	72.54
8	30	2	92.78	85.58	-67.07	-53.15
8	31	2	97.13	100.52	66.70	75.20
8	33	2	112.66	119.96	98.54	63.42
8	34	2	61.89	66.62	20.44	63.41
9	1	2	63.23	55.25	-25.54	-49.00
9	3	2	63.34	47.30	15.93	44.54
9	4	2	109.66	116.44	104.78	50.79
9	5	2	87.00	99.77	86.63	49.50
9	6	2	119.09	137.98	-91.15	-103.58
9	8	2	74.96	83.30	19.26	81.05
9	9	2	81.66	85.03	21.31	82.37
9	10	2	101.47	102.74	-66.88	-78.00
9	11	2	101.61	93.77	-60.82	-71.37
9	12	2	140.20	167.06	-103.32	-131.29
9	13	2	85.12	102.20	79.06	64.77
9	14	2	143.79	154.59	-88.82	-126.53
9	15	2	166.79	207.27	-153.99	-139.74
9	16	2	71.56	92.98	72.94	57.66
9	19	2	117.55	131.63	-34.11	-101.26
10	0	2	60.19	42.45	42.29	-3.67
10	1	2	82.02	90.26	-33.72	-33.73
10	2	2	191.68	214.77	136.58	165.74
10	3	2	101.73	104.75	53.63	89.98
10	4	2	90.98	84.52	-70.14	-47.15
10	5	2	76.77	71.41	22.60	67.95
10	6	2	118.10	116.10	76.14	87.65
10	7	2	64.24	64.08	-34.02	-54.30
10	10	2	93.18	87.87	-55.89	-67.81
10	14	2	62.80	78.76	38.82	68.53
10	15	2	139.38	146.30	103.58	103.32
10	16	2	61.77	60.42	53.13	23.67
10	18	2	79.80	101.26	-76.60	-65.23
10	26	2	135.28	163.27	-93.41	-133.91
10	27	2	77.26	76.45	-36.54	-67.15
11	2	2	104.31	103.09	-63.99	-80.38
11	3	2	76.95	68.52	-37.32	-57.46
11	6	2	187.20	214.41	151.38	151.85
11	7	2	120.40	117.94	-85.59	-81.14
11	16	2	99.08	105.89	83.00	45.76

H	K	L	FO	FC	A	B
11	17	2	76.95	69.27	53.72	43.73
11	18	2	84.96	77.47	18.25	75.29
11	19	2	91.24	95.50	-56.37	-77.09
11	21	2	50.87	66.95	-53.51	-40.25
11	22	2	57.64	61.42	-7.44	-60.97
11	23	2	74.72	91.50	-67.69	-61.57
11	24	2	142.75	154.21	-101.12	-116.42
11	25	2	67.62	70.27	14.22	68.81
11	26	2	40.06	53.42	-5.71	53.12
11	27	2	82.46	90.53	61.38	66.54
12	0	2	88.09	99.37	60.52	78.82
12	1	2	54.91	57.79	-24.29	52.44
12	2	2	58.61	57.45	57.32	3.87
12	3	2	54.70	43.14	34.75	25.55
12	4	2	54.52	72.54	-27.70	-67.04
12	6	2	111.77	114.44	-56.52	-99.45
12	8	2	72.52	78.63	-63.70	-46.10
12	10	2	129.29	150.37	100.48	111.36
12	17	2	107.84	115.03	84.09	78.49
12	18	2	129.71	148.26	128.00	74.81
12	19	2	111.98	118.35	-75.97	-90.75
12	20	2	116.10	134.06	76.04	110.40
12	21	2	64.45	71.36	62.30	34.79
12	22	2	88.24	101.27	-80.58	-61.34
9	24	2	61.66	70.91	-52.33	-47.85
9	25	2	69.44	42.62	34.64	-24.82
9	26	2	118.44	116.34	-63.90	-97.22
9	27	2	140.89	147.75	-95.75	-112.52
9	28	2	88.72	79.23	50.89	60.72
13	4	2	69.77	66.22	51.05	42.18
13	5	2	85.81	98.56	-66.17	-73.04
13	6	2	138.54	157.07	-111.14	-111.00
13	8	2	69.36	74.62	-60.05	-44.28
13	11	2	129.76	154.69	-86.78	-128.05
13	12	2	68.36	77.41	-50.56	-58.61
13	13	2	71.94	85.42	56.86	63.75
13	16	2	66.19	69.86	-34.00	-61.02
13	17	2	60.04	69.97	54.26	44.18
13	19	2	60.52	70.06	-42.56	-55.66
13	20	2	63.17	72.68	-67.21	-27.68
0	2	3	42.80	56.13	14.06	-54.34
0	4	3	122.65	112.93	67.07	90.85
0	6	3	26.90	26.13	-24.39	-9.37
0	8	3	129.18	128.14	-38.20	-122.31
0	10	3	89.57	90.02	13.18	-89.05
0	12	3	88.34	81.54	-28.87	-76.26
0	14	3	41.05	55.47	54.10	12.25
0	16	3	45.28	51.62	-28.43	-43.09
0	20	3	91.94	93.75	86.09	37.14
0	22	3	108.62	96.39	-1.41	-94.38
0	24	3	238.82	230.27	149.01	175.55
0	30	3	132.54	115.84	-99.10	-59.98
1	1	3	77.61	67.14	-63.64	21.42
1	2	3	113.64	109.90	-69.91	-84.80
1	4	3	30.00	27.24	-13.17	23.85
1	5	3	100.83	98.67	29.90	94.03
1	6	3	175.53	189.19	-53.65	-181.43
1	7	3	70.28	70.77	16.24	68.88
1	8	3	93.67	99.97	4.33	99.88
1	9	3	196.78	192.38	70.01	179.19
1	10	3	51.81	50.03	-28.61	-41.04
1	12	3	138.72	152.35	-50.35	-143.79
1	13	3	91.90	98.19	66.35	72.37
1	20	3	96.73	87.84	-58.78	-65.27
1	21	3	261.33	225.96	91.45	206.62
1	22	3	104.63	101.80	42.78	-92.38
1	23	3	79.26	81.66	-12.52	80.70
1	24	3	155.94	133.52	73.01	111.78
1	25	3	59.90	56.47	41.87	37.90
1	28	3	88.63	69.64	6.68	68.21
1	31	3	106.38	80.77	13.71	79.59
1	32	3	65.13	58.68	39.44	43.45
2	0	3	117.77	118.83	-1.07	-118.82
2	1	3	50.41	55.02	-53.95	-10.81
2	2	3	127.47	129.14	111.85	64.55
2	3	3	104.59	97.02	11.60	96.33
2	4	3	121.68	132.20	-66.19	-114.43
2	5	3	33.18	73.47	1.72	73.45
2	6	3	159.76	150.60	22.76	148.87
2	7	3	79.92	70.47	42.07	59.54
2	9	3	151.15	140.64	-43.64	-133.70
2	11	3	56.66	63.40	-29.76	-55.98
2	12	3	40.18	51.46	-38.27	-34.41
2	13	3	38.77	53.07	-52.35	-4.87
2	14	3	45.24	60.70	20.67	-57.07
2	16	3	44.84	43.41	36.38	22.89
2	18	3	163.32	146.27	-82.06	-121.08
2	24	3	117.44	111.47	-74.42	-82.99
2	26	3	66.24	73.32	26.06	-68.53
2	27	3	67.56	66.93	-1.07	-66.92
2	30	3	158.04	133.80	12.34	-133.23
2	33	3	155.73	136.65	70.82	116.86
2	34	3	159.30	131.98	-13.18	-131.32
2	35	3	68.19	65.60	39.79	52.16
2	36	3	161.16	169.93	78.81	150.55
3	1	3	114.66	109.93	5.53	109.79
3	2	3	47.00	44.89	20.10	40.14
3	3	3	162.17	161.80	71.74	145.03
3	4	3	127.47	120.93	-60.77	-104.55
3	5	3	59.62	73.57	-36.19	64.05
3	6	3	210.63	234.06	89.02	216.46
3	8	3	117.29	98.20	-57.05	-79.93
3	9	3	134.07	126.07	64.47	108.34
3	10	3	0.28	52.02	37.63	35.93

H	K	L	FO	FC	A	B
3	11	3	43.76	41.43	-4.15	41.22
3	14	3	54.27	55.53	47.56	23.65
3	15	3	130.92	112.16	-59.64	-96.23
3	16	3	65.13	75.14	1.89	74.11
3	17	3	75.92	93.29	-27.02	73.79
3	18	3	173.84	168.05	15.65	167.36
3	19	3	74.12	73.57	25.62	69.04
3	23	3	66.60	64.64	-51.69	-38.35
3	24	3	215.50	200.05	-49.26	-193.83
3	25	3	54.16	55.43	33.73	33.61
4	1	3	51.98	50.09	16.60	47.19
4	2	3	61.93	64.34	4.33	-61.93
4	3	3	151.49	173.90	53.42	166.49
4	5	3	43.31	51.11	-46.73	-23.58
4	6	3	87.30	92.69	-34.72	-85.94
4	7	3	35.28	41.06	13.95	-38.59
4	10	3	62.75	64.42	37.20	52.59
4	14	3	54.09	44.24	41.50	15.33
4	16	3	58.08	63.19	5.01	-62.99
4	21	3	102.50	88.93	54.67	71.48
4	22	3	144.76	129.49	-51.15	-119.97
4	24	3	61.59	43.71	27.67	33.92
4	27	3	192.70	186.80	-85.37	-165.03
4	28	3	89.86	68.65	52.76	43.94
4	32	3	63.37	70.90	31.64	-61.45
4	35	3	117.16	107.23	-53.25	-93.13
5	1	3	77.56	71.86	1.36	71.85
5	4	3	92.16	96.63	-14.13	93.57
5	5	3	55.09	60.26	-7.67	59.77
5	6	3	91.27	85.94	-32.99	-79.35
5	8	3	44.61	36.62	18.40	31.66
5	9	3	61.82	60.07	-29.79	-52.16
5	11	3	63.31	55.63	-30.67	-44.42
5	12	3	75.78	93.20	4.26	-93.13
5	13	3	93.07	106.08	55.17	90.60
5	14	3	96.97	98.15	68.37	70.62
5	15	3	215.37	234.24	129.90	195.59
5	16	3	148.52	154.38	-106.99	-111.28
5	17	3	87.92	75.47	19.37	72.95
5	18	3	89.91	91.57	26.64	87.61
5	21	3	157.08	141.10	82.32	114.60
5	22	3	68.51	74.95	29.95	-63.70
5	26	3	77.22	77.49	8.96	-76.97
5	27	3	76.87	71.36	-22.66	67.67
5	28	3	79.05	71.79	-4.17	71.67
5	29	3	58.65	53.20	23.95	47.51
5	31	3	51.55	59.32	46.97	36.23
5	32	3	62.39	76.09	63.38	42.12
5	33	3	41.44	33.45	14.90	-30.00
5	34	3	61.64	77.76	-66.02	-41.08
6	0	3	101.97	100.88	-76.43	-65.84
6	1	3	58.17	54.33	-4.93	-56.11
6	2	3	82.41	62.62	28.19	55.92
6	3	3	56.15	46.32	28.92	34.18
6	5	3	65.42	67.91	-52.27	-43.36
6	6	3	59.30	51.76	-14.05	-43.30
6	7	3	64.10	72.25	58.01	43.07
6	8	3	78.14	76.23	-31.57	-63.44
6	9	3	189.02	221.27	-89.67	-202.29
6	12	3	63.96	52.57	17.23	49.65
6	21	3	47.85	47.26	14.17	45.09
6	23	3	141.44	98.30	-20.65	-96.11
6	24	3	78.99	69.34	-30.55	-62.24
6	25	3	72.17	49.85	40.07	-21.67
6	27	3	55.43	46.29	8.53	-45.50
6	28	3	49.34	55.10	-52.17	-17.72
6	29	3	52.64	49.49	29.82	39.50
6	30	3	58.88	58.83	52.33	26.47
6	31	3	50.85	43.30	9.22	-42.31
6	32	3	52.50	84.16	44.42	71.48
6	33	3	78.11	119.67	48.89	109.23
6	34	3	91.73	103.84	-9.75	-104.40
7	2	3	103.29	96.59	-5.19	96.49
7	3	3	136.22	219.42	109.47	190.06
7	4	3	150.47	135.64	-65.49	-118.78
7	6	3	129.24	115.61	62.81	97.06
7	8	3	111.52	87.05	-16.93	-85.38
7	9	3	89.64	88.07	-10.26	-87.67
7	12	3	129.65	114.15	-44.79	-104.99
7	13	3	116.20	114.08	-13.50	110.29
7	15	3	138.01	117.65	48.18	107.33
7	19	3	60.40	63.25	60.49	15.17
7	20	3	75.76	71.84	8.47	-71.33
7	21	3	174.46	139.78	-34.83	-135.37
7	22	3	82.92	77.75	-12.08	75.81
7	25	3	80.63	76.62	63.75	59.15
7	28	3	88.23	72.46	-27.39	-67.04
8	0	3	139.75	207.48	52.96	200.60
8	1	3	96.44	90.19	2.14	-90.17
8	2	3	103.94	88.37	4.85	-87.93
8	3	3	60.01	66.96	-30.84	-59.44
8	5	3	60.02	64.86	8.86	-64.25
8	6	3	105.37	103.21	-22.51	-100.72
8	7	3	48.97	54.45	34.70	41.97
8	8	3	54.70	66.92	59.68	30.23
8	9	3	166.53	155.52	75.15	135.14
8	-12	3	59.29	53.76	-42.31	-33.17
8	14	3	75.63	63.47	35.52	52.61
8	16	3	57.51	48.07	-6.15	-47.67
8	18	3	45.72	46.34	-12.91	-44.51
8	19	3	57.28	52.56	-24.30	-46.61
8	21	3	102.02	96.13	-52.80	-80.34
8	23	3	65.69	54.07	9.60	-53.25
8	24	3	75.64	81.18	-50.26	-63.76

H	K	L	FO	FC	A	B
8	25	3	121.86	111.94	71.47	86.15
8	26	3	62.71	65.33	-12.63	-64.09
8	27	3	78.89	67.55	-39.38	-54.88
9	4	3	76.20	65.65	13.76	64.19
9	11	3	68.09	67.22	-0.08	67.22
9	12	3	75.02	70.30	20.95	67.10
9	13	3	82.61	72.26	-51.43	-50.76
9	14	3	101.22	89.95	31.25	84.34
9	15	3	92.01	79.21	45.26	65.01
9	16	3	110.85	106.25	-38.77	-98.92
9	19	3	50.32	48.15	33.71	34.38
9	21	3	66.81	51.88	30.86	41.71
9	22	3	47.26	41.87	3.00	41.76
9	23	3	35.37	43.99	-43.64	5.57
9	24	3	67.85	62.58	-12.12	61.39
9	25	3	51.58	54.80	-12.36	53.39
9	27	3	75.86	75.20	24.62	71.06
10	0	3	88.80	91.61	-36.94	-83.84
10	5	3	97.52	77.92	-26.46	-73.29
10	6	3	109.34	84.94	-26.74	-80.62
10	7	3	63.39	49.97	7.41	49.42
10	9	3	73.11	73.67	-67.41	-29.7[illegible]
10	11	3	52.78	47.12	40.96	23.31
10	12	3	45.06	58.63	52.11	26.87
10	13	3	80.94	68.64	49.21	-47.86

H	K	L	FO	FC	A	B
10	14	3	66.46	71.39	-31.66	-63.99
10	18	3	128.82	108.63	42.88	99.81
10	24	3	49.07	67.36	-21.44	-63.86
11	2	3	99.93	91.63	58.07	70.88
11	3	3	43.57	39.80	8.82	38.81
11	4	3	84.27	77.78	-16.85	-75.93
11	5	3	45.40	54.34	9.59	-53.49
11	6	3	60.40	58.67	-33.89	-47.83
11	7	3	115.37	112.17	52.18	97.29
11	8	3	63.82	60.64	5.83	-60.36
11	10	3	66.15	69.55	-19.47	55.77
11	11	3	67.53	56.32	34.62	44.26
11	18	3	99.91	116.70	-30.91	-112.53
11	19	3	94.98	89.59	28.62	84.89
11	20	3	83.07	76.65	59.65	-48.14
12	2	3	110.67	114.33	-9.54	-113.93
12	0	3	72.81	63.48	40.75	48.67
12	3	3	53.66	68.80	-43.11	-53.62
12	4	3	105.71	97.33	23.92	94.34
12	6	3	32.75	48.66	33.23	35.54
12	7	3	35.94	42.73	-21.52	-36.92
12	9	3	56.13	49.22	23.25	43.39
12	10	3	65.18	79.54	-23.08	-75.12
12	11	3	42.43	52.78	-48.18	-21.54
12	12	3	71.50	69.86	-18.05	-66.45
12	13	3	40.34	46.81	32.55	32.64

7. Discussion of the Crystal Structure of $3Bi_2O_3.17Nb_2O_5$.

A large number of compounds have structures which may be considered to be built up of two-dimensional networks of corner-sharing octahedra. In the third dimension, these networks are often placed directly one upon the other, and are joined by sharing corners of the octahedra.

The two-dimensional network may contain holes formed by rings of octahedra, which become tunnels in three dimensions. Tunnels formed by 3-, 4-, 5- or 6-membered rings of octahedra are known[I.20-23]. These may be empty[I.32] or filled, wholly or partially.

Tetragonal potassium bronze[I.19], Figure 6.2, is such a structure, in which the square and pentagonal cross-section tunnels contain the alkali cations.

$Nb_{16}W_{18}O_{94}$ was described as related to the bronze structure, with all the four-cornered, and two thirds of the five-cornered holes empty. The remaining one third of the pentagonal tunnels contain both metal and oxygen atoms, giving rise to a pentagonal bipyramidal co-ordination for the metal atom. Sleight[I.18] pictured this structure as one of a family of $(MeO)_yMeO_3$ structures, based on various MeO_3 octahedral networks in which some tunnels are filled with (Me-O) chains. He predicted a family of $A_x(MeO)_yMeO_3$ compounds, containing further cations, A, in some

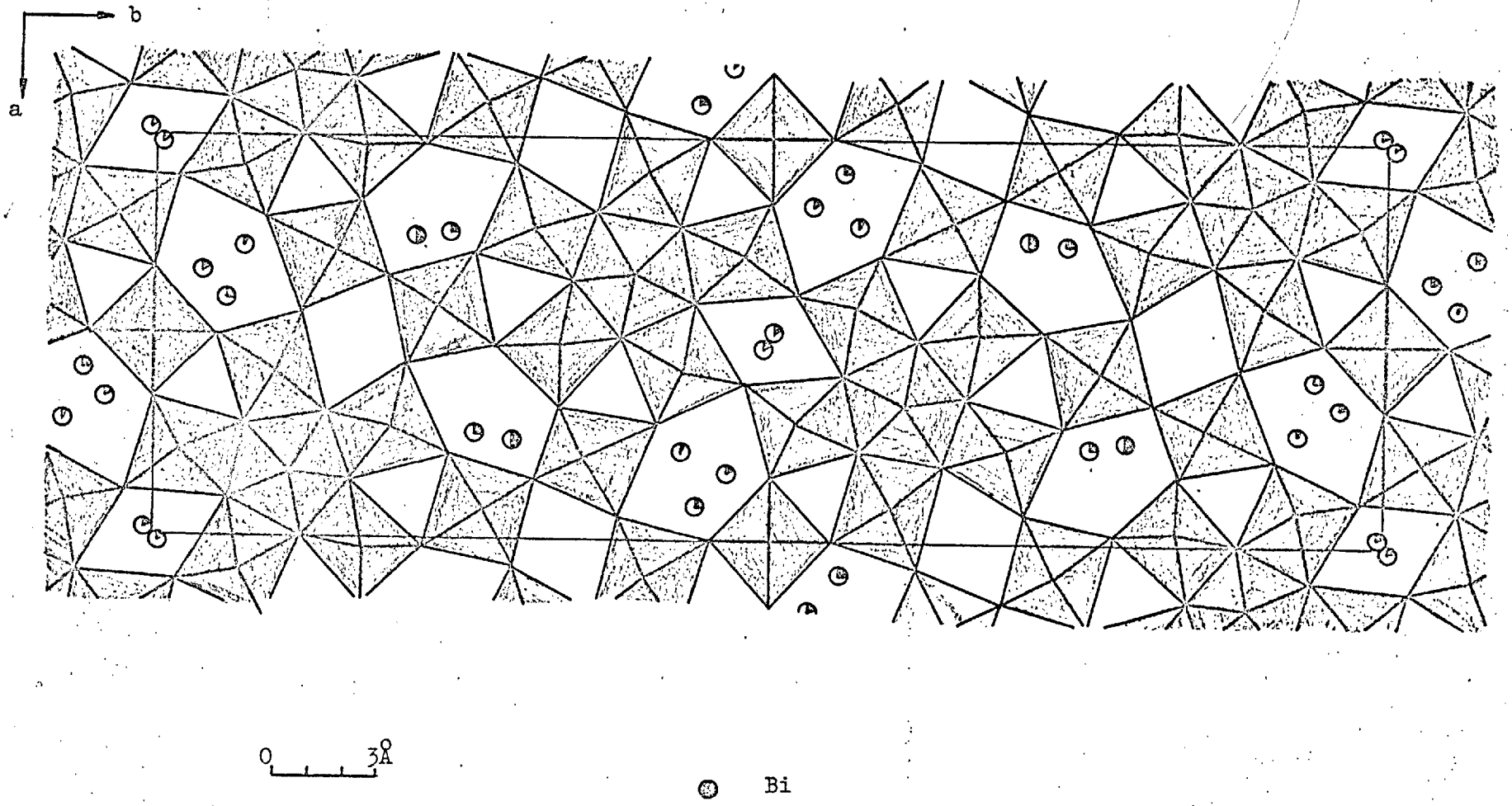


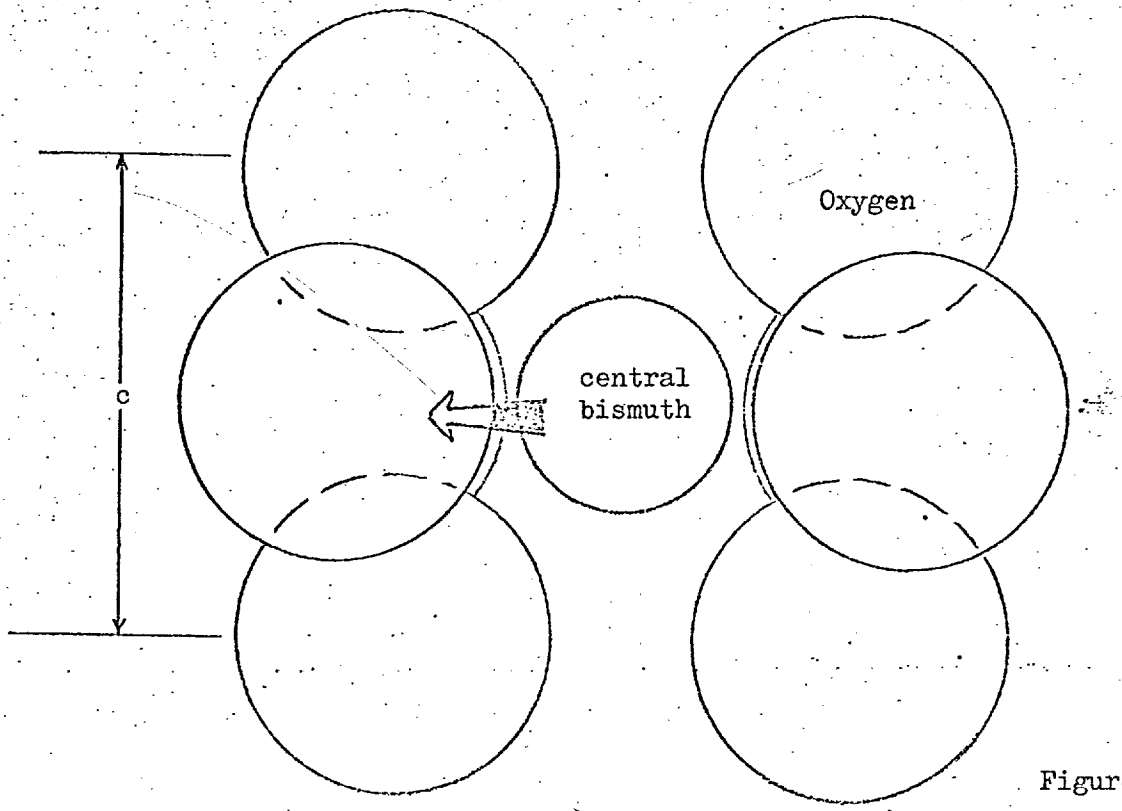
Figure 7.1 - The [001] projection of the structure of $3Bi_2O_3.17Nb_2O_5$, showing the $Me_{34}O_{94}$ matrix and the occupancies of the bismuth sites.

or all of the unfilled tunnels.

$3Bi_2O_3.17Nb_2O_5$ is just such a compound, and may be re-written as $Bi_6(NbO)_4(NbO_3)_{30}$ or x=1/5, y=2/15. Figure7.1 shows a schematic diagram of the $(NbO)_4(NbO_3)_{30}$ matrix found in $3Bi_2O_3.17Nb_2O_5$, with the bismuth occupancies indicated at sites where this exceeded 0.08.

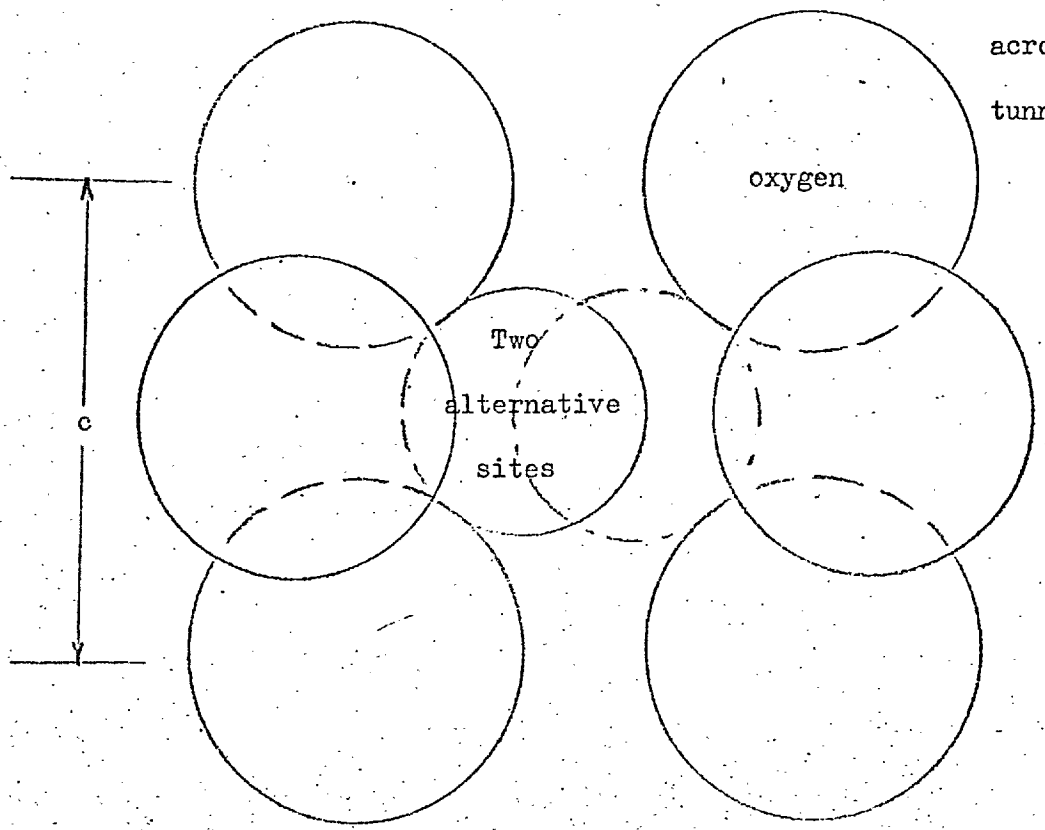
The fact that the bismuth atoms are spread out among a number of sites of fractional occupancy, is not unreasonable. The pentagonal tunnels are over 5Å across at the height of the bismuths, and are therefore too large for these atoms, (ionic radius 0.96Å), as shown in Figure 7.2. The diamond shaped tunnels are smaller than the pentagons (~4Å at the height of the bismuths) but are still too large for a central bismuth atom.

Consequently, the bismuths are located away from the centres of the holes. They show a very strong tendency towards a one-sided four-fold co-ordination, similar to that found in a number of other oxides and oxyhalides of bismuth[I.24-28]. The bismuth atoms could achieve this co-ordination at a number of sites. The bismuth occupancies at these sites are uneven, but add up to 5.5 per unit cell, whereas 6 would be expected from the formula. With a standard deviation of 0.2 in the total occupancy, this difference is only marginally significant. There are several further sites of similar oxygen environments which may have very low occupancies of bismuth atoms. Small peaks were observed in Fourier maps at two such places. This could bring the total number of bismuth atoms from the "observed" total of 5.5 to the expected total of six, if indeed this difference is real.



(a)

Figure 7.2
Showing a cut
across a pentagonal
tunnel



(b)

The low occupancies of the bismuth sites account for the remarkable similarity of the intensities of reflections of $3Bi_2O_3.17Nb_2O_5$ to the corresponding ones of $Nb_{16}W_{18}O_{94}$. Had the six bismuth atoms been localised to six sites of unit occupancy, they would have had a much more marked effect on reflection intensities.

While the distribution of the bismuth atoms may represent real energy differences between the available sites, and therefore would be expected to be the same in different crystals, no generalisation can be made on this. The actual occupancy of any given site may well be a variable quantity from crystallite to crystallite, and could be dependent on the mode of preparation and subsequent heat treatment. This crystal structure determination might, therefore, be regarded as the elucidation of the structure of the particular crystal examined. The Nb-O matrix found will certainly be the same for all crystals of $3Bi_2O_3.17Nb_2O_5$, as would be the tendency of bismuth atoms to achieve a one-sided four-fold co-ordination.

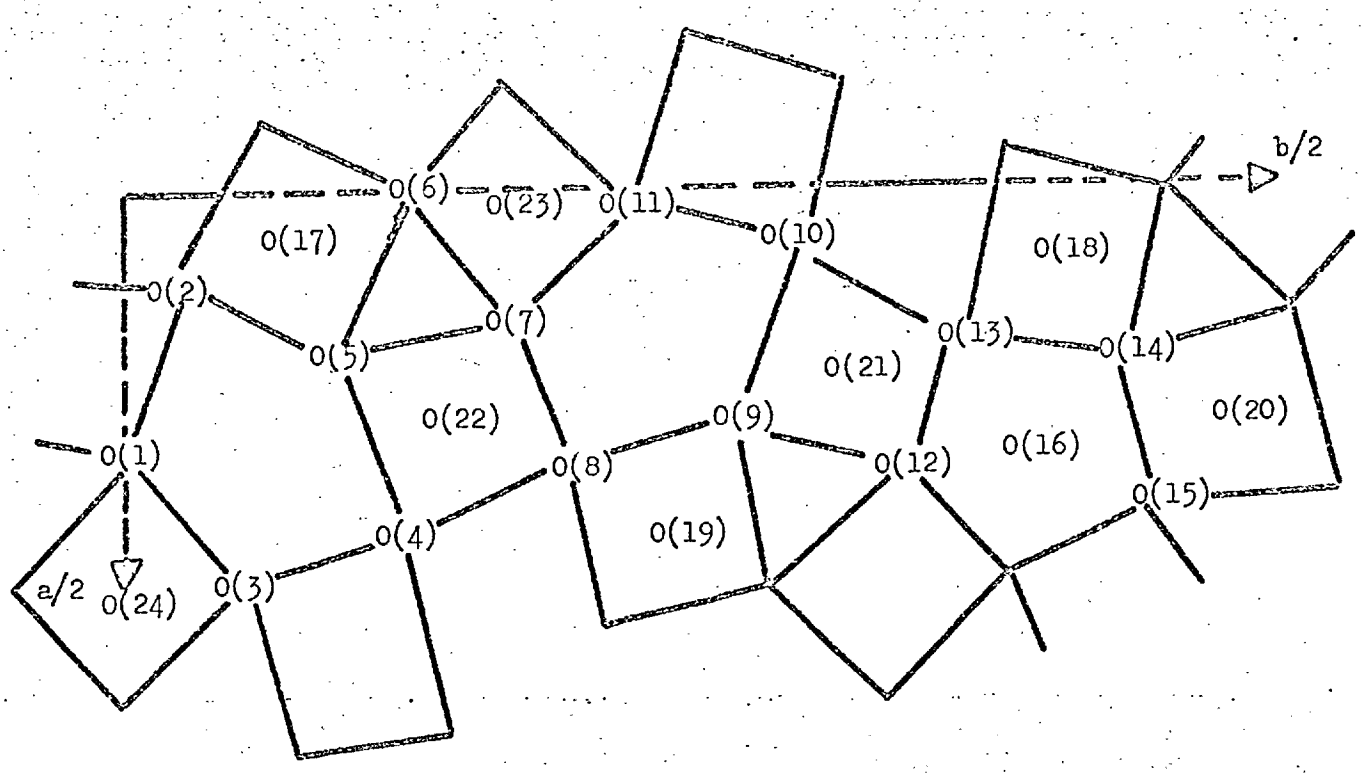
The ideal structure corresponds to the formula $3Bi_2O_3.17Nb_2O_5$. A formula of $Bi_2O_3.6Nb_2O_5$, as originally proposed, would have $5\frac{2}{3}$ bismuth atoms per unit cell, but electrical neutrality would require the random removal of half an oxygen atom per unit cell. This would in fact correspond to a cell content of $Bi_{5\frac{2}{3}}Nb_{34}O_{93\frac{1}{2}}$. Thus it is felt that there are no reasonable grounds for supposing that the ideal formula is not in fact the true one.

All atoms in $3Bi_2O_3.17Nb_2O_5$ are situated near two levels which are

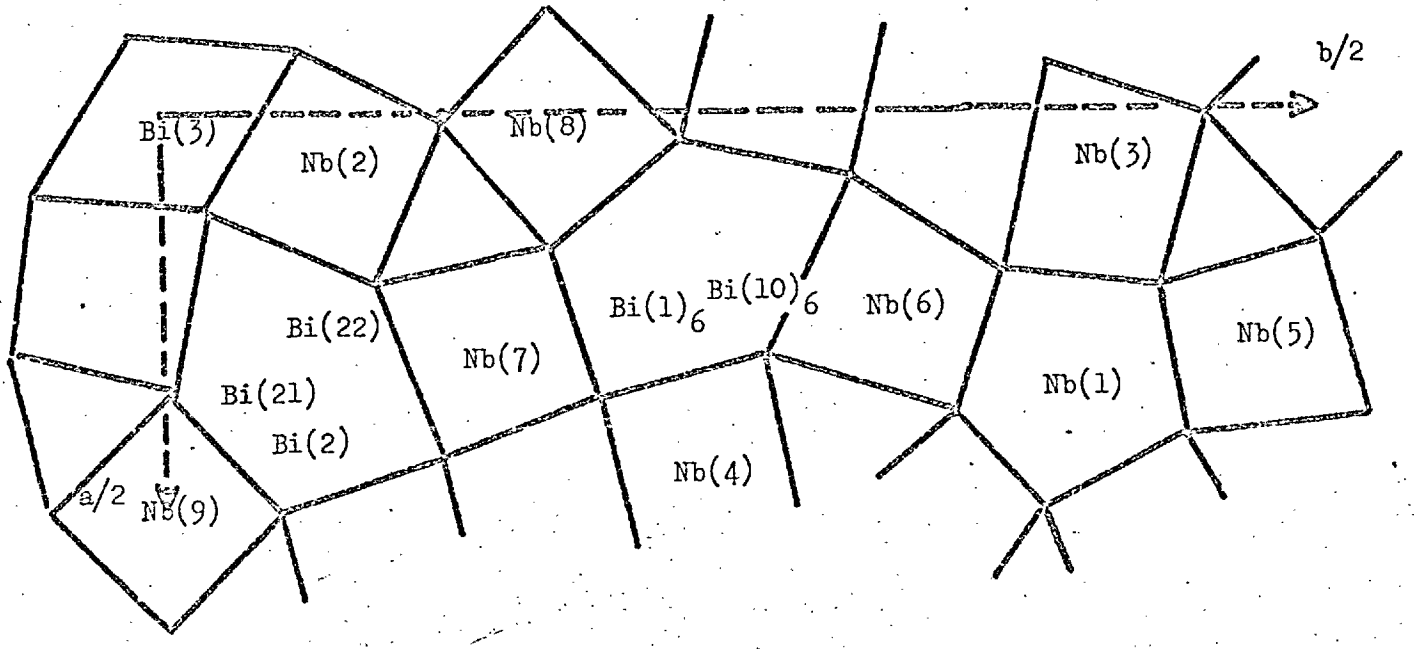
approximately c/2 apart. The holosymmetric space group, Pbam, would have required all atoms to be exactly at $z = 0$, or $z = \frac{1}{2}$. Refinement in the space group Pba2 showed that this was not the case, since the sheet of octahedra is significantly buckled. In any case Pba2 must be regarded as an 'overall' space group. On an atomic level, it is the exact arrangement of the bismuth atoms that determines the local symmetry. It is only possible to say that the statistical distribution of the bismuth atoms is such that the overall effect is that of orthogonal crystal class and of the apparent space group Pba2.

The final set of positional parameters (Table 6.3) were used to calculate the various inter-atomic distances, angles and standard deviations given in Tables 7.1 and 7.2 respectively. Figures 7.3 (a) and (b) indicate the positions of the appropriately named atoms within the asymmetric portion of the unit cell. The suffices in the tables refer to the following symmetry operations:

1. $\frac{1}{2} + x,\ \frac{1}{2} - y,\ z$
2. $x,\ y,\ z + 1$
3. $x,\ y,\ z - 1$
4. $\frac{1}{2} - x,\ \frac{1}{2} + y,\ z$
5. $1 - x,\ -y,\ z$
6. $x - \frac{1}{2},\ \frac{1}{2} - y,\ z$
7. $\frac{1}{2} - x,\ y - \frac{1}{2},\ z$
8. $-x,\ -y,\ z$


b/2
O(6)
O(23)
O(11)
O(10)
O(17)
O(18)
O(2)
O(7)
O(13)
O(14)
O(5)
O(21)
O(22)
O(9)
O(20)
O(1)
O(8)
O(12)
O(16)
O(15)
O(4)
O(19)
a/2
O(24)
O(3)

(a)


b/2
Bi(3)
Nb(2)
Nb(8)
Nb(3)
Bi(22)
Bi(1)6
Bi(10)6
Nb(6)
Nb(5)
Nb(7)
Bi(21)
Nb(1)
Bi(2)
Nb(4)
a/2
Nb(9)

(b)

Figure 7.3

Table 7.1 - $3Bi_2O_3 \cdot 17Nb_2O_5$, Some Inter-Atomic Distances and Standard Deviations in Å.

Niobium-Oxygen Distances

Nb(1) - $O(6)_1$	2.02	0.02			
Nb(1) - O(12)	2.08	0.03	Nb(2) - O(2)	1.94	0.03
Nb(1) - O(13)	2.11	0.02	Nb(2) - O(5)	1.87	0.03
Nb(1) - O(14)	2.08	0.02	Nb(2) - O(6)	2.03	0.02
Nb(1) - O(15)	2.14	0.02	Nb(2) - $O(15)_6$	2.09	0.02
Nb(1) - O(16)	1.65	0.03	Nb(2) - O(17)	2.34	0.04
Nb(1) - $O(16)_2$	2.29	0.03	Nb(2) - $O(17)_2$	1.60	0.04
Mean	2.05		Mean	1.98	
Nb(3) - O(13)	2.04	0.02	Nb(4) - O(8)	2.00	0.03
Nb(3) - O(14)	2.07	0.02	Nb(4) - O(9)	2.28	0.03
Nb(3) - $O(3)_6$	2.00	0.03	Nb(4) - $O(10)_1$	1.83	0.03
Nb(3) - $O(4)_6$	1.93	0.03	Nb(4) - $O(11)_1$	1.82	0.03
Nb(3) - O(18)	1.66	0.06	Nb(4) - O(19)	1.81	0.07
Nb(3) - $O(18)_2$	2.27	0.06	Nb(4) - $O(19)_2$	2.19	0.07
Mean	1.99		Mean	1.99	

Table 7.1 - continued

Nb(5) - O(14)	2.04	0.02	Nb(6) - O(9)	1.87	0.03
Nb(5) - O(15)	2.03	0.02	Nb(6) - O(10)	2.00	0.02
Nb(5) - $O(2)_4$	1.97	0.03	Nb(6) - O(12)	2.02	0.03
Nb(5) - $O(1)_4$	1.90	0.03	Nb(6) - O(13)	2.10	0.02
Nb(5) - O(20)	1.59	0.04	Nb(6) - O(21)	1.59	0.05
Nb(5) - $O(20)_2$	2.35	0.04	Nb(6) - $O(21)_2$	2.35	0.04
Mean	1.98		Mean	1.99	
Nb(7) - O(4)	1.87	0.03	Nb(8) - O(6)	2.03	0.02
Nb(7) - O(5)	2.06	0.03	Nb(8) - O(7)	1.97	0.03
Nb(7) - O(7)	1.92	0.03	Nb(8) - O(11)	1.98	0.03
Nb(7) - O(8)	2.06	0.03	Nb(8) - $O(12)_4$	1.98	0.03
Nb(7) - O(22)	1.72	0.09	Nb(8) - O(23)	1.70	0.07
Nb(7) - $O(22)_2$	2.23	0.09	Nb(8) - $O(23)_2$	2.23	0.07
Mean	1.98		Mean	1.98	
Nb(9) - O(1)	2.05	0.03	(x2)		
Nb(9) - O(3)	1.91	0.03	(x2)		
Nb(9) - O(24)	2.46	0.06			
Nb(9) - $O(24)_2$	1.48	0.06			
Mean	1.98				

Table 7.1 - continued

Bismuth-Oxygen Distances

Bi(2) - O(3)$_3$	2.16	0.05
Bi(2) - O(3)	2.45	0.06
Bi(2) - O(24)	2.51	0.01
Bi(2) - O(18)$_1$	2.64	0.06
Bi(2) - O(1)	2.89	0.05
Bi(2) - O(4)$_3$	3.00	0.05
Bi(2) - O(1)$_3$	3.09	0.04
Bi(2) - O(4)	3.23	0.04
Bi(2) - O(5)	3.27	0.04
Bi(2) - O(22)	3.40	0.06
Bi(22) - O(5)	2.12	0.06
Bi(22) - O(5)$_3$	2.52	0.06
Bi(22) - O(17)	2.59	0.03
Bi(22) - O(22)	2.77	0.06
Bi(22) - O(1)	3.07	0.05
Bi(22) - O(1)$_3$	3.34	0.05
Bi(22) - O(3)$_3$	3.37	0.06
Bi(22) - O(4)$_3$	3.38	0.05
Bi(22) - O(2)$_3$	3.40	0.06
Bi(21) - O(1)	2.24	0.06
Bi(21) - O(1)$_3$	2.39	0.06
Bi(21) - O(24)	2.47	0.02
Bi(21) - O(20)$_7$	2.71	0.04
Bi(21) - O(3)$_3$	2.75	0.06
Bi(21) - O(3)	3.06	0.06
Bi(21) - O(5)	3.19	0.05
Bi(21) - O(5)$_3$	3.32	0.05
Bi(21) - O(2)$_3$	3.40	0.06
Bi(3) - O(2)$_3$	2.18	0.06
Bi(3) - O(2)	2.42	0.05
Bi(3) - O(17)	2.51	0.03
Bi(3) - O(20)$_7$	2.52	0.04
Bi(3) - O(2)$_9$	2.64	0.06
Bi(3) - O(2)$_8$	2.84	0.05
Bi(3) - O(20)$_6$	2.93	0.04
Bi(3) - O(15)$_6$	2.95	0.04
Bi(3) - O(15)$_7$	3.08	0.04

Table 7.1 - continued

$Bi(10)_6 - O(9)_3$	2.26	0.08	$Bi(1)_6 - O(19)$	2.34	0.04
$Bi(10)_6 - O(9)$	2.31	0.08	$Bi(1)_6 - O(8)_3$	2.37	0.08
$Bi(10)_6 - O(19)$	2.34	0.04	$Bi(1)_6 - O(8)$	2.38	0.08
$Bi(10)_6 - O(21)$	2.55	0.04	$Bi(1)_6 - O(7)_3$	2.49	0.04
			$Bi(1)_6 - O(22)$	2.49	0.06
$Bi(10)_6 - O(8)$	2.94	0.06			
$Bi(10)_6 - O(8)_3$	2.98	0.06	$Bi(1)_6 - O(9)_3$	2.86	0.06
$Bi(10)_6 - O(11)$	3.28	0.04	$Bi(1)_6 - O(7)$	2.92	0.04
$Bi(10)_6 - O(7)_3$	3.25	0.03	$Bi(1)_6 - O(9)$	2.95	0.06
			$Bi(1)_6 - O(23)$	3.16	0.03

Niobium-Niobium Distances - Pentagonal Nb-s

$Nb(1) - Nb(2)_1$	3.340	0.005
$Nb(1) - Nb(5)$	3.287	0.004
$Nb(1) - Nb(3)$	3.260	0.005
$Nb(1) - Nb(6)$	3.376	0.005
$Nb(1) - Nb(8)_1$	3.276	0.005

Table 7.1 - continued

Oxygen-Oxygen Distances

Nb(1) Pentagon

$O(6)_1$ - O(12)	2.39	0.03
O(12) - O(13)	2.38	0.03
O(13) - O(14)	2.53	0.03
O(14) - O(15)	2.51	0.03
O(15) - $O(6)_1$	2.43	0.03
O(16) - $O(6)_1$	2.58	0.05
O(16) - O(12)	2.51	0.04
O(16) - O(13)	2.56	0.04
O(16) - O(14)	2.59	0.04
O(16) - O(15)	2.62	0.04
$O(16)_2$ - $O(6)_1$	3.09	0.06
$O(16)_2$ - O(12)	3.20	0.04
$O(16)_2$ - O(13)	3.21	0.04
$O(16)_2$ - O(14)	3.19	0.04
$O(16)_2$ - O(15)	3.25	0.04

Nb(3) Octahedron

O(13) - O(14)	2.53	0.03

Nb(2) Octahedron

O(2) - O(5)	2.99	0.04
O(5) - O(6)	2.87	0.04
O(6) - $O(15)_6$	2.43	0.03
$O(15)_6$ - O(2)	2.83	0.04
O(17) - O(2)	3.14	0.06
O(17) - O(5)	2.85	0.06
O(17) - O(6)	3.04	0.06
O(17) - $O(15)_6$	3.01	0.05
$O(17)_2$ - O(2)	2.41	0.05
$O(17)_2$ - O(5)	2.56	0.06
$O(17)_2$ - O(6)	2.65	0.05
$O(17)_2$ - $O(15)_6$	2.75	0.05

Nb(4) Octahedron

O(8) - O(9)	2.74	0.05
O(9) - $O(11)_1$	2.86	0.04
$O(11)_1$ - $O(10)_1$	2.68	0.04
$O(10)_1$ - O(8)	2.90	0.04

Table 7.1 - continued

Nb(3) Octahedron (cont.)

$O(14) - O(3)_6$	2.82	0.04
$O(3)_6 - O(4)_6$	2.76	0.04
$O(4)_6 - O(13)$	3.18	0.04
$O(18) - O(13)$	2.41	0.06
$O(18) - O(14)$	2.49	0.06
$O(18) - O(3)_6$	2.66	0.06
$O(18) - O(4)_6$	2.58	0.06
$O(18)_2 - O(13)$	3.26	0.07
$O(18)_2 - O(14)$	3.28	0.07
$O(18)_2 - O(3)_6$	3.00	0.07
$O(18)_2 - O(4)_6$	2.90	0.07

Nb(5) Octahedron

$O(14) - O(15)$	2.51	0.03
$O(15) - O(2)_4$	2.92	0.04
$O(2)_4 - O(1)_4$	2.94	0.04
$O(1)_4 - O(14)$	2.81	0.04
$O(20) - O(14)$	2.51	0.05
$O(20) - O(15)$	2.49	0.05

Nb(4) Octahedron (cont.)

$O(19) - O(8)$	2.53	0.09
$O(19) - O(9)$	2.71	0.08
$O(19) - O(10)_1$	2.91	0.07
$O(19) - O(11)_1$	2.58	0.07
$O(19)_2 - O(8)$	2.79	0.09
$O(19)_2 - O(9)$	2.87	0.09
$O(19)_2 - O(10)_1$	2.88	0.07
$O(19)_2 - O(11)_1$	3.06	0.07

Nb(6) Octahedron

$O(9) - O(10)$	2.99	0.04
$O(10) - O(13)$	2.96	0.04
$O(13) - O(12)$	2.38	0.03
$O(12) - O(9)$	2.87	0.04
$O(21) - O(9)$	2.43	0.07
$O(21) - O(10)$	2.59	0.05
$O(21) - O(12)$	2.47	0.05
$O(21) - O(13)$	2.53	0.05
$O(21)_2 - O(9)$	2.97	0.08

Table 7.1 - continued

Nb(5) Octahedron (cont.)

O(20) - $O(2)_4$	2.59	0.06
O(20) - $O(1)_4$	2.36	0.06
$O(20)_2$ - O(14)	3.26	0.05
$O(20)_2$ - O(15)	3.25	0.05
$O(20)_2$ - $O(2)_4$	2.91	0.06
$O(20)_2$ - $O(1)_4$	3.12	0.07

Nb(7) Octahedron

O(4) - O(5)	3.12	0.04
O(5) - O(7)	2.81	0.04
O(7) - O(8)	2.41	0.04
O(8) - O(4)	2.82	0.04
O(22) - O(4)	2.78	0.09
O(22) - O(5)	2.69	0.08
O(22) - O(7)	2.71	0.08
O(22) - O(8)	2.53	0.10
$O(22)_2$ - O(4)	2.78	0.08
$O(22)_2$ - O(5)	3.26	0.09
$O(22)_2$ - O(7)	2.67	0.08
$O(22)_2$ - O(8)	2.93	0.10

Nb(6) Octahedron (cont.)

$O(21)_2$ - O(10)	2.92	0.05
$O(21)_2$ - O(12)	3.34	0.05
$O(21)_2$ - O(13)	3.36	0.05

Nb(8) Octahedron

O(6) - O(7)	2.85	0.04
O(7) - O(11)	2.97	0.04
O(11) - $O(12)_6$	2.98	0.04
$O(12)_6$ - O(6)	2.39	0.04
O(23) - O(6)	2.70	0.07
O(23) - O(7)	2.87	0.07
O(23) - O(11)	2.62	0.07
O(23) - $O(12)_6$	2.59	0.07
$O(23)_2$ - O(6)	2.94	0.07
$O(23)_2$ - O(7)	2.59	0.06
$O(23)_2$ - O(11)	3.01	0.07
$O(23)_2$ - $O(12)_6$	3.03	0.07

Table 7.1 - continued

Nb(9) Octahedron

O(1) - O(3)	2.74	0.04
O(3) - $O(1)_5$	2.88	0.04
O(24) - O(1)	3.04	0.06
O(24) - O(3)	3.21	0.07
$O(24)_2$ - O(1)	2.64	0.06
$O(24)_2$ - O(3)	2.34	0.06

Bi(21) Environment

O(1) - O(24)	3.04	0.06
O(1) - $O(20)_7$	2.36	0.07
$O(1)_3$ - O(24)	2.64	0.06
$O(1)_3$ - $O(20)_7$	3.12	0.07
$O(20)_7$ - O(24)	>3.5	
$O(3)_3$ - O(1)	>3.5	
$O(3)_3$ - $O(1)_3$	2.74	0.04
$O(3)_3$ - O(24)	2.34	0.05

Bi(2) Environment

O(3) - O(24)	3.21	0.07
O(3) - $O(18)_1$	2.66	0.06
$O(3)_3$ - O(24)	2.34	0.06
$O(3)_3$ - $O(18)_1$	3.00	0.06
O(24) - $O(18)_1$	>3.5	

Bi(22) Environment

O(5) - O(17)	2.85	0.06
O(5) - O(22)	2.69	0.08
$O(5)_3$ - O(17)	2.56	0.07
$O(5)_3$ - O(22)	3.26	0.08
O(17) - O(22)	>3.5	

Bi(3) Environment

O(2) - $O(20)_7$	2.59	0.06
O(2) - O(17)	3.14	0.06
$O(2)_3$ - $O(20)_7$	2.92	0.07
$O(2)_3$ - O(17)	2.40	0.06
O(20) - O(17)	>3.5	

Table 7.1 - continued

Bi(10) Environment				Bi(1) Environment			
O(9)	- O(19)	2.71	0.08	O(8)	- O(19)	2.53	0.10
O(9)	- O(21)	2.43	0.07	O(8)	- O(22)	2.53	0.09
$O(9)_3$	- O(19)	2.87	0.08	$O(8)_3$	- O(19)	2.79	0.08
$O(9)_3$	- O(21)	2.97	0.08	$O(8)_3$	- O(22)	2.93	0.09
O(19)	- O(21)	>3.5		O(19)	- O(22)	>3.5	
				O(9)	- O(7)	>3.5	
				O(9)	- $O(7)_3$	>3.5	

Table 7.2 - $3Bi_2O_3.17Nb_2O_5$, Some Inter-Atomic Angles and Standard Deviations in Å.

Nb(1) Pentagon			Nb(2) Octahedron		
$O(6)_1$ - Nb(1) - O(12)	71.4	0.9	O(2) - Nb(2) - O(5)	103.6	1.2
O(12) - Nb(1) - O(13)	69.4	1.0	O(5) - Nb(2) - O(6)	95.1	1.1
O(13) - Nb(1) - O(14)	74.2	0.9	O(6) - Nb(2) - $O(15)_6$	72.4	0.9
O(14) - Nb(1) - O(15)	72.9	0.8	$O(15)_6$ - Nb(2) - O(2)	98.3	1.0
O(15) - Nb(1) - $O(6)_1$	71.5	0.8			
			O(17) - Nb(2) - O(2)	94.3	1.8
O(16) - Nb(1) - $O(6)_1$	89.1	1.7	O(17) - Nb(2) - O(5)	84.5	2.0
O(16) - Nb(1) - O(12)	83.8	1.7	O(17) - Nb(2) - O(6)	88.0	1.8
O(16) - Nb(1) - O(13)	84.8	1.4	O(17) - Nb(2) - $O(15)_6$	85.5	1.4
O(16) - Nb(1) - O(14)	87.3	1.4			
O(16) - Nb(1) - O(15)	87.9	1.3	$O(17)_2$ - Nb(2) - O(2)	85.0	2.0
			$O(17)_2$ - Nb(2) - O(5)	95.0	2.1
$O(16)_2$ - Nb(1) - $O(6)_1$	91.3	1.7	$O(17)_2$ - Nb(2) - O(6)	93.0	2.0
$O(16)_2$ - Nb(1) - O(12)	94.1	1.3	$O(17)_2$ - Nb(2) - $O(15)_6$	95.3	1.6
$O(16)_2$ - Nb(1) - O(13)	93.4	1.3			
$O(16)_2$ - Nb(1) - O(14)	93.8	1.4	O(17) - Nb(2) - $O(17)_2$	178.9	1.3
$O(16)_2$ - Nb(1) - O(15)	94.4	1.3			
O(16) - Nb(1) - $O(16)_2$	177.6	0.9			

Table 7.2 - continued

Nb(3) Octahedron			Nb(4) Octahedron		
O(13) - Nb(3) - O(14)	76.0	0.9	O(8) - Nb(4) - O(9)	79.4	1.2
O(14) - Nb(3) - $O(3)_6$	87.9	1.1	O(9) - Nb(4) - $O(11)_1$	88.0	1.2
$O(3)_6$ - Nb(3) - $O(4)_6$	89.1	1.3	$O(11)_1$ - Nb(4) - $O(10)_1$	94.6	1.2
$O(4)_6$ - Nb(3) - O(13)	104.6	1.1	$O(10)_1$ - Nb(4) - O(8)	98.6	1.2
O(18) - Nb(3) - O(13)	80.4	2.1	O(19) - Nb(4) - O(8)	83.0	2.8
O(18) - Nb(3) - O(14)	83.2	2.2	O(19) - Nb(4) - O(9)	82.1	2.5
O(18) - Nb(3) - $O(3)_6$	93.0	2.6	O(19) - Nb(4) - $O(10)_1$	106.3	1.9
O(18) - Nb(3) - $O(4)_6$	91.4	2.3	O(19) - Nb(4) - $O(11)_1$	90.5	2.1
$O(18)_2$ - Nb(3) - O(13)	98.2	1.8	$O(19)_2$ - Nb(4) - O(8)	83.5	2.7
$O(18)_2$ - Nb(3) - O(14)	98.4	1.8	$O(19)_2$ - Nb(4) - O(9)	80.0	2.4
$O(18)_2$ - Nb(3) - $O(3)_6$	89.1	2.3	$O(19)_2$ - Nb(4) - $O(11)_1$	99.2	2.0
$O(18)_2$ - Nb(3) - $O(4)_6$	87.1	2.0	$O(19)_2$ - Nb(4) - $O(10)_1$	91.3	1.8
O(18) - Nb(3) - $O(18)_2$	177.4	2.2	O(19) - Nb(4) - $O(19)_2$	159.2	1.6

Table 7.2 - continued

Nb(5) Octahedron			Nb(6) Octahedron		
O(14) - Nb(5) - O(15)	76.0	0.9	O(9) - Nb(6) - O(10)	101.6	1.2
O(15) - Nb(5) - $O(2)_4$	93.8	1.0	O(10) - Nb(6) - O(13)	92.7	1.0
$O(2)_4$ - Nb(5) - $O(1)_4$	99.2	1.2	O(13) - Nb(6) - O(12)	70.7	1.0
$O(1)_4$ - Nb(5) - O(14)	91.0	1.0	O(12) - Nb(6) - O(9)	94.9	1.3
O(20) - Nb(5) - O(14)	86.9	1.8	O(21) - Nb(6) - O(9)	88.8	2.9
O(20) - Nb(5) - O(15)	86.1	1.8	O(21) - Nb(6) - O(10)	92.0	1.8
O(20) - Nb(5) - $O(2)_4$	93.1	2.1	O(21) - Nb(6) - O(12)	85.3	1.8
O(20) - Nb(5) - $O(1)_4$	84.8	2.2	O(21) - Nb(6) - O(13)	85.5	1.8
$O(20)_2$ - Nb(5) - O(14)	95.8	1.6	$O(21)_2$ - Nb(6) - O(9)	88.7	2.8
$O(20)_2$ - Nb(5) - O(15)	95.7	1.6	$O(21)_2$ - Nb(6) - O(10)	84.0	1.6
$O(20)_2$ - Nb(5) - $O(2)_4$	84.4	1.8	$O(21)_2$ - Nb(6) - O(12)	99.5	1.6
$O(20)_2$ - Nb(5) - $O(1)_4$	94.0	2.0	$O(21)_2$ - Nb(6) - O(13)	98.0	1.5
O(20) - Nb(5) - $O(20)_2$	177.1	1.5	O(21) - Nb(6) - $O(21)_2$	174.8	1.5

Table 7.2 - continued

Nb(7) Octahedron			Nb(8) Octahedron		
O(4) - Nb(7) - O(5)	105.2	1.3	O(6) - Nb(8) - O(7)	90.8	1.1
O(5) - Nb(7) - O(7)	90.0	1.2	O(7) - Nb(8) - O(11)	97.6	1.2
O(7) - Nb(7) - O(8)	74.6	1.3	O(11) - Nb(8) - $O(12)_6$	97.7	1.1
O(8) - Nb(7) - O(4)	91.7	1.3	$O(12)_6$ - Nb(8) - O(6)	73.2	1.0
O(22) - Nb(7) - O(4)	96.4	2.5	O(23) - Nb(8) - O(6)	92.2	1.9
O(22) - Nb(7) - O(5)	90.4	2.6	O(23) - Nb(8) - O(7)	102.7	1.5
O(22) - Nb(7) - O(7)	96.1	2.3	O(23) - Nb(8) - O(11)	90.2	1.9
O(22) - Nb(7) - O(8)	83.8	3.1	O(23) - Nb(8) - $O(12)_6$	89.3	1.7
$O(22)_2$ - Nb(7) - O(4)	85.1	2.2	$O(23)_2$ - Nb(8) - O(6)	87.0	1.8
$O(22)_2$ - Nb(7) - O(5)	99.0	2.3	$O(23)_2$ - Nb(8) - O(7)	75.8	1.4
$O(22)_2$ - Nb(7) - O(7)	80.0	1.9	$O(23)_2$ - Nb(8) - O(11)	90.8	1.7
$O(22)_2$ - Nb(7) - O(8)	86.1	2.9	$O(23)_2$ - Nb(8) - $O(12)_6$	91.9	1.5
O(22) - Nb(7) - $O(22)_2$	169.8	2.4	O(23) - Nb(8) - $O(23)_2$	178.3	1.3

Nb(9) Octahedron					
O(1) - Nb(9) - O(3)	87.4	1.2	O(24) - Nb(9) - O(3)	93.6	1.9
O(3) - Nb(9) - $O(1)_5$	93.3	1.2	$O(24)_2$ - Nb(9) - O(1)	95.7	1.9
O(24) - Nb(9) - O(1)	84.3	1.7	$O(24)_2$ - Nb(9) - O(3)	86.4	1.9
			O(24) - Nb(9) - $O(24)_2$	180	

The Niobium Co-ordination

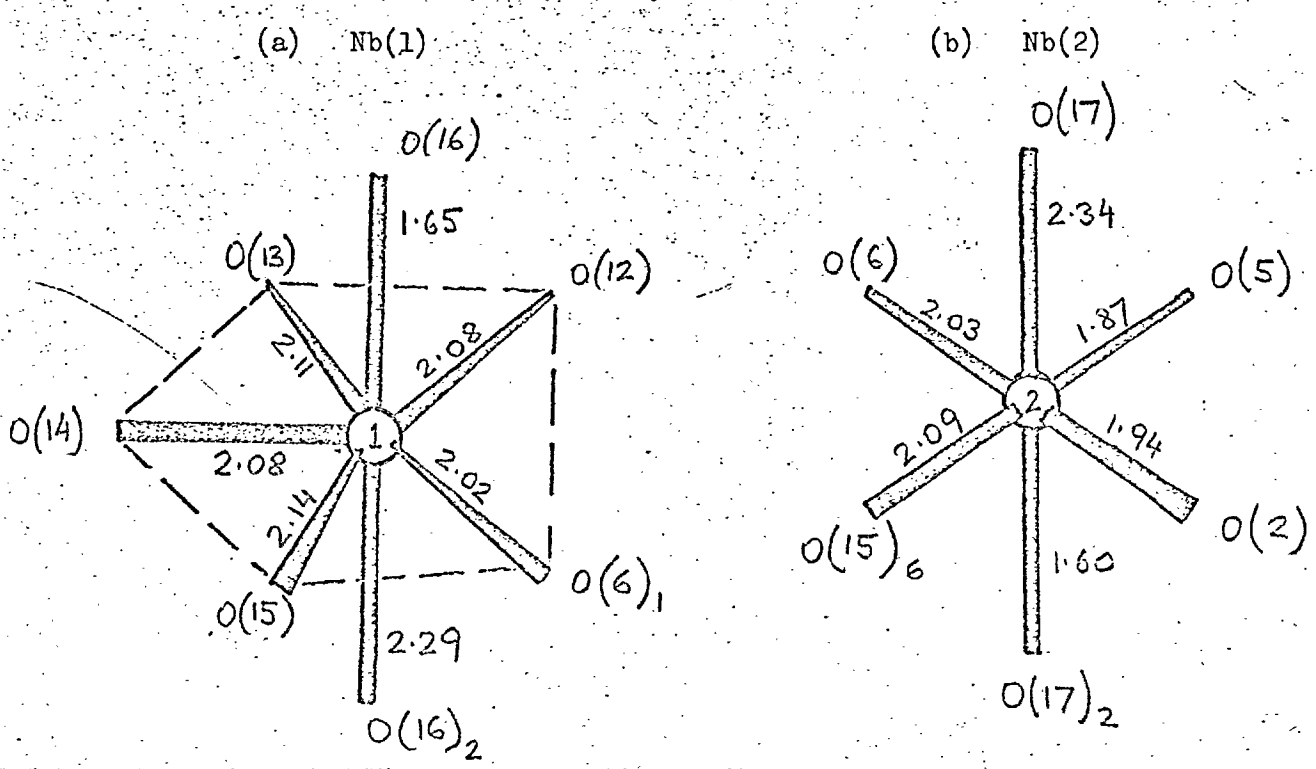
One niobium atom has a pentagonal bipyramidal co-ordination, whereas the eight others are octahedrally surrounded by oxygen atoms (Figure 7.4).

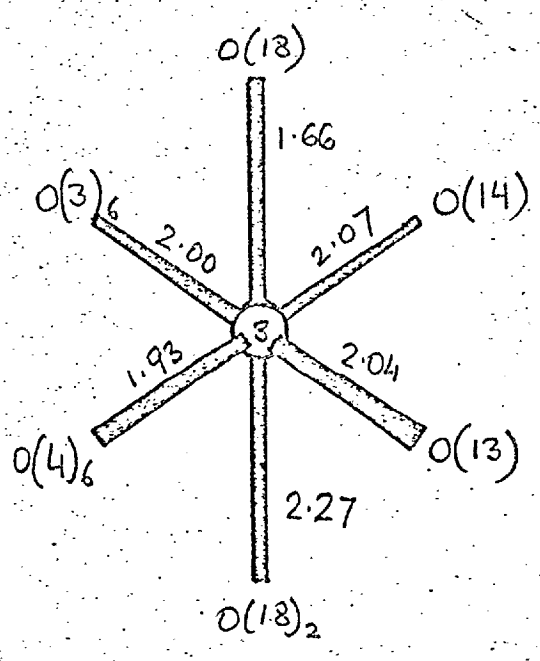
The octahedra are all distorted but have mean Nb-O distances ranging from 1.98 to 1.99Å, which are quite usual. In every case however, there is one very short Nb-O bond perpendicular to the octahedral sheet, but not always in the same sense. These short distances are usually of the order of 1.60Å, except in one case, $(Nb(9) - O(24)_2)$, where there is an ultra short distance of 1.48 ± 0.06 Å. It is thought that the constraint of these two atoms to the diad axis is responsible for this very short distance. The disorder of the bismuth atoms inevitably leads to a breakdown in the symmetry at the unit cell level, and these two atoms must move off the'diad' axis slightly, as required by the local environment. It is therefore reasonable to suppose that the $Nb(9) - O(24)_2$ distance quoted does not represent reality. The other short Nb-O distances may be compared with the shortest Nb-O distance reported[I.63,I.64] of 1.57 Å.

The fact that the bismuth atoms are disordered, makes the positions of the oxygen atoms at the same height as the bismuths much less certain than the estimated standard deviations would imply. The high temperature factors of some oxygen atoms are also an indication that the refined positions represent mean values of slightly different positions, depending on the presence or absence of a bismuth atom in the vicinity. Since the short bond is not always in the same sense, it is not thought to be a function

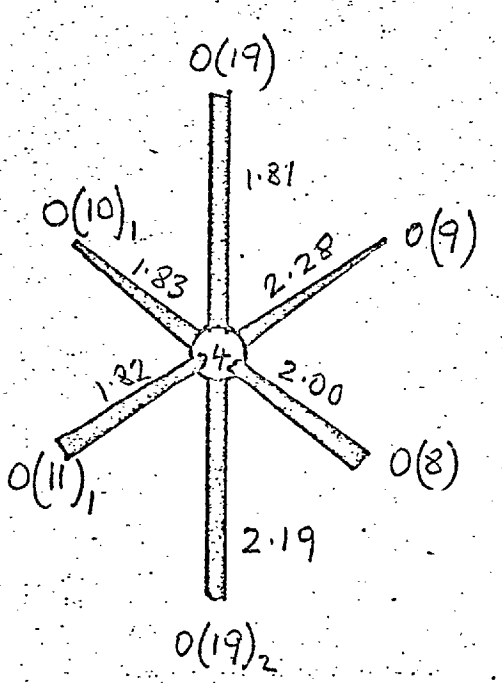
Figure 7.4 (a) - (i)

$3Bi_2O_3.17Nb_2O_5$, Nb-O co-ordinations and distances (Å)

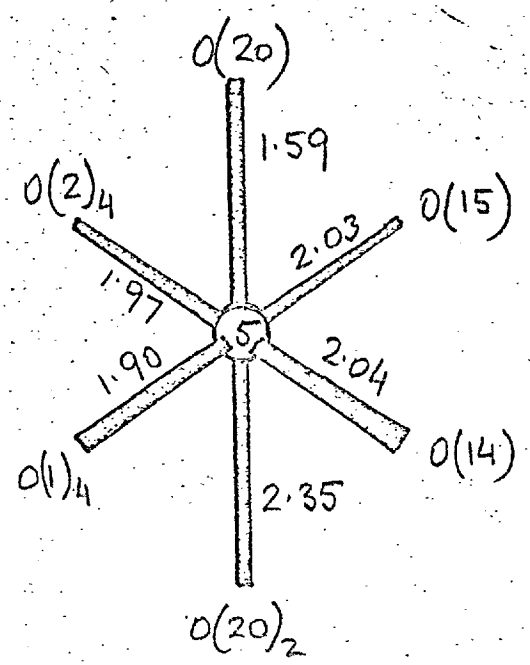




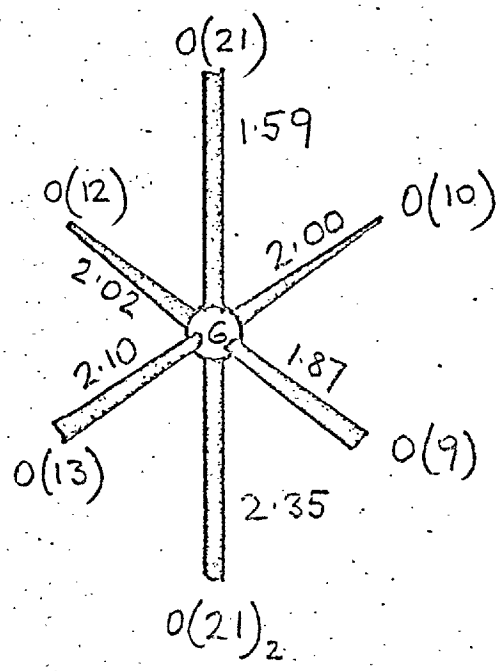
(c) Nb(3)



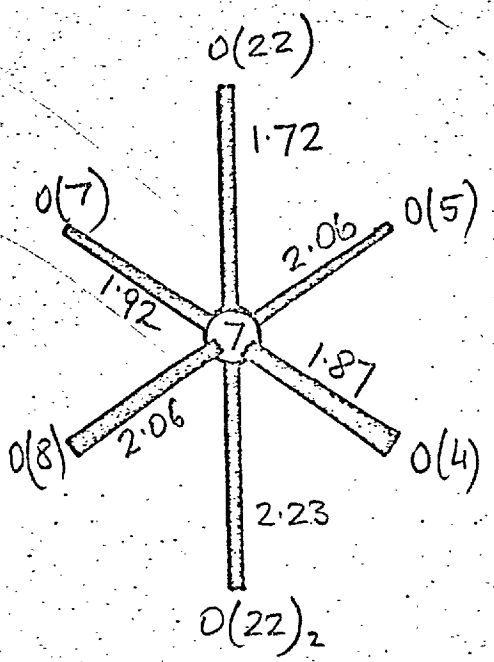
(d) Nb(4)



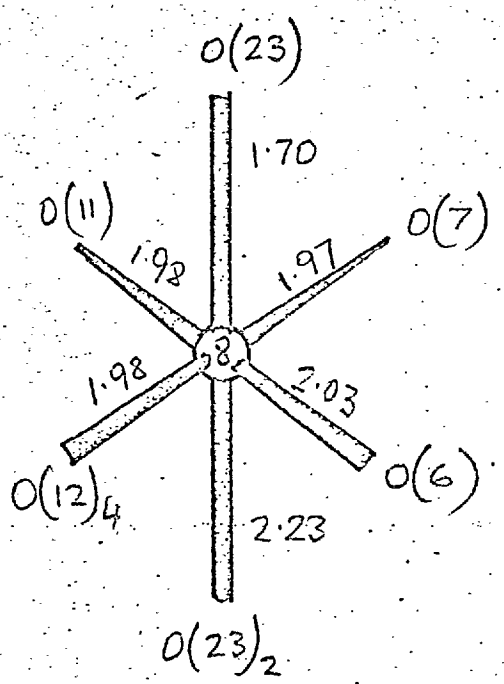
(e) Nb(5)



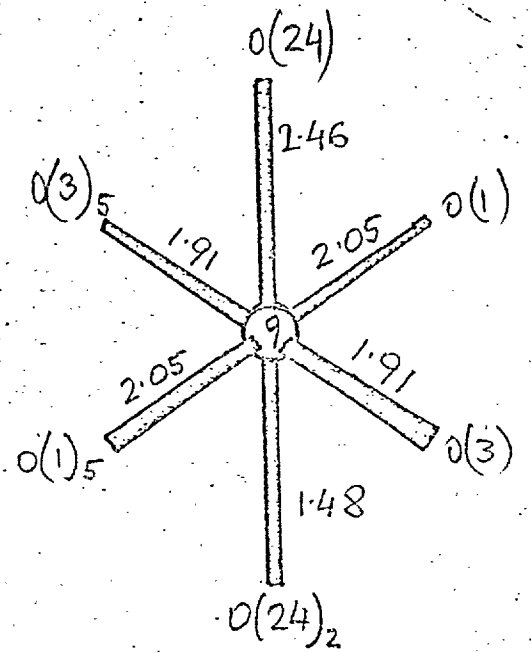
(f) Nb(6)



(g) Nb(7)



(h) Nb(8)



(i) Nb(9)

of some systematic error or erroneous refinement. It may be concluded that the presence of very short Nb-O bonds is a structural feature. ($Nb_{16}W_{18}O_{94}$ was solved in projection only).

The very short Nb-O distance is accompanied by a longer than usual one to the opposite apex. Very short Nb-O distances have been found in some "shear" compounds e.g. $Nb_{16}O_{42}F$ (1.57Å)[I.63,I.64] and $TiNb_2O_7$ (1.64Å)[I.65]. In both these cases, as in $3Bi_2O_3.17Nb_2O_5$, the average of the six octahedral Nb-O distances is quite normal at 2.0Å, and there is one longer distance (2.33Å and 2.34Å respectively) to compensate for the short one.

The oxygen-oxygen contacts and the oxygen-niobium-oxygen angles in Tables 7.1 and 7.2 respectively, indicate the distortions of the octahedra in $3Bi_2O_3.17Nb_2O_5$.

Since the very short Nb-O distance is accompanied by a longer than usual one to the opposite apex, one may conclude that the niobium atom is displaced along the body-diagonal of the octahedron, perpendicular to the octahedral sheet in $3Bi_2O_3.17Nb_2O_5$. This is an over-simplified picture however, only true of some octahedra. Consideration of the displacement of the niobium atom from the plane of the equatorial oxygens for each octahedron (Figure 7.5) shows that in only five cases is this displacement towards the close apical oxygen. In the other three instances, as well as in the case of the pentagonal niobium, the metal atom is in the half of the octahedron (or pentagonal bipyramid) opposite to the close oxygen atom. This is illustrated schematically in Figure 7.6.

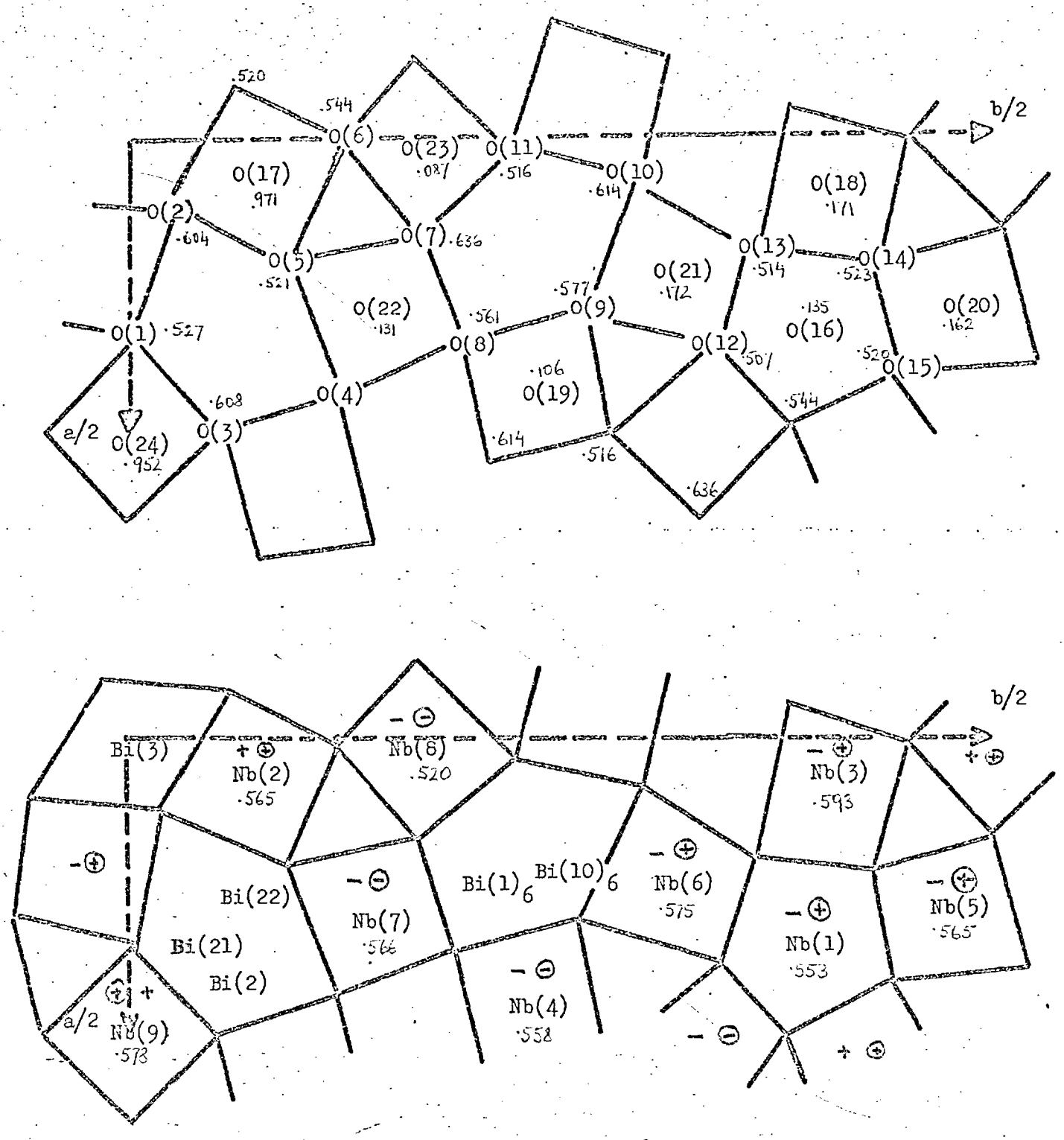


Figure 7.5 - showing the fractional heights of the oxygen and niobium atoms . Octahedra are marked + if the niobium atom is closer to the "top" apical oxygen than the bottom, and ⊕ if the niobium atom is above the plane of the equatorial oxygens.

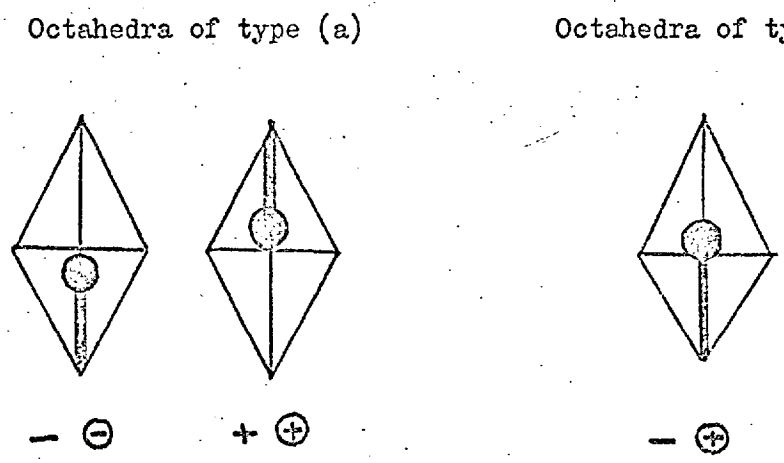


Figure 7.6 - Schematic diagram of the various types of displacements of the niobium atoms in their octahedra. The short Nb-O distance is indicated by a heavy line ═══.

Octahedra of type (a), where the niobium atoms are displaced towards the close oxygen, would be expected to show relatively large dipole moments. Octahedra of type (b) would be expected to be rather less polar, since they are distorted to minimise the effect of the displaced niobium atom. Therefore type (a) octahedra are the principal contributors to dipole fields.

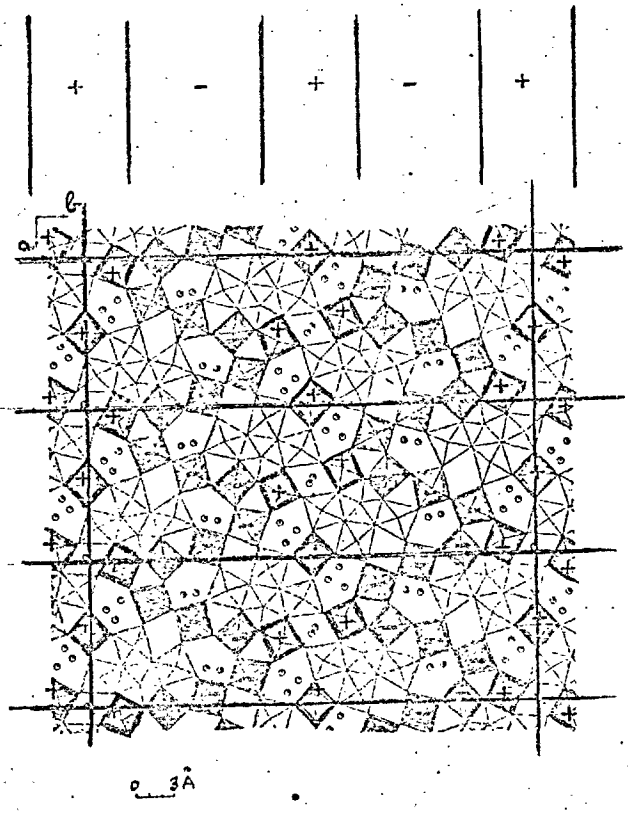
Table 7.3 lists the ratios of the two apical Nb-O distances for each octahedron. Of the type (a) octahedra Nb(2) and Nb(9) have larger niobium displacements than do their "negative" counterparts. Therefore, in spite of the fact that "positive" and "negative" octahedra are not equal in number

the variations in the magnitudes of their displacements tend to minimise the dipole fields set up.

Table 7.3 - $3Bi_2O_3.17Nb_2O_5$, ratios of apical Nb-O distances

Nb	Nb-O/Nb-O_2	Ratio	Type
1.	1.65/2.29	0.72	b
2.	2.34/1.60	1/0.69	a+
3.	1.66/2.27	0.73	b
4.	1.81/2.19	0.83	a-
5.	1.59/2.35	0.68	b
6.	1.59/2.35	0.68	b
7.	1.72/2.23	0.77	a-
8.	1.70/2.23	0.76	a-
9.	2.46/1.48	1/0.60	a+

It is interesting to note the manner in which type (a) octahedra are arranged in the continuous structure. Figure 7.7 shows that polar regions occur in sheets perpendicular to c, and are stacked alternately along b. A schematic [100] projection, Figure 7.8, shows these sheets running through the structure, giving rise to a small scale "domain" effect.



(a) type "-ve" octahedra are blocked in

(a) type "+ve" octahedra are boldly outlined

Figure 7.7

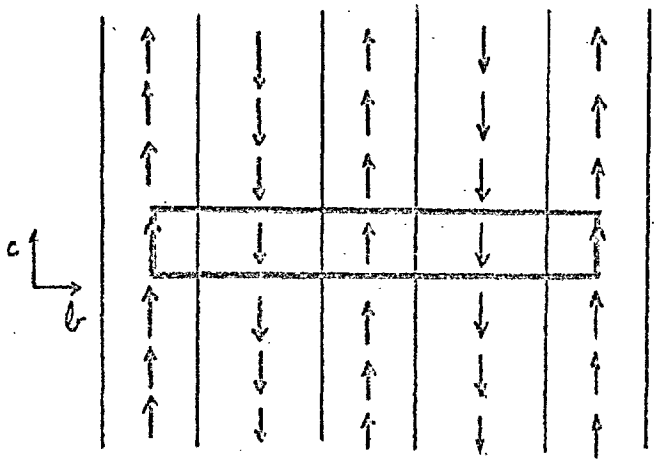


Figure 7.8

A comparison of the space groups Pba2 of $3Bi_2O_3.17Nb_2O_5$ and $P2_12_12$ as in $Nb_{16}W_{18}O_{94}$ (Figure 7.9) shows that although the [001] projections are identical, all equi-points are at the same z height in Pba2, but they are not in $P2_12_12$. It is therefore inevitable that the buckling of the sheet of octahedra, as well as the arrangement of the "domains" must be different in the two compounds.

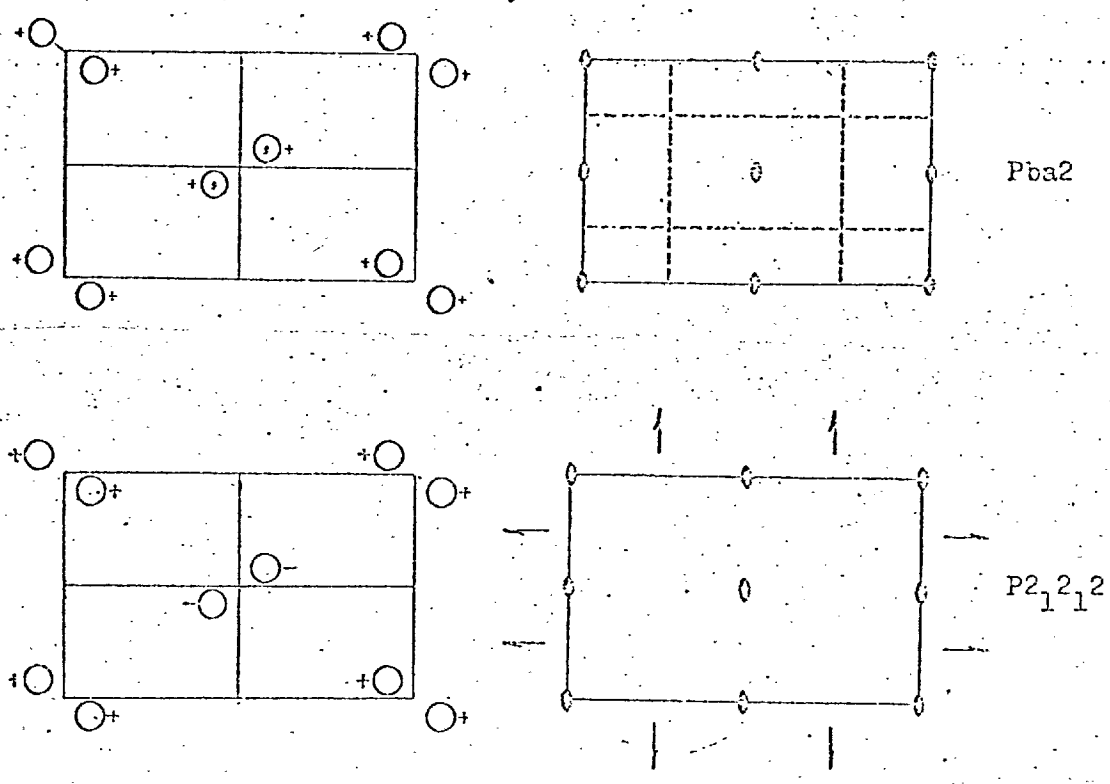


Figure 7.9 - Comparison of space groups Pba2 and $P2_12_12$

The mean niobium-oxygen distance in the pentagonal bipyramid is 2.05Å. Again the diagonal consists of a rather short and a longish Nb-O distance as in the case of the octahedra. The pentagonal bipyramid was treated as a (b) type octahedron in the preceeding discussion.

The pentagon itself is quite regular and rather compact. Both these features are quite usual(I.18,I.57-59). The shortest oxygen contact occurs in the pentagonal ring, and in fact all five distances are below 2.53Å.

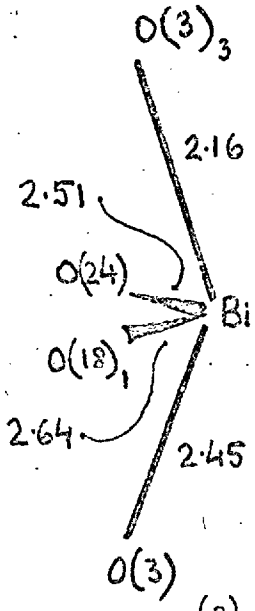
The closest niobium-niobium distance also occurs in the vicinity of the pentagon, where there are five such distances between 3.26 and 3.38Å. (This does not correspond to metal-metal bonding.)

The Bismuth Co-ordination

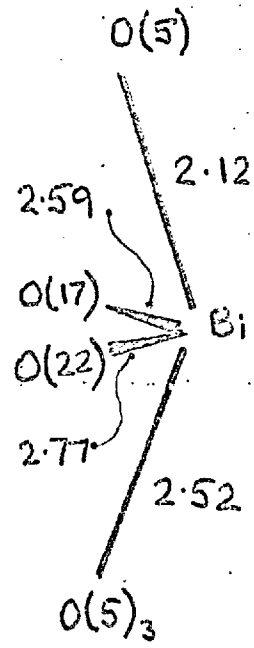
Of the six separate bismuth sites included in least-squares refinement four may be described as having a one-sided four-coordination (although one of these, Bi(3), is a border-line case). The other two also have this environment, but with a fifth close oxygen neighbour.(Figure 7.10). It is difficult to decide where the upper limit of Bi-O distances should be drawn, and Table 7.1 goes up to ~3.2Å.

In almost every case there is one very short Bi-O contact of ~2.1Å, (similarly to triclinic $BiNbO_4$) and three or four rather longer ones. There is a gap of 0.2 - 0.4Å in the list of Bi-O distances between those representing the inner co-ordination of 4 or 5, and the next shortest ones.

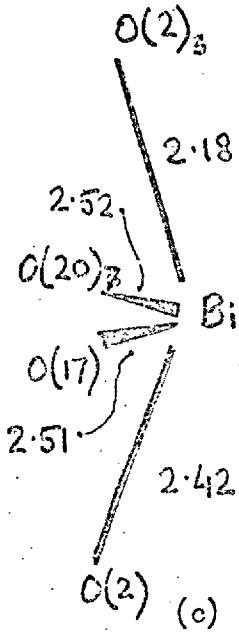
Figure 7.10 (a) - (f); $3Bi_2O_3.17Nb_2O_5$, Inner Bismuth Co-ordination and Bi-O Distances in Å.



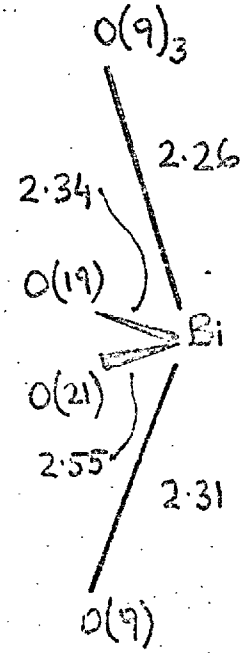
(a) Bi(2)



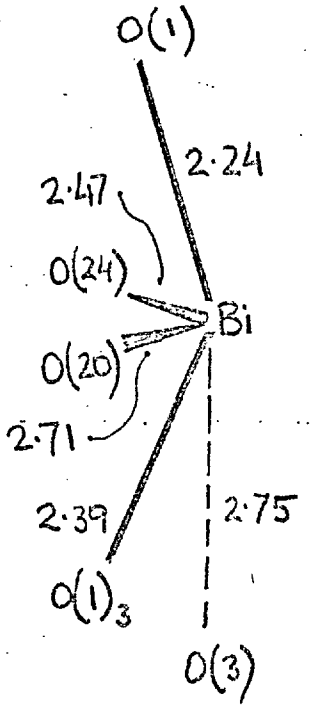
(b) Bi(22)



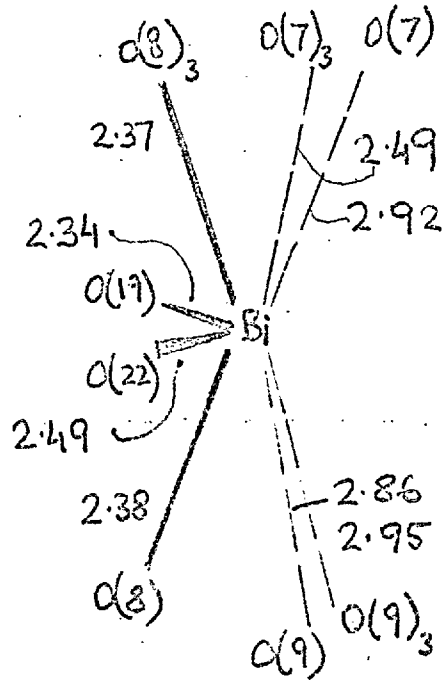
(c) Bi(3)



(d) $Bi(10)_6$


O(1)
2·24
2·47
O(24)
Bi
O(20)
2·71
2·39
2·75
O(1)3
O(3)

(e) Bi(21)


O(8)3
O(7)3
O(7)
2·37
2·49
2·92
2·34
O(19)
Bi
O(22)
2·49
2·38
2·86
2·95
O(8)
O(9)
O(9)3

(f) $Bi(1)_6$

The one-sided four-coordination, a consequence of a lone pair of electrons, is found in a number of oxides and oxy-halides of bismuth, (Refs. I.24-28), but it is more often associated with tervalent antimony, (Refs. I.1,I.30), and is also found for arsenic[I.31].

The mean of the first four Bi-O distances are in the range 2.40 - 2.50Å. The oxygen-oxygen distances within these sets of four indicate that there is a rectangular distortion, such that two pairs of oxygens are rather close together, while the pairs themselves are further apart; Figure 7.11.

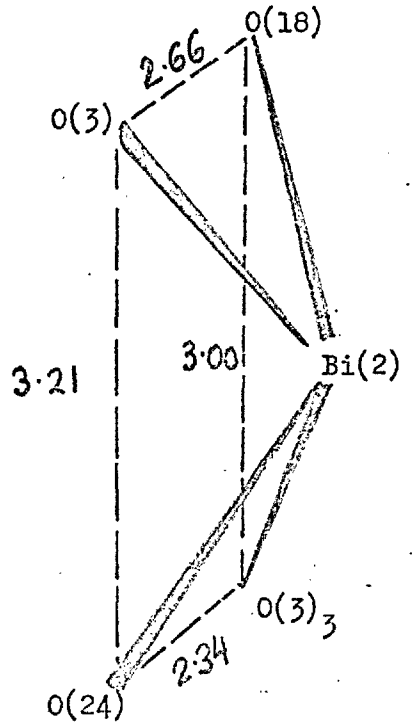


Figure 7.11

Oxygen-oxygen distances in Å.

Of the other two bismuth atoms one, Bi(21), may be pictured as having a fifth oxygen atom co-ordinated to it as well as the four which form a one-sided four-coordination.

The most frequently occupied bismuth site, Bi(1), may also be thought of as eight co-ordinated, there being a one-sided four set of oxygens, and a further four almost coplanar with the bismuth atom.

Oxygen-oxygen contacts

Generally oxygen atoms are over 2.5Å from one another. Oxygen-oxygen distances below this limit are found essentially in two places: either in the ring about the pentagonal niobium atom, or on the contracted sides of the rectangles of the one-sided bismuth co-ordinations.

All the oxygen atoms are associated with the $Nb_{34}O_{94}$ matrix.

8. Investigations on "$Bi_2O_3 \cdot 5Nb_2O_5$" and Discussion of Some Related Compounds

The compound "$Bi_2O_3 \cdot 5Nb_2O_5$" was first prepared by Roth. He found it to be stable from room temperature to a dissociation temperature of 1095°C. He recorded its powder pattern, but did not index it.

Unit Cell

It was found possible to index and refine by least-squares the previously unindexed powder pattern given by Roth for $Bi_2O_3 \cdot 5Nb_2O_5$ (Table 8.1) with the exception of the first doublet of d = 12.2 and 12.4Å, on the basis of an orthorhombic unit cell with

$$a = 17.632 \pm 0.006$$

$$b = 3.949 \pm 0.002$$

$$c = 17.167 \pm 0.006 \text{ Å}.$$

Given this unit cell, there should only be one line in the powder pattern in the neighbourhood of d = 12Å, which is the 101 at d ~ 12.3Å.

A Guinier photograph of the products of preparation (d), (Section 3), which consisted mainly of the 1:5 compound, showed only a single line

Table 8.1 - "$Bi_2O_3 \cdot 5Nb_2O_5$", X-ray Powder Pattern

Cu Kα radiation

λ = 1.54178 Å

Roth and Waring (I.2) I	Roth and Waring (I.2) d(Å)	$\sin^2\theta_{obs}$	h	k	l	$\sin^2\theta_{calc}$
15	12.4	0.00386	1	0	1	0.00393
15	12.2	0.00397				
15	8.55	0.00813	0	0	2	0.00807
100	3.945	0.03818	0	1	0	0.03810
45	3.921	0.03865	4	0	2	0.03865
30	3.854	0.04001	2	0	4	0.03991
30	3.599	0.04588	2	1	0	0.04575
20	3.523	0.04788	2	1	1	0.04776
20	3.453	0.04984	5	0	1	0.04981
80	3.367	0.05242	1	0	5	0.05233
15	3.319	0.05395	2	1	2	0.05381
15	3.276	0.05537	3	1	0	0.05531
50	3.196	0.05818	1	1	3	0.05816
20	3.073	0.06293	4	0	4	0.06285
30	3.062	0.06338	3	1	2	0.06337
90	3.001	0.06599	5	0	3	0.06594
35	2.964	0.06764	3	0	5	0.06762

Table 8.1 continued -

I	d(Å)	$\sin^2\theta_{obs}$	h	k	l	$\sin^2\theta_{calc}$
65	2.940	0.06875	6	0	0	0.06882
5	2.900	0.07066	4	1	1	0.07070
30	2.859	0.07270	0	0	6	0.07259
45	2.843	0.07352	3	1	3	0.07345
60	2.781	0.07634	6	0	2	0.07688
15	2.763	0.07784	2	1	4	0.07801
15	2.722	0.08021	2	0	6	0.08024
20	2.601	0.08784	5	1	1	0.08791
5	2.566	0.09026	1	1	5	0.09043
5	2.487	0.09593	7	0	1	0.09565
			2	1	5	0.09617
5	2.424	0.10114	6	0	4	0.10108
45	2.373	0.10553	3	1	5	0.10572

at the appropriate θ angle. In order to verify this, further careful preparations, (f), were carried out. The Guinier photograph of the product showed only a single line at d ~ 12.3Å. Several high-resolution scans on the General Electric XRD-6 powder diffractometer also showed a unique line in each case at the appropriate 2θ angle.

A manual step-scan was made on the diffractometer to examine the

neighbourhood of $2\theta \sim 7.1^{\circ}$ more thoroughly. The line was rather weak, and therefore three ten-second counts were taken every 0.02° of 2θ. Their average and spread is plotted out in Figure 8.0 (a), while a smoothed out function is plotted in (b). This latter set of points was obtained by plotting the means of three successive intervals. A curve is drawn in each case, showing a single peak.

The conclusion drawn from the above results was that no splitting occurred. The rest of the powder pattern was identical with Roth's for $Bi_2O_3.5Nb_2O_5$, but contained a number of extra lines. These could all be explained by

(a) the presence of a small proportion of $3Bi_2O_3.17Nb_2O_5$, and a trace of high-temperature $BiNbO_4$, and

(b) some weaker lines, not recorded by Roth, but indexable on the same cell data.

Comparison with $Sb_{0.67}Nb_2O_6$

Roth's powder pattern of $Bi_2O_3.5Nb_2O_5$ showed a remarkable similarity to that of the compound $Sb_2O_3.3Nb_2O_5$, recently prepared by Skapski(I.33). He recorded its powder pattern, which resembled those of the tetragonal bronzes, and indexed it on the basis of an orthorhombic unit cell of

$$a = 17.635$$

$$b = 3.968$$

$$c = 17.219 \text{ Å}.$$

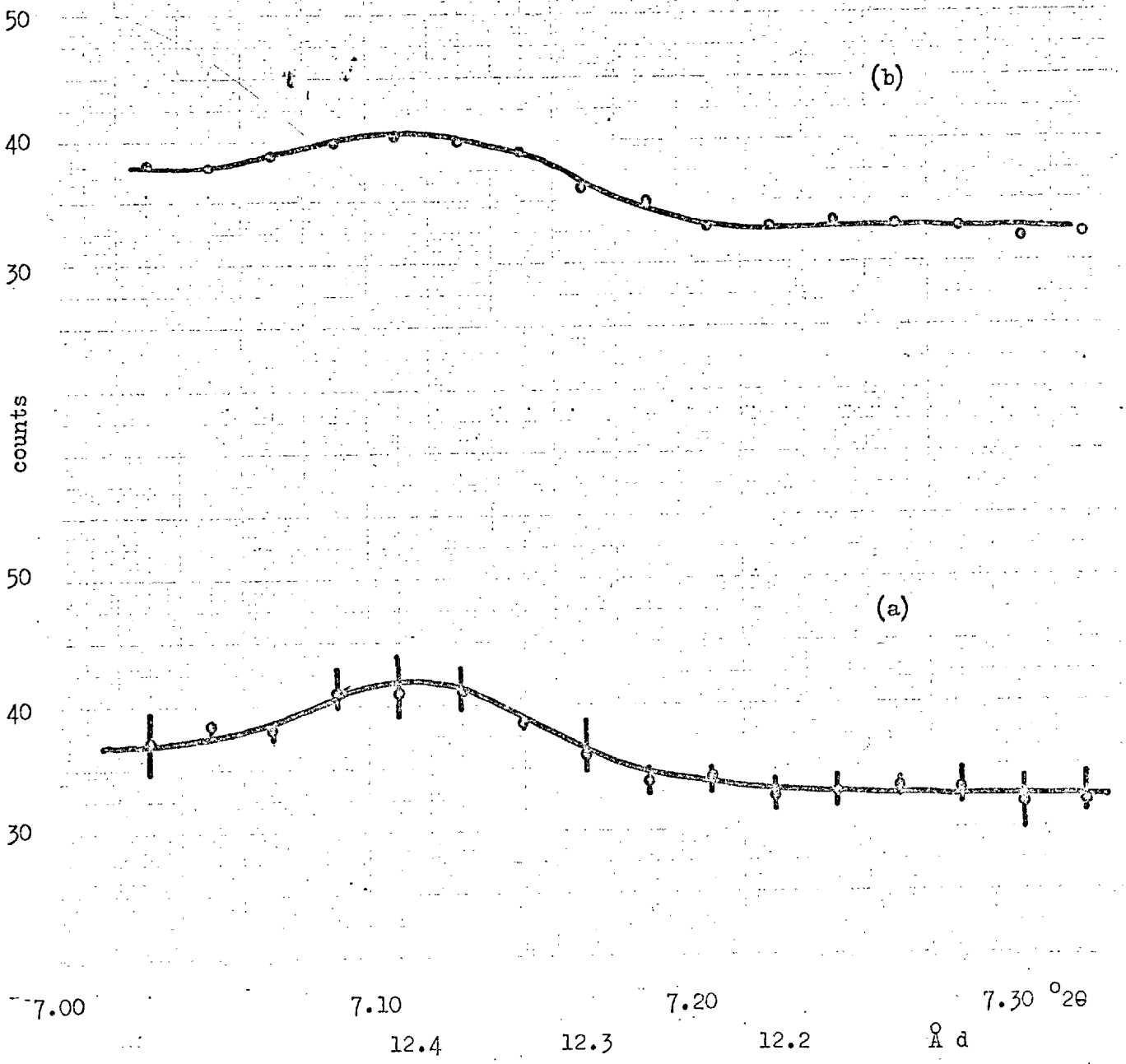


Figure 8.0

There was single-crystal evidence that this was the true cell and absences showed the possible space-groups to be $Pmn2_1$ or Pmnm.

As mentioned above, the author's powder pattern of "$Bi_2O_3.5Nb_2O_5$" included several weak lines not recorded by Roth. The equivalents of these weak lines are however, present in the powder pattern of $Sb_2O_3.3Nb_2O_5$.

The resemblence of these two powder patterns, and the fact that in the case of the antimony compound there is single-crystal evidence for a 17 x 17 cell, is taken as further justification in regarding the unit cell of "$Bi_2O_3.5Nb_2O_5$" as analogous.

The powder patterns of the two compounds are compared in Table 8.2. Since the indices are the same in all but one case, the powder pattern of "$Bi_2O_3.5Nb_2O_5$" satisfies the same absence conditions as the antimony compound, i.e. hkl, no conditions, h0l, h+l=2n present. These imply $Pmn2_1$ or Pmnm as possible space groups, although absences in powder patterns cannot be considered as conclusive.

Relationship with the Tetragonal Bronze Structure

The $\sim$17Å unit-cell edge corresponds to a diagonal of the tetragonal bronze structure (Figure 8.1), which was described in Section 6.

It is proposed that the crystal structure of "$Bi_2O_3.5Nb_2O_5$" is based on a distortion of such a 17 x 17 Å unit cell.

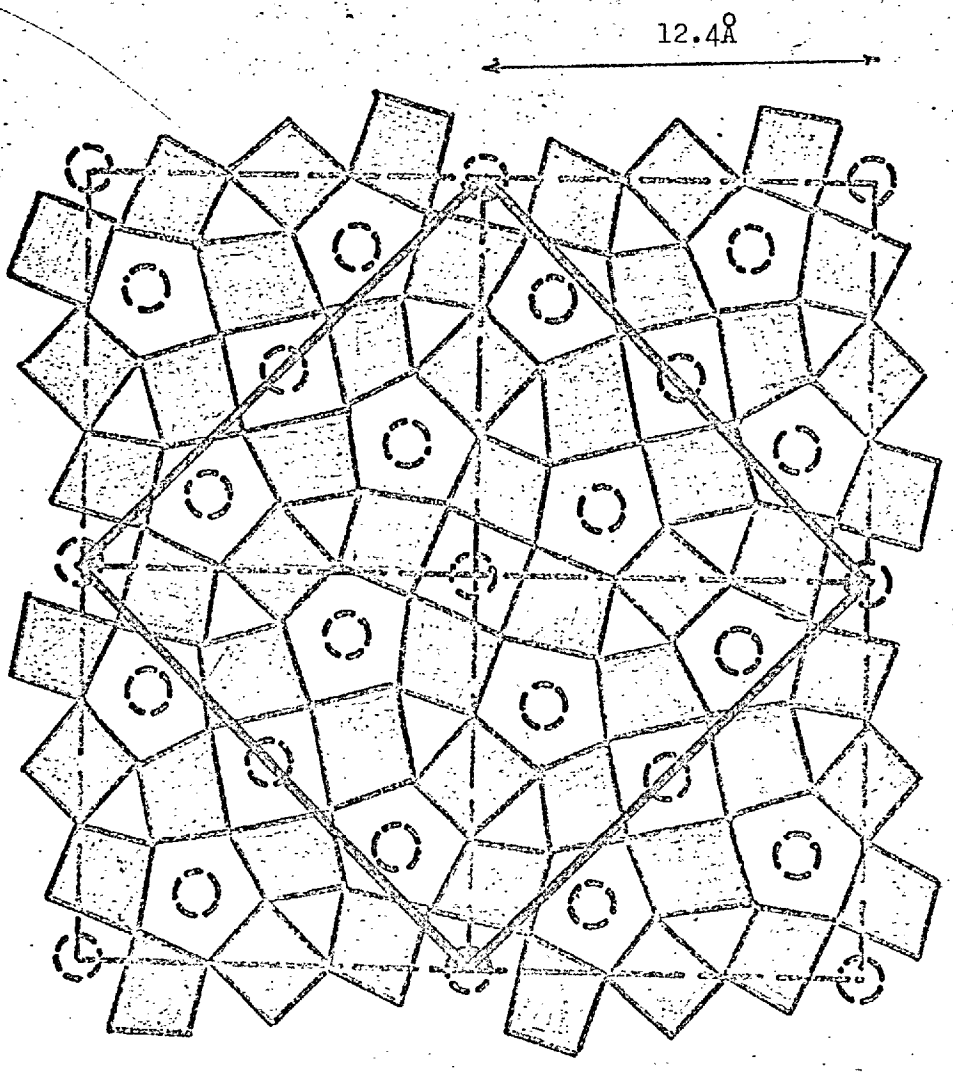
The normal complement of such a cell would be 20 Nb + 60 O. A compound of the type $xA_2O_3.yNb_2O_5$ would require y = 10 and x = 10/3,

Table 8.2 - Powder patterns of the compounds "$Bi_2O_3 \cdot 5Nb_2O_5$" and $Sb_2O_3 \cdot 3Nb_2O_5$.

"$Bi_2O_3 \cdot 5Nb_2O_5$"			$Sb_2O_3 \cdot 3Nb_2O_5$
$d(\text{Å})_{\text{Roth}}$	$d(\text{Å})_{\text{Author}}$	h k l (in both cases)	$d(\text{Å})_{\text{Skapski}}$
12.4			
	12.3	1 0 1	12.42
12.2			
	8.8	2 0 0	
8.55	8.6	0 0 2	8.65
	6.1	2 0 2	6.17
	5.52	1 0 3	5.46
	4.40	4 0 0	4.412
		3 0 3	4.110
3.945	3.94	0 1 0	3.971
3.921	3.91	4 0 2	3.927
3.854	3.87	2 0 4	3.873
		1 1 1	3.781
3.599	3.60	2 1 0	3.621
		0 1 2	3.609
3.523	3.51	2 1 1	3.542
3.453	3.44	5 0 1	3.456
3.367	3.37	1 0 5	3.380
3.319	3.32	2 1 2	
3.276	3.28	3 1 0	3.292

3.196	3.20	1 1 3	3.211
3.073		4 0 4	3.077
3.062		← 2 1 3 | 3 1 2 →	3.063
3.001	2.99	5 0 3	3.004
2.964	2.96	3 0 5	2.971
		4 1 0	2.950
2.940	2.93	6 0 0	2.941
2.900		4 1 1	2.907
2.859	2.85	0 0 6	2.870
2.843	2.84	3 1 3	2.856
		4 1 2	2.790
2.781	2.77	6 0 2	2.782
2.763	2.76	2 1 4	2.771
2.722	2.72	2 0 6	2.730
		4 1 3	2.622
		3 1 4	2.614
2.601	2.59	5 1 1	2.605
2.566		1 1 5	2.573
		5 1 2	2.520
2.487	2.48	2 1 5, 7 0 1	2.495
2.424	2.42	6 0 4	2.426
	2.39	4 0 6	2.405
	2.38	5 1 3	2.396
2.373	2.37	3 1 5	2.378

Figure 8.1 - Showing four unit cells of the tetragonal bronze structure



Basic Structure	No. of Nb-filled pentagons per 17 x 17 cell	Cell Content (17x17)			Formula
	n	Bi	Nb	O	
	0	$6\frac{2}{3}$	20	60	$Bi_2O_3 \cdot 3Nb_2O_5$
	1	$5\frac{2}{3}$	21	61	$Bi_2O_3 \cdot 3\frac{11}{17}Nb_2O_5$
20 Nb + 60 O	2	$4\frac{2}{3}$	22	62	$Bi_2O_3 \cdot 4\frac{5}{7}Nb_2O_5$
+ n(Nb,O)	3	$3\frac{2}{3}$	23	63	$Bi_2O_3 \cdot 6\frac{3}{11}Nb_2O_5$
	4	$2\frac{2}{3}$	24	64	$Bi_2O_3 \cdot 9Nb_2O_5$
	5				
4 per 12 x 37 cell = average per 17x17 cell of		(17 x 17)			
	$2\frac{2}{3}$	4	$22\frac{2}{3}$	$62\frac{2}{3}$	$Bi_2O_3 \cdot 5\frac{2}{3}Nb_2O_5$
					$(3Bi_2O_3 \cdot 17Nb_2O_5)$

Table 8.3

i.e. a formula of $A_2O_3 \cdot 3Nb_2O_5$. This fits the formula given for $Sb_{0.67}Nb_2O_6$ (or $Sb_2O_3 \cdot 3Nb_2O_5$), but not $Bi_2O_3 \cdot 5Nb_2O_5$.

A structure of this type may achieve a Nb:Bi ratio greater than three

either by oxygen deficiency in the matrix, or by the presence of some niobium (plus oxygen) atoms in some of the pentagonal tunnels. By analogy with the $3Bi_2O_3.17Nb_2O_5$ structure, (Section 6 and 7), it is reasonable to take the second alternative.

The basic bronze framework contains four pentagonal tunnels per 12 x 12Å unit cell, which is equivalent to 8 per 17 x 17Å cell. By adding successive (Nb-O) units into the pentagons, one achieves the possible formulae shown in Table 8.3.

Clearly the closest approach to 1:5 occurs when two pentagonal tunnels are filled. The formula then becomes $Bi_2O_3.4\frac{5}{7}Nb_2O_5$, only a small deviation from the nominal 1:5. A cell content of two filled pentagonal tunnels is easily accomodated by some orthorhombic space groups (including $Pmn2_1$) . The non-integral number of bismuth atoms per cell is understandable, if the $4\frac{2}{3}$ bismuths are unevenly distributed at a number of sites of fractional occupancy in the other tunnels, as in the $3Bi_2O_3.17Nb_2O_5$ structure.

Due to the short oxygen-oxygen distances found in the ring of a pentagonal bipyramidal niobium atom, it is extremely unlikely that two neighbouring pentagons should be filled with niobium. If this were the case, Figure 8.2, the central octahedron would have to have two very short oxygen-oxygen distances clamping down on the niobium atom at the centre. No such configuration has yet been found, and it seems reasonable therefore to exclude it from consideration.

There are two potential sets of mirror planes inherent in the basic Nb-O structure as seen in Figure 8.3. (The possibility of a third

transverse mirror plane in the plane of the paper exists, but is unlikely, cf. $3Bi_2O_3.17Nb_2O_5$). It is clear that in the presence of both mirror planes, the filling of any one pentagon in Figure 8.3 produces a situation such as shown in Figure 8.2. Thus if such a situation is to be avoided, one of the mirror planes has to be broken (changed into a glide or a screw for instance). In this case, a sensible structure may be

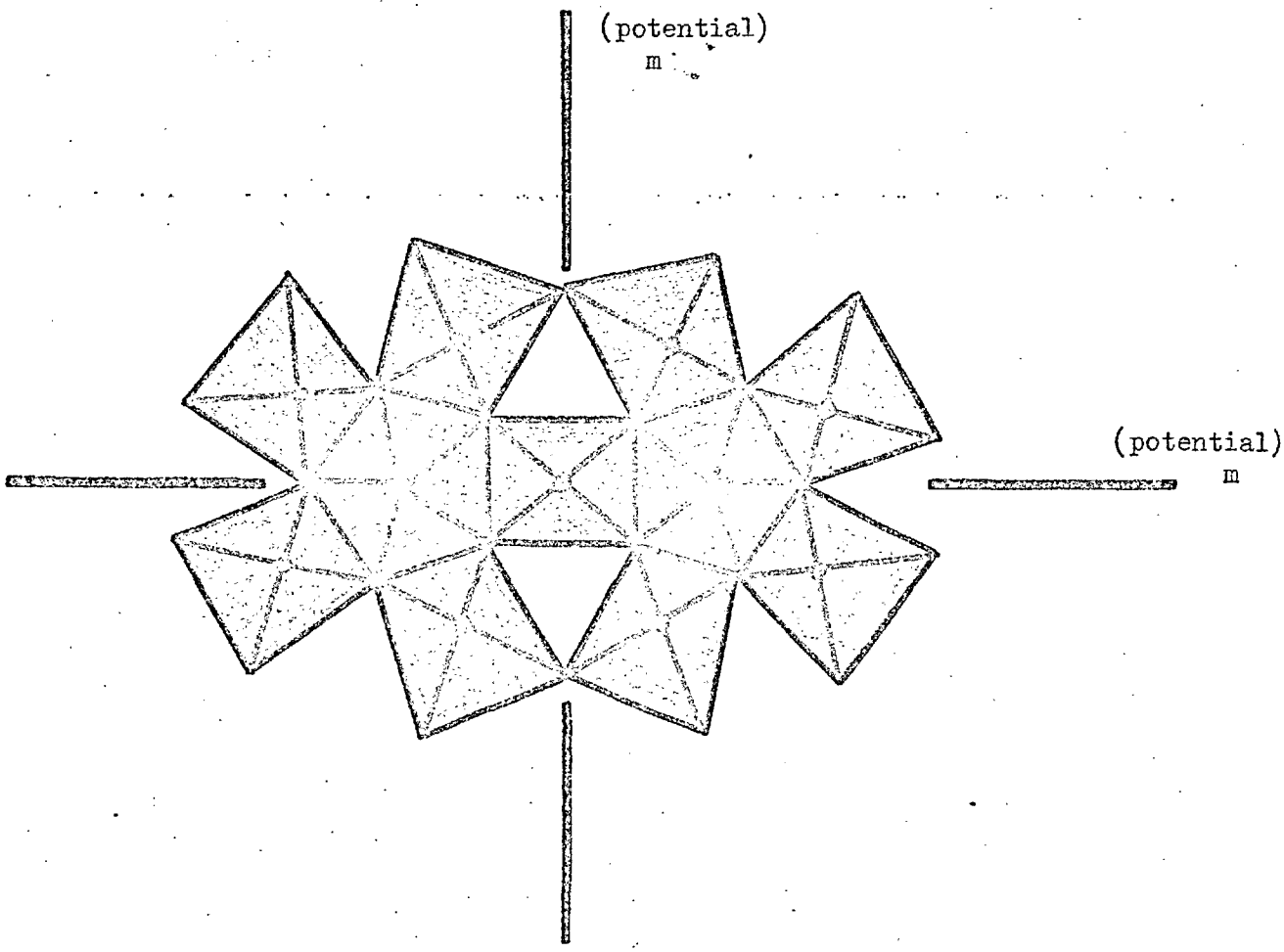
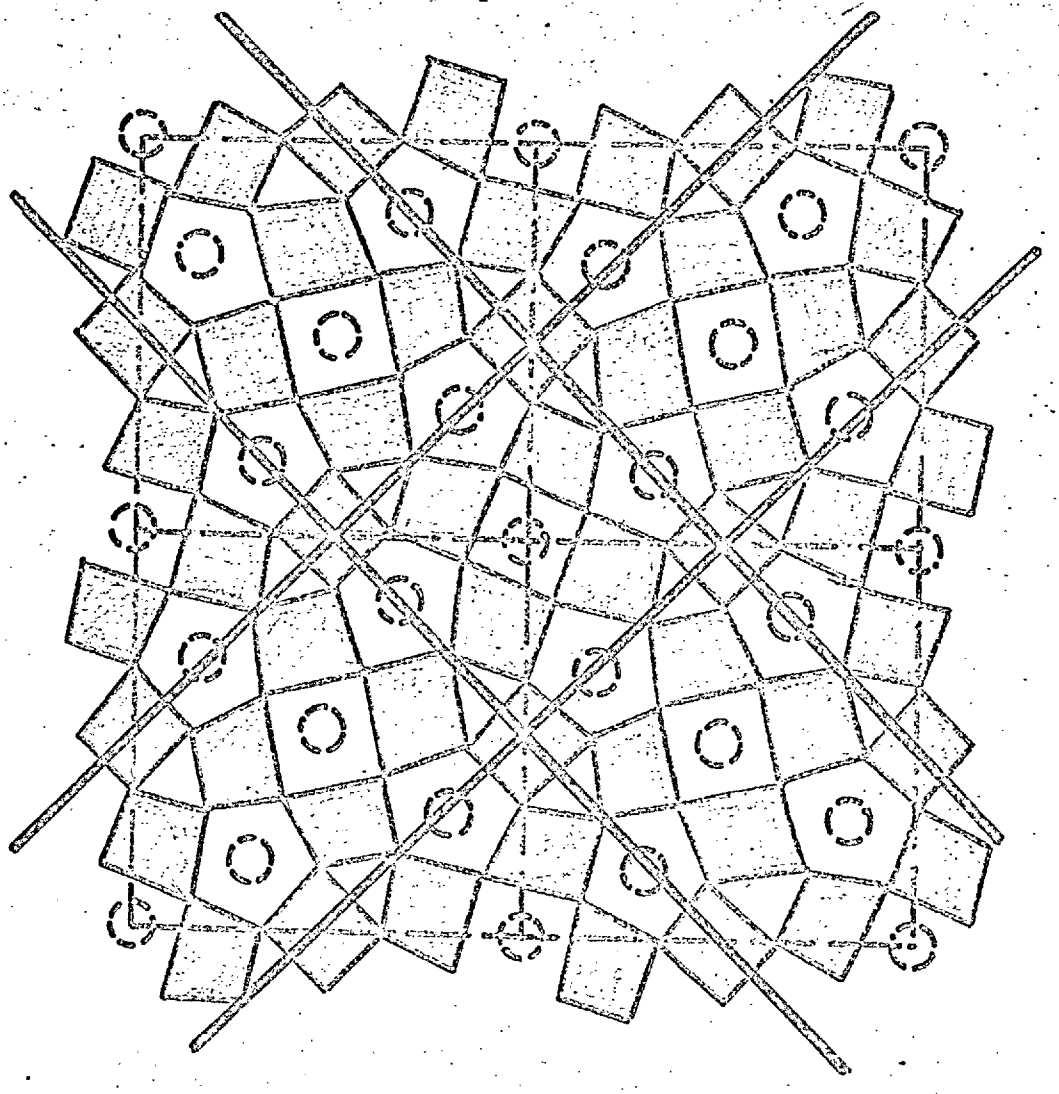


Figure 8.2

Figure 8.3 - Showing four unit cells of the tetragonal bronze structure, with two potential sets of mirror planes

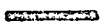




Me-O octahedron



Possible cation positions



potential mirror planes

drawn, as in Figure 8.4. Since the structure is essentially planar, the presence of the screw axis or the glide plane give two alternative ways of buckling the sheet of octahedra. The projection shown is valid in either case.

It is interesting to note that two filled pentagonal tunnels per 17 x 17 cell represents the maximum allowed by these considerations. If the last basic mirror plane is also broken, a greater number of tunnels can be filled, but the 17Å unit cell repeat is lost. In fact the maximum density of $2\frac{2}{3}$ tunnels per 17 x 17Å cell can be deduced, corresponding to the $Nb_{34}O_{94}$ network of the $3Bi_2O_3.17Nb_2O_5$ structure (space group Pba2, with the sheet of octahedra in the ab plane). The $3Bi_2O_3.17Nb_2O_5$ structure therefore contains the maximum possible number of niobium-filled pentagonal tunnels, given the restriction that a situation such as shown in Figure 8.2 should not arise.

The resemblence in all respects (positions of lines, indices, intensities) of the powder patterns of "$7Bi_2O_3.33Nb_2O_5$" and $Sb_2O_3.3Nb_2O_5$ implies that the bismuth compound also has the space group Pmnm or $Pmn2_1$. The former is inconsistent with two niobium-filled pentagonal tunnels per cell, as the two-fold positions are already occupied, and in any case a pentagon (in 2D) cannot have mm symmetry. Pmnm is also excluded by the above structural arguments. $Pmn2_1$ however is one of the space groups which fit the requirements.

The available evidence for the structure of "$Bi_2O_3.5Nb_2O_5$" may be summarised as follows:-

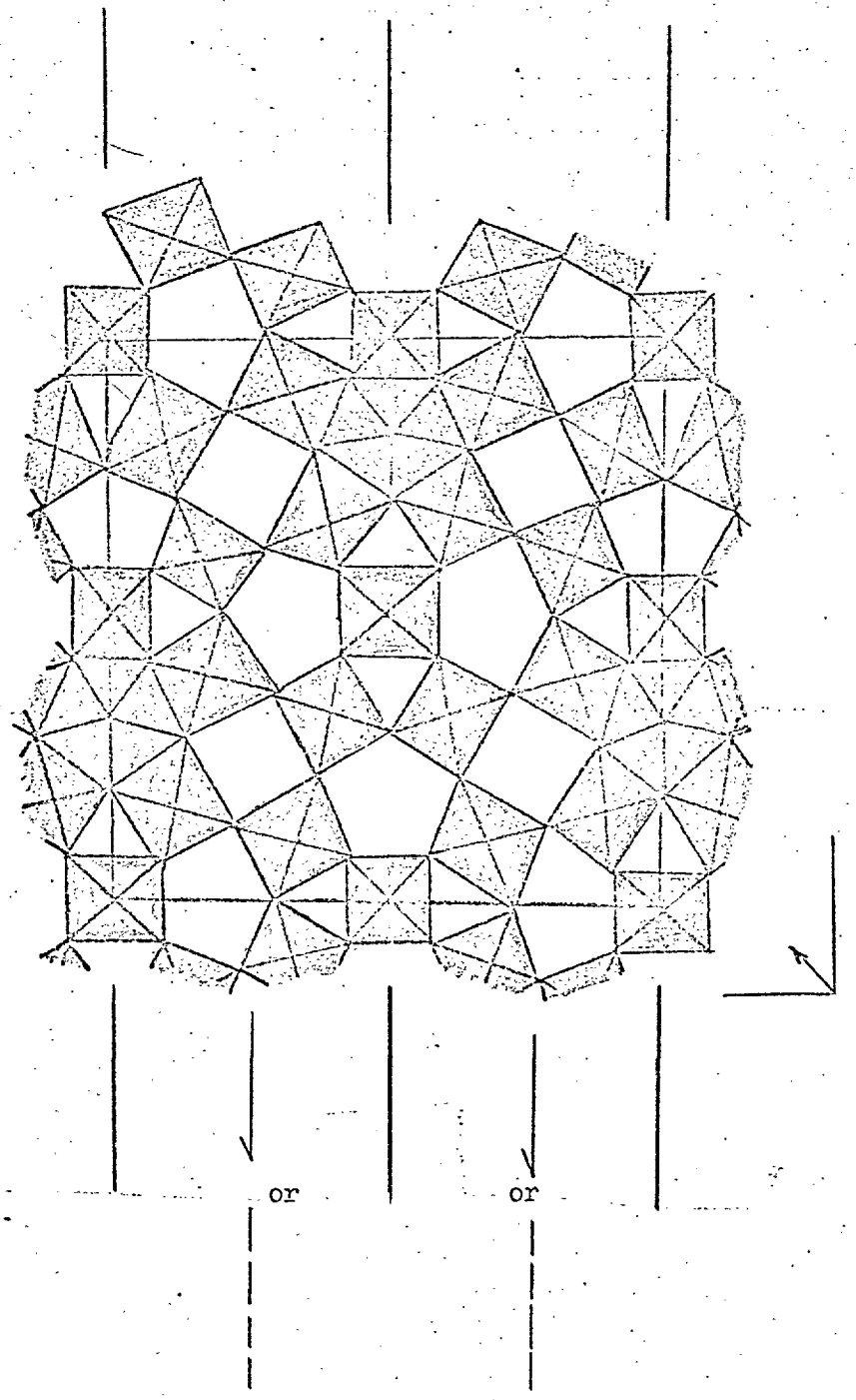


Figure 8.4 - Projection of the $Nb_{22}O_{62}$ framework proposed for $7Bi_2O_3 \cdot 33Nb_2O_5$

(a) the composition is near $Bi_2O_3.5Nb_2O_5$

(b) the powder pattern can be indexed on the basis of an orthorhombic unit cell related to tetragonal bronze

(c) the powder pattern is almost identical with that of $Sb_2O_3.3Nb_2O_5$, from which a probable space group may be deduced.

This evidence, together with

(a) considerations of various structural features.

(b) structural knowledge of the 3:17 compound, led to the postulate of the following structure.

In a 17 x 17Å unit cell of the basic bronze network a maximum of two of the eight pentagonal tunnels may be filled with Nb and O atoms without producing clashes of the type shown in Figure 8.2. To achieve electrical neutrality $4\frac{2}{3}$ bismuth atoms have to be included in the pentagonal and diamond-shaped tunnels at a number of sites, in a manner exactly analogous to that in $3Bi_2O_3.17Nb_2O_5$. In fact the ratio of the number of bismuth atoms to available sites is quite similar to that in $3Bi_2O_3.17Nb_2O_5$. The proposed framework for this structure is illustrated in Figure 8.4. The "overall" space group is probably $Pmn2_1$.

The actual formula of $7Bi_2O_3.33Nb_2O_5$ is very near to $Bi_2O_3.5Nb_2O_5$ (17.5% Bi_2O_3, 82.5% Nb_2O_5 for 7:33; 16.7% Bi_2O_3, 83.3% Nb_2O_5 for 1:5). The difference is of the same order, and in the same sense as that between "3:17" and "1:6" (Section 7). The overall effect is simply to move the appropriate region of the phase diagram (Figure 3.1) slightly towards the bismuth-rich end.

$PbO.xNb_2O_5$; $BaO.xNb_2O_5$

There is evidence for the existence of similar compounds in the systems $PbO-Nb_2O_5$ and $BaO-Nb_2O_5$.

$PbO.xNb_2O_5$ is known to be variable in the range $1 \leqslant x \leqslant 3$. At the composition $PbNb_2O_6$ it has a rhombohedral[I.34,I.35], tetragonal[I.36] and a ferroelectric orthorhombic form[I.36,I.37]. According to Francombe and Lewis[I.37], for $x > 1$, the symmetry appears orthorhombic with a cell of 17.6 x 17.9 x 7.72 Å. As $x \rightarrow 3$ the orthorhombic distortion disappears, as does the doubling of c, until at $x=3$ the structure is truely tetragonal. Roth[I.36] however arrives at a different conclusion, and states that there is a range of composition $1 \leqslant x \leqslant 2$ and that there is an ordered phase at $PbO.2Nb_2O_5$.

Later work of Roth and Waring[I.38] on the $BaO—Nb_2O_5$ system stated that $3BaO.5Nb_2O_5$ and $BaO.3Nb_2O_5$ were end members of a solid-solution series.

All workers realised that these structures were all based on the tetragonal bronze structure in some manner, which was unexplained. The powder patterns were not indexed, except for the 1:1 compounds[I.36,I.38,I.39].

The powder patterns of $PbO.2Nb_2O_5$ and $3BaO.5Nb_2O_5$ were virtually identical, and showed family resemblence to that of $BaO.3Nb_2O_5$. The former two were also very similar to "$Bi_2O_3.5Nb_2O_5$" and $Sb_2O_3.3Nb_2O_5$, though not as close as these two patterns were to one another.

An attempt was made by the author to index the powder patterns of

Table 8.4 - X-ray powder patterns of $3BaO.5Nb_2O_5$, $PbO.2Nb_2O_5$, $Sb_2O_3.3Nb_2O_5$ and "$Bi_2O_3.5Nb_2O_5$"

$3BaO.5Nb_2O_5$ (I.38)		$PbO.2Nb_2O_5$ (I.36)		$Sb_2O_3.3Nb_2O_5$ (I.33)			"$Bi_2O_3.5Nb_2O_5$" (I.2)	
d	I	d	I	d	I	←hkl→	d	I
8.81	10	8.84	7					
				8.65	m	002	8.55	15
6.25	14	6.18	15	6.17	vw	202		
5.60	6	5.576	15					
				5.46	w	103		
				4.412	m	400		
				4.110	m	303		
3.964	51	3.948	32	3.971	s	010	3.945	100
				3.927	m	402	3.921	45
3.860	5	3.857	6	3.873	ms	204	3.854	30
3.778	4			3.781	vw	111		
3.619	10	3.601	5	3.621	mw	210	3.599	30
				3.609	vw	012		
3.545	9	3.528	8	3.542	w	211	3.523	20
3.463	35	3.455	14	3.456	m	501	3.453	20
3.350	25			3.380	s	105	3.367	80
		3.333	16			212	3.319	15
3.233	80	3.218	55	3.292	w	310	3.276	15
3.091	5	3.109	5	3.211	m	113	3.196	50
		3.067	8	3.077	m	404	3.073	20
				3.063	w	213|312	3.062	30
3.026	100	3.020	100	3.004	s	503	3.001	90
				2.971	ms	305	2.964	35
2.945	52	2.942	32	2.950	m	410		
				2.941	m	600	2.940	65
				2.907	w	411	2.900	5
2.872	6	2.861	5	2.870	mw	006	2.859	30
				2.856	m	313	2.843	45
2.796	90	2.786	60	2.790	mw	412		
				2.782	m	602	2.781	60
				2.771	w	214	2.763	15
				2.730	w	206	2.722	15
2.636	6	2.627	4	2.622	w	413		
				2.614	w	314		

Table 8.4 - continued

$3BaO.5Nb_2O_5$		$PbO.2Nb_2O_5$		$Sb_2O_3.3Nb_2O_5$			"$Bi_2O_3.5Nb_2O_5$"	
d	I	d	I	d	I	hkl	d	I
2.601	35	2.596	23	2.605	m	511	2.601	20
				2.573	m	115	2.566	5
		2.520	4	2.520	vvw	512		
				2.495	mw	215/701	2.487	5
2.453	15	2.441	9					
				2.426	mw	604	2.424	5
				2.405	vvw	406		
				2.396	mw	513		
2.365	5			2.378	ms	315	2.373	45

$3BaO.5Nb_2O_5$ and $PbO.2Nb_2O_5$ on the basis of an orthorhombic unit cell of approximately 17.2 x 17.6 x 3.9Å. This was not entirely successful, for although all the lines were indexed, the agreement was not as good as expected.

These powder patterns are reproduced in Table 8.4, together with those of the bismuth and antimony compounds, to show the very marked resemblance.

It is interesting to note that the ordered compound analogous to $7Bi_2O_3.33Nb_2O_5$ in an $xAO.yNb_2O_5$ system would be $7AO.11Nb_2O_5$, not far from those reported (Table 8.5).

$xAO.yNb_2O_5$	%A	%Nb
$7AO.11Nb_2O_5$	24.1	75.9
$3BaO.5Nb_2O_5$	23.1	76.9
$PbO.2Nb_2O_5$	20.0	80.0

Table 8.5

It seems probable that in the lead and barium systems two phases are present concurrently. One may have a random arrangement of niobium-filled pentagonal tunnels and is therefore pseudo-tetragonal. The other phase, definitely orthorhombic, may be of the type discussed, with two niobium-filled tunnels per cell, arranged in an ordered manner. The presence of two phases was realised by Francombe and Lewis[I.37] for $PbO.xNb_2O_5$. This would explain some of the contradiction and confusion apparent in the literature.

The present interpretation considers both phases to contain niobium atoms in pentagonal tunnels, but only the second phase to be ordered. This goes some way toward explaining the range of compositions of $PbO.xNb_2O_5$ and $BaO.xNb_2O_5$.

Survey of Some Tetragonal Bronze-Type Structures

It is becoming increasingly clear that the tetragonal bronze structure

is a basic unit upon which many compounds are based. The three types of interstitial site in the parent structure may accomodate various metal atoms. A large number of compounds crystallise with variants of this structure. Jamieson et al[I.40] divided these compounds into three categories:-

1. conducting, highly-coloured, non-stoichiometric bronzes,
2. compounds of the type $(AO)_x(B_2O_5)$
3. ferroelectric materials of the type $(A1)_2(A2)_4(C)_4(B1)_2(B2)_8O_{30}$

The list of tetragonal bronze-type structures given by Jamieson et al is reproduced here, with the addition of some compounds of the type $(A_2O_3)_x(B_2O_5)$ to category 2.

Table 8.6 - Some tetragonal bronze-type structures

Cat.	Formula	Composition Range x =	aÅ	bÅ	cÅ	Ref.
1	$K_xW_2O_6$	0.9-1.1	12.31	-	3.84	(I.19)
	$Na_xW_2O_6$	0.56-0.76	12.10	-	3.75	(I.41)
	$Pb_xW_2O_6$	0.3-0.7	12.20	-	3.78	(I.42)
	$Ba_xW_2O_6$	0.22-0.44	12.15	-	3.84	(I.44)
	$K_xMo_2O_6$	~1.0	12.32	-	3.86	(I.45)
	$BaNb_2O_5$		12.60	-	3.95	(I.46)
	$BaTa_2O_5$		12.60	-	3.95	(I.46)

Table 8.6 - continued

Cat.	Formula	x	aÅ	bÅ	cÅ	Ref.
2	$Na_2O.4Nb_2O_5$		12.42	3x12.32	3.91	(I.47,I.48)
	$K_2O.3Nb_2O_5$		3x12.57	-	3.94	(I.48)
	$K_2O.2Ta_2O_5$		3x12.43	-	3.88	(I.48)
	$PbO.xNb_2O_5$	1-3	17.52	17.59	2x3.94 (at x=2)	(I.37)
	$BaO.xNb_2O_5$	1.7-3.0	?	?	?	(I.38)
	$SrO.2\frac{1}{2}(Nb_2O_5)$		12.34	-	3.94	(I.49)
	$BaO.2Ta_2O_5$		17.55	17.65	3.91	(I.50)
	"$Bi_2O_3.5Nb_2O_5$"		17.63	17.17	3.95	(Section 8)
	$Sb_2O_3.3Nb_2O_5$		17.64	17.22	3.97	(I.33)
	$Nb_{16}W_{18}O_{94}$		12.25	3x12.21	3.94	(I.18)
	$3Bi_2O_3.17Nb_2O_5$		12.52	3x12.38	3.92	(I.51)
3	$Pb_5Nb_{10}O_{30}$		17.65	17.91	2x3.84	(I.37)
	$Pb_5Ta_{10}O_{30}$		17.61	17.91	2x3.87	(I.52,I.53)
	$Sr_5Ta_{10}O_{30}$		12.45	-	2x3.85	(I.52)
	$Ba_5Ta_{10}O_{30}$		12.59	-	2x3.92	(I.52)
	$(Pb,X)_5Nb_{10}O_{30}$,	X= Ca,Sr,Ba	17.85 (for 60%Pb, 40%Ba)	18.14	2x3.90	(I.52,I.50, I.53)
	$Ba_4R_2Fe_2Nb_8O_{30}$	R=Nd,Sm,Gd	12.47	-	3.93	(I.54)
	$Ba_xSr_{5-x}Nb_{10}O_{30}$	1.25-3.75	12.43	-	3.91 (at x=1.35)	(I.40)
	$Ba_6Nb_8Ti_2O_{30}$		12.54	-	4.01	(I.55)
	$Ba_4Na_2Nb_{10}O_{30}$		17.59	17.63	4.00	(I.56)

.....

9. "$4Bi_2O_3 \cdot 9Nb_2O_5$"

Preparations from 4:9 mixtures of Bi_2O_3 and Nb_2O_5 did not yield single crystals. Some crystals of the 4:9 compound were however found in the products of preparations (c) and (e), (Section 3), which consisted mainly of $3Bi_2O_3 \cdot 17Nb_2O_5$.

The crystals were badly formed hexagonal plates. Oscillation and Weissenberg photographs showed the Laue symmetry to be 6/mmm, and gave an approximate value of the unit cell as $a \sim 7.5$, $c \sim 19.5$ Å.

Much better quality crystals were grown accidentally at a later time, during an investigation of the solid solution range between $SbNbO_4$ and orthorhombic $BiNbO_4$. A mixture of the composition 30% Sb_2O_3, 20% Bi_2O_3, and 50% Nb_2O_5 was sealed in a platinum capsule and heated to 670°C for 24 hours, and then fired for one week at 970°C. The quenched product was highly crystalline, and contained well formed hexagonal plates of the 4:9 compound. Sb_2O_3 seems to have acted, unexpectedly, as an excellent flux for the growth of these crystals. There is however a possibility of Sb contamination in this product.

Unit Cell and Space Group

Roth recorded the powder pattern of the 4:9 compound and indexed it fully on the basis of a hexagonal unit cell with a = 6.441, c = 19.778Å. In view of the values obtained from oscillation and Weissenberg photographs, the powder pattern was re-indexed on the basis of the larger cell, using $a_{new} = 2a_{old}/\sqrt{3}$, $c_{new} = c_{old}$. The transformation of indices therefore affected h and k only. The re-indexed powder pattern is listed in Table 9.1. These cell parameters were checked using a single crystal on the Siemens four-circle diffractometer. Exact agreement was found between the transformed and measured values.

The unit cell may therefore be taken as

$$a = 7.445 \pm 0.0004 \text{ Å}$$

$$c = 19.778 \pm 0.003 \text{ Å}$$

The Laue symmetry observed was 6/mmm. Absences were found for $hh2\bar{h}l$, when $l \neq 2n$. This indicated $P6_3mc$, $P\bar{6}2c$ or $P6_3/mmc$ as possible space groups. It was also noted that reflections of the type hkl, $h-k=3n$ and $l \neq 2n$ were generally weak and often unobserved. This is consistent with metal atoms in special positions in each of the possible space groups.

The formula for the cell contents, $4Bi_2O_3.9Nb_2O_5$ is inconsistent with any of these space groups. Thus a unit-cell content of Z=1 would give an odd number of oxygen atoms per cell. In all three space groups, all positions have an even number of equipoints. For $Z < 1$, only $Z=2/3$ gives even integer numbers of niobium and oxygen atoms per cell, i.e. $Bi_{5\frac{1}{3}}Nb_{12}O_{38}$.

Table 9.1 - X-ray powder pattern of "$4Bi_2O_3 \cdot 9Nb_2O_5$"

Cu Kα radiation

λ = 1.54178Å

Roth and Waring(I.2) I	d(Å)	$\sin^2\theta_{obs}$	h	k	l	$\sin^2\theta_{calc}$
13	9.86	0.00611	0	0	2	0.00608
4	4.946	0.02429	0	0	4	0.02431
93	3.294	0.05477	0	0	6	0.05470
83	3.179	0.05880	2	0	1	0.05869
100	3.063	0.06334	2	0	2	0.06324
10	2.895	0.07091	2	0	3	0,07084
73	2.699	0.08158	2	0	4	0.08148
28	2.499	0.09516	2	0	5	0.09515
6	2.471	0.09733	0	0	8	0.09724
4	2.308	0.11156	2	0	6	0.11186
11	2.125	0.13160	2	0	7	0.13161
7	1.9778	0.15192	0	0	10	0.15193
29	1.9616	0.15444	2	0	8	0.15440
57	1.8610	0.17159	2	2	0	0.17150
11	1.8158	0.18024	2	0	9	0.18023
27	1.6857	0.20913	2	0	10	0.20910
8	1.6483	0.21873	0	0	12	0.21878
39	1.6210	0.22616	2	2	6	0.22620

Table 9.1 - continued

11	1.6070	0.23012	4	0	1	0.23019
11	1.5913	0.23468	4	0	2	0.23475
18	1.5703	0.24100	2	0	11	0.24101
14	1.5324	0.25307	4	0	4	0.25298
9	1.4931	0.26657	4	0	5	0.26665
5	1.4869	0.26880	2	2	8	0.26874
2	1.4133	0.29752	0	0	14	0.29779
4	1.4000	0.30320	4	0	7	0.30312
3	1.3554	0.32348	2	2	10	0.32344
4	1.3503	0.32593	4	0	8	0.32591
5	1.2496	0.38058	4	0	10	0.38060
10	1.2340	0.39026	2	2	12	0.39029
5	1.2203	0.39907	2	0	15	0.39902
5	1.2162	0.40177	4	2	1	0.40169
4	1.2096	0.40616	4	2	2	0.40625
3	1.2003	0.41243	4	0	11	0.41251
5	1.1833	0.42442	4	2	4	0.42448
4	1.1646	0.43816	4	2	5	0.43816
3	1.1539	0.44632	2	0	16	0.44612
2	1.0749	0.51434	6	0	0	0.51451
3	1.0376	0.55198	4	2	10	0.55211
2	1.0215	0.56952	6	0	6	0.56920
4	1.0088	0.58395	4	2	11	0.58401

The quotient of the unit cell volume divided by the number of oxygen atoms is usually about 18 - 21 for this type of compound. The measured volume (949.2Å^3) would therefore indicate 45 - 52 oxygen atoms per cell.

With the observed unit cell, a small deviation from the supposed formula to, for example $3Bi_2O_3.7Nb_2O_5$, would give an acceptable and even number of metal (6 + 14) and oxygen (44) atoms per cell for Z = 1.

Single-crystal intensity data have been collected for this compound on the Siemens automatic diffractometer. The indications so far are that the structure is not straight-forward, and in the time available, no conclusive results have been obtained. This work is being continued.

10. Summary to Part I

Structural Features of the Bi_2O_3-Nb_2O_5 System

The present work has resulted in a better understanding of the compounds occurring in the Bi_2O_3-Nb_2O_5 system, in the region from 1:1 towards the niobium-rich end.

The crystal structure of triclinic $BiNbO_4$ was fully analysed and was shown to be an entirely novel structure. It is built up of sheets of Nb-O octahedra, each infinite in two dimensions, and linked in the third only through the bismuth atoms.

The formula of $Bi_2O_3 \cdot 6Nb_2O_5$ was corrected to the ideal of $3Bi_2O_3 \cdot 17Nb_2O_5$ on the basis of single crystal structural work. The powder pattern of this compound was indexed on the basis of an orthorhombic unit cell of $a = 12.516$, $b = 37.14$, $c = 3.922$ Å. The structure was shown to be based on that of the tetragonal bronzes, with an $Nb_{34}O_{94}$ matrix, continuous in three dimensions. The bismuth atoms are distributed among a number of sites. The $Me_{34}O_{94}$ matrix is rigid, and can exist on its own (e.g $Nb_{16}W_{18}O_{94}$). The bismuth atoms, which hold the octahedral sheets together in triclinic $BiNbO_4$, are in that sense redundant in this structure.

The powder pattern published for $Bi_2O_3 \cdot 5Nb_2O_5$ has been indexed on the

basis of an orthorhombic unit cell of a = 17.632, b = 3.949, c = 17.167Å, in which a and c correspond to distortions of the diagonal of the tetragonal bronze unit cell (a = 12.4Å, $\sqrt{2}$a = 17.5Å). If the structure proposed for this phase is correct, then the formula would ideally be $7Bi_2O_3.33Nb_2O_5$. The proposed structure would have much in common with $3Bi_2O_3.17Nb_2O_5$, essentially differing only in the positions (and number) of niobium-filled pentagonal tunnels. The slight errors in these formulae are both in the same sense, and of similar magnitudes, effectively displacing the appropriate part of the phase diagram away from the niobium-rich end.

The unit cell published for "$4Bi_2O_3.9Nb_2O_5$" has been corrected on the basis of single-crystal work and the powder pattern re-indexed. Reasons have been advanced for considering the structural formula to be incorrect.

Niobium Co-ordinations

In all these structures, as would be expected, the basic building block is the niobium-oxygen octahedron. The only exception to this is the pentagonal-bipyramidal niobium atom in $3Bi_2O_3.17Nb_2O_5$. This co-ordination however, can be regarded as a secondary effect, the niobium atom filling a pentagonal hole which is left by Nb-O octahedra.

All the Nb-O octahedra encountered were distorted, with the niobium atom displaced from the centre of the octahedron. The average Nb-O bondlengths for each octahedron were, however, very uniform at just under 2Å.

The displacement of the metal atom from the centre of the octahedron in some oxides and other compounds is often associated with ferroelectric behaviour. $3Bi_2O_3.17Nb_2O_5$ belongs to one of the crystal classes with unique polar axes, and therefore there is a definite possibility of its exhibiting ferroelectric properties.

The pentagonal bipyramidal niobium co-ordination is rare but not novel. The pentagon of oxygens in $3Bi_2O_3.17Nb_2O_5$, as in earlier examples, (Refs. I.18,I.57,I.58,I.59), was found to be regular and compact. Some of the shortset oxygen-oxygen distances encountered were in this "five-membered ring". The niobium atom was found to be dispaced toward one of the apices of the bipyramid, by a fraction similar to that in the octahedra of the same structure.

Bismuth Co-ordination

One of the difficulties in describing the oxygen environments of the bismuth atoms is the setting of a meaningful upper limit on the Bi-O distances considered.

In $BiNbO_4$ the two independent bismuth atoms had very similar co-ordinations, which were one-sided and irregular. The co-ordination number of 8 is arrived at by considering Bi-O distances of up to 3.0Å. There is a distinct gap above 3.0Å, the next nearest ones being at approximately 3.5Å.

In $3Bi_2O_3.17Nb_2O_5$ six independent bismuth sites were encountered.

In all of these there was an almost continuous range of Bi-O distances to well over 3Å, except for a gap of usually 0.2 - 0.4Å after the fourth or the fifth distance. In the cases where the cut-off could be considered after four, the geometry was clearly that of a one-sided four-co-ordination similar to ones reported previously(I.24-I.28). The other two bismuth atoms could also be considered to have such a co-ordination, with one further oxygen attached on the side, but one of these was better described by a rectangular anti-prism, more regular than in the case of triclinic $BiNbO_4$. It is interesting to note that this last site was the one with the largest bismuth occupancy in the $3Bi_2O_3.17Nb_2O_5$ structure.

Some bismuth-oxygen co-ordinations and distances have recently been reviewed by Abrahams et al(I.60). Their table is reproduced here, (Table 10.1), with the addition of the independent bismuth co-ordinations found in triclinic $BiNbO_4$, $3Bi_2O_3.17Nb_2O_5$, and four other mixed oxides and oxyhalides with one-sided four-co-ordinations. In each case, an inner co-ordination, with Bi-O distances less than the limit stated is considered separately from the total co-ordination. In some cases, one or other of these is rather indistinct. For example, the inner co-ordination can only be found by drawing an arbitrary limit in the case of triclinic $BiNbO_4$. For $3Bi_2O_3.17Nb_2O_5$ on the other hand it is the total co-ordination that is difficult to decide for some of the bismuth sites.

Table 10.1 - Some bismuth co-ordinations

Compound	Total Co-ord.	Range of Bi-O distances in Å	Upper break in distance Å	Inner Co-ord.	Average Bi-O distance Å	Reference
$Bi_4Si_3O_{12}$	9	2.15 - 3.55	2.62	6	2.39	I.61
Bi_2GeO_5	7	2.13 - 3.18	2.66	6	2.35	I.62
$BiOHCrO_4$(mono)	9	2.228-3.326	2.579	6	2.376	I.17
$BiOHCrO_4$(ortho)	9	2.185-3.089	2.678	6	2.382	I.17
$Bi_2O_2SO_4.H_2O$	10	2.22 - 3.45	2.57	6	2.38	I.16
"	10	2.10 - 3.35	2.59	5	2.32	I.16
$BiOHSeO_4.H_2O$	9	2.19 - 3.16	2.64	6	2.40	I.16
$Bi_{12}GeO_{20}$	7	2.076-3.170	2.640	5	2.357	I.60
$BiNbO_4$(tric) Bi(1)	8	2.10 - 3.01	-	-	-	Section 5.
Bi(2)	8	2.10 - 2.96	-	-	-	"
$3Bi_2O_3.17Nb_2O_5$ Bi(1)	8	2.34 - 2.95	2.49	5	2.41	Section 7.
Bi(21)	?	-	2.74	5	2.51	"
Bi(2)	?	-	2.64	4	2.40	"

Table 10.1 - continued

Compound	Total Co-ord.	Range of Bi-O distances Å	Upper break in distance Å	Inner Co-ord.	Average Bi-O distance Å	Reference
$3Bi_2O_3.17Nb_2O_5$						
Bi(22)	?	-	2.77	4	2.50	Section 7.
Bi(10)	?	-	2.55	4	2.36	"
Bi(3)	?	-	2.52	4	2.41	"
$BaBi_4Ti_4O_{15}$	8	2.28 - 2.89	2.3	4	2.28	(I.27)
Bi_2NbO_5F	8	2.29 - 2.90	2.3	4	2.29	(I.28)
$Bi_4Ti_3O_{12}$	12	2.29 - 2.79	2.3	4	2.29	(I.26)
$PbBi_2Nb_2O_9$	8	2.29 - 2.82	2.3	4	2.29	(I.25)

Oxygen Environments

In both the structures fully investigated, i.e. triclinic $BiNbO_4$ and $3Bi_2O_3.17Nb_2O_5$, as well as orthorhombic $BiNbO_4$, all oxygen atoms are associated with the niobium-oxygen network, usually in octahedra. The structure proposed for $7Bi_2O_3.33Nb_2O_5$ would also be included in this.

Closest oxygen-oxygen contacts occurred in $3Bi_2O_3.17Nb_2O_5$ in the pentagonal ring, and in the rectangles of the one-sided bismuth co-ordinations.

.....

References I

I.1. D.Rogers and A.C.Skapski, Proc.Chem.Soc., 1964,400.

I.2. R.S.Roth and J.L.Waring, J.Res.Nat.Bur.Stand., Sect.A., 1962,66,451.

I.3. R.S.Roth and J.L.Waring, Amer.Mineralogist, 1963,48,1348.

I.4. B.Aurivillius, Arkiv Kemi, 1949,1,463.

I.5. A.C.Skapski and D.Rogers, Chem.Commun., 1965,611.

I.6. A.C.Skapski, Ph.D. Thesis, London, 1963.

I.7. D.Cromer, Acta Cryst., 1964,17,1044.

I.8. L.H.Thomas and K.Umeda, J.Chem.Phys., 1957,26,293.

I.9. International Tables for X-ray Crystallography, Kynoch Press, Birmingham, Volumes I, II and III.

I.10. E.W.Hughes, J.Am.Chem.Soc., 1941,63,1737.

I.11. S.Geller, Acta Cryst., 1961,14,1025.

I.12. A.I.M.Rae and E.M.Maslen, Acta Cryst., 1949,2,318.

I.13.(a) A.J.C.Wilson, Acta Cryst., 1949,2,318.

I.13.(b) E.R.Howells, D.C.Phillips and D.Rogers, Acta Cryst., 1950,3,210.

I.14. S.N.Ruddlesden and P.Popper, Acta Cryst., 1958,11,54.

I.15. B.Aurivillius, Arkiv Kemi, 1949,1,463.

I.16. B.Aurivillius, Acta Chem. Scand., 1964,18,2375.

I.17. B.Aurivillius and A.Lowenheim, Acta Chem. Scand., 1964,18,1937.

I.18. A.W.Sleight, Acta Chem. Scand., 1966,20,1102.

I.19. A.Magneli, Arkiv Kemi, 1949,1,213.

I.20. A.Magneli, Nova Acta Regiae Soc. Scient. Upsaliensis,IV, 1950,14,8.

I.21. A.Magneli, Acta Chem. Scand., 1953,7,315.

I.22. G.Hagg and A.Magneli, Rev. Pure Appl. Chem., 1954,4,235.

I.23. A.D.Wadsley, Rev. Pure Appl. Chem., 1955,5,165.

I.24. B.Aurivillius, Arkiv Kemi, 1951,3,165.

I.25. B.Aurivillius, Arkiv Kemi, 1949,1,463.

I.26. B.Aurivillius, Arkiv Kemi, 1949,1,499.

I.27. B.Aurivillius, Arkiv Kemi, 1950,2,519.

I.28. B.Aurivillius, Arkiv Kemi, 1952,5,39.

I.29. P.B.Jamieson, S.C.Abrahams and J.L.Bernstein, J. Chem. Phys., to be published.

I.30. M.Estrand, Svensk. Kem. Tidskr., 1955,67,230.

I.31. A. C. Skapski, Chem. Commun., 1966,10.

I.32. J. Graham and A. D. Wadsley, Acta Cryst., 1961,14,379.

I.33. A. C. Skapski, Acta Chem. Scand., 1966,20,580.

I.34. R. Mahe, Bull. Soc. Chim. France, 1967,6,1879.

I.35. R. Mahe, Bull. Soc. Chim. France, 1966,11,3401.

I.36. R. S. Roth, J. Res. Nat. Bur. Stand., 1959,62,27.

I.37. M. H. Francombe and B. Lewis, Acta Cryst., 1958,11,696.

I.38. R. S. Roth and J. L. Waring, J. Res. Nat. Bur. Stand., 1961,65A,337.

I.39. R. S. Roth, Acta Cryst., 1957,10,437.

I.40. P. B. Jamieson, S. C. Abrahams and J. L. Bernstein, J. Chem. Phys., in press.

I.41. A. Magneli and B. Blomberg, Acta Chem. Scand., 1957,5,375.

I.42. R. A. Benroff and L. E. Conroy, J. Am. Chem. Soc., 1960,82,6261.

I.43. A. C. Skapski, private communication.

I.44. L. E. Conroy and T. Yokokawa, Inorg. Chem., 1965,4,994.

I.45. T. A. Bither, J. L. Gillson and H. S. Young, Inorg. Chem., 1966,5,1559.

I.46. A. Galasso, L. Katz and R. Ward, J. Amer. Chem. Soc., 1959,81,5898.

I.47. A. Reisman and F. Holtzberg, J. Amer. Chem. Soc., 1958,80,37.

I.48. C. D. Whiston and A. J. Smith, Acta Cryst., 1965,19,169.

I.49. M. H. Francombe, Acta Cryst., 1960,13,131.

I.50. M. Gasperin, Bull. Soc. Min. Crist., 1967,90,172.

I.51. E. T. Keve and A. C. Skapski, Nature, 1968,217,841.

I.52. I. G. Ismailzade, Kristallografiya, 1959,4,658. (Sov. Phys. Cryst., 1959,4,618.)

I.53. E. C. Subbarao, G. Shirane and F. Jona, Acta Cryst., 1960,13,226.

I.54. N. N. Krainik, V. A. Isupov, M. F, Bryzhina and A. L. Agranovskaya, Sov. Phys. Cryst., 1964,9,281.

I.55. N. C. Stephenson, Acta Cryst., 1965,18,496.

I.56. J. J. Rubin, L. G. Van Uitert and H. J. Levinstein, Int. J. Cryst. Growth, 1967,1,315.

I.57. A. Magneli, Arkiv Kemi, 1949,1,223.

I.58. L. Kihlborg, Acta Chem. Scand., 1963,17,1485.

I.59. L. Kihlborg, Acta Chem. Scand., 1960,14,1612.

I.60. S. C. Abrahams, P. B. Jamieson and J. L. Bernstein, J. Chem. Phys., 1967,47,4034.

I.61. D. J. Segal, R. P. Santos, and R. E. Newnham, Z. Krist., 1966,123,73.

I.62. B. Aurivillius, C.I. Linblom, and P. Stenson, Acta Chem. Scand., 1964,18,1555.

I.63. S. Andersson, Acta Chem. Scand., 1965,19,1401.

I.64. A. Åstrom, Acta Chem. Scand., 1966,20,1102.

I.65. A. D. Wadsley, Acta Cryst., 1961,14,660.

"This agreeth not well with me, therefore
I will not continue it."

Francis Bacon

PART II

STUDIES ON SOME NOVEL FLUORITE-TYPE SUPERSTRUCTURES

11. Some Superstructures of the Fluorite-Type

Introduction

The compounds which are discussed in this Part were all supplied by Dr A. E. D. White of the Crystal Growing Laboratory of the Electrical Engineering Department, Imperial College. They were by-products in the preparation of some rare-earth niobates.

Equimolar proportions of the rare-earth oxides (Nd_2O_3, La_2O_3 or Y_2O_3) and niobium pentoxide were heated together with an eight-fold excess of PbF_2 to 1250°C in a platinum crucible. Crystals were grown by evaporation at constant temperature or by slow cooling to 900°C over a period of five or six days, then quenched to room temperature. In either case, two types of products were obtained, one of which was identified as the niobate, and the other was an unknown compound. These three compounds are given the name ND, LA or Y according to the rare-earth present in the preparation.

A fourth compound named PB/NB was prepared by the above method, but the rare-earth oxide was omitted.

When the powder patterns and unit cells of these four compounds were obtained, a thorough search in the literature revealed that they were

entirely novel compounds.

This Part of the Thesis offers an account of some of the work done in connection with these compounds. Since their formulae are still not established, they are referred to by the symbols quoted above. Single-crystal intensity data were collected for LA and ND, but their solution, which is not yet complete, is not described in any detail.

Preliminary Analysis

The LA and ND samples were analysed by the Inter-Collegiate Analytical Service, using X-ray fluorescence methods. The ratio (at.%) of metals found were:-

LA	La:Pb:Nb	19.4:19.1:18.8
ND	Nd:Pb:Nb	1:8.7:11.2

It was not possible to analyse for oxygen or fluorine at the time.

Since the accuracy of the analysis is rather crucial in the single-crystal structure determination, it is being repeated by the Service using a combination of X-ray fluorescence, electron probe and classical wet methods. It is hoped that accurate percentage contents will be obtained for the metals, as well as a less accurate indication of the oxygen and fluorine contents.

Optical Examination

All four materials were highly crystalline hexagonal plates, sometimes

several millimetres in size. ND crystals were pale violet, LA very pale yellow, while Y and PB/NB were both yellow. Crystals of ND and LA were examined under a polarising microscope. Both showed uniform extinction when viewed normal to the plate with parallel light. With convergent polarised light, the isogyres and the concentric isochromes characteristic of a uniaxial crystal could be seen in both cases.

X-ray Powder Photographs

Guinier photographs were taken of powders of all four compounds; these are shown in Plate 11.1. The photographs were rather complex, with a few very strong lines, and a large number of weak ones.



Plate 11.1

The photographs show much resemblence, those of ND and Y are apparently identical.

Tables 11.1, 2 and 3 list the powder lines of these compounds. Those of ND and LA have been indexed on the basis of the unit cells obtained from single crystals on the four-circle diffractometer. The ND powder pattern is fully indexed on the basis of a hexagonal cell of $a = 7.468$, $c = 66.78$ Å with rhombohedral absences, while all but five weak (impurity) lines of the LA powder pattern could be indexed on the basis of a hexagonal unit cell of $a = 7.458$, $c = 48.21$ Å, again with rhombohedral absences.

The powder pattern of Y is listed alongside that of ND for comparison. That of PB/NB is not indexed, except for some of the very strong lines. These are indexed on the basis of a hexagonal cell of $a = 7.5$, $c = 96$ Å, obtained from single-crystal photographs.

All the powder patterns were corrected for film shrinkage, using the accurately known d spacings of some of the uniquely indexed lines of the ND powder pattern as a standard.

Unit Cells and Space Groups

Accurate values of the unit-cell parameters for LA and ND were obtained from the four-circle diffractometer, using a slit collector aperture for maximum θ resolution to perform $\theta/2\theta$ scans for a number of reflections.

Table 11.1 - X-ray powder pattern for ND and Y.

Guinier camara, Cu K_α radiation

(- h + k + l = 3n)

Y		ND					
I	θ°_{obs-Y}	I	θ°_{obs-ND}	h	k	l	$\theta^\circ_{calc-ND}$
		vw	1.95	0	0	3	1.98
		vw	3.98	0	0	6	3.97
m	6.02	m	5.97	0	0	9	5.96
ms	6.95	s	6.99	0	1	2	6.97
w	7.37	w	7.37	1	0	4	7.34
w	7.62	w	7.62	0	1	5	7.60
w	7.96			0	0	12	
vw	8.25	w	8.25	1	0	7	8.27
w	11.04	w	11.07	1	0	13	11.04
vw	11.98	w	11.98	0	0	18	11.98
vw	12.59	w	12.58	1	1	3	12.57
w	12.71	w	12.71	1	0	16	12.69
m	13.36	m	13.37	1	1	9	13.35
w	13.86	w	13.87	2	0	2	13.85
vs	14.03	vs	14.02	0	0	21	14.02
w	14.19	w	14.19	2	0	5	14.19
vs	14.58	vs	14.60	0	2	7	14.57

Table 11.1 continued

w	15.04	w	15.05	0	1	20	15.05
w	15.66	w	15.66	2	0	11	15.66
w	16.09	w	16.06	0	0	24	16.07
vs	16.73	vs	16.73	2	0	14	16.72
m	16.93	w	16.91	0	1	23	16.91
m	17.56	w	17.54	0	2	16	17.54
m	18.44	m	18.42	2	1	1	18.38
ms	18.69	m	18.67	1	2	5	18.68
m	18.90	w	18.85	0	1	26	18.82
w	19.18	w	19.19	1	2	8	19.17
w	19.60	vw	19.61	2	1	10	19.61
w	20.20	w	20.21	1	1	24	20.20
				0	0	30	20.24
m	20.41	w	20.42	2	1	13	20.42
m	20.87	w	20.90	2	0	23	20.89
				3	0	0	20.93
m	21.44	m	21.44	2	1	16	21.42
m	21.82	w	21.83	3	0	9	21.84
m	21.94	w	21.96	0	2	25	21.96
ms	22.54	m	22.54	2	0	26	22.52
				3	0	12	22.53
				2	1	19	22.57

Table 11.1 - continued

vw	23.39	vvw	23.40	3 0 15	23.39
vs	23.64	vs	23.65	0 2 28	23.66
vs	24.35	vs	24.37	2 2 0	24.37
w	25.18	w	25.19	2 2 9	25.18
m	25.46	m	25.46	0 2 31	25.44
				1 3 1	25.44
				3 1 2	25.47
w	25.62	vw	25.64	1 1 33	25.65
				3 1 5	25.67
w	25.80	w	25.80	1 2 26	25.79
vw	26.03	w	26.05	3 1 8	26.05
				2 0 32	26.06
vw	26.30			1 0 37	26.30
vw	27.30	vw	27.36	1 2 29	27.36
vw	27.52	vw	27.51	2 2 18	27.51
vs	28.00	s	27.93	2 0 35	27.95
vw	28.30			3 0 27	28.30
vs	28.62	vs	28.62	2 2 21	28.58
				4 0 4	28.59
vs	28.94	vs	28.92	4 0 7	28.89
				0 0 42	28.98
m	29.05			1 2 32	29.03

Table 11.1 - continued

vw	29.30	vw	29.27	0	2	37	29.26
w	29.85	vw	29.82	3	0	30	29.83
s	30.21	s	30.23	0	4	14	30.20
				2	1	31	30.20

Table 11.2 - LA, X-ray powder pattern

Guinier camera, Cu K_α radiation

(- h + k + l = 3n)

I	$\theta^{o}_{obs\text{-}LA}$	h	k	l	$\theta^{o}_{calc\text{-}LA}$
m	5.50	0	0	6	5.50
ms	6.92	1	0	1	6.91
w	7.10	0	1	2	7.09
m	7.81	1	0	4	7.78
w	8.28	0	0	9	8.27
w	11.08	0	0	12	11.05
w	11.94	1	1	0	11.92
w	12.19	1	1	3	12.24
m	12.23	0	1	11	12.26
w	12.43		-		
m	13.15	1	1	6	13.16
vs	13.87	0	0	15	13.87
w	14.33	0	2	4	14.30
vs	14.59	2	0	5	14.57
vw	15.27	0	2	7	15.27
m	16.45	1	0	16	16.38
vs	16.71	0	2	10	16.68
m	17.27	0	1	17	17.26
vw	17.54		-		

Table 11.2 - continued

m	18.48	1	2	2	18.49
m	18.80	2	1	4	18.78
m	19.08	2	0	14	19.09
vw	19.61	0	0	21	19.60
w	19.92	1	2	28	19.90
		0	1	20	19.94
w	20.52	0	2	16	20.46
w	20.74	1	1	18	20.74
vw	20.97	0	3	0	20.96
m	21.17	0	3	3	21.16
		1	2	11	21.17
vw	21.75	0	3	6	21.74
w	21.87		-		
vw	22.16	2	1	13	22.19
w	22.43		-		
m	22.68	0	2	19	22.71
vs	23.51	2	0	20	23.50
w	23.95	0	3	12	23.95
		2	1	16	23.96
vs	24.39	2	2	0	24.40
w	25.06	2	2	6	25.09

Table 11.2 - continued

vw	25.30		-		
w	25.50	1	3	1	25.49
		0	3	15	25.51
vw	25.81	1	1	24	25.82
w	25.97	2	1	19	25.97
		2	0	23	25.98
w	26.31	1	3	7	26.38
vw	27.08	2	2	12	27.09
vw	27.31	1	3	10	27.30
s	27.69	0	2	25	27.72
vs	28.53	2	2	15	28.53
vs	28.69	0	0	30	28.64
		4	0	4	28.77
vw	29.39	0	3	21	29.37
s	30.20	4	0	10	30.20

Table 11.3 - X-ray powder pattern for PB/NB.

Guinier camera, Cu Kα radiation

I	θ_{obs}	h	k	l	I	θ_{obs}	h	k	l
vw	6.06				vw	16.16			
vw	6.26				s	16.85	0	2	20
m	6.91				m	17.03			
m	7.06				vw	17.66			
vw	7.30				vw	17.85			
vw	8.81				w	18.52			
w	12.59				w	18.61			
vw	12.91				w	18.75			
w	13.17				vw	18.91			
vw	13.41				vw	19.07			
vw	13.53				vw	20.57			
vw	13.90				vw	20.90			
m	14.10				w	21.04			
m	14.21				vw	21.32			
vs	14.66	2	0	10	vw	21.57			
vw	15.11				w	21.70			
vw	15.78				w	22.11			
vw	15.86				w	22.35			
vw	15.99				w	22.60			

Table 11.3 - continued

vw	23.64			vw	27.48			
m	23.80			vw	27.67			
m	23.95			vw	27.98			
vw	24.09			m	28.14			
vs	24.49	2	2 0	m	28.33			
w	25.36			vw	28.57			
w	25.62			ms	28.79	2	2 20	
vw	25.89			m	28.81			
vw	26.23			w	29.45			
vw	26.83			ms	30.43	4	0 20	
vw	27.18							

The values obtained for the hexagonal cell were:-

LA	a = 7.458 Å	c = 48.21 Å
ND	a = 7.468 Å	c = 66.78 Å

It was found possible to align an LA crystal about the 48 Å axis, and a Laue symmetry of $\bar{3}m$ was observed photographically.

In the case of ND, it was not possible to find the 66 Å axis photographically, and therefore no photographs could be taken to show the full Laue symmetry. This was checked however on the four-circle diffractometer, both for the intensities of equivalent reflections and for the angle between the a^* and b^* axes.

In both cases rhombohedral absences were found on the Weissenberg photographs and on a $\theta/2\theta$ scan of a central lattice row. Since there were no absences other than $h - k + l = 3n$ (or the converse) in either case, there is a choice of space groups from $R\bar{3}m$, $R3m$ or $R32$.

Interpretation of Single-Crystal Photographs

Oscillation and Weissenberg photographs were taken of single crystals of ND, LA and PB/NB. From the numerous crystals of the first two compounds examined it was clear that each was a highly crystalline, definate phase. All photographs of each sample appeared to come from identical structures.

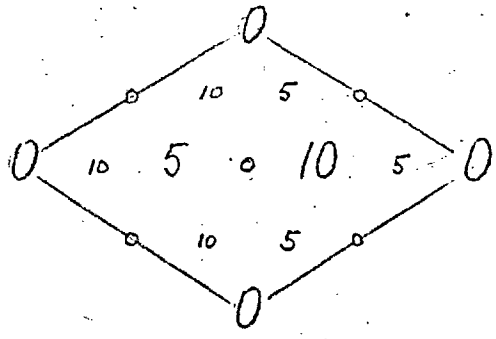
From these photographs it was clear that all the compounds were built up from a subcell which was rhombohedral. The equivalent hexagonal subcell has $a_{sub} \sim 3.75$, $c_{sub} \sim 9.45$ Å. The three compounds LA, ND and PB/NB represent five-fold, seven-fold and ten-fold super-lattices of the subcell. In fact

a_{LA}	=	$2a_{sub}$		c_{LA}	=	$5c_{sub}$	
a_{ND}	=	$2a_{sub}$		c_{ND}	=	$7c_{sub}$	
$a_{PB/NB}$	=	$2a_{sub}$		$c_{PB/NB}$	=	$10c_{sub}$	
(a_Y	=	$2a_{sub}$		c_Y	=	$7c_{sub}$	by analogy with ND)

The subcell reflections were 100 to 1000 times as intense as the weaker ones in between them.

In each case, the positions of the metal atoms are essentially arranged on a rhombohedral lattice, shown in Figures 11.1, 11.2 and 11.3, for LA, ND and PB/NB respectively. For LA there are 15 discrete "layers" per true cell, for ND there are 21 and for PB/NB there are 30.

In any rhombohedral space group one third of the hexagonal cell is repeated three times along c (with a rhombohedral stacking sequence). In space groups R32 and $R\bar{3}m$ the presence of the diad or centre of symmetry ensure that the contents of only 1/6 of the cell are independent. If one of these space groups is assumed, the number of crystallographically independent layers is 3 for LA, 4 for ND and either 5 or 6 for PB/NB. This is illustrated schematically below, where the various layers are



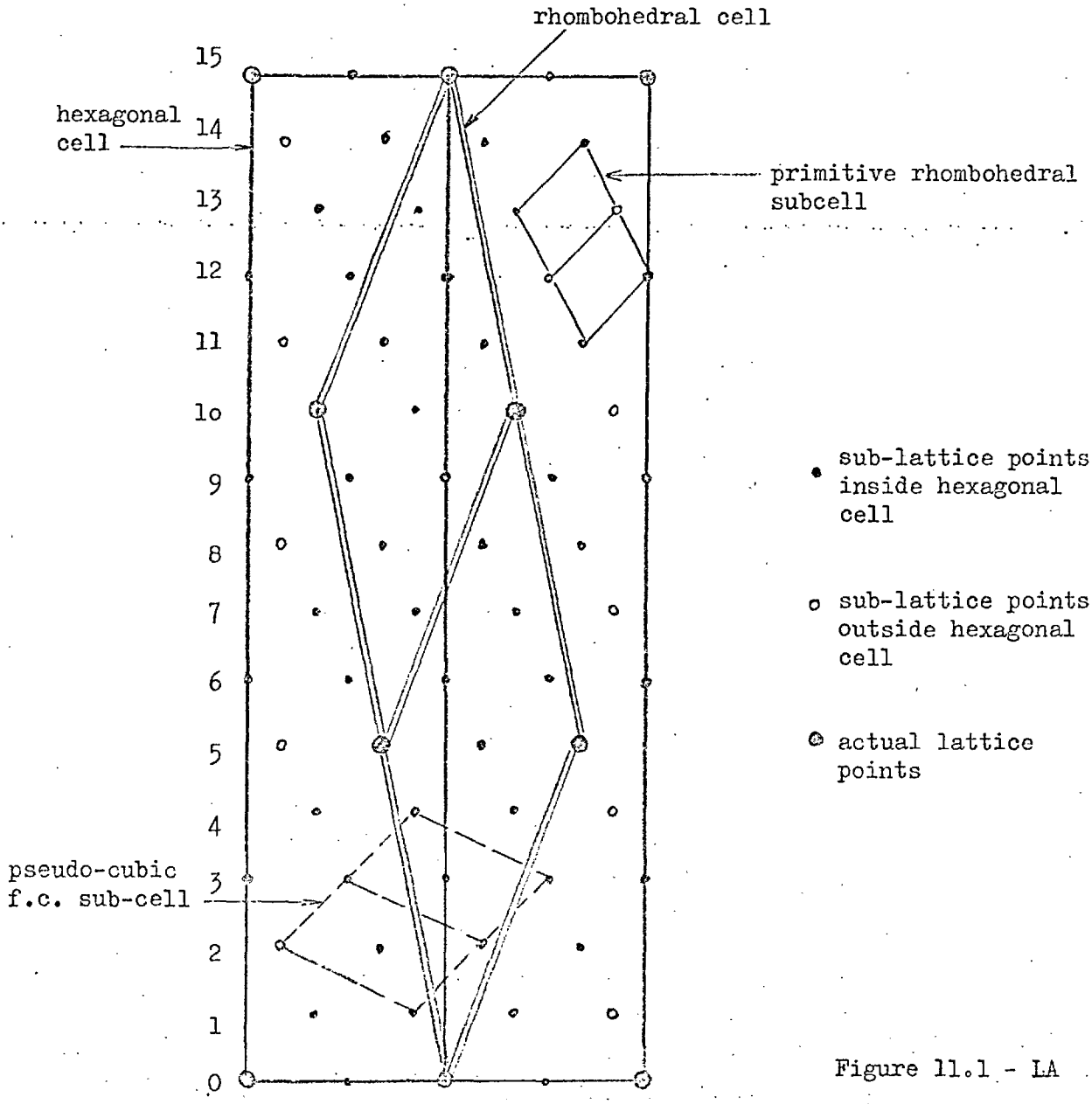


Figure 11.1 - LA

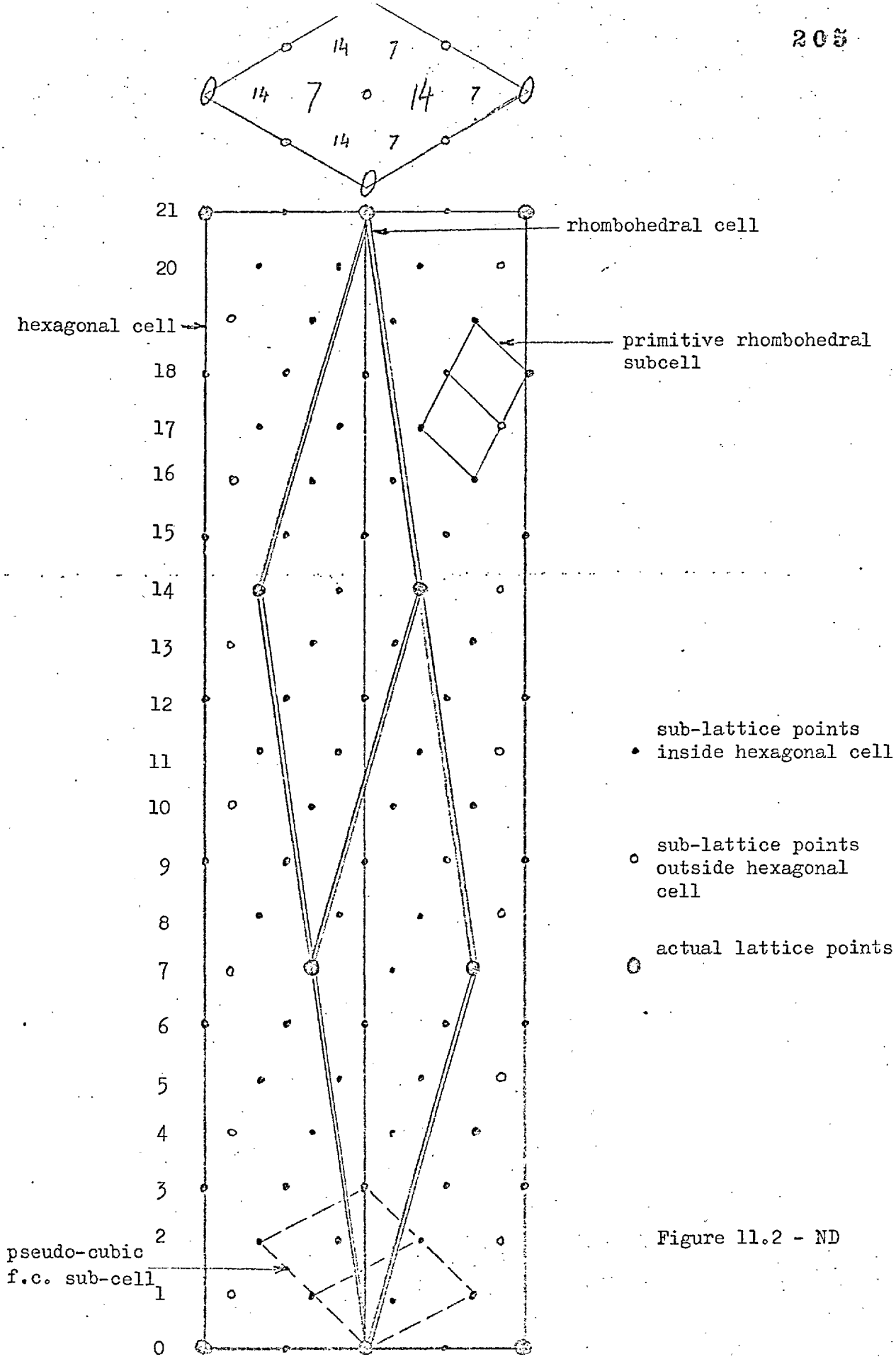
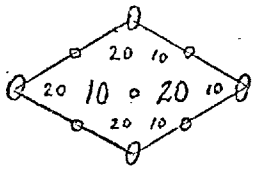


Figure 11.2 - ND



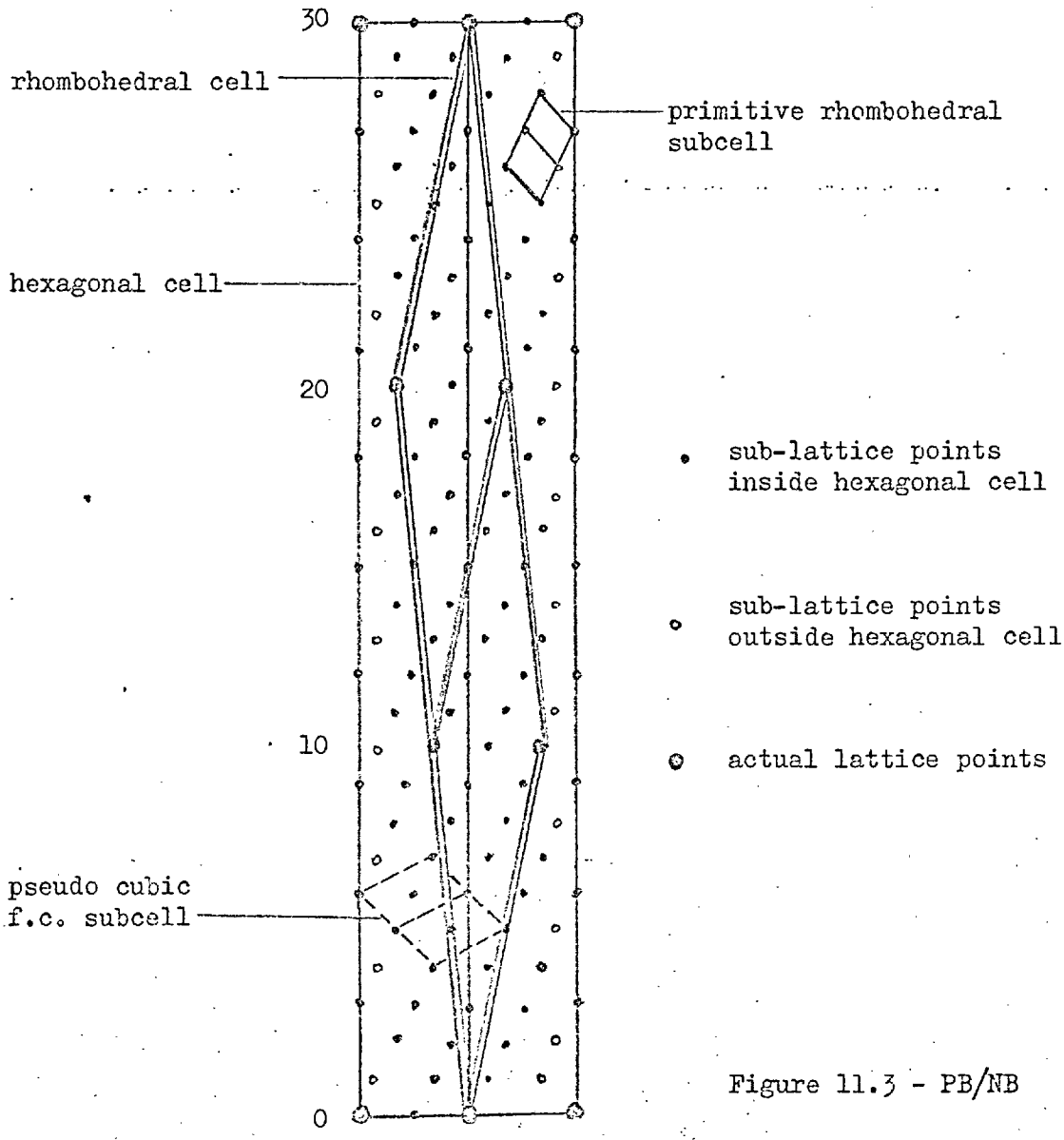
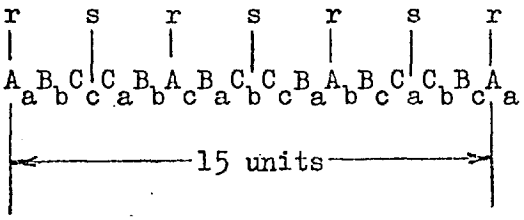


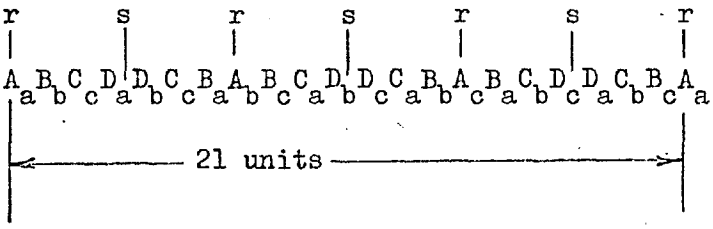
Figure 11.3 - PB/NB

stacked in a "cubic" close packed pattern, having positions denoted by a, b, c. The crystallographically independent layers are denoted by a sequence of capitals A, B, C etc. The symmetry operation of 2 or $\bar{1}$ is denoted by s, and the rhombohedral repeat by r.

LA

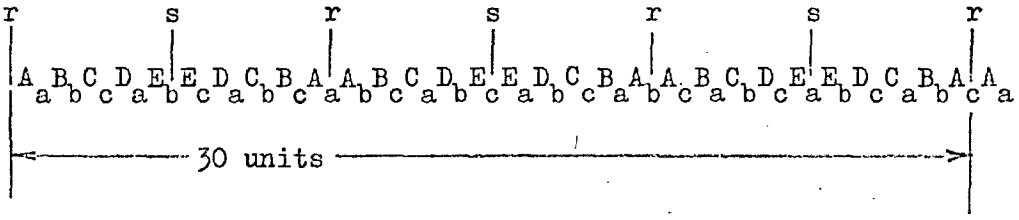


ND

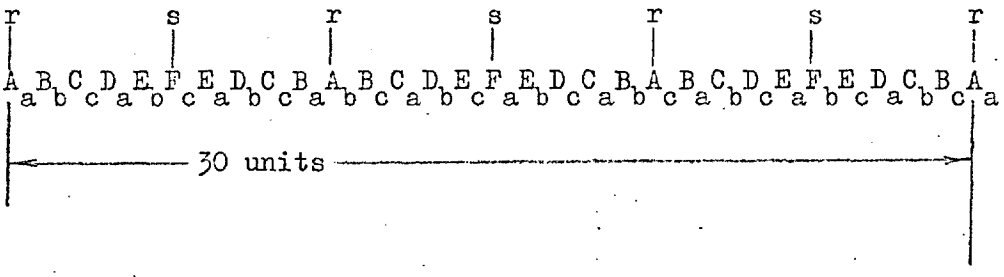


PB/NB

1)

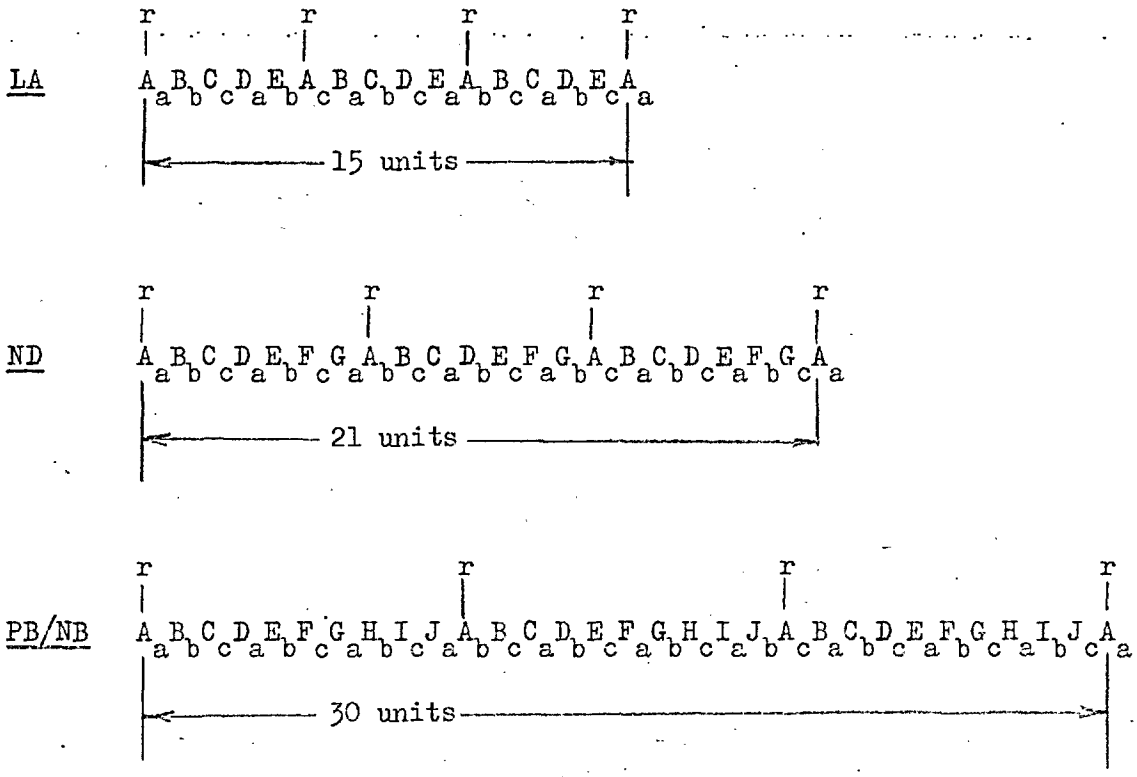


2)



The number of possible metal atom positions in each layer is four, one in a three-fold, and a crystallographically independent one in a one-fold position. The total number of metal sites are 60, 84 and 120 for LA, ND and PB/NB respectively.

In the space group R3m there is no symmetry operation relating the layers within one third of the cell. There would then be 5, 7 or 10 independent layers for the three compounds, as shown below.



Strictly speaking, the materials need not have the same space groups, but in any case, space groups R32 or R$\bar{3}$m offer a much simpler and more plausible

structural reason for the 5, 7 or 10-folding than does R3m.

The fact that the subcell has $a_{sub} = a/2$ differentiates between the one-fold and three-fold positions in a layer. On some layers at least, the one-fold and three-fold positions must be distinguishable, either chemically (including the possibility of a vacancy, or of differing environments) or by displacements from the ideal positions.

Geometrical Considerations

Inspection of Figures 11.1-3 shows that for LA the actual rhombohedral cell and the rhombohedral subcell both have the same sense, both obverse say. In the other two cases the subcells are of the opposite sense to the actual cell.

It is simple to show that for "N-fold" compounds (i.e. 3N layers per hexagonal cell) will have subcells of the same sense if N=3n-1, and opposite senses if N=3n+1. If N=3n, the structure cannot have true rhombohedral symmetry.

Structural Speculations

The sublattice can be interpreted on the basis of a primitive rhombohedral cell, or a pseudo-cubic face centred cell. (Both are shown in Figures 11.1-3.) The pseudo-cubic cells for all structures in this group have a parameters close to 5.4 Å. This may be compared

with 5.94 Å for the fluorite-type structure of PbF_2[II.1], which was present in the preparation as a flux, and which contains just such a lattice of Pb positions. It seemed natural therefore to try to interpret the diffraction results as an ordered variant of the PbF_2 fluorite-type lattice. NdOF also has a fluorite strucure[II.2] with a = 5.59 Å, as has LaOF[II.3] with a = 5.8 Å.

It was difficult to see at first how niobium, which prefers an octahedral co-ordination, could fit into a fluorite-type structure, where the co-ordination of the metal is eight-fold and takes the form of a cubic hexahedron, but this can in fact be accomplished in two ways.

(1) A single niobium may be placed on the triad axis. An octahedron may be formed by the displacement of the apical anions in a typical fluorite co-ordination (see Figure 11.4 (a) and (b)).

(2) As an alternative, the three symmetry related atoms in a single layer could have octahedral environments of the type encountered in the hexagonal bronzes[II.4], Figure 11.5, where the structure is truly hexagonal, consisting of the Me-O octahedral sheets shown in the Figure, stacking directly on top of one another. A hexagonal layer is exactly the right size for such a configuration, since in $K_{0.31}WO_3$ for instance the hexagonal cross section has a = 7.37 Å. This may be compared with a = 7.46 and 7.47 Å for LA and ND respectively. In these structures however, the metal sites are on a rhombohedral lattice and not directly above one another, as in the bronzes. A discrete bronze-type layer (Figure 11.6 (a)) could fit into a fluorite lattice (Figure 11.6 (b)) connecting by the apical oxygens on the octahedra. The fluorite-type

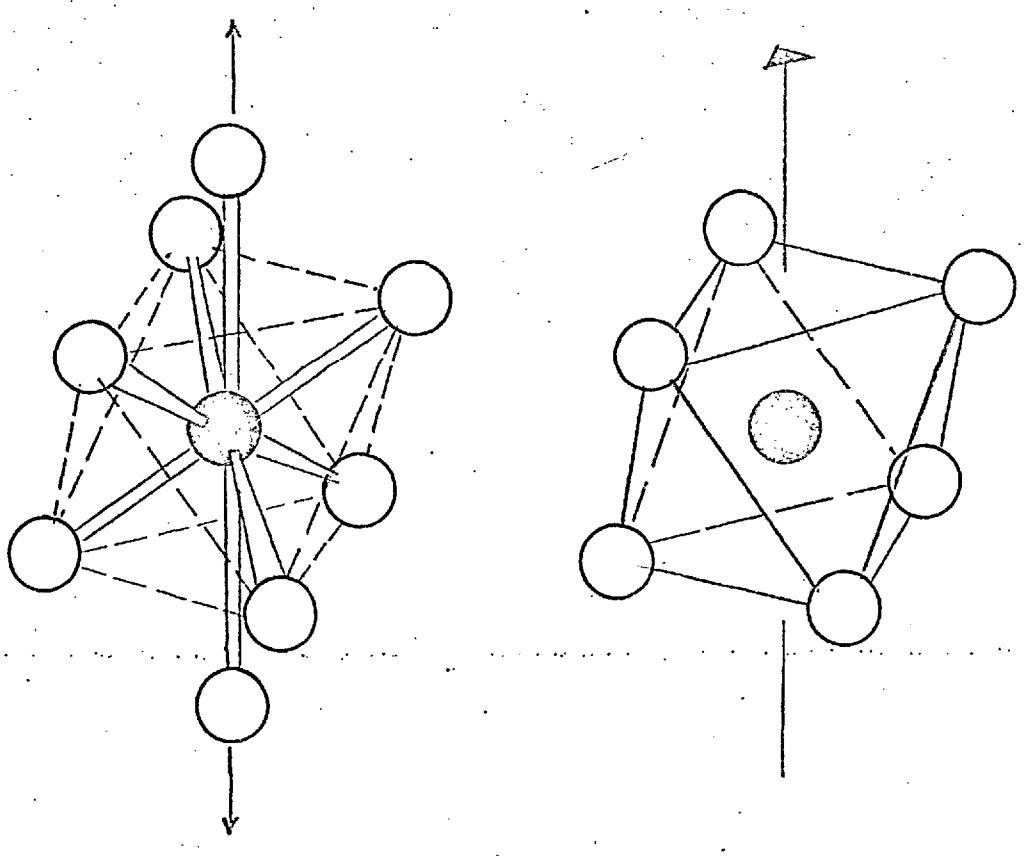


Figure 11.4

(a) (b)

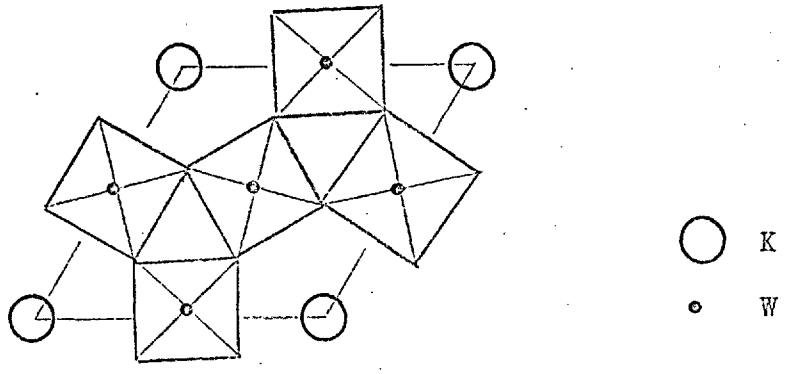
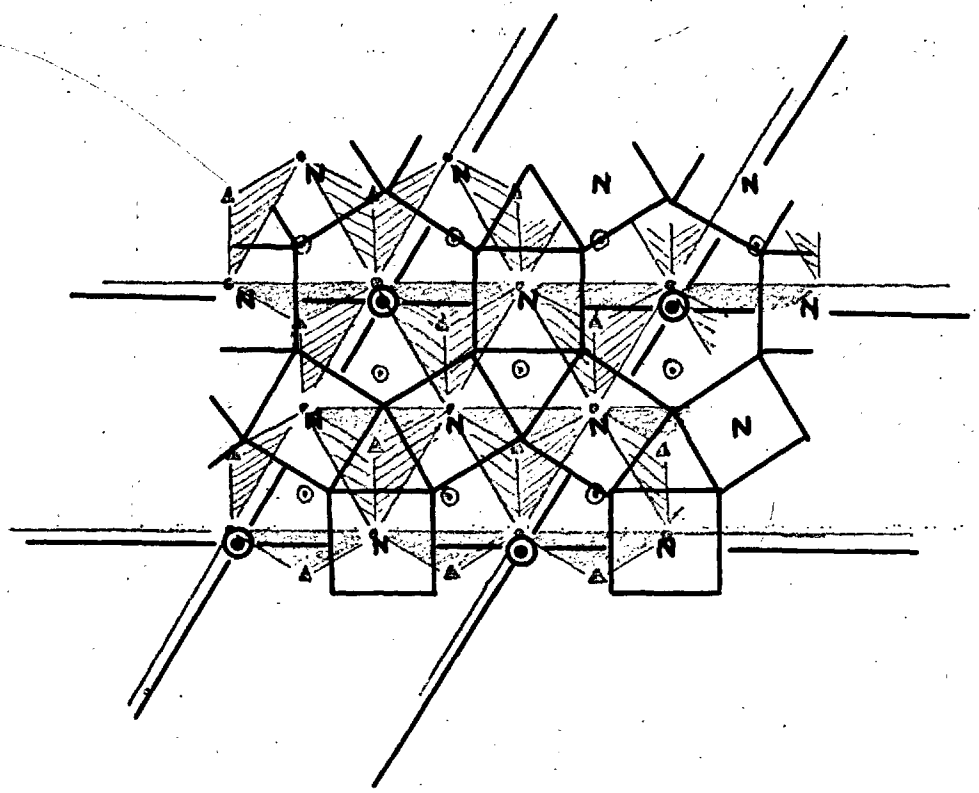


Figure 11.5

The hexagonal bronze structure (K_xWO_3)



N **Niobium at centre of octahedron**

⊙ Metal with fluorite-type environment
(oxygen directly above and below)
(oxygen directly above and below)

◉ **Metal with fluorite-type environment**

• O above plane of metals
(oxygen above and below)

▲ O below plane of metals

Figure 11.6 (a)
Figure 11.6 (b)

network can continue across this layer through the six-membered hole. An atom at this one-fold position in the layer is surrounded by the apical anions of the metals in the neighbouring layers. With two more anions directly above and below this metal, a normal fluorite co-ordination is obtained. (There are six further "oxygens" forming a ring in the layer making the total co-ordination 8 + 6.)

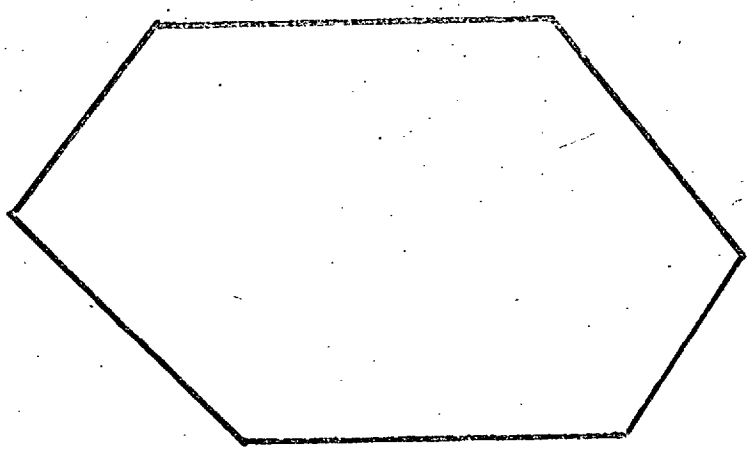
The structures envisaged therefore have a mixture of fluorite-type and octahedral environments for metal atoms, which are arranged on a rhombohedral sublattice. The overall formulae would then be near MX_2.

It was decided to collect single-crystal intensity data for two of the compounds, LA and ND, so that the full three-dimensional structure could be determined.

Collection of Single Crystal Intensity Data for LA

At the time of the collection of single-crystal intensity data for LA and ND, only copper radiation was available on the diffractometer. There was no prospect in the then foreseeable future of obtaining a molybdenum X-ray tube, which would have been far more appropriate for these compounds.

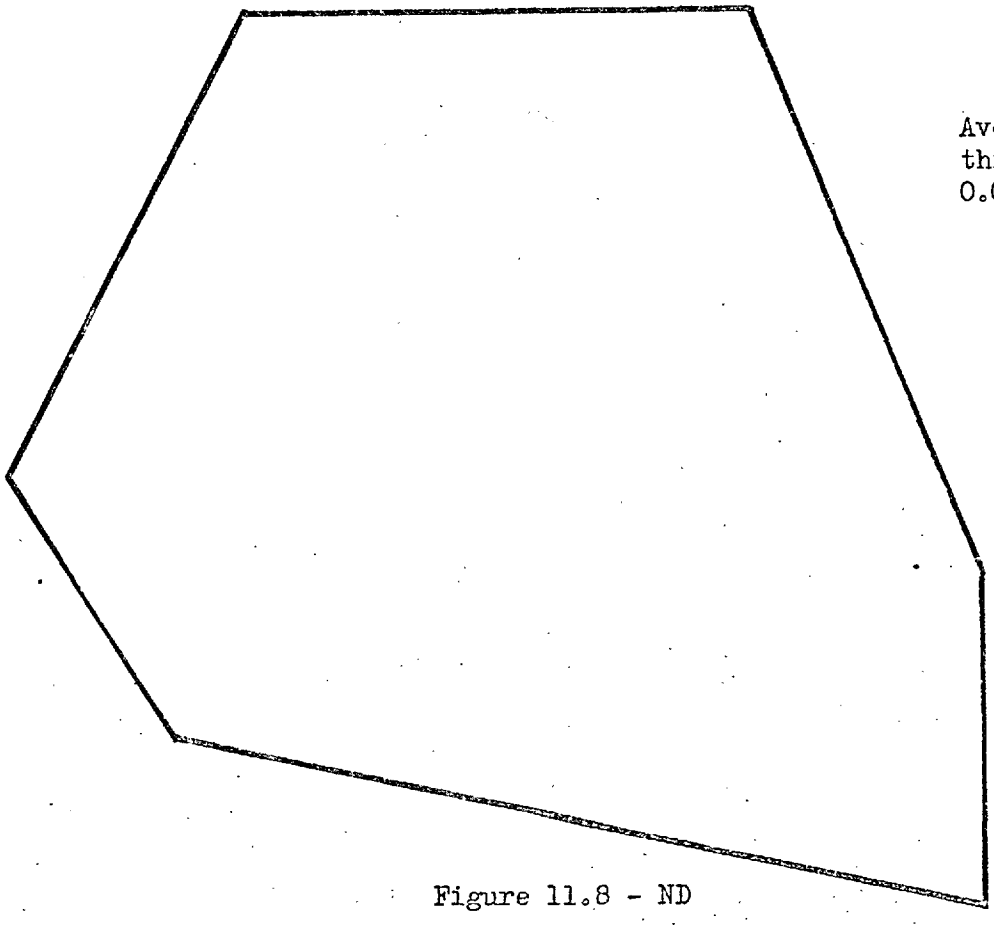
A crystal (Figure 11.7) of LA was mounted with the c axis parallel to the axis of ϕ on the four-circle diffractometer. It quickly became apparent that additional peaks were present among the weaker ones, which occurred in unexpected positions. A continuous $\theta/2\theta$ scan along the 00ℓ



Average
thickness
0.005 cm

0 5 x 10^{-3}cm

Figure 11.7 - LA



Average
thickness
0.003 cm

Figure 11.8 - ND

row revealed that these were the Fe and W radiation peaks of the strong subcell reflections. The dirty radiation from the tube had not previously been detected since it was only about 1% of the Cu-Kα radiation. The subcell reflections were however 100 to 1000 times as strong as the others, and 1% of such a strong peak was exactly of the order of the weaker ones, among which it fell. Furthermore, the close spacing of the reciprocal lattice in the c^* direction meant that these extra peaks often interfered with either the background or the peak counts for a given intensity measurement.

This typified the difficulties encountered with LA and ND in the fact that any error which would normally be negligible, e.g. extinction, Renninger effects, radiation streaks, caused by the subcell reflections affects the weaker ones to an unusual extent.

When a "clean" X-ray tube became available, (Cu), automatic data collection proceeded normally. The five-values method was used to measure 618 reflections in a twelfth segment of the reflecting sphere. 68 of these had peak counts which were less than 2.6 standard deviations above the background, and were treated as unobserved reflections.

The intensity data were corrected for the Lorentz and polarisation factors and for absorption errors. (μ was estimated at 1500 cm^{-1}).

Collection of Single-Crystal Intensity Data for ND

A crystal (Figure 11.8) of ND was mounted on the diffractometer

with a_2 parallel to the axis of ϕ. Intensity data were collected automatically for an octant of the reflecting sphere, of which only the independent twelfth was used. A total of 860 independent reflections were measured, of which 45 were rejected on the basis of counting statistics, and were treated as unobserveds.

The data were corrected for the Lorentz and polarisation factors and for absorption errors (μ was estimated at 1460cm^{-1}). Table 11.4 lists F^2 after absorption correction for two symmetry equivalent rows. The discrepencies of the first few reflections are caused by inaccuracy in the absorption correction.(The lowest transmission factors were of the order of 0.003.)

	$3\,\bar{1}\,\ell$	$2\,1\,\ell$		$3\,\bar{1}\,\ell$	$2\,1\,\ell$		$3\,\bar{1}\,\ell$	$2\,1\,\ell$
	F^2	F^2		F^2	F^2		F^2	F^2
ℓ			ℓ			ℓ		
1	306	132	25	54	58	49	13	17
4	133	57	28	39	36	52	333	379
7	175	98	31	488	508	55	380	380
10	339	219	34	524	586	58	354	422
13	862	636	37	693	789	61	9	6
16	1614	1319	40	20	35	64	82	105
19	532	481	43	40	45	67	54	58
22	32	24	46	35	43	70	5	7
						73	98	109

Table 11.4

Progress of Structure Solution

Work on the solution of the structures of LA and ND is being carried on simultaneously. Although current values of R are as low as 15 and 18, there is an abundance of false minima.

While the current structure for ND gives good agreement with the results of the first analysis, that of LA indicates a different result. Most of the light atoms have been localised, and the structures appear to be based, as proposed, on fluorite and hexagonal-bronze type building blocks. As a molybdenum tube has recently become available on the four-circle diffractometer, it is proposed to collect a new set of intensity data for ND, using a crystal of more optimum shape. It is hoped that the results of an accurate analysis will be available shortly.

The reduction in absorption errors and the analytical results should enable the completion of the solution of the structure.

References II

II.1. J.Sanka, Z.Fiz.Khim.S.S.S.R., 1951,25,41.

II.2.(a) L.Mazza and A.Iandelli, Atti Accad.Ligure sci. e lett., 7,44.

II.2.(b) W.Finkelnburg and A.Stein, J.Chem.Phys., 1950,18,1296.

II.3. A.F.Wells, Structural Inorganic Chemistry, Oxford University Press.

II.4. A.Magneli, Acta Chem.Scand., 1953,7,315.

"The fly sate upon the axle-tree of the chariot wheel, and said, What a dust do I raise!"

Aesop

PART III

THE CRYSTAL STRUCTURE OF DICALCIUM NITRIDE

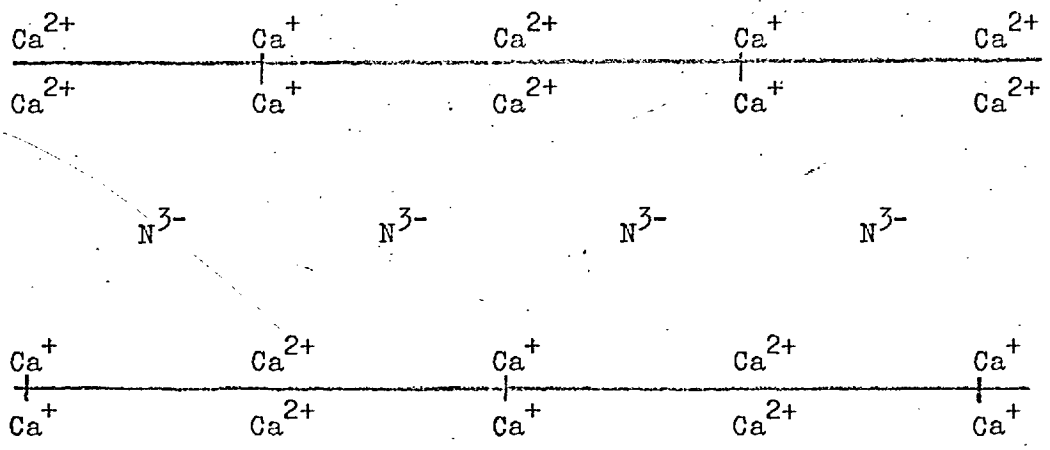
Introduction

Dicalcium nitride was first prepared by Ahmad and Tomlinson[1] during an investigation of the thermodynamics of the Ca-Ca_3N_2 system. They showed that the new phase found had the stoicheiometry Ca_2N. The compound was prepared by heating a 1:1 ratio of pure calcium and Ca_3N_2 in a sealed iron tube for 20 hours at 1100°C, and quenching. The X-ray powder pattern of Ca_2N was recorded by Ahmad, and an investigation of the electrical properties of powder compacts was subsequently carried out by Tomlinson.

Ca_2N forms greenish black lustrous crystals, which quickly decompose in air. Ammonia and hydrogen are given off on contact with water. The analoguous subnitrides of strontium and barium, Sr_2N and Ba_2N, are also known. They were prepared by Arya and Prokofyava[2], who measured the electrical conductivity of powdered Ba_2N, and found it to be 10^{-2} $ohms^{-1}cm^{-1}$.

Tomlinson's preliminary measurements showed powdered Ca_2N to have a conductivity of 0.2 $ohm^{-1}cm.^{-1}$ at room temperature, i.e. well in the semiconductor range, with a positive temperature coefficient.

Ahmad[3] postulated an ionic, as opposed to an interstitial model for Ca_2N, which he pictured as consisting of layers of Ca^+ and Ca^{2+} ions, with N^{3-} ions sandwiched between them in the manner shown.



Other Calcium Nitrides

The usual nitride of calcium is Ca_3N_2, which so far has been shown to exist in four phases.

1.) α-Ca_3N_2 is black and is formed at temperatures below 350°C. It is pseudohexagonal[4].

2.) β-Ca_3N_2 is brown and is prepared at temperatures up to 1050°C. It has a body centered cubic lattice with a = 11.40Å [5], and has an anti-Mn_2O_3 structure. The N-Ca distance found is 2.47Å.

3.) γ-Ca_3N_2 is yellow and is formed above 1050°C[4,24].

4.) High-pressure Ca_3N_2 - formed at 1800°C and 90kb, (Bradley et al[6] called this the γ phase.).

Ca_3N_4 and $Ca_{11}N_8$ [7,23] are also known.

The Importance of the Structure of Ca_2N

Ca_2N is a chemically interesting novel nitride, for which an ionic model had been proposed, An accurate determination of the structure would help to decide between this and a possible interstitial model. If Ca_2N proved to be ionic, the structure might explain the unusual valency of calcium.

Electrical measurements showed powdered Ca_2N to have an electrical conductivity in the semiconductor range at room temperature. Knowledge of the structure, it was hoped, would provide an insight into the electrical properties and behaviour of a single crystal.

This section offers an account of the determination of the crystal structure of dicalcium nitride by three-dimensional X-ray methods.

12. The Crystal Structure of Dicalcium Nitride

Crystal Data

Ca_2N, M = 100.2, Rhombohedral, a = 6.603 Å, $\alpha = 31^{\circ}59'$, U = 71.7 $Å^3$, D_m = 2.17g.cm.$^{-3}$, D_c = 2.18 g.cm.$^{-3}$ for Z = 1, F(000) = 47

Space Group $R\bar{3}m$, (D_{3d}^5, No.166)

For CuKα radiation, μ = 301 cm.$^{-1}$

Hexagonal Cell; a = 3.638 ± 0.003, c = 18.78 ± 0.009 Å, U = 215.1 $Å^3$, Z = 3.

Experimental Account and Results

Preliminary Examination

Crystals of Ca_2N, sealed in Lindemann tubes under argon, were supplied by Professor J. W. Tomlinson. The samples were prepared by Mr. C. Lammas, using the tubes themselves to chip off small pieces from a larger block of the material. Obtaining a single crystal was therefore a matter of trial and error, and proved quite difficult in practice.

The crystals were examined under a microscope. All samples appeared lustrous and greenish black in colour. No clearly defined habit was observable since the large majority of the samples were not single crystals, but some triangular faces could occasionally be seen.

The crystals which were usable for taking photographs were the size of the diameter of the Lindemann tubes, (0.3mm). Smaller crystals, which had a higher probability of being single were loose in the tube, and as it was impossible to wedge them in any way, they were not usable for photographic methods.

Oscillation photographs of some thirty crystals were taken, and if these looked promising, a zero-layer Weissenberg photograph was obtained.

One crystal was selected for the determination of the unit cell and space-group, and preliminary collection of three-dimensional data. Examination of further crystals was meanwhile continued.

Unit Cell and Space-group

From oscillation and Weissenberg photographs the crystal class initially appeared to be monoclinic, with a = 6.299, b = 3.638, c = 7.535 Å, $\beta = 123^{\circ}51'$. This corresponds to a volume of 143.4 $Å^3$. A cell content of 2 formula units gave a calculated value for density of 2.18 $g.cm.^{-3}$, compared with the observed value[10] of 2.17 $g.cm.^{-3}$.

The absences found were $h + k \neq 2n$ for h k l, and no extra conditions for axial reflections, indicating C2 (No 5), Cm (No 8) or C2/m (No 12) as possible space-groups. (The numbers in parentheses refer to International Tables[11] Volume I.) C2/m emerged as the correct monoclinic space-group, but the symmetry was in fact higher than this.

An alternative monoclinic cell is a = 6.299, b = 3.638, c = 6.603 Å, $\beta = 109^{\circ}4'$, but the former cell was found tc be more convenient computationally and more sensible structurally.

On plotting out the lattice, it was evident that the monoclinic side-step brought every third lattice point into line. (Figure 3.1). The ab plane, which was centred, was clearly hexagonal since $a/b = \frac{6.299}{3.638} = 1.731 \quad (\sim\sqrt{3})$. (Figure 3.2). The structure, which was solved as monoclinic refined to positions consistent with rhombohedral symmetry.

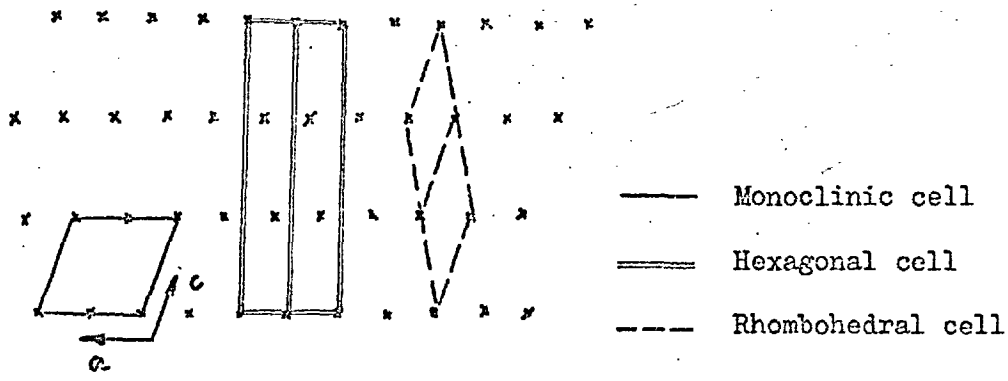


Figure 3.1

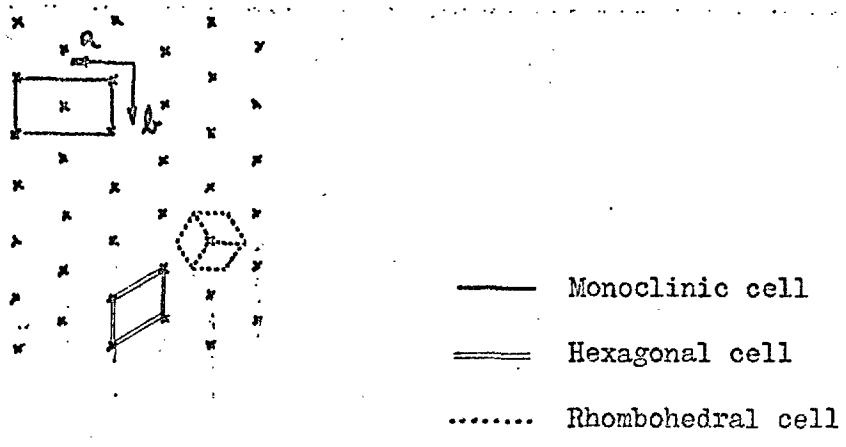


Figure 3.2

Ahmad's powder pattern was therefore indexed on the basis of the hexagonal cell a = 3.638, c = 18.78 Å, using the relationship

$$\sin^2\theta_{hkl} = \frac{\lambda^2}{3a^2}(h^2 + hk + k^2) + \frac{\lambda^2}{4c^2}l^2,$$ with the rhombohedral

condition that only h - k + l = 3n are present.

The rhombohedral cell has a = 6.603 Å, $\alpha = 31^{\circ}59'$, with the volume of 71.7 $Å^3$, and contains one formula per unit cell. The dimensions quoted for the various cells are those derived from the hexagonal cell, which was obtained by least-squares refinement of the inter-planar spacings, d, as given by Ahmad[3]. The indexed powder pattern with observed and calculated values of d is listed in Table 3.2. The least-squares refinement of cell-dimensions was performed using a program written for the Atlas computer by R. Diamand. The program has an optional weighting scheme of the type $w = 1/\sin\theta\cos\theta$. Two refinements, one using this scheme, the other with unit weights were performed, but showed no significant difference. The standard deviations in both cases were 0.003Å for a, and 0.009Å for c.

Figures 3.1 and 3.2 show the relationship of the hexagonal and rhombohedral cells to the monoclinic cell which was used in the structure determination. Table 3.1 summarises the dimensions of the various cells.

	a Å	b Å	c Å	α	β	V $Å^3$	Z
HEXAGONAL	3.638		18.78			215.1	3
RHOMBOHEDRAL	6.603			$31^{\circ}59'$		71.7	1
MONOCLINIC	6.299	3.638	7.535		$123^{\circ}51'$	143.4	2
	D_{obs}[3] = 2.17 $g.cm^{-3}$ D_{calc} = 2.18 $g.cm^{-3}$						

Table 3.1

Table 3.2

X-ray powder data for Ca_2N

Cu Kα radiation — Philips 11.54 cm. camera

Key

ss	very strong
s	strong
ms	medium strong
m	medium
f	faint
ff	very faint

Line No.	Intensity	h k l (hexagonal)	d_{obs} (3)	d_{calc}
1	ss	0 0 3	6.21	6.21
2	ms	0 0 6	3.13	3.12
3	s	1 0 2	2.98	2.98
4	ss	0 1 4	2.62	2.61
5	f	1 0 5	2.427	2.407
6	ff	0 0 9	2.080	2.082
7	f	0 1 7	2.034	2.038
8	ms	1 0 8	1.875	1.878
9	s	1 1 0	1.815	1.815
10	ff	1 1 3	1.743	1.743

Line No.	Intensity	h k l (hexagonal)	d_{obs} (3)	d_{calc}
11	ff	0 1 10	1.605	1.611
12	ms	2 0 1	1.567	1.567
13	f	0 2 2	1.549	1.551
14	ms	1 0 11	1.494	1.499
15	f	1 1 9	1.369	1.369
16	f	2 0 7	1.356	1.357
17	f	0 2 8	1.309	1.307
18	f	0 0 15	1.253	1.251
19	f	2 1 2	1.180	1.180
20	f	1 2 4	1.155	1.153
21	ff	1 2 7	1.089	1.088
22	ff	2 0 13	1.063	1.064
23	ff	3 0 0	1.051	1.050
24	ff	0 0 18	1.043	1.043
25	ff	3 0 3	1.033	1.035
26	ff	3 1 10 (α_1)	0.792	0.792
27	ff	3 1 10 (α_2)	0.792	0.792

Collection of Data

Three-dimensional data were collected using the equi-inclination

Weissenberg technique and visual estimation of the intensities. A Unicam Weissenberg camera was used with Cu Kα radiation. The crystals, sealed under argon in Lindemann tubes, were mounted on Nonius goniometer heads. The crystal was set to rotate about the monoclinic a axis, which being approximately 6.3 Å, made it possible to photograph layers 0kl to 5kl.

The multiple-film technique was used, placing four Ilford Industrial G films in the camera-pot for each exposure. With Cu Kα radiation film ratios of about 2.8:1 could be expected, giving a ratio of 22:1 between the top and bottom films. This proved to be adaquate, and only one 24 hour exposure per layer was made.

The films for each layer were developed and fixed together, in total darkness, for five minutes each. The intensities were estimated by means of a stepped wedge, made by exposing a reflection for a known number of small oscillations of the crystal. The wedge stretched from 1 to 40 on an arbitrary scale, with 16 enequal intervals. Every reflection was then measured, using the wedge, on each of the films of the pack on which it appeared.

Film ratios were calculated from the intensity totals of reflections common to the given two films. All measurements were scaled up to the top film of the pack. A mean intensity was then calculated for each reflection using subjective weights to give maximum account to measurements on the central part of the wedge, as these estimates were felt to be most accurate.

No subsidary layer photographs were taken, as it was not possible to turn the crystal round in its tube, nor was it possible to obtain another crystal. Thus no interlayer scaling was applied at this stage.

A final reflection list of 124 was then prepared. These were all regarded as independent in the space-group C2/m. The reflection data was punched on cards ready for input into the -X-ray 63- system.

Solution of the Structure of Ca_2N

The $(Lp)^{-1}$ correction was applied to the raw intensity data and square-roots were calculated using the DATRDN link of the -X-ray 63- system. In the same run a three-dimensional Patterson map was calculated by utilizing the reduced data as input to the FOURR link of the system.

This map is shown in eight sections for the full unit cell in Figure 3.3.

For the purposes of structure determination Ca_2N was considered to be monoclinic, especially as this suited our programs better. The cell used was:

$a = 6.299$ Å

$b = 3.638$ Å

$c = 7.535$ Å

$\beta = 123^{\circ}51'$

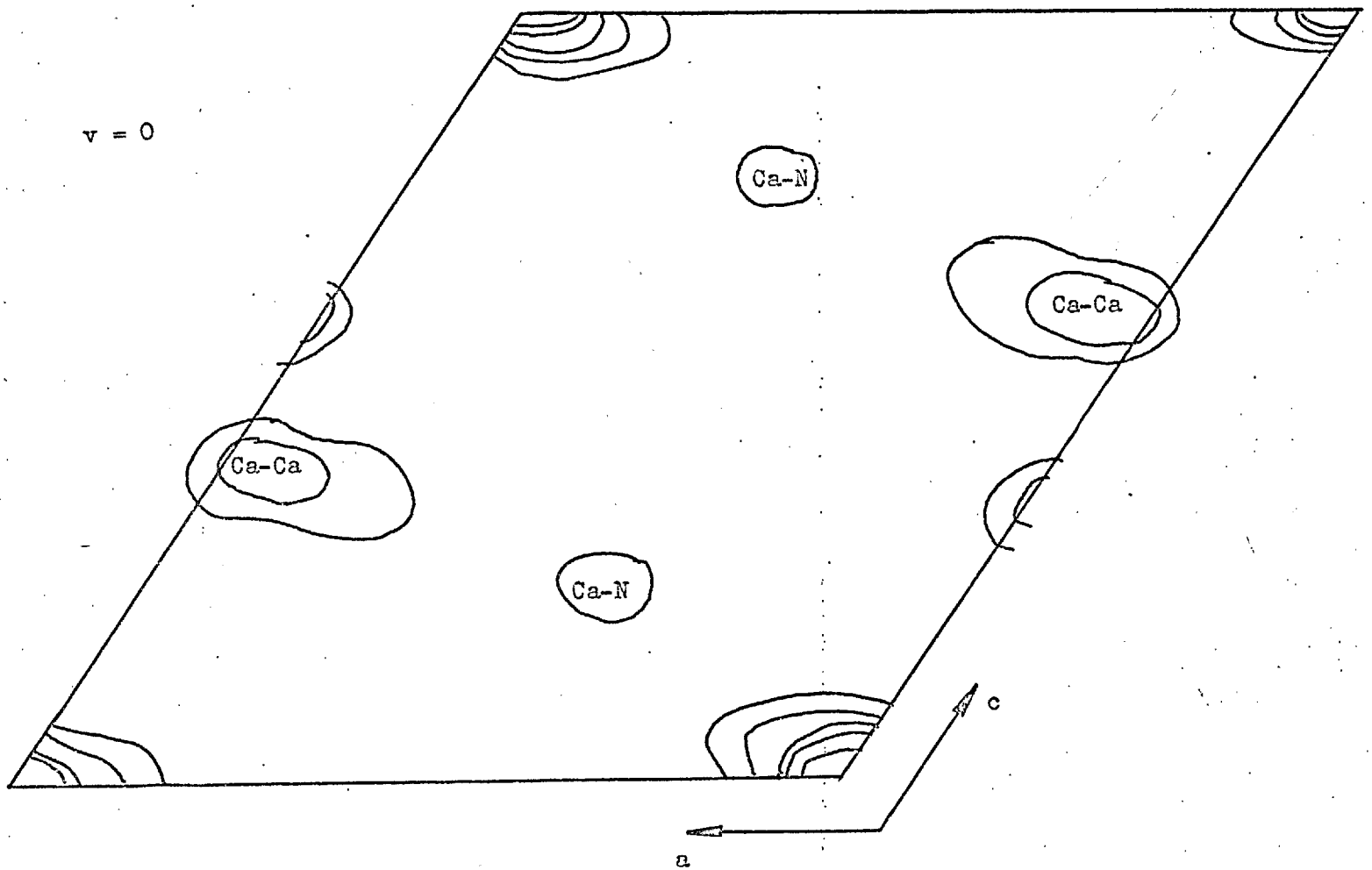
$Z = 2$

The three possible space-groups were C2, Cm or C2/m, of which the last appeared most likely. This was assumed to be the actual space-group until it could be shown to be otherwise. It was clear that with a

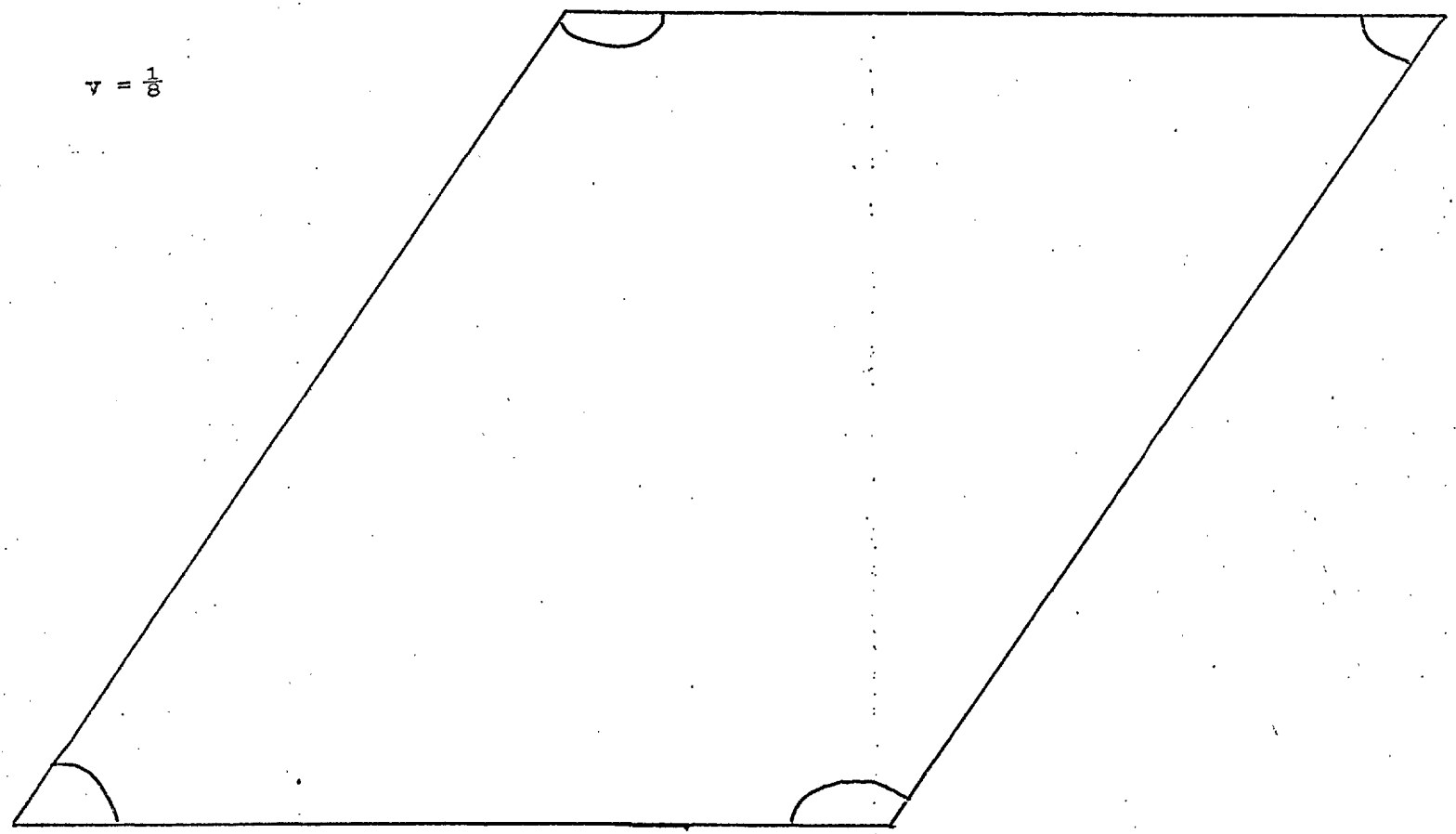
Figure 3.3

Sections of Patterson Synthesis

Contours at equal but arbitrary intervals.

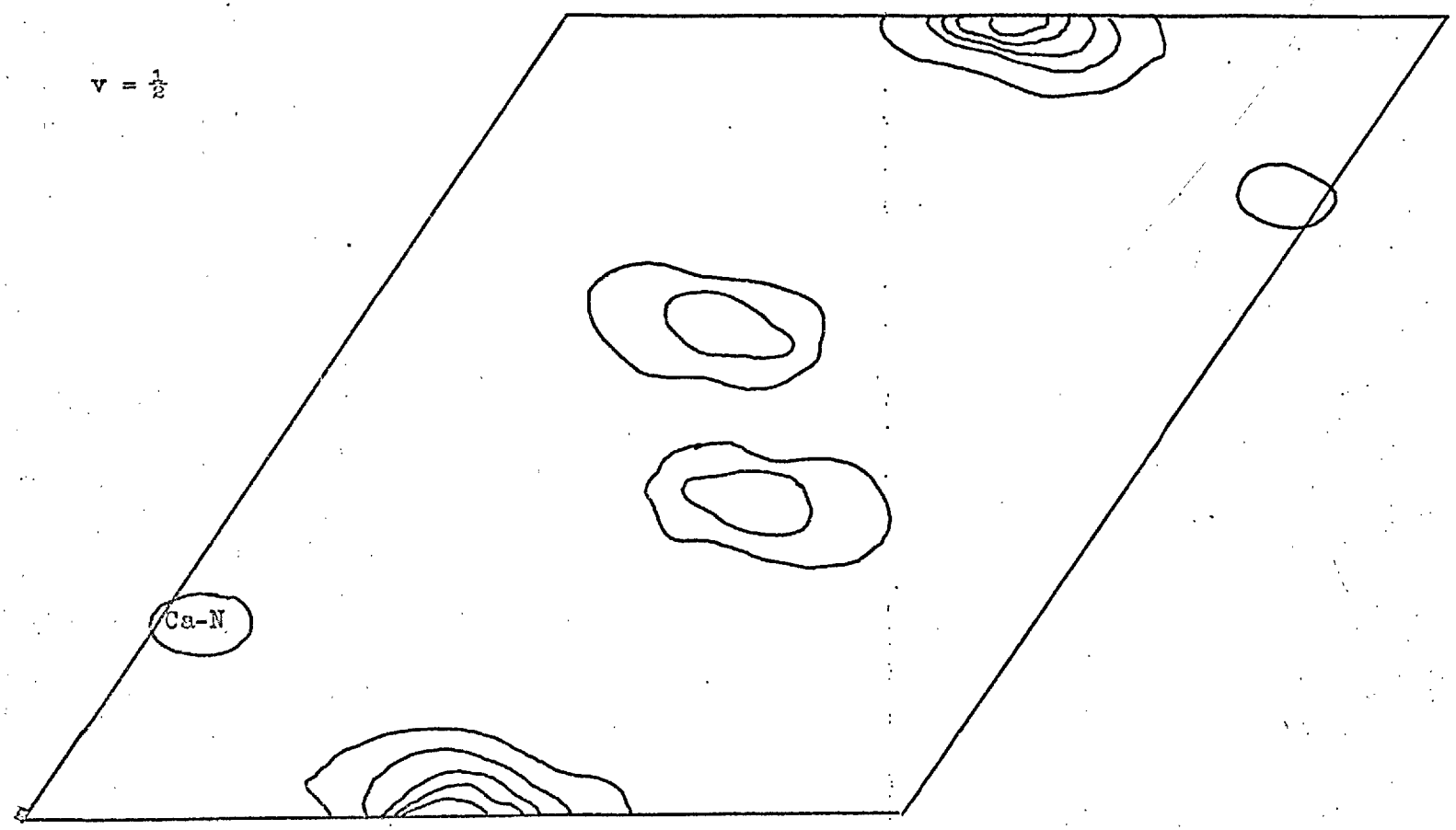

v = 0
Ca-N
Ca-Ca
Ca-Ca
Ca-N
c
a

$v = \frac{1}{8}$



$\nu = \frac{1}{4}$

$V = \frac{3}{8}$

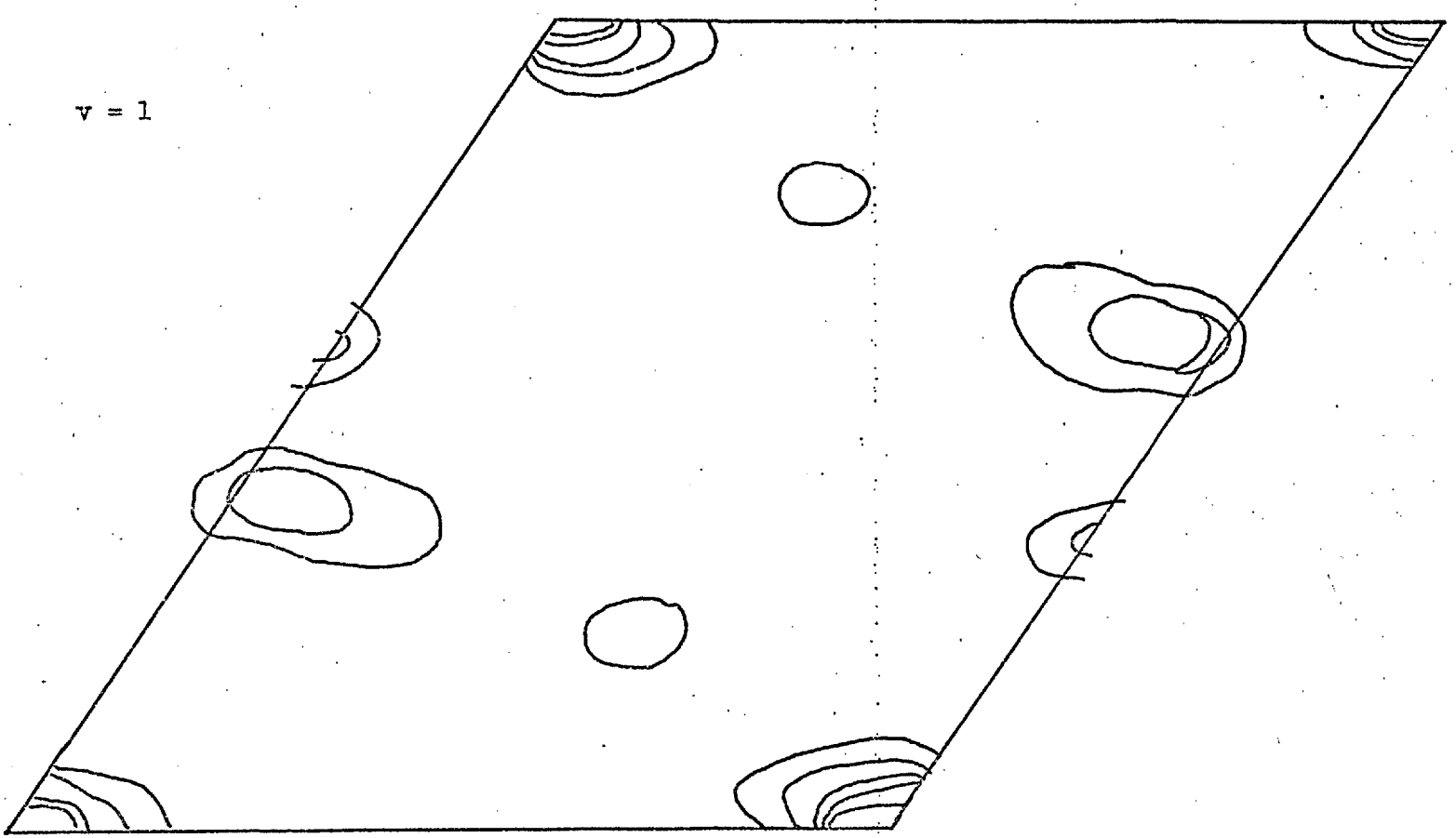

v = ½
Ca-N

$v = \frac{5}{8}$

$v = \frac{3}{4}$

$v = \frac{7}{8}$

v = 1



unit cell content of $2(Ca_2N)$, the nitrogen atoms would have to be in two-fold, and the calciums in four-fold, special positions.

The two-fold special positions in C2/m are points of symmetry 2/m at:

(d) 0, $\frac{1}{2}$, $\frac{1}{2}$

(c) 0, 0, $\frac{1}{2}$

(b) 0, $\frac{1}{2}$, 0

(a) 0, 0, 0, and equivalent positions with respect to $(\frac{1}{2},\frac{1}{2},0)$. The four-fold ones are at:

(i)	m	x,	0,	z;	$\bar{x}$,	0,	$\bar{z}$	
(h)	2	0,	y,	$\frac{1}{2}$;	0,	$\bar{y}$,	$\frac{1}{2}$	
(g)	2	0,	y,	0;	0,	$\bar{y}$,	0	
(f)	$\bar{1}$	$\frac{1}{4}$,	$\frac{1}{4}$,	$\frac{1}{2}$;	$\frac{1}{4}$,	$\frac{3}{4}$,	$\frac{1}{2}$	
(e)	$\bar{1}$	$\frac{1}{4}$,	$\frac{1}{4}$,	0;	$\frac{1}{4}$,	$\frac{3}{4}$,	0,	and equivalent

positions with respect to $(\frac{1}{2},\frac{1}{2},0)$.

In the Patterson map all peaks are on v = 0 or $\frac{1}{2}$, therefore all atoms occur on layers separated by $y = \frac{1}{2}$. The strongest (2/5 of the origin peak and therefore representing two Ca-Ca vectors) are at $\pm(0.075,0,0.60)$, (with another origin peak at $\frac{1}{2},\frac{1}{2},0$, due to the C-face centring vectors between all kinds of atoms) and other 2Ca-Ca peaks at $\pm(0.575, \frac{1}{2},0.60)$, which again is related to the earlier peak (A) by C-face centring vectors. Thus only peak A, (0.075,0,0.60) has to be considered.

This is incompatible with special positions e,f,g,h, but it is compatible with i if x = 0.0375 and z = 0.30. Drawing the calcium

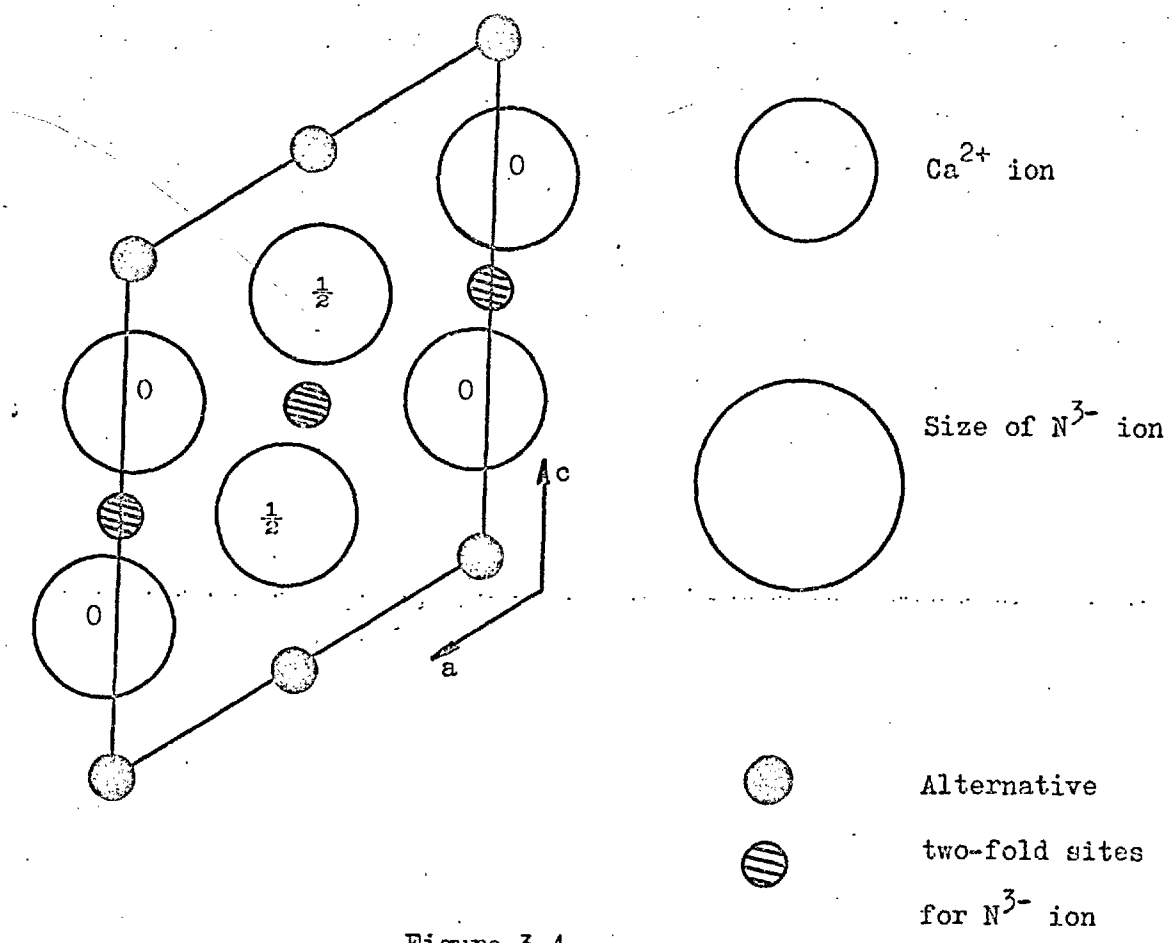


Figure 3.4

atoms in the unit cell at these approximate co-ordinates, (Figure 3.4), using a radius equivalent to 1 Å, it was thought reasonable that the nitrogen atoms should go at (0,0,0), (black circles in Figure 3.4) instead of the other available two-fold sites.

As the total content of the unit cell was apparently determined, it was decided to refine the structure by least-squares immediately without calculating a Fourier on the basis of the Ca atoms only. For this, the DATRDN and ORFLS links of the system were utilised.

The latter is a revised version of the Busing-Levy full-matrix least-squares program[9].

Atomic scattering factors were supplied in the DATRDN link for 0.1 intervals of $\frac{\sin\theta}{\lambda}$. The scattering factors used were those for $Ca^{1\frac{1}{2}+}$ and N^{3-}. These were obtained by interpolation between values for Ca^{+} and Ca^{2+}, and extrapolation from N and N^{-}, found in International Tables[11], Volume III. The program uses a four-point interpolation function to evaluate the required values of form-factors for a given θ.

The input parameters were:

	x	y	z	B
Ca	0.037	0.0	0.3	0.0
N	0.0	0.0	0.0	0.0

After five cycles of unweighted refinement on calcium x, z, B, and nitrogen B, as well as the interlayer scales as parameters, produced an R factor of 0.227 and the following parameters and standard deviations

	x	y	z	B
Ca	0.03978	0.0	0.30571	-0.641
σ	0.00315	-	0.00156	0.267
N	0.0	0.0	0.0	31.89
σ	-	-	-	19.44

Clearly the calcium position was correct, and this atom refined normally, the negative temperature factor being a result of large, uncorrected absorption errors. It was equally clear from the temperature factor that the nitrogen position was incorrect.

A Fourier map was therefore calculated, using the refined Ca position to phase the data. The interlayer scales obtained in the refinement were also used. This was accomplished using the DATRDN, FC and FOURR links of the system.

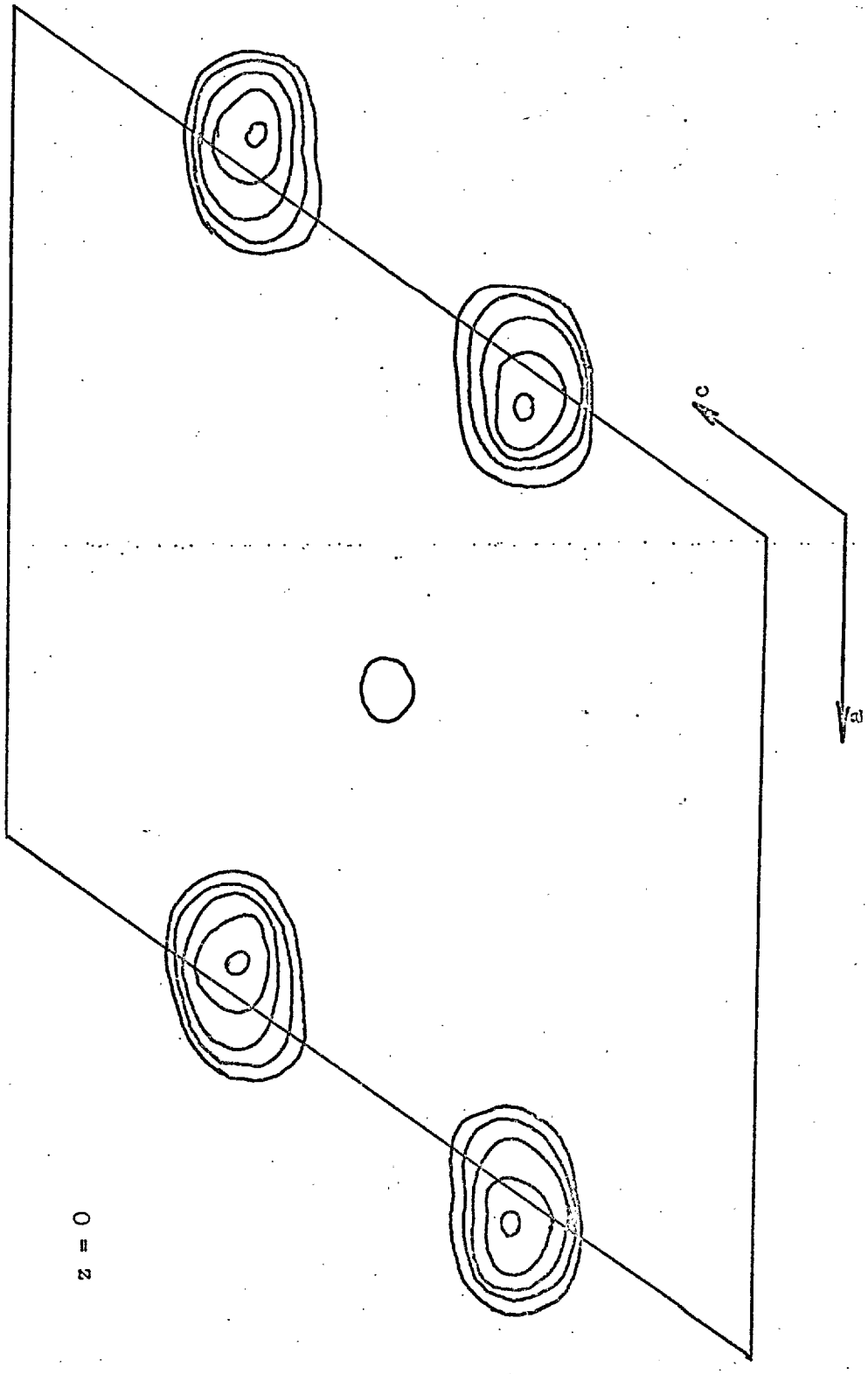
The Fourier obtained is shown in Figure 3.5 for half the cell in $\frac{1}{8}$ sections. The map shows clearly the position of the nitrogen atom at $(\frac{1}{2},0,\frac{1}{2})$, plus the symmetry related position. The next highest peaks are of the order of half the height of the nitrogen peak, forming ripples around the heavy atoms. The nitrogen position of $(\frac{1}{2},0,\frac{1}{2})$ is consistent with the Patterson, where the corresponding Ca-N peaks appear.

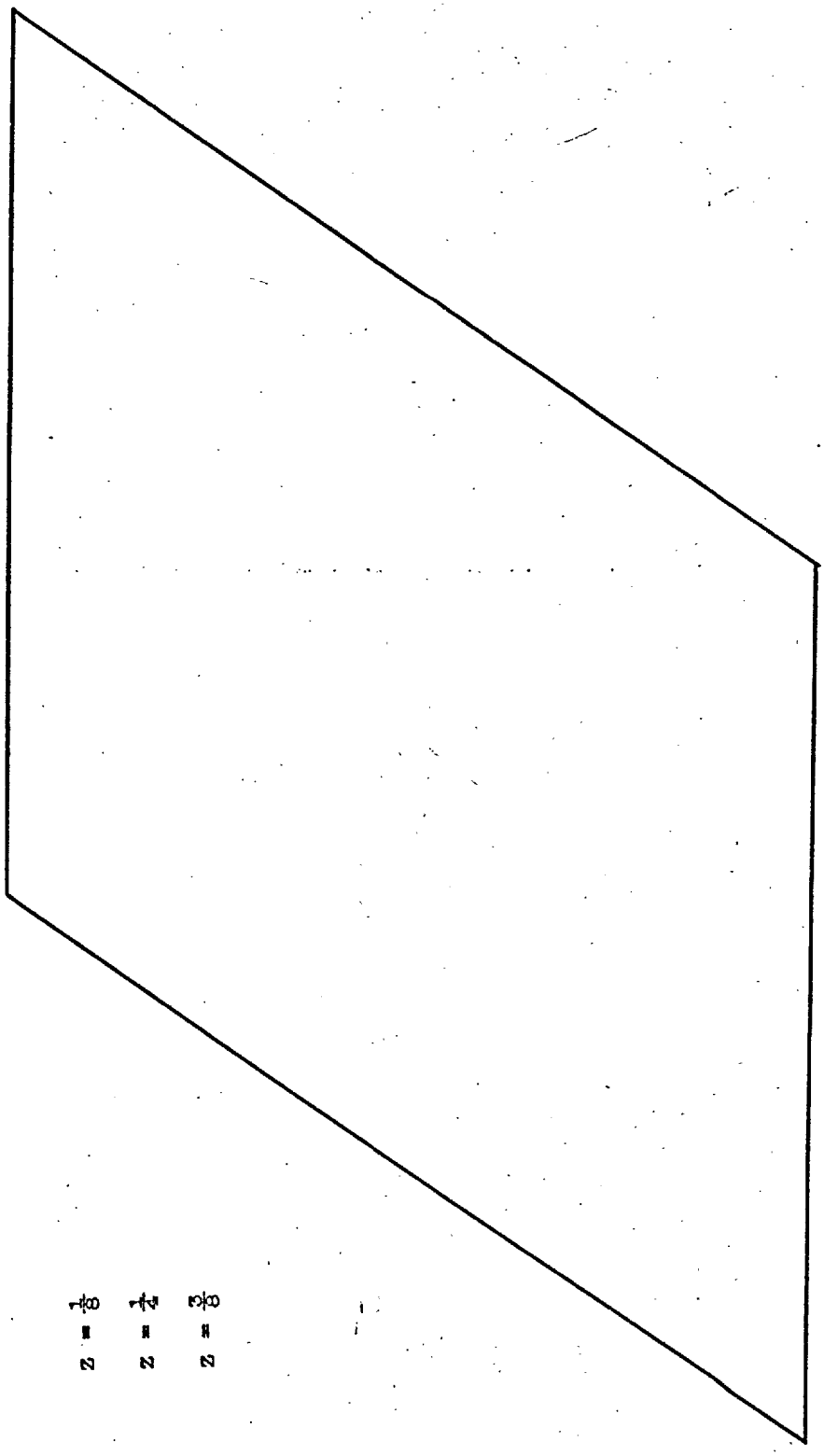
Five cycles of least-squares refinement of the calcium and nitrogen parameters gave an R factor of 0.188 and

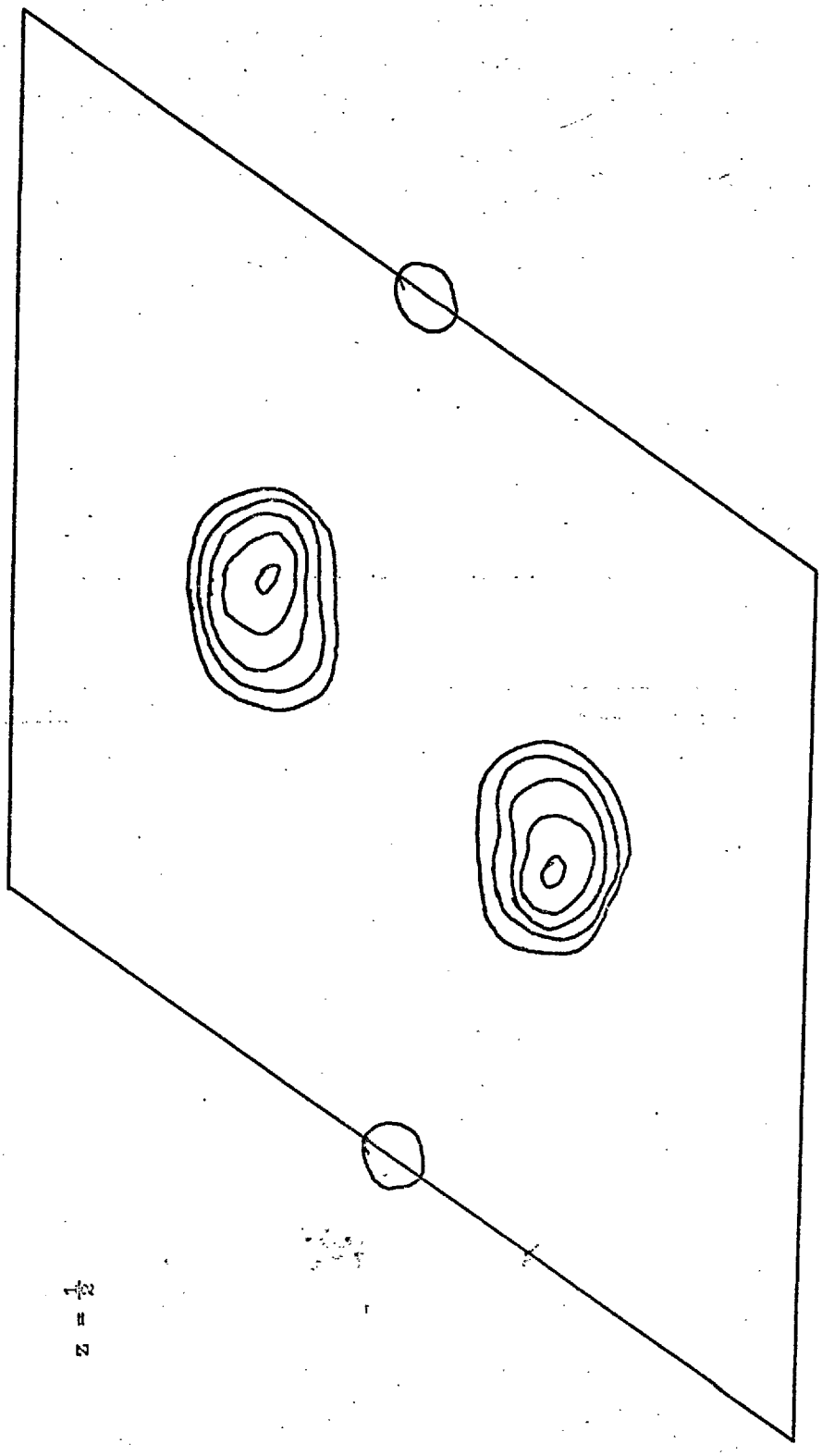
	x	y	z	B
Ca	0.03688	0.0	0.30448	-0.677
σ	0.00141	-	0.00093	0.190
N	0.5	0.0	0.5	0.016
σ	-	-	-	0.781

Figure 3.5

Fourier synthesis using calcium positions for phasing.


o
y
z = 0


1/8
1/4
3/8
2
2
2



The largest shift on the last cycle was 0.005 standard deviations, with an average shift of 0.002 standard deviations.

On correcting six misindexed reflections, using the final unit cell constants, and removing three strong low-angle reflections which were thought to suffer from extinction, two refinements were carried out simultaneously. The first used unit weights, giving after five cycles R = 0.160 and parameters:

	x	y	z	B
Ca	0.03520	0.0	0.30453	-0.972
σ	0.00160	-	0.00103	0.177
N	0.5	0.0	0.5	0.016
σ	-	-	-	0.781

Maximum shift/error 0.0140

Average shift/error 0.0070

The second refinement used a weighting scheme of the type

$$w = 1 \quad \text{for} \quad F < F^*$$

$$\sqrt{w} = \frac{F^*}{F} \quad \text{for} \quad F \geqslant F^*, \text{ with } F^* = 8 \text{ on an absolute scale.}$$

Five cycles gave an R of 0.162 and parameters:

	x	y	z	B
Ca	0.03538	0.0	0.30426	-0.86
σ	0.00130	-	0.00081	0.17
N	0.5	0.0	0.5	0.14
σ	-	-	-	0.68

On the last cycle the maximum shift was 0.0035 standard deviations, while the average was 0.0015 standard deviations.

These parameters are the final ones for refinement in the monoclinic space group. Table 3.4 lists the observed structure amplitudes and the calculated structure factors corresponding to these parameters. Reflections are indexed in the monoclinic system; the scale is ten times absolute.

As a final check, an error synthesis was calculated. This showed no unusual features and the highest peak was equivalent to 1/6 of the height of a nitrogen peak.

Of the possible space groups in the monoclinic system, only C2/m is centrosymmetric. Since the structure refined with a centre of symmetry, C2/m must be regarded as the correct monoclinic space group.

Table 3.3 shows the final hexagonal and rhombohedral co-ordinates. Figure 3.6 (b) illustrates the symmetry of the space group $R\bar{3}m$.

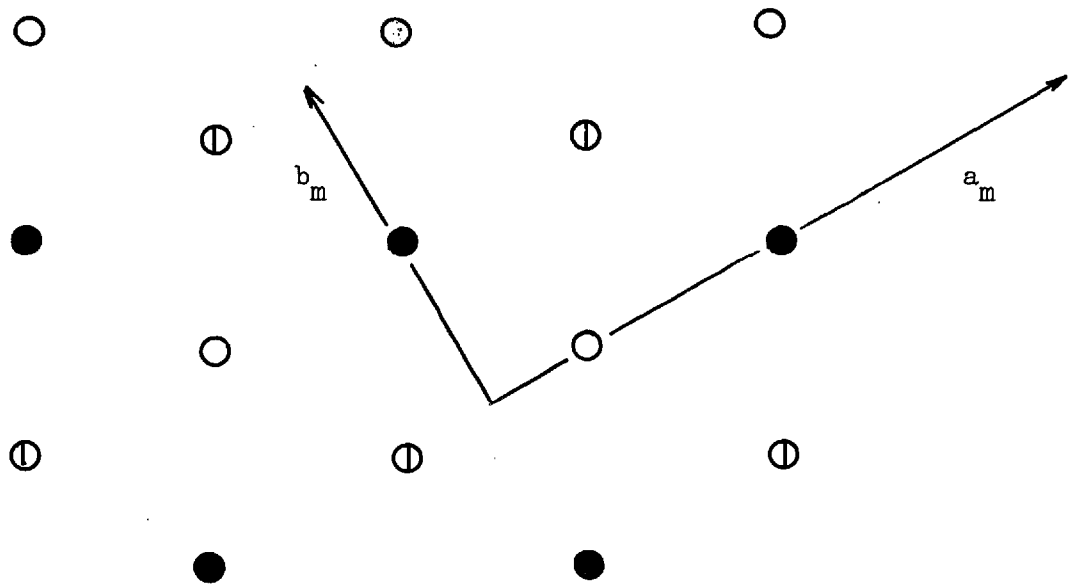


Figure 3.6 (a)

● { N at z = 0
  Ca at z = 0.268
  Ca at z = 0.732

◐ { N at z = $\frac{1}{3}$
  Ca at z = $\frac{1}{3}$ + 0.268
  Ca at z = $\frac{1}{3}$ - 0.268

○ { N at z = $\frac{2}{3}$
  Ca at z = $\frac{2}{3}$ + 0.268
  Ca at z = $\frac{2}{3}$ - 0.268

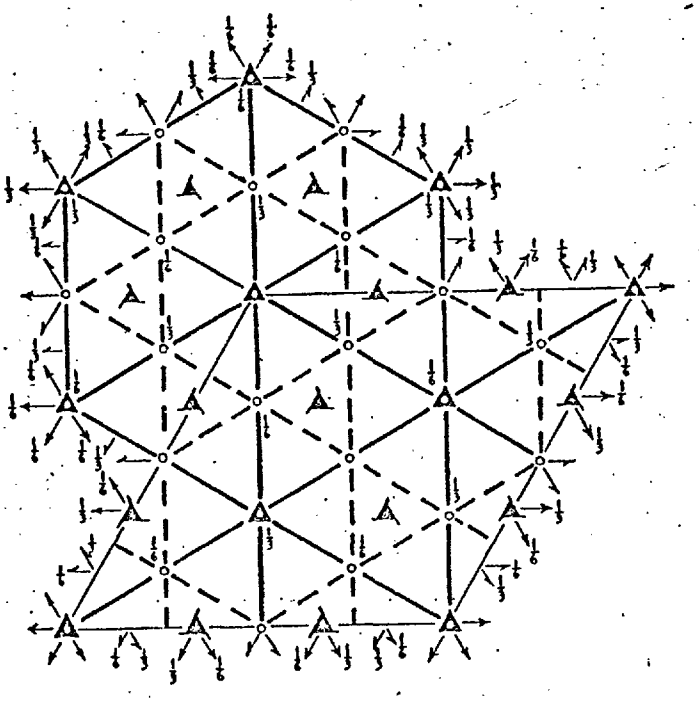


Figure 3.6 (b)

The positions obtained from the monoclinic refinement are superimposed (Figure 3.6 (a)) on this diagram to show that they comply with the symmetry requirements of the rhombohedral space-group.

	Hexagonal	Rhombohedral
N	0, 0, 0 $\frac{1}{3}, \frac{2}{3}, \frac{2}{3}$ $\frac{2}{3}, \frac{1}{3}, \frac{1}{3}$	0, 0, 0
Ca	$\pm$ 0, 0, z $\pm \frac{1}{3}, \frac{2}{3}, \frac{2}{3}+z$ $\pm \frac{2}{3}, \frac{1}{3}, \frac{1}{3}+z$ z = 0.268	$\pm$ x, x, x x = 0.268

Table 3.3

Table 3.4

Observed Structure Amplitudes and

Calculated Structure Factors for

Ca_2N

Scale: 10 x absolute

Format: 1 $|F_o|$ F_c

0,0,L		
1	146	-199
2	199	-189
3	257	197
4	121	79
5	300	-240
6	151	113
7	128	121
8	93	-170

0,2,L		
0	250	296
1	142	-119
2	167	-160
3	148	170
4	67	65
5	178	-222
6	119	108
7	97	122

0,4,L		
0	205	218
1	90	-84
2	141	-139
3	179	155
4	48	56

1,1,L		
-8	199	-177
-7	234	184
-5	269	-200
-4	99	72
-3	274	236
-2	272	-317
0	280	251
1	137	-111
2	200	-200
3	244	254
5	120	-174
6	72	112

1,3,L		
-5	168	-183
-4	59	67
-3	187	169
-2	238	-211
0	184	188
1	100	-92
2	135	-147
3	163	210
5	95	-173

2,0,L		
-9	123	-115
-8	143	-114
-7	249	173
-6	58	28
-5	357	-255
-4	190	197
-3	109	115
-2	152	-250

2,2,L		
0	262	243
1	200	-186
2	77	-71
3	166	187
5	119	-184

2,4,L		
-5	137	-208
-4	174	137
-3	111	93
-2	160	-178
0	177	197
1	134	-154

3,1,L		
-9	130	-120
-8	164	-111
-7	291	222
-6	105	-62
-5	180	-172

3,1,L		
-4	145	158
-3	114	122
-2	263	-297
-1	135	115
0	135	163
1	160	-169
2	80	-68
3	139	223

3,3,L		
-7	206	215
-6	61	-54
-5	145	-156
-4	137	138
-3	98	90
-2	198	-225
-1	76	84
0	144	142

4,0,L		
-7	269	187

4,0,L		
-6	100	-65
-5	207	-191
-4	191	240
-1	59	96
0	96	166
1	195	-222
3	202	172
4	130	-111

4,2,L		
-6	64	-64
-5	159	-171
-4	186	210
-2	179	-189
-1	80	90
0	178	150
1	237	-209
2	40	16
3	149	174

4,4,L		
-2	183	-182

5,1,L			5,3,L		
-7	284	212	-6	142	-135
-6	167	-142	-5	92	-96
-5	125	-98	-4	146	178
-4	189	187	-2	179	-198
-2	164	-215	-1	143	155
-1	158	165			
0	92	72			
1	155	-183			

Least-Squares Refinement in the Space Group $R\bar{3}m$.

Due to no further single crystals being available, no single-crystal photograph has been taken which shows a three-fold axis. However, since the powder pattern could be indexed fully on the basis of a hexagonal cell with rhombohedral absences, and the size of the unit cell is consistent with a rhombohedral cell, it is fairly safe to assume that the symmetry is in fact rhombohedral, especially if the simplicity of the structure is taken into account.

As a final step in the refinement of this structure, the space group $R\bar{3}m$ was assumed and all monoclinic indices were transformed to

rhombohedral using the transformation

$$\begin{pmatrix} h \\ k \\ l \end{pmatrix}_{\text{rhomb.}} = \begin{pmatrix} \frac{1}{2} & \frac{1}{2} & 1 \\ 1 & 0 & 1 \\ \frac{1}{2} & -\frac{1}{2} & 1 \end{pmatrix} \begin{pmatrix} h \\ k \\ l \end{pmatrix}_{\text{mono.}}$$

This produced 71 independent values of (hkl). Duplicate values of (hkl), equivalent in the rhombohedral system were averaged. Calculation of structure factors using the final monoclinic positions transformed to this cell gave $R = 0.133$.

The full-matrix refinement program was patched at this stage to confine the calcium atom to the body-diagonal of the rhombohedral cell. Thus the number of parameters was reduced to three plus one overall scale factor. Five cycles of least-squares refinement produced virtually no change from the original transformed parameters. This is understandable since the structure had been fully refined as monoclinic. The improved agreement is thought to result from the fact that some of the error introduced by absorption had been eliminated by taking mean values for duplicate reflections recorded in different directions. The refinement was based on all the data; no reflections were removed for extinction. The weighting scheme used was the same as in the monoclinic refinement. The final output parameters referred to rhombohedral axes are given in Table 3.5. The list of observed structure amplitudes and the structure factors calculated from these parameters are given in Table 3.6.

Table 3.5 - Ca_2N, final positional parameters, rhombohedral refinement

	d	x	y	z	B
Ca	0.2680	0.2680	0.2680	0.2680	-0.59
σ	0.003				
N	0.0	0	0	0	0.30
σ	-				0.67

(where $d\underline{D} = x\underline{a} + y\underline{b} + z\underline{c}$ and $\underline{D} = \underline{a} + \underline{b} + \underline{c}$)

Unobserved reflections are included in the Table as the minimum locally observable and are marked by "L". The scale is absolute.

Table 3.6 - Ca_2N, observed structure amplitudes and calculated structure factors, rhombohedral refinement

0	0	1	L	1.59	2.06	2	3	-1		16.44	17.45
0	0	2		19.98	-18.74	2	3	3		17.57	18.96
0	0	3		8.89	7.96	2	3	4		14.55	-15.25
0	1	-3		14.20	-15.68	2	3	5		6.52	-6.01
0	1	-2	L	2.99	-0.11	2	3	6		12.91	17.99
0	1	-1		22.83	27.83	2	4	4		8.03	-6.22
0	1	1		19.60	-23.84	2	4	5		20.63	18.91
0	1	2		11.39	11.35	2	4	6		4.19	5.16
0	1	3		17.61	19.30	3	3	3		22.57	-17.98
0	1	4		9.45	-7.91	3	3	4		8.37	-6.56
0	2	-2		18.00	19.48	3	3	5		19.66	20.24
0	2	2		20.63	22.39	3	3	6		5.57	5.33
0	2	3		9.15	-8.23	3	4	4		27.32	23.51
0	2	4		12.47	-12.22	3	4	5		7.47	6.20
0	3	3		12.99	-12.43	3	4	6		14.50	-16.15
0	3	4		12.76	14.03	3	5	5		19.47	-16.66
1	1	-3	L	1.41	-0.52	3	5	6		3.63	1.83
1	1	-2		17.37	20.36	4	4	4		10.62	7.73
1	1	-1	L	2.47	0.47	4	4	5		20.69	-17.94
1	1	1		12.82	19.47	4	4	6	L	2.67	2.03
1	1	2		23.31	30.56	4	4	7		18.56	16.87
1	1	3		7.98	-8.82	4	5	5		5.48	2.41
1	1	4		12.39	-12.43	4	5	6		18.13	20.09
1	2	-2	L	2.41	-0.42	4	5	7	L	1.96	-2.64
1	2	-1		16.49	-16.83	4	6	7		13.34	-14.98
1	2	2		11.22	-10.31	5	5	5		26.29	21.95
1	2	3		14.16	-14.44	5	5	7		18.65	-15.12
1	2	4		14.98	15.27	5	5	6	L	2.27	-2.53
1	2	5		14.67	12.35	5	6	6		16.96	-15.52
1	3	-1		7.98	7.55	5	6	7		12.65	9.62
1	3	3		18.39	17.20	5	7	7		11.16	16.27
1	3	4		14.20	13.36	6	6	6		13.25	10.12
1	3	5		15.71	-13.45	6	6	7		20.30	16.75
2	2	-2		15.93	-15.60	6	6	8		11.27	-9.70
2	2	-1		6.91	7.96	6	7	7		9.93	-9.74
2	2	2		17.44	-16.12	6	7	8		10.14	-10.68
2	2	3		21.53	22.26	7	7	7		11.2	-10.73
2	2	4		12.99	14.89	7	7	8		17.70	15.46
2	2	5		13.09	-13.62	7	8	8		11.57	10.46
						8	8	8		8.20	-14.47

13. Discussion of the Crystal Structure of Ca_2N

Description of the Structure of Ca_2N

Figure 4.1 shows Ca_2N to have a layer structure of the anti-$CdCl_2$ type. The projection shown corresponds to [010] of the monoclinic cell. The rhombohedral cell is also drawn in, with its calcium content hatched. The [111] rhombohedral axis runs down the page, through these two atoms and a nitrogen at the origin. Figure 4.2 shows a view of a single layer of the Ca_2N structure looking down the rhombohedral [111] axis.

The structure may be thought of as consisting of two sheets of calcium with a sheet of nitrogen sandwiched in between. Such a triple sheet is considered to form a single layer of the Ca_2N structure.

The set of positional parameters and standard deviations from rhombohedral refinement were used to calculate the various interatomic lengths and angles. These are listed in Table 4.0. The standard deviations include the estimated error in the unit cell.

The final atomic co-ordinates from monoclinic refinement were also used to calculate the various distances and angles. These are listed in Table 4.1 with their standard deviations (errors in the unit cell were not included). The symmetry operations used, (monoclinic cell), are

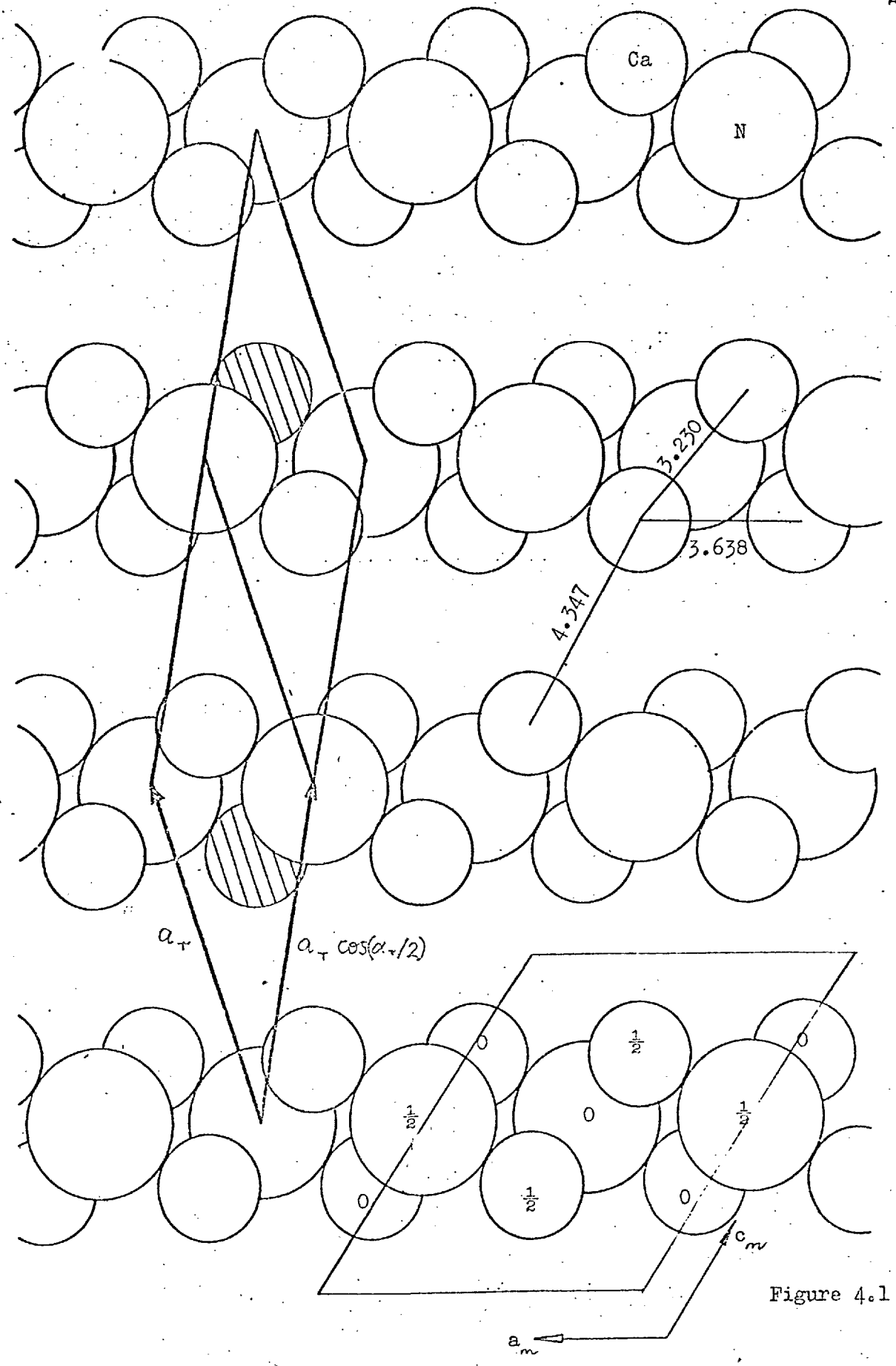


Figure 4.1

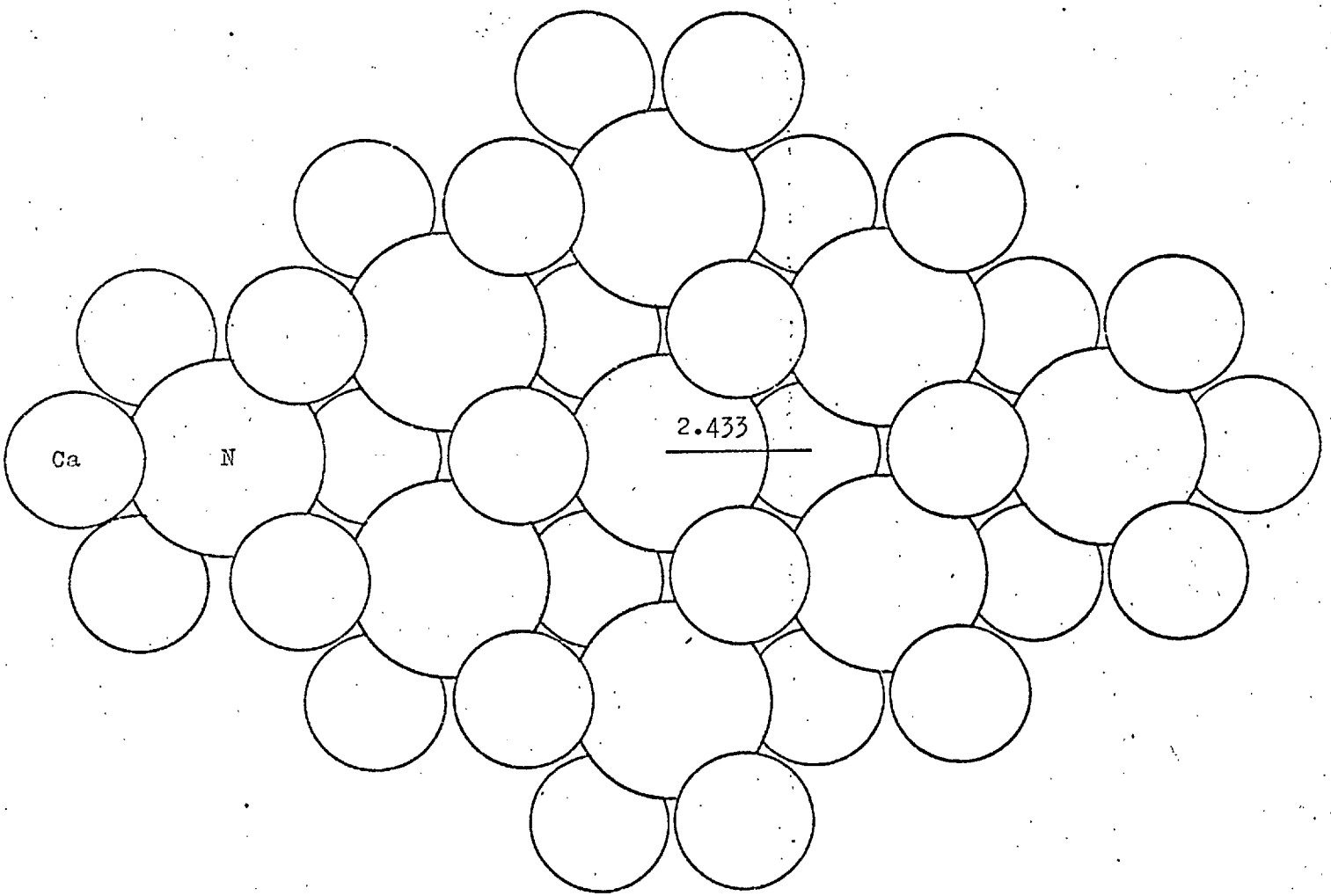


Figure 4.2

indicated by Roman numerals according to the following scheme;

I	$x+\frac{1}{2}, \frac{1}{2}, z$	III	$\bar{x}, 0, \bar{z}$
II	$\frac{1}{2}-x, \frac{1}{2}, 1-z$	IV	$x+\frac{1}{2}, -\frac{1}{2}, z.$

Bond lengths and angles which are equivalent in the higher symmetry are averaged. In all cases the values obtained from monoclinic refinement are within one standard deviation of the mean, and are in agreement with those in Table 4.0

The nitrogen and calcium co-ordinations are illustrated in Figures 4.0 (a) and (b).

Table 4.0 - Ca_2N, Inter-atomic distances angles and their standard deviations - Rhombohedral Refinement

		σ
N - Ca	6 at 2.433 Å	0.007 Å
Ca - N	3 at 2.433	0.007
Ca - Ca	3 at 3.230	0.008
	6 at 3.638	0.003
	3 at 4.347	0.008
Ca - N - Ca	96.9 or 83.1°	0.2°
N - Ca - N	96.9°	0.2°

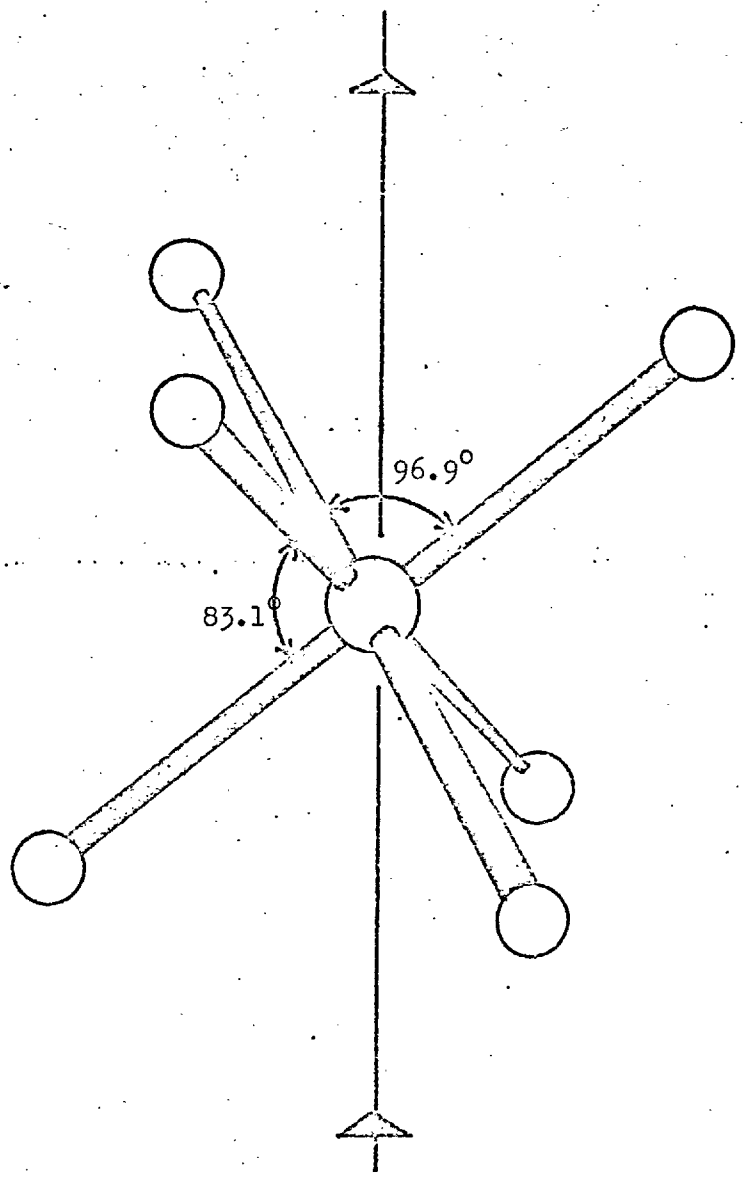


Figure 4.0 (a)

The nitrogen co-ordination

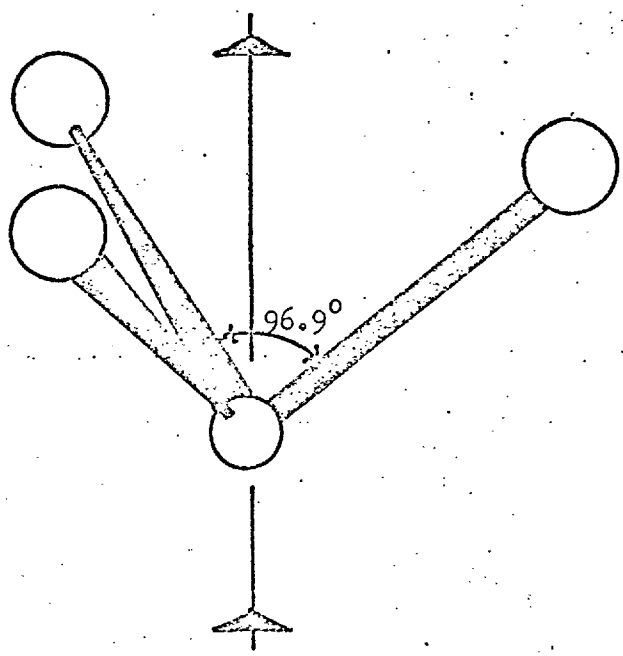


Figure 4.0 (b)

The calcium co-ordination

Ca_2N, Inter-atomic distances and angles; Monoclinic Refinement

Bond	Bond-length Å	σ Å	Bond	Mean Length Å	σ Å
N - Ca	2.436	0.007	N - Ca	2.433	0.004
N - Ca_{II}	2.429	0.005			
Ca - Ca_I	3.638	0.011	Ca - Ca_1	3.638	0.011
Ca - Ca_{II}	3.230	0.005	Ca - Ca_2	3.225	0.006
Ca_I - Ca_{II}	3.220	0.011			
Ca - Ca_{III}	4.353	0.010	Ca - Ca_3	4.353	0.010
Angle		σ	Angle	Mean	σ
Ca-N-Ca_I	96.78°	0.19°	Ca-N-Ca_1	96.9°	0.15°
Ca-N-Ca_{IV}	96.97°	0.20°			
Ca-N-Ca_{II}	83.22°	0.19°	Ca-N-Ca_2	83.1°	0.15°
Ca_I-N-Ca_{II}	83.03	0.20°			

Table 4.1

The nitrogen atoms lie at centres of symmetry on inversion triads. They have an octahedral environment with six equal N - Ca distances of 2.433 Å, but there is some angular distortion and the octahedra are flattened in the c direction. The N - Ca distance in β-Ca_3N_2 is 2.47 Å.

Within a layer, each calcium atom is in contact with three nitrogens at 2.433 Å. There are three nearest neighbour calcium atoms at 3.230 Å,

and six more at 3.638 Å. The nearest calciums in the next layer are at 4.347 Å. This is in fact the closest approach of the adjacent layers. Thus the Ca-Ca distance between the layers is very significantly longer than that found in the metal; 3.947 Å in the α-form and 3.877 Å in the γ-form[12].

Therefore Ca_2N may be described as consisting of anti-$CdCl_2$ type layers, separated by remarkably large gaps, and stacked in an ABC sequence.

Ionic Nature of Ca_2N

Clearly, the postulated structure of Ahmad is only partially correct in predicting a layer arrangement, but is incorrect in that it requires two crystallographically non-equivalent calcium atoms.

It appears best , however, to think of the structure as being essentially ionic. The fact that Ca_2N gives off ammonia and hydrogen in contact with water, and the difference in the electronegativities of the two elements support this contention. There would be an excess of one electron per formula unit, which would be essentially "free", and would give rise to the lustrous, graphitic appearance of the crystals.

Comparison with Other M_2X Compounds

A structural comparison may be made with Cs_2O[13]. This compound

also has an anti-$CdCl_2$ type structure, the main difference being that in Ca_2N the shortest metal-metal distance between layers is substantially greater than the corresponding one within the layer, whereas for Cs_2O (where there is no excess of electrons) they are of the same order.

Other compounds known with the general formula M_2X, which contain excess electrons are Ag_2F[14], Ti_2O[15], Ti_2S[16], and Nb_2S[17] apart from the barium and strontium analogues of Ca_2N. The conductivities of Ti_2S, Ti_2Se and Ti_2Te had been measured by McTaggart[16], although he was not certain whether these compounds exist as a separate phase or not.

Ag_2F is hexagonal with $a = 2.989$, $c = 5.710$ Å, $Z = 1$, and has an anti-CdI_2 structure. This differs from the anti-$CdCl_2$ type only in the manner of stacking the layers, the sequence in this case being ABAB. The atomic parameters were determined from powder data by Terrey and Diamond as F at (0,0,0) and Ag at $(\frac{1}{3}, \frac{2}{3}, u)$ and $(\frac{2}{3}, \frac{1}{3}, \bar{u})$, where u is approximately 0.3.

Ti_2O is trigonal with $a = 2.959$, $c = 4.845$ Å, $Z = 1$, space-group $P\bar{3}m1$ (No 164). The atomic co-ordinates were stated by Andersson et al[15] as O at (0,0,0) and Ti at $(\frac{1}{3},\frac{2}{3},z)$ and $(\frac{2}{3},\frac{1}{3},\bar{z})$ where $z = 0.263$.

Ti_2S is hexagonal[18], but nothing further is known about it at the present time. Its structure is soon to be published[19].

Nb_2S is tetragonal with $a = 16.794$, $c = 3.359$ Å, and has the

space-group I4/m. Its structure is being investigated by Franzen et al[17].

The first two compounds have metal-metal distances between the layers shorter than within them, though in the case of Ti_2O the difference is not great. A "layer" is still being defined as an anion sheet between two metallic sheets. Thus these compounds appear to have structures contradictory to that of Ca_2N, as illustrated in Figure 4.3.

Because of this apparent contradiction, an attempt was made to check the structures of Ag_2F and Ti_2O. In each case the published

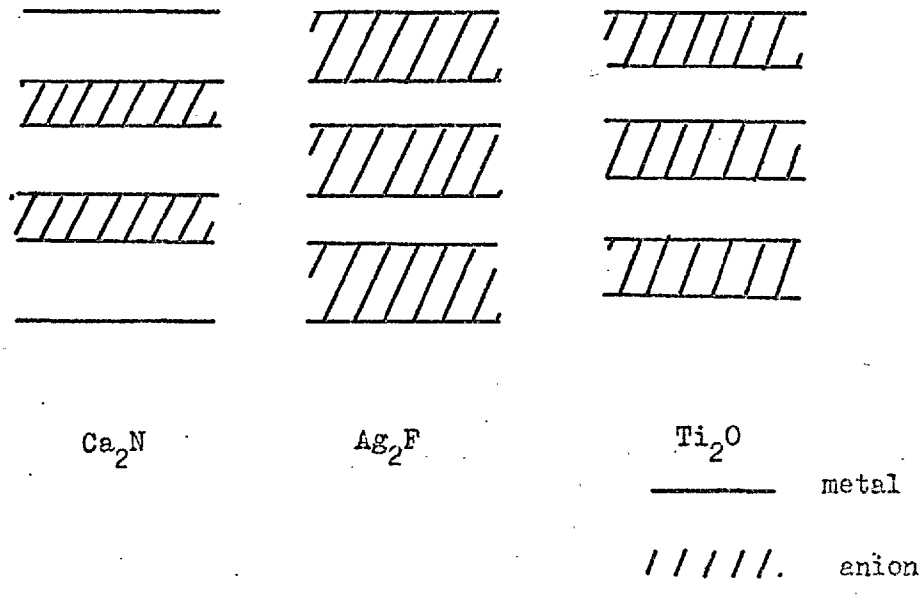


Figure 4.3

structure and the alternative structure analogous to Ca_2N were refined by least-squares of the powder data. Table 4.2 summarises the various

agreement factors obtained.

Compound	Atoms	R
Ag_2F	Ag + F at (0,0,0)	0.312
	Ag + F at $(0,0,\frac{1}{2})$	0.301
	Ag only	0.312
Ti_2O	Ti + O at (0,0,0)	0.169
	Ti + O at $(0,0,\frac{1}{2})$	0.181
	Ti + $\frac{1}{2}$O at (0,0,0) and $\frac{1}{2}$O at $(0,0,\frac{1}{2})$	0,169
	Ti only	0.169

Table 4.2

In both cases the results are inconclusive. Neither version leads to a significantly better agreement. Fourier methods were also tried, and seemed to indicate in the case of Ti_2O that there may be disorder, and both sites may be occupied by oxygens. With the Ti atom at $\pm$ 0.263 in z, the two sites are almost identical, and therefore disorder may well be present.

In the case of Ag_2F the results appear inconclusive, though the ability of silver to form metal-metal bonds, and the reasonable Ag-F distances would favour the published structure.

No data are available for Nb_2S and Ti_2S, thus these compounds cannot be considered at this stage.

Comparison with Cs_3O

Ca_2N was compared structurally with Cs_2O, but its electrical properties would favour comparison with a lower oxide of caesium, Cs_3O. Tsai et al[20] have found that powdered Cs_3O shows metallic conductivity.

Cs_3O contains columns of O-Cs octahedra. A slice perpendicular to these columns is shown in Figure 4.4[21]. The metal-metal distance within the columns is 2.89 Å, similar to that in Cs_2O, but the Cs-Cs distance between the columns is ~5.8 Å, compared with only 5.24 Å in metallic caesium.

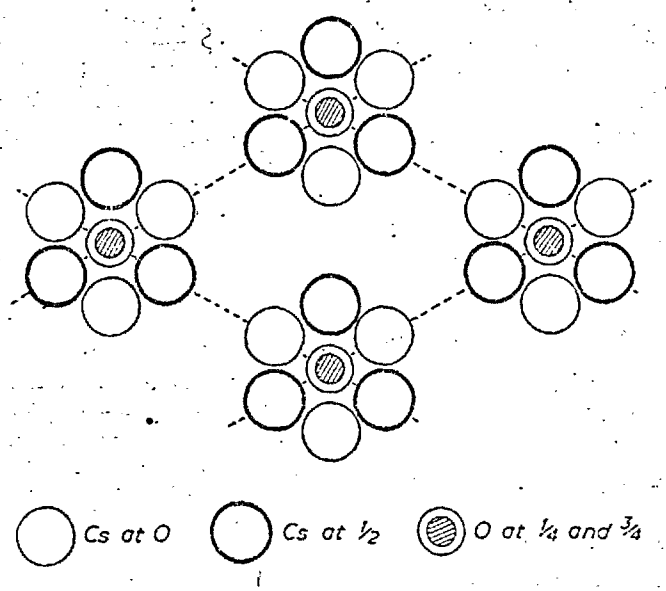


Figure 4.4

The metallic conductivity of powdered Cs_3O implies that a single crystal have metallic conductivity in all directions, and therefore suggests that the "free" electrons are situated in the gaps between the columns as opposed to being localised to the columns themselves. The latter alternative would result in a uni-directional conductivity, which would contradict the experimental observation.

This implies that in Ca_2N the excess electrons should be localised to the large gaps between the layers. Such an arrangement would give the required electrostatic stability to the Ca^{2+} environment. The layers without the excess electrons remain essentially ionic in character and form a barrier to conduction through them.

Thus the "free" electrons should be able to move with ease parallel to the basal plane of the hexagonal cell, (i.e. in the gaps between the layers), The layers themselves form barriers which become less effective as the electrons become more energetic with a rise in temperature. Under such conditions more electrons are able to surmount the barriers, so that in the trans-layer direction a much lower value of conductivity may be expected, which however would increase with an increase in temperature in the manner of a semi-conductor.

These properties would explain the experimental observation for a powder compact, since it is the poorer "conductor" which would govern the conductivity of a powder which was composed of a mixture of two different conductors. The temperature coefficient of a mixture

would however be a proportional average of the components. In the case of Ca_2N we can therefore say that at least one direction in a single crystal must have a positive temperature coefficient of conductivity. Before a full proposal of the electrical properties of Ca_2N is made reference should be made to the known properties of other M_2X compounds.

Electrical Properties of M_2X Compounds

Most electrical measurements on these compounds were made in the powder form. The values of conductivity at room temperature are listed in Table 4.3 with the conductivity of the appropriate metal given for comparison. The ratio of the two conductivities is also stated in each case.

The general trend in the Table shows that M_2X compounds, other than Ca_2N and Ba_2N have metallic conductivities. They are of the order of 1/10th of the value for the appropriate metal. The conductivities of Ca_2N and Ba_2N can only be described as semiconducting, the actual values being of the order of 10^{-6} of the metallic value.

Two conclusions may, therefore be drawn from the Table. First, that there is likely to be a significant structural difference between Ca_2N and the other compounds. (Ba_2N and Sr_2N are assumed to be isostructural with Ca_2N, although there is no direct evidence for this) The significant structural difference is the size of the interlayer metal-metal distance compared with that within the layer in each case.

Compound	Conductivity of powder $ohm^{-1}cm^{-1}$	Metal	Conductivity of metal $ohm^{-1}cm^{-1}$	Ratio M/M_2X
Ca_2N	$2x10^{-1}$	Ca	$3x10^5$	$1.5x10^6$
Ba_2N	$1x10^{-2}$	Ba	$1.4x10^4$	$1.4x10^6$
Ti_2O	-			-
Ti_2S	$3x10^3$			6
Ti_2Se	$5x10^3$	Ti	$2x10^4$	4
Ti_2Te	$5x10^3$			4
Ag_2F	graphitic ($\sim 10^3$)	Ag	$6x10^5$	$\sim 6x10^2$
Nb_2S	$>10^2$	Nb	$8x10^4$	10

Table 4.3

The second conclusion is that only Ca_2N and its barium and strontium analogues should be semiconductors, as the other compounds should show single-crystal conductivities which are almost metallic, though they should still exhibit marked anisotropy. The direction of poorest conductivity still cannot be much worse than the values for the powder, since as stated previously, it is this direction that governs overall conductivity of the powder sample.

Of this group, only Ag_2F had been examined in detail for the

electrical properties of a single crystal. Andres et al[22] have found that flakes of Ag_2F, being roughly normal to the crystallographic c axis, showed conductivities of 4×10^4 ohm^{-1}cm^{-1} at room temperature. It was not possible to measure the conductivity of the flakes in the perpendicular direction, but it was stated by the authors to be almost certainly considerably lower. They also found that Ag_2F became a superconductor at 0.066°K and a critical field of 2.5 Oe at 0°K. Measurements of the Meissner effect in single crystals showed that the supercurrents flow in all three directions.

The last observation is important since it implies that the marked anisotropy inherent in such layer compounds disappears in the superconducting state, although there may be a structural change accompanying the transition. If one pictures Ag_2F as consisting of alternate layers of twin sheets of bonded metallic silvers and sheets of F^- ions, one can localise the "free" electrons in between the bonded silver atoms. Metallic conduction would then be expected in this plane, with lower conduction perpendicular to it. The effectiveness of the ionic barrier of the F^- ions is expected to be lower than that of the ionic layer in Ca_2N, which effectively consists of the triple sheet of Ca^{2+}, N^{3-}, Ca^{2+} ions. A less effective barrier gives better conduction through itself, and therefore the value of the conductivity for a powder specimen is much higher for Ag_2F than for Ca_2N. Thus the presence of the gap between the layers of Ca_2N implies excellent conductivity parallel to them, possibly even better than in the metal.

Since electrically the major difference between the two compounds

appears to be the effectiveness of the ionic barrier, and since this barrier disappears in the superconducting state, it is quite likely that Ca_2N would also become a superconductor at a suitably low temperature. Superconductivity is already known to be exhibited by some other nitrides, e.g. Mo_2N, MoN, NbN, TiN, VN, ZrN etc.

Likely Electrical Properties of Single Crystals of Ca_2N

At room temperature, the electrical conductivity of Ca_2N is likely to be markedly anisotropic. In a direction parallel to the layers of the structure, conductivity should be metallic. Perpendicular to the sheets it should exhibit semiconductivity. The temperature coefficients should be negative and positive in the two directions respectively, as for a usual metal and a semiconductor. Ca_2N (as well as Ba_2N and Sr_2N) should be the only M_2X compound of the group discussed that exhibits semiconductivity.

In view of its structure, and by analogy with Ag_2F, Ca_2N is likely to be a superconductor at low temperatures.

In the powder form, no contradictions arise between the measured values and the properties proposed.

Clearly, a thorough electrical investigation of single crystals of Ca_2N is very desirable, and should give interesting results. It is hoped that this work will scon be undertaken at a different laboratory.

References III

(1) I. Ahmad and J. W. Tomlinson, to be published.

(2) S. M. Arya and E. A. Prokofyeva, J.Gen.Chem.(U.S.S.R.), 1955,25,813.

(3) I. Ahmad, Ph.D. thesis, London, 1963.

(4) Y. Laurent, J. David and J. Lang, Compt.Rend., 1964,259(5),1132.

(5) M. von Stackelberg and R. Paulus, Z.Phys.Chem., 1933,B22,305.

(6) R. S. Bradley, D. C. Munro and M. Whitefield, J.Inorg.Nucl.Chem., 1966,28,1803.

(7) Y. Okamoto and J. C. Goswani, Inorg.Chem., 1966,July, 5,1281.

(8) University of Maryland Technical Report TR-64-6, NsG-396.

(9) W. R. Busing, K. O. Martin and H. A. Levy, Oak Ridge National Laboratory Report, ORNL-TM-305.

(10) J. W. Tomlinson, private communication.

(11) International Tables for X-ray Crystallography,
Kynoch Press, Birmingham,
Volume I 1952,
Volume II 1959,
Volume III 1962.

(12) J. F. Smith, O. N. Carlson and R. W. West, Trans.Electrochem.Soc., 1956,103,409.

(13) Khi-Ruey Tsai, P. M. Harris and E. N. Lassetre, J.Phys.Chem., 1956,60,338.

(14) H. Terrey and A. Diamond, J.Chem.Soc., 1928,2820.

(15) S. Andersson, S. Asbrink, B. Holmberg and A. Magnelli, Bul.Nat.Inst.Sci.India, 1958,14,136.

(16) F. K. McTaggart, Aust.J.Chem., 1958,11,471.

(17) H. F. Franzen, V. W. Dejong, B. R. Conard, J.Inorg.Nucl.Chem., 1966,28,3052.

(18) K. E. Wetzlac and G. Lennartz, DEW(Deut.Edelstahlenwerke).Tech.Ber., 1961,1,15.

(19) J. P. Owens, B. R. Conard and H. F. Franzen, Acta Cryst, to be published.

(20) Khi-Ruey Tsai, P. M. Harris and E. N. Lassetre, J.Phys.Chem., 1956,60,345.

(21) A. F. Wells, "Structural Inorganic Chemistry", Clarendon Press, Oxford, 1962.

(22) K. Andres, N. A. Kuebler and M. B. Robin, J.Phys.Chem.Solids, 1966,27,1747.

(23) Y. Laurent, J. Lang and M.Th.Le Bihan, Acta Cryst., to be published.

(24) Y. Laurent, J. Lang and M.Th.L. Bihan, Acta Cryst., 1968,B24,494.

APPENDIX

(*Reprinted from Nature, Vol. 217, No. 5131, p. 841 only, March 2, 1968*)

Structure corresponding to the Ideal Composition $3Bi_2O_3.17Nb_2O_5$

As part of a study[1] of the structures of compounds in the Bi_2O_3–Nb_2O_5 binary system, we have determined the crystal structure of $3Bi_2O_3.17Nb_2O_5$, which we believe to be the ideal formula of the compound prepared by Roth and Waring[2] and referred to as $Bi_2O_3.6Nb_2O_5$.

The pale yellow plates of this material are orthorhombic with $a = 12{\cdot}516 \pm 0{\cdot}005$, $b = 37{\cdot}14 \pm 0{\cdot}02$, $c = 3{\cdot}922 \pm 0{\cdot}002$ Å, $U = 1828{\cdot}3$ Å^3. Using this unit cell we have been able to index fully the X-ray powder pattern published by Roth and Waring[2]. Single crystal photographs suggested that the structure was of the tetragonal bronze type[3] but with one cell edge tripled, and the intensities showed a remarkable similarity to those found by Sleight[4] for $Nb_{16}W_{18}O_{94}$.

The structure has been determined from some 1,300 independent reflexions, obtained with Cu–$K\alpha$ radiation and visually estimated. Least-squares refinement, in space group *Pba*2, has now reached $R = 0{\cdot}10$ and is being continued.

All atoms in $3Bi_2O_3.17Nb_2O_5$ are situated near two levels approximately $c/2$ apart. The structure is based on an $Me_{34}O_{94}$ matrix in which four of the twelve pentagonal tunnels are regular (in contrast with the other eight) and contain niobium atoms in pentagonal bipyramidal co-ordination. All the other niobium atoms have an octahedral co-ordination. The remaining eight pentagonal and six diamond-shaped tunnels, which are empty in $Nb_{16}W_{18}O_{94}$, contain all the bismuth atoms. We have found that these are statistically distributed among a number of possible sites, and have used the occupancy at each site as a parameter in the least-squares refinement. The resulting structure is shown schematically in Fig. 1.

The apparent chaos among the bismuth atoms is not unreasonable. The pentagonal and even the diamond-shaped tunnels are too large for the bismuth atom (ionic radius 0·96 Å) and, consequently, these atoms are located away from the centre of the hole. Furthermore, the bismuth atoms show a very strong tendency towards a one-sided four-fold co-ordination similar to that found, for example, in $BiSbO_4$ (ref. 5) and a number of other complex oxides and oxyhalides of bismuth[6–9]. This kind of co-ordination, a consequence of a lone pair of electrons, is more often associated with tervalent antimony[10,11] and is even found for arsenic[12]. The bismuth atoms could achieve this co-ordination at a number of sites. The bismuth occupancies of these sites are uneven (see Fig. 1)

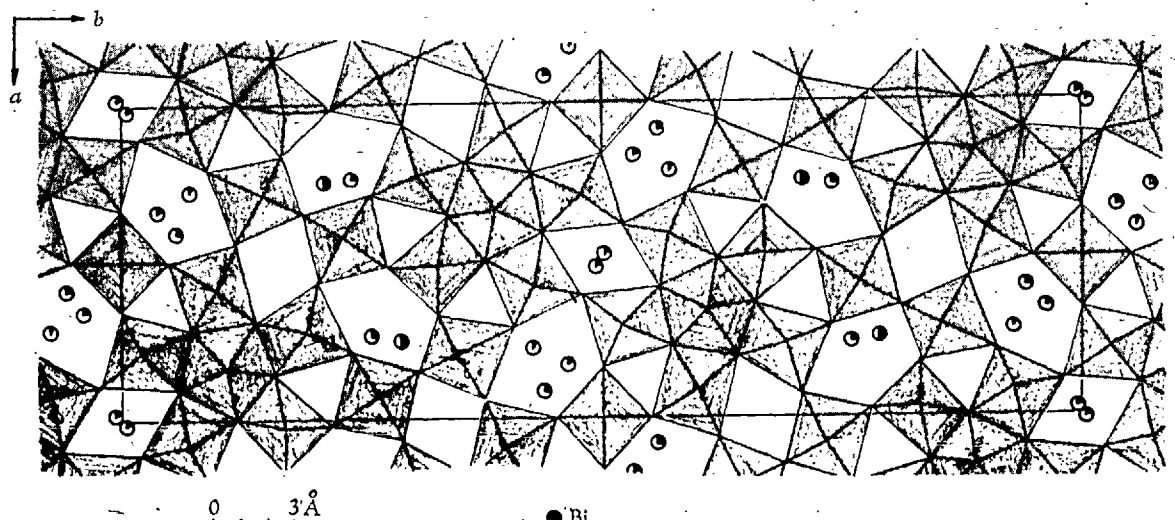


Fig. 1. The [001] projection of the structure of $3Bi_2O_3.17Nb_2O_5$ showing the $Me_{34}O_{64}$ matrix (shaded) and the occupancies of the bismuth sites.

but add up to 5·7 ($2\sigma = 0{\cdot}2$) per unit cell, whereas 6 would be expected from the formula. It seems likely that the remaining 0·3 atoms are spread out thinly among some or all of the other possible sites. If, however, the true formula is $Bi_2O_3.6Nb_2O_5$, there would be $5\frac{2}{3}$ bismuth atoms per unit cell, but electrical neutrality would require the random removal of half an oxygen atom per unit cell.

It is difficult to reach a clear-cut decision between the two compositions, the difference between which is very slight (15·0 per cent Bi_2O_3, 85·0 per cent Nb_2O_5, D_{calc} = 5·37 g cm^{-3} for 3 : 17, and 14·3 per cent Bi_2O_3, 85·7 per cent Nb_2O_5, $D_{calc} = 5{\cdot}30$ g cm^{-3} for 1 : 6). We consider, however, that $3Bi_2O_3.17Nb_2O_5$ represents the ideal structural formula.

E. T. Keve
A. C. Skapski

Chemical Crystallography Laboratory,
Imperial College,
London.

Received January 24, 1968.

[1] Keve, E. T., and Skapski, A. C., *Chem. Commun.*, 281 (1967).
[2] Roth, R. S., and Waring, J. L., *J. Res. Nat. Bur. Stand., Sect. A*, **66**, 451 (1962).
[3] Magnéli, A., *Arkiv Kemi*, **1**, 213 (1949).
[4] Sleight, A. W., *Acta Chem. Scand.*, **20**, 1102 (1966).
[5] Aurivillius, B., *Arkiv Kemi*, **3**, 153 (1951).
[6] Aurivillius, B., *Arkiv Kemi*, **1**, 463 (1949).
[7] Aurivillius, B., *Arkiv Kemi*, **1**, 499 (1949).
[8] Aurivillius, B., *Arkiv Kemi*, **2**, 519 (1950).
[9] Aurivillius, B., *Arkiv Kemi*, **5**, 39 (1952).
[10] Edstrand, M., *Svensk. Kem. Tidskr.*, **67**, 230 (1955).
[11] Rogers, D., and Skapski, A. C., *Proc. Chem. Soc.*, 400 (1964).
[12] Skapski, A. C., *Chem. Commun.*, 10 (1966).

Printed in Great Britain by Fisher, Knight & Co., Ltd., St. Albans.

Reprinted from CHEMICAL COMMUNICATIONS, 1967, page 281.

The Structure of Triclinic $BiNbO_4$ and $BiTaO_4$

By E. T. KEVE and A. C. SKAPSKI

(*Chemical Crystallography Laboratory, Imperial College, London, S.W.7*)

THE group of ABO_4 compounds shown in the Table falls into three structure types, all of which are unique to this system. Previous studies[1,2] have shown the monoclinic and orthorhombic forms to be related in a very simple manner. We have now determined the crystal structure of triclinic $BiNbO_4$, a representative of the third type, and find it to have unusual features.

The triclinic forms of $BiNbO_4$ and $BiTaO_4$ were first prepared by Aurivillius[3] who showed them to

be isomorphous. Subsequently Roth and Waring[4,5] found them to be the high-temperature forms and prepared the low-temperature orthorhombic modifications of these compounds. Triclinic $BiNbO_4$ forms pale yellow elongated prisms. The crystals are normally twinned on the *bc* plane in two

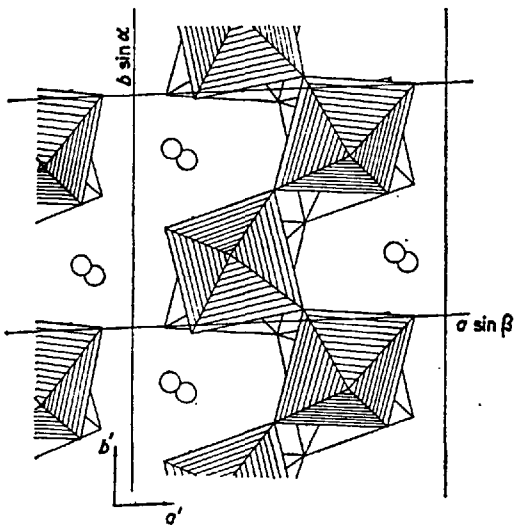


FIGURE 1a. [001] *Projection of triclinic* $BiNbO_4$.

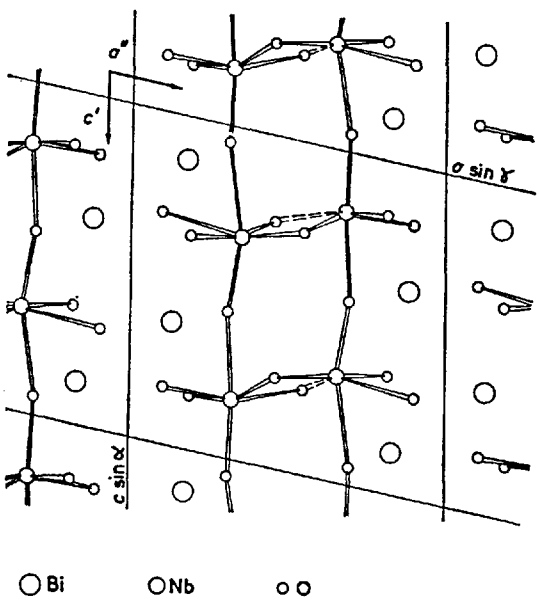


FIGURE 1b. [010] *Projection of triclinic* $BiNbO_4$. (*Dashed lines indicate bonds between niobium and oxygens in the cell above. The octahedra are joined at corners, not edges*).

different ways, one of them being polysynthetic. The unit-cell dimensions[4] are: $a = 7{\cdot}611$, $b = 5{\cdot}536$, $c = 7{\cdot}919$ Å, $\alpha = 89°\ 54'$, $\beta = 77°\ 28'$; $\gamma = 87°\ 9'$, U = 325·2 Å.[3] The unit-cell content is $4(Bi^{III}Nb^{V}O_4)$.

TABLE

	Nb^V	Sb^V	Ta^V
Sb^{III}	$SbNbO_4$ (o-rh.)	α-Sb_2O_4 (o-rh.)	$SbTaO_4$ (o-rh.)
	—	β-Sb_2O_4 (mon.)	—
Bi^{III}	$BiNbO_4$ (o-rh.)	—	$BiTaO_4$ (o-rh.)
	$BiNbO_4$ (tric.)	$BiSbO_4$ (mon.)	$BiTaO_4$ (tric.)

One form of twinning could be removed by splitting a crystal, but because of the very small size of the resulting fragment Cu-K_α radiation was used to collect the visually estimated data. The structure was solved by standard methods and all the oxygen atoms were observed in a difference Fourier. Least-squares refinement on 642 independent reflections, assuming space group $P\bar{1}$, has reached $R = 0{\cdot}122$. No absorption correction could be applied because of the polysynthetic twinning.

Figures (1a) and (1b) show that the structure contains puckered sheets in the *bc* plane consisting of Nb–O octahedra joined by corners only. It can be derived by slicing an ReO_3-type structure diagonally [parallel to (110) of the ReO_3 unit cell], separating the sheets of octahedra so formed, and sidestepping them to permit more economical packing (Figure 1b). The voids in this framework (Figure 1a) are then filled by the bismuth atoms.

The type of sheet found in this structure is novel in having octahedra joined at four vertices so that the two free ones are adjacent. The other way of joining octahedra at four vertices to form a sheet of the composition $(AX_4)_n$ is found, among others, in β-Sb_2O_4[1] and $SbNbO_4$.[2] This type of sheet, however, together with those, two-octahedra thick, found in $Sr_3Ti_2O_7$[6] and Bi_3NbTiO_9[7] (as perovskite units) are analogous to slices parallel to (100) of the ReO_3 structure.

The octahedra are distorted and the Nb–O distances are within the normal range. The co-ordination of the bismuth atoms is one-sided and very irregular. Each of the two crystallographically independent bismuth atoms has eight oxygen neighbours in the range 2·10—3·00 Å; there are other oxygens at distances greater than 3·48 Å. The standard deviations are 0·04—0·08 Å.

There are no unusually short oxygen–oxygen contacts.

Both the nature and frequency of the two modes of twinning can be explained in terms of alternative ways of stacking adjacent sheets.

(*Received, October 25th,* 1966; *Com.* 824.)

[1] D. Rogers and A. C. Skapski, *Proc. Chem. Soc.*, 1964, 400.
[2] A. C. Skapski and D. Rogers, *Chem. Comm.*, 1965, 611.
[3] B. Aurivillius, *Arkiv Kemi*, 1951, **3**, 153.
[4] R. S. Roth and J. L. Waring, *J. Res. Nat. Bur. Stand., Sect. A*, 1962, **66**, 451.
[5] R. S. Roth and J. L. Waring, *Amer. Mineralogist*, 1963, **48**, 1348.
[6] S. N. Ruddlesden and P. Popper, *Acta Cryst.*, 1958, **11**, 54.
[7] B. Aurivillius, *Arkiv Kemi*, 1949, **1**, 463.

Reprinted from CHEMICAL COMMUNICATIONS, 1966, page 829.

Ca_2N: A Nitride with a Layer Structure

By E. T. KEVE and A. C. SKAPSKI

(*Chemical Crystallography Laboratory, Imperial College, London, S.W.7*)

AHMAD and TOMLINSON[1] have recently prepared a new nitride of the stoicheiometry Ca_2N and recorded its *X*-ray powder pattern. Corresponding subnitrides of strontium and barium are also known.[2] We have determined the structure of dicalcium nitride by three-dimensional *X*-ray methods, and find it to have some unusual features.

Ca_2N forms greenish black lustrous crystals which quickly decompose in air, and have to be sealed under argon. Their symmetry is rhombohedral, and the unit-cell dimensions, determined by indexing Ahmad's powder data, are a = 6·603 Å, α = 31° 59′, U = 71·7 Å^3, D_m = 2·17 g. cm.$^{-3}$, D_c = 2·18 g. cm.$^{-3}$ for Z = 1. The corresponding hexagonal cell has a = 3·638, and c = 18·78 Å. The space group has proved to be $R\bar{3}m$.

The structure was solved by standard methods on the basis of a morphologically and computationally convenient monoclinic unit cell (a = 6·299, b = 3·638, c = 7·535 Å, β = 123° 51′, Z = 2 and space group $C2/m$). Least-squares refinement has now reached R = 0·16 for 121 reflections, collected with Cu-K_α radiation and visually estimated. Further refinement using data from a better-quality crystal will be carried out.

Figures 1a and b show that Ca_2N has a layer structure. The nitrogen atoms lie on inversion triads, and their co-ordination is octahedral with some angular distortion (Ca–N–Ca angles of 96·9° and 83·1°) and six equal N–Ca distances of 2·43 Å. By comparison the N–Ca distance found in the usual nitride, Ca_3N_2, is 2·47 Å.[3] Within each layer every calcium atom is in contact with three nitrogens at 2·43 Å. Its nearest calcium neighbours are three at 3·23 Å and six at 3·64 Å. The shortest Ca–Ca distance between the layers is 4·35 Å. The Ca–Ca distances found in the metal are 3·947 Å in the α-form and 3·877 Å in the γ-form.[4]

The nearest structural equivalent is Cs_2O,[5] which has an anti-$CdCl_2$ type structure. The main difference is that in Ca_2N the shortest metal–metal distance between layers is substantially greater than the corresponding one within the layer (see Figure 1a), whereas they are of the same order in Cs_2O. Further comparison can be made with a lower oxide of cæsium, Cs_3O,[6] which is reported to have a greenish metallic appearance. It has columns of O–Cs octahedra with interatomic distances similar to those in Cs_2O, but the Cs–Cs distances between the columns are about 0·5 Å greater than those in the metal.

It is probably best to think of the structure as being essentially ionic. Thus Ca_2N gives off

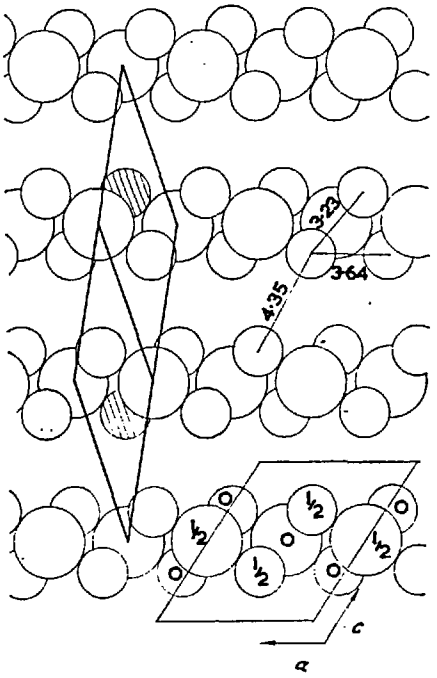


FIGURE 1a

A view of the layer structure of Ca_2N *showing the rhombohedral cell and its calcium content (hatched). The projection corresponds to* [010] *of the monoclinic cell indicated. The estimated standard deviations of the bond lengths are* ~0·01 Å.

ammonia and hydrogen in contact with water,[1] and the difference in the electronegativities of the two elements also favours this view. The greenish black graphitic appearance is due to the excess electrons.

Tsai *et al.*[5] have found that powdered Cs_3O shows metallic conductivity. This implies that single crystals must have metallic conductivity

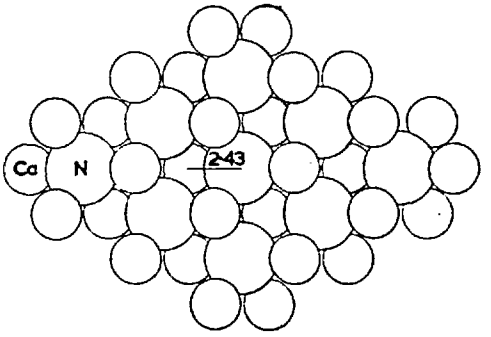


FIGURE 1b

A single layer in the Ca_2N *structure.*

in all directions, and therefore suggests that the "free" electrons are situated in the gaps between the columns of O–Cs octahedra. We favour an analogous view of Ca_2N, with the excess electrons being situated in the large gaps between layers, which, being essentially ionic, form a barrier to conduction. Such a view also gives the calcium ions a more balanced electrostatic environment.

A preliminary investigation of the electrical properties of powder compacts of Ca_2N[7] indicates that the conductivity is in the semiconductor range (about 0·2 ohm^{-1} $cm.^{-1}$ at room temperature) and that the temperature coefficient is positive. These observations are consistent with the structure. A single crystal should have excellent conductivity parallel to the layers, but a much lower conductivity normal to them. A rise in temperature should reduce the effectiveness of the ionic layers as barriers, so conduction perpendicular to the layers, which in a powder specimen would be the determining factor governing overall conductivity, should increase.

(*Received, October* 21*st*, 1966; *Com.* 805.)

[1] I. Ahmad, Ph.D. Thesis, London, 1963; I. Ahmad and J. W. Tomlinson, to be published. We thank Prof. J. W. Tomlinson and Mr. C. Lammas for supplying us with crystals.
[2] S. M. Arya and E. A. Prokofyeva, *J. Gen. Chem.* (*U.S.S.R.*), 1955, **25**, 813.
[3] M. Stackelberg and R. Paulus, *Z. phys. Chem.*, 1933, **B22**, 305.
[4] J. F. Smith, O. N. Carlson, and R. W. Vest, *Trans. Electrochem. Soc.*, 1956, **103**, 409.
[5] Khi-Ruey Tsai, P. M. Harris, and E. N. Lassetre, *J. Phys. Chem.*, 1956, **60**, 338.
[6] Khi-Ruey Tsai, P. M. Harris, and E. N. Lassetre, *J. Phys. Chem.*, 1956, **60**, 345.
[7] J. W. Tomlinson, private communication.